TID-4500, UC-48 ACRH-34

ARGONNE CANCER RESEARCH HOSPITAL
950 EAST FIFTY-NINTH STREET • CHICAGO • ILLINOIS 60637

Semiannual Report to
THE ATOMIC ENERGY COMMISSION

SEPTEMBER 1970

ALEXANDER GOTTSCHALK, M.D.
Editor

MARGOT DOYLE, Ph.D.
Associate Editor

OPERATED BY THE UNIVERSITY OF CHICAGO
UNDER
CONTRACT AT-(11-1)-69

DISCLAIMER

LEGAL NOTICE

Printed in the U.S.A.
Available from the National Technical Information Service, National Bureau of Standards, U.S. Department of Commerce, Springfield, Virginia 22151

Price: Printed copy $3.00; Microfiche $0.65

TID-4500, UC-48 ACRH-34

ARGONNE CANCER RESEARCH HOSPITAL
950 EAST FIFTY-NINTH STREET · CHICAGO · ILLINOIS 60637

Semiannual Report to
THE ATOMIC ENERGY COMMISSION

SEPTEMBER 1970

ALEXANDER GOTTSCHALK, M.D.
Editor

MARGOT DOYLE, Ph.D.
Associate Editor

OPERATED BY THE UNIVERSITY OF CHICAGO
UNDER
CONTRACT AT-(11-1)-69

TABLE OF CONTENTS

ERYTHROPOIESIS AND ERYTHROPOIETIN IN PATIENTS WITH CHRONIC RENAL FAILURE TREATED WITH HEMODIALYSIS AND TESTOSTERONE*

By

R. L. DeGowin,† A. R. Lavender,‡ M. Forland,§ D. Charleston, and A. Gottschalk

Advanced renal disease compromises the endocrine function of the kidney as well as its excretory function. Diminished erythropoietin levels[1] are associated with an anemia of underproduction in patients with chronic renal failure. Maintenance of the nonuremic state by periodic hemodialysis does not fully correct deficient erythropoiesis.[2] Consequently, repeated blood transfusions, with their attendant sequelae,[3] are needed to maintain the hematocrit at levels compatible with optimal rehabilitation. This acquired erythropoietin deficiency should be treated by replacement of the hormone, as physicians treat other endocrine deficiencies, such as diabetes mellitus, Addison's disease or myxedema. The fact that erythropoietin is not available in quantities sufficient to test its efficacy in replacement therapy makes it necessary to seek alternative solutions to this problem.

Several related observations suggest one possible approach. Patients who have had bilateral nephrectomy continue to produce erythrocytes, although the rate of erythropoiesis is insufficient to attain normal hemoglobin concentrations.[4,5] Endocrine control of erythropoiesis, responsive to hypoxia or plethora, probably occurs in anephric patients since they response to hemorrhage with reticulocytosis and to blood transfusion with a reduction in marrow erythroblasts.[6] Moreover, erythropoietin has been detected in the plasma of anephric patients.[6,7] Since the release of erythropoietin from extrarenal sites appears responsive to hypoxia, a qualitatively normal stimulus, we wondered if agents that enhance erythropoietin production in normal man would correct the anemia in the patient undergoing periodic hemodialysis. Androgens increase erythropoiesis in rodents[8] and man[9] and act, at least in part, by increasing erythropoietin production.[10-12] Recent studies show that androgens increase plasma erythropoietin levels in anephric patients[13] bur not in anephric rodents.[14]

Seeking an agent to reduce transfusion requirements for patients with chronic renal failure undergoing hemodialysis, we administered testosterone to 2 such patients to test whether androgens would stimulate either residual renal tissue or some extrarenal site to produce erythropoietin and accelerate erythropoiesis. Responses to testosterone were evaluated by assays of erythropoietin and by morphologic and ferrokinetic measurements of erythropoiesis in the blood and bone marrow.

*This report is taken from a paper that appeared in Amer. Int. Med., 72:913, 1970. The work was supported in part by U. S. Public Health Service, the National Heart Institute, and Hines VA Hospital, Hines, Ill.

†Recipient of a Research Career Development Award from the National Cancer Institute, U. S. Public Health Service. Present address: Department of Medicine, University of Iowa Medical School, Iowa City, Ia.

‡Recipient of a Research Career Development Award from the National Heart Institute, U. S. Public Health Service. Present address: Hines VA Hospital and Stritch School of Medicine, Hines, Ill.

§Present address: University of Texas Medical School, San Antonio, Texas.

METHODS AND MATERIALS

Evaluation of erythropoiesis. Erythropoiesis was evaluated from changes in the patients' transfusion requirements with therapy, and from changes in hemoglobin, hematocrit, red blood cell count and reticulocyte count. Sections and smears were made of spicules of bone marrow obtained by aspiration,[15] and the percentage of normoblasts in 1,000 nucleated marrow cells was determined from smears. Iron stores were evaluated from Prussian-blue-stained marrow sections. The serum iron and total iron-binding capacity, ferrokinetic studies, and linear profile scanning were performed by methods previously described.[16]

Assay of plasma erythropoietin. Arterial blood, obtained in a heparinized container immediately before dialysis, was used for determination of blood counts and plasma erythropoietic activity. The plasma erythropoietin was assayed with the posthypoxic plethoric mouse.[17,18] One milliliter of plasma per mouse was injected into groups of 5 to 10 assay mice. The mean erythrocyte ^{59}Fe incorporation of saline-injected controls was subtracted from the mean erythrocyte ^{59}Fe incorporation induced by the patient's sample of plasma in assay mice. One-tenth of a cobalt unit of erythropoietin prepared from human urine elicited about 5 per cent ^{59}Fe uptake, and saline elicited about 0.5 per cent ^{59}Fe incorporation into newly formed red cells in this assay system.

Testosterone administration. Testosterone enanthate 200 mg was injected intramuscularly twice weekly after each dialysis.

Anephric patient. A 39-year-old white man (J.M.) gave evidence of renal disease for approximately 15 years. Bilateral nephrectomy was performed in March 1966, and extracorporeal renal transplantation in July 1966.[19] Rejection of the transplant occurred 25 days later, and since that time the patient has been maintained on twice weekly 6-hour therapy with the Kolff twin-coil dialyzer. His BUN averaged 50 to 60 mg/100. During the last two and one-half years he has developed neuropathy requiring leg braces, hyperpigmentation secondary to iron overload from transfusions, gynecomastia, testicular atrophy, and muscular wasting. After beginning therapy with testosterone, his nutrition and sense of well-being greatly improved. There were no undesirable side effects of the therapy.

Patient with kidneys. A 44-year-old Serbian minister (D.P.) with chronic glomerulonephritis received hemodialysis twice weekly for 5 months before the beginning of the study in May 1968. His BUN averaged 30 to 60 mg/100 ml. He suffered no complications from therapy or disease. During testosterone administration, this patient developed a voracious appetite, gained weight and became very active, preaching in various parts of Chicago. After three months of vigorous activity he complained of a recurrence of angina pectoris with effort which he had experienced before beginning periodic hemodialysis. The testosterone was discontinued, he became less active, and the angina disappeared.

RESULTS

Anephric patient. About 3 units (1500 ml) of blood per week were required to maintain this patient's hematocrit between 20 and 25 per cent (23 ± 2.1 per cent)* (Figure 1). During therapy with testosterone, transfusions of blood were reduced to 1 unit every three weeks, because the patient seemed to require fewer transfusions to assure a sense of well-being. With less blood

*(mean ± standard deviation, n = 8).

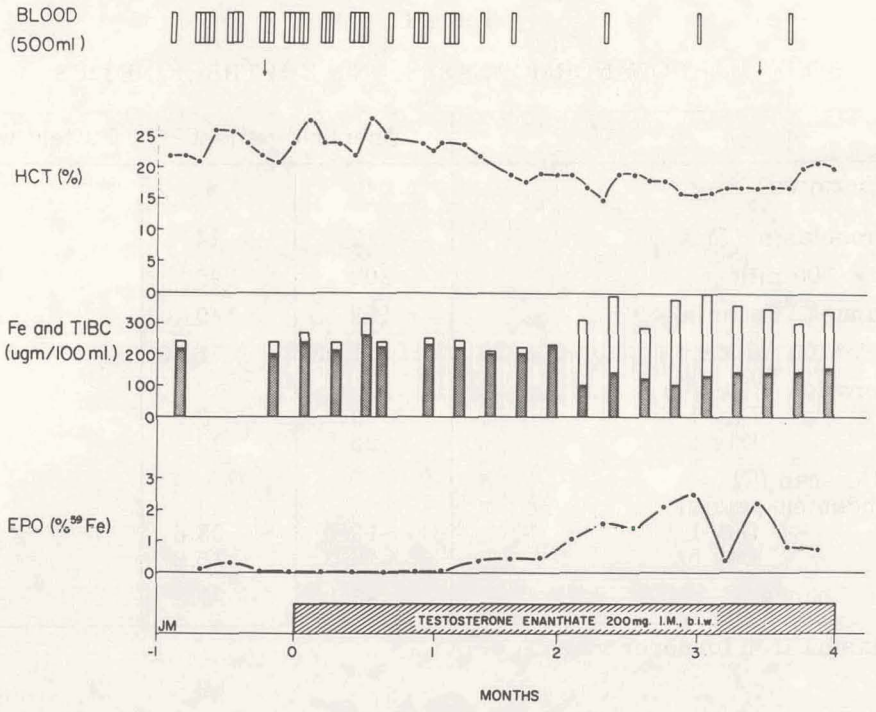

Figure 1. Chronology of blood transfusions, marrow normoblast counts and ferrokinetic studies (arrows), hematocrit (HCT), serum iron (Fe = shaded bar) and total iron-binding capacity (TIBC = open portion of bar), plasma erythropoietic activity (EPO), and twice-weekly intramuscular injections of testosterone. Withholding testosterone administration from the anephric patient (J.M.) produced a diminished hematocrit and increased erythropoietic activity of the plasma.

transfusions the hematocrit fell below levels of 20 per cent during the second month of therapy (20 ± 2.3 per cent)*. At this time, erythropoietic activity of the plasma was first detected. During the third month, after the fall in hematocrit and increase in plasma erythropoietic activity had occurred, the total iron-binding capacity increased and the serum iron and saturation of transferrin markedly decreased (Figure 1).

Bone marrow aspirates were performed during the week before therapy with testosterone and during the fourth month of therapy. The percentage of normoblasts present in the marrow increased by one-third from 18 to 24 per cent of the marrow's nucleated cells. Simultaneous ferrokinetic and linear profile scanning studies demonstrated an increased clearance of ^{59}Fe from the plasma (Table 1) to slightly greater than normal, and increasing erythrocyte radioiron incorporation by the fifth day. Radioiron clearance and utilization, however, were still subnormal.

A comparison of the linear profile scan made 24 hours after injection of ^{59}Fe (day 1) and before therapy (Figure 2), with scans made by Alfrey et al,[20] reveals a pattern characteristic of diminished erythropoiesis; normally, uptake of radioiron by the pelvis exceeds that in the abdomen. After 4 months of therapy, the 24-hour uptake of ^{59}Fe in the abdominal-pelvic region increased 20 per cent toward normal (Figure 3). The 5-day scans before and after therapy

*(mean ± standard deviation, n = 8).

Table 1

BONE MARROW NORMOBLASTS AND ERYTHROKINETICS

	Anephric patient		Patient with kidneys
Months of Therapy	0	4	0
Marrow normoblasts (%)	18	24	21
Serum Fe (μg/100 ml)	202	195	102
T 1/2 clearance ^{59}Fe (min)	198	140	111
PITR* (mg Fe/100 ml/day)	1.02	1.39	0.92
RBC incorporation ^{59}Fe (%)			
Day 1	3	3	6
Day 5	22	32	69
Linear profile scan (%) [cts. in abdomen-pelvis]			
Day 1	19.7	23.6	28.5
Day 5	16.6	15.8	17.1
Change:	-3.1	-7.8	-11.4

*PITR = plasma iron turnover rate.

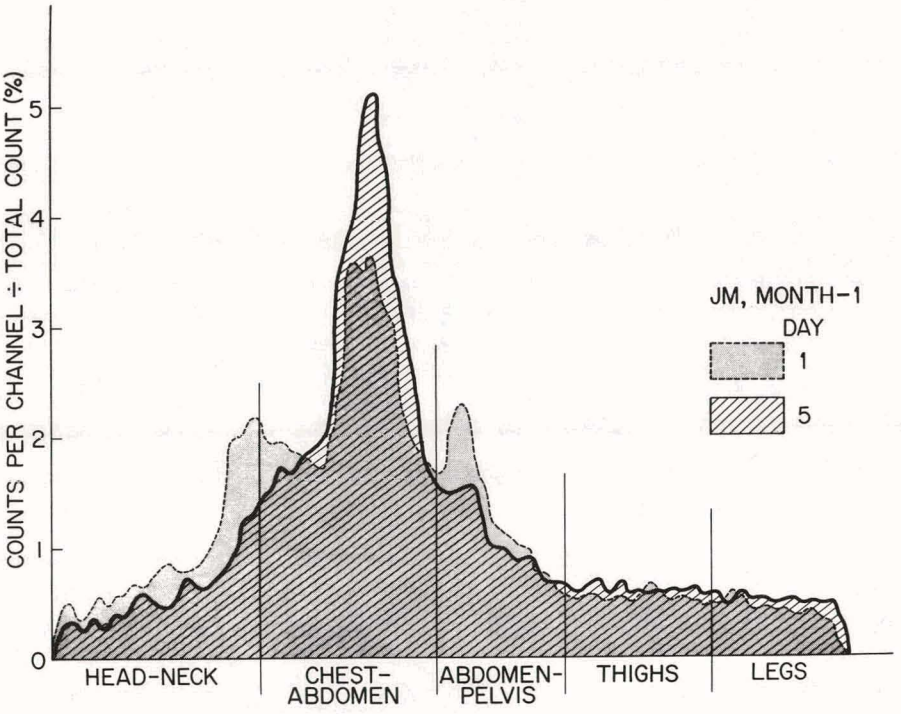

Figure 2. Pretreatment linear profile scans at 24 hours (day 1) and at 5 days after intravenous injection of ^{59}Fe in the anephric patient (J.M., month-1) show very little uptake and release of ^{59}Fe in the abdominal-pelvic region, indicating greatly diminished erythropoiesis.

showed very little change and represent ^{59}Fe in storage sites and in the hemoglobin of intravascular erythrocytes (Table 1). After completing these studies, the dose of testosterone was doubled for several months, but this failed to change hemoglobin or serum iron levels.

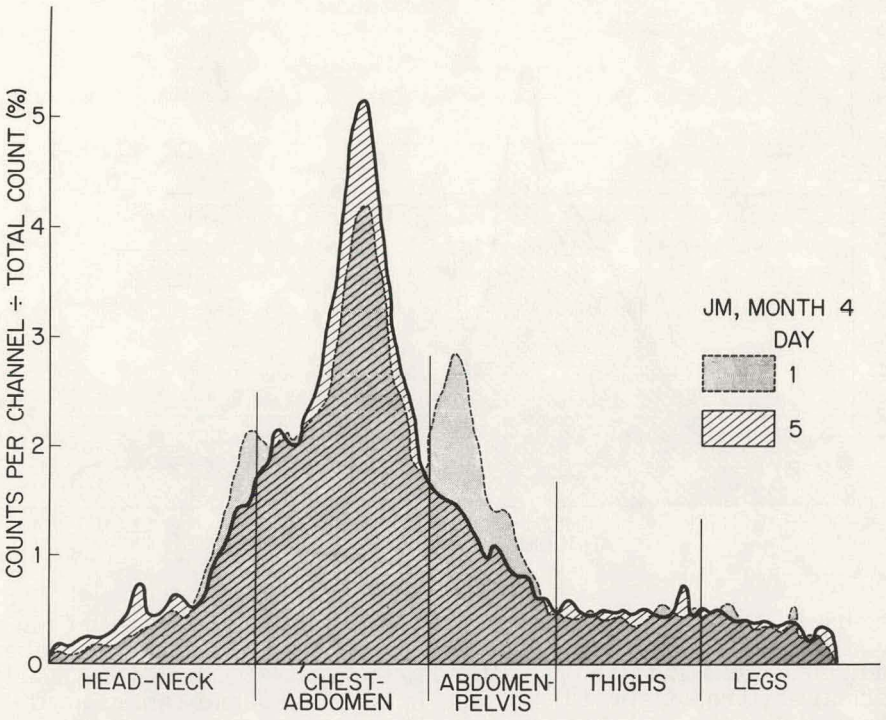

Figure 3. Linear profile scans after therapy in the anephric patient (J.M., month 4) indicate a 20% increase in ^{59}Fe uptake in the abdominal-pelvic region at one day, suggesting increased erythropoiesis.

In summary, when the hematocrit was permitted to fall below levels of 20 per cent by decreasing the frequency of blood transfusions in this anephric patient receiving testosterone, the erythropoietin level increased, and the percentage of saturated transferrin decreased. Marrow normoblast counts, ferrokinetic studies and linear profile scanning all demonstrated a distinct increase in erythropoiesis, although the hematocrit did not increase.

Patient with kidneys. Ferrokinetic studies and linear profile scanning before giving testosterone to this patient with kidneys (Table 1, Figure 4), revealed a pattern similar to that reported for normal subjects.[20] At that time, transfusion of one unit of blood per week was required to maintain the hematocrit at about 23 per cent (23 ± 1.3 per cent)*. During the month of baseline studies the hematocrit never exceeded 25 per cent. After therapy with testosterone, blood transfusions were diminished and then discontinued. Despite this, the hematocrit rose and, during the second month of therapy, usually exceeded 25 per cent (26 ± 1.7 per cent)*. Although erythropoietic activity was barely detectable during the first and second months of therapy, it was clearly present at low levels in the plasma during the third month of therapy. During the second month of therapy the mean level of transferrin increased, and the percentage saturation

*(mean ± standard deviation, n = 8).

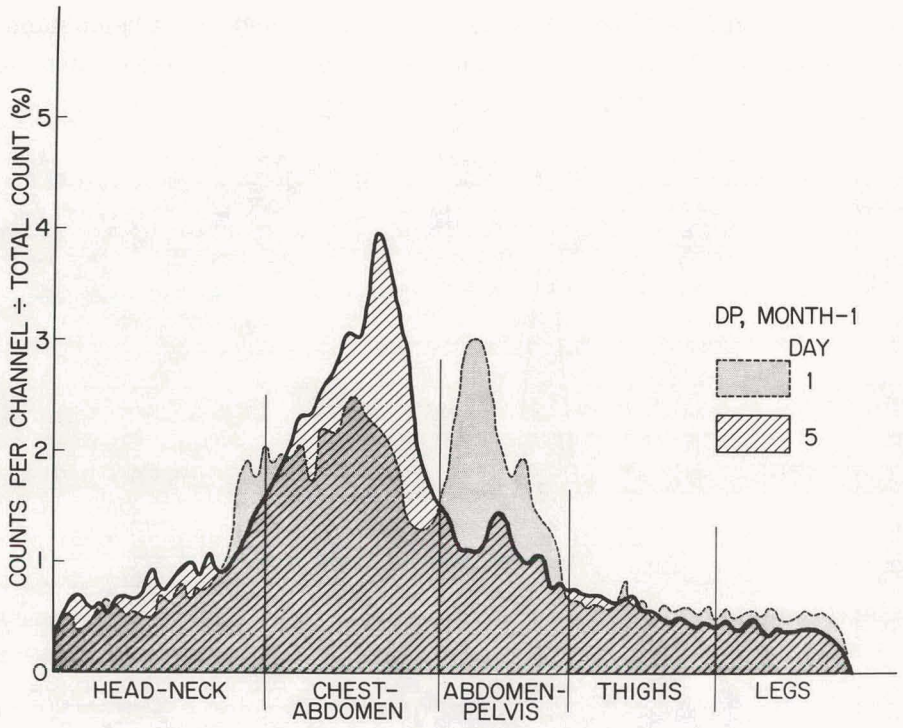

Figure 4. Pretreatment linear profile scans of the patient with damaged kidneys (D.P., month-1), show a nearly normal pattern of uptake and release one and five days after injection of ^{59}Fe, indicating nearly normal erythropoiesis at the outset. In fact, "a normal rate of erythropoiesis" was insufficient to correct the anemia.

of transferrin decreased by about one-third of that of the baseline or of that noted in the fourth month. After testosterone had been discontinued (Figure 5), the hematocrit progressively fell from levels above 25 per cent to levels as low as 20 per cent (22 ± 1.4 per cent* during the fourth month), and the patient was given another blood transfusion.

In summary, therapy with testosterone was associated with an increasing hematocrit,† which permitted the discontinuance of blood transfusions, and evidence of increasing erythropoietic activity of the blood. When therapy with testosterone was discontinued, erythropoietin levels decreased, the hematocrit diminished to levels below 25 per cent, and blood transfusions were initiated once again.†

DISCUSSION

As his blood transfusions were withheld, increasing erythropoiesis and elevated plasma levels of erythropoietin accompanied a progressive anemia in our anephric patient. We cannot tell from these studies whether therapy with testosterone facilitated this qualitatively normal response to hypoxia, but erythropoietic activity of the plasma was detected at slightly higher hematocrit values (16 and 19 per cent) than in Naets' patient who did not receive androgens;[6]

*(mean ± standard deviation, n = 8).

†There is a significant increase from the baseline hematocrits to those during the second month of therapy ($P < 0.01$). Hematocrits during the fourth month were significantly lower than during the second month ($P < 0.001$).

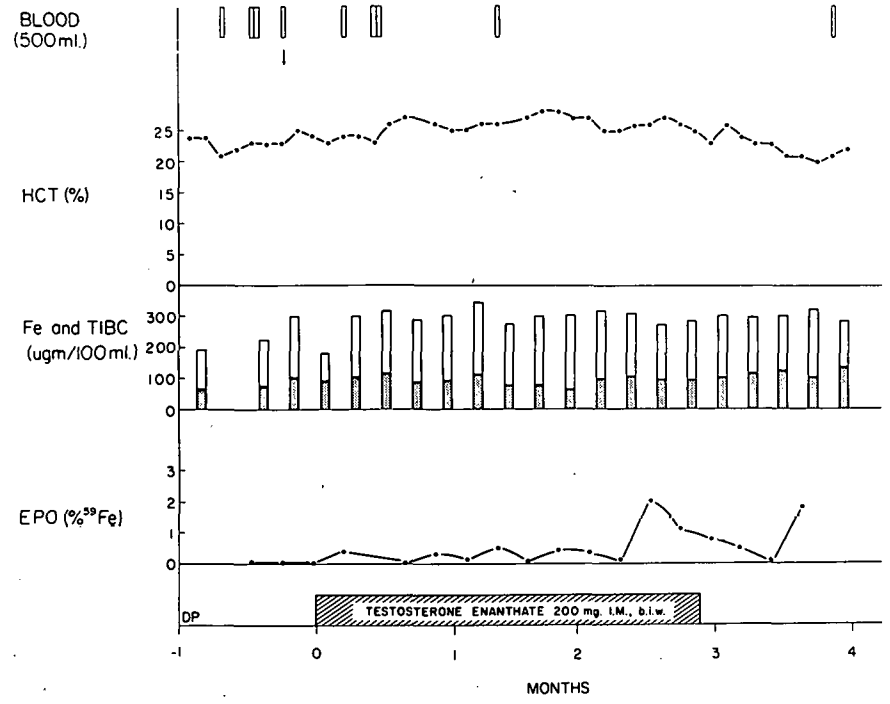

Figure 5. Chronology of the patient with damaged kidneys (D.P.) showing that plasma erythropoietin increased during the increase in hematocrit. Discontinuation of the testosterone resulted in a diminished hematocrit suggesting that testosterone had induced higher levels of erythropoietin and an increase in hematocrit.

Naets was unable to demonstrate activity until his patient's hematocrit had fallen to 14 per cent immediately after a hemorrhage.[6] Our studies suggest that anemia (and/or testosterone administration) raised erythropoietin levels and thereby induced an accelerated erythropoiesis. These observations are consistent with those reported by Nathan,[4] Naets,[6] Eschbach,[2] and Mirand[7] and their coworkers, but not with those of Erslev et al.[5] Although fewer blood transfusions were given to the patient with kidneys, the hematocrit increased, reflecting enhanced erythropoiesis. The fact that the hematocrit and erythropoietin levels diminished when therapy with testosterone was discontinued further supports the idea that the androgen was responsible for the increases in these values which accompanied its administration.

The hematocrits of both patients were equal at the beginning of the investigation. Measurements of the marrow normoblasts, serum iron and transferrin concentrations, erythrocytes ^{59}Fe utilization, linear profile scanning, and transfusion requirements gave evidence that the rate of erythropoiesis in the patient with kidneys exceeded the rate in the anephric patient. As blood transfusions were withheld, the hematocrit of the patient with kidneys increased, while that of the anephric patient diminished. We presume that the decrease in serum iron in the latter was secondary to the augmented iron utilization that accompanies accelerated erythropoiesis.

The mechanism by which androgens enhance erythropoiesis is still not completely understood. Since high levels of erythropoietin were already present in patients with aplastic anemia who are known to respond, some believed that androgens directly stimulated the bone marrow.[21]

In vitro studies testing the effects of testosterone[22] or androgenic metabolites[23] on mammalian bone marrow cultures support that thesis. However, doubling the dose of testosterone in our anephric patient did not increase his hematocrit, as might have been expected if the androgen was highly stimulatory to the marrow. The possible effects of androgen on protein synthesis, and particularly, on transferrin in such patients deserve further study.

Fried and Gurney,[10] Mirand et al,[11] and Alexanian et al,[12] have demonstrated that rodents and human beings treated with testosterone develop increased levels of erythropoietin. Mirand's studies in nephrectomized patients suggest that renal tissue need not be present,[13] and our studies agree with his in that both of our patients developed increased levels of erythropoietin and erythropoiesis while receiving testosterone. Fried and Kilbridge's recent studies in nephrectomized rats showed an effect with cobalt and anemia, but not with testosterone.[14] Rats and man, however, may respond differently to nephrectomy. The presence of erythropoietically active plasma in nephrectomized patients raises the interesting consideration that the "renal erythropoietic factor (REF)"[24] might be produced in an extrarenal site.

There is a pressing need for an agent that will induce erythropoiesis and obviate the need for blood transfusions which carry with them the risks of hepatitis[3] and hemosiderosis,[2] and the costs of blood and hospitalizations. Such an agent would help to provide effective programs of hemodialysis for many patients who are awaiting or are ineligible for renal transplantation. Further studies with analogs or metabolites of androgens should be carried out, because some anabolic steroids have a greater erythropoietic effect than others.[25] In the light of our studies and those of Mirand and coworkers,[13] clinical trials of testosterone or its analogs are needed to provide evidence for the usefulness of such a regimen in the therapy of anemia in the renoprival patient.

ACKNOWLEDGMENTS

We wish to thank Mrs. Claudette Perry, Miss Vi Stark, Miss Terry Gogol, and Mr. Walter Shipley for their valuable technical assistance.

LITERATURE CITED

1. Gurney, C. W., E. Goldwasser, and C. Pan. J. Lab. Clin. Med., 50:534, 1957.
2. Eschbach, J. W., D. Funk, J. Adamson, I. Kuhn, B. H. Scribner, and C. A. Finch. New Eng. J. Med., 276, 653, 1967.
3. Friedman, E. A., and G. E. Thomson. Lancet, 2:675, 1966.
4. Nathan, D. G., E. Schupak, F. Stohlman, Jr., and J. P. Merrill. J. Clin. Invest., 43:2158, 1964.
5. Erslev, A. J., P. J. McKenna, J. P. Capelli, R. J. Hamburger, H. E. Cohn, and J. E. Clark. Arch. Intern. Med. (Chicago), 122:230, 1968.
6. Naets, J. P., and M. Wittek. Lancet, 1:941, 1968.
7. Mirand, E. A., and G. P. Murphy. JAMA, 209:392, 1969.
8. Fried, W., R. L. DeGowin, and C. W. Gurney. Proc. Soc. Exptl. Biol. Med., 117:839, 1964.
9. Kennedy, B. J., and A. S. Gilbertsen. New Eng. J. Med., 256:719, 1957.
10. Fried, W., and C. W. Gurney. Nature, 206:1160, 1965.

11. Mirand, E. A., A. S. Gordon, and J. Wenig. Nature, 206:270, 1965.

12. Alexanian, R., W. K. Vaughn, and M. W. Ruchelman. J. Lab. Clin. Med., 70:777, 1967.

13. Mirand, E. A., G. P. Murphy, R. A. Steeves, J. M. Groenewald, and J. N. DeKleek. J. Lab. Clin. Med., 73:121, 1969.

14. Fried, W., and T. Kilbridge. J. Lab. Clin. Med., 74:623, 1969.

15. Block, M. Illinois Med. J., 98:16, 1950.

16. DeGowin, R. L., L. B. Sorensen, D. B. Charleston, A. Gottschalk, and J. H. Greenwald. Ann. Intern. Med., 69:1213, 1968.

17. DeGowin, R. L., D. Hofstra, and C. W. Gurney. Proc. Soc. Exptl. Biol. Med., 110:48, 1962.

18. DeGowin, R. L., D. Hofstra, and C. W. Gurney. J. Lab. Clin. Med., 60:846, 1962.

19. Lavender, A. R., M. Forland, J. J. Rams, J. S. Thompson, H. P. Russe, and B. H. Spargo. JAMA, 203:265, 1968.

20. Alfrey, C. P., Jr., V. Cook, and J. P. Pittman. J. Nucl. Med., 8:859, 1967.

21. Gardner, F. H., and D. G. Nathan. New Eng. J. Med., 274:420, 1966.

22. Reisner, E. H., Jr. Blood, 27:460, 1966.

23. Necheles, T. F., and U. S. Rai. Blood, 34:380, 1969.

24. Contrera, J. F., A. S. Gordon, and A. H. Weintraub. Blood, 28:330, 1966.

25. Sanchez-Medal, L., A. Gomez-Leal, L. Duarte, and M. G. Rico. Blood, 28:283, 1969.

SPLENIC HEMORRHAGE IN A HEMOPHILIAC: DIAGNOSIS OF OCCULT RUPTURE, PREOPERATIVE EVALUATION, AND POST OPERATIVE SUPPORT*

By

J. M. Baron, H. S. Kingdon, G. E. Block,† A. Gottschalk

In the past, severe spontaneous or surgically induced hemorrhages in hemophiliacs have resulted in death due to the inability of the physician to administer to the patient enough Factor VIII (Antihemophilic Factor) to control hemorrhage without overloading the vascular system with excessive plasma.[1] This difficulty has been overcome in recent years by the use of Factor VIII concentrates. These materials can normalize blood clotting sufficiently to permit the performance of even major operations in the hemophiliac with little more than normal risk.[2] This report describes how the use of Factor VIII concentrates protected against serious bleeding during splenectomy in a severe hemophiliac.

The value of serial spleen scanning in documenting the presence of splenomegaly and detecting the appearance of the splenic hematoma is emphasized.

CASE REPORT

H.S., a 17-year-old white male college student, was admitted to Argonne Cancer Research Hospital in February 1968 complaining of pain of four days' duration in the left upper quadrant of the abdomen. Previous studies had established the diagnosis of Hemophilia A, on the basis of pretreatment plasma levels of Factor VIII of less than 1 per cent of normal and plasma Factor IX levels of 100 per cent of normal.

Five days prior to admission, the patient had imbibed a substantial quantity of alcohol and had vomited five times. The following morning he awoke with severe pain in the left upper quadrant of the abdomen and left shoulder. Splenic pathology was suspected, but, because his blood counts and vital signs were normal, he was treated initially with analgesics in the outpatient department. Admission was arranged when the pain became more severe.

At the time of admission, the pain was made more intense by deep breathing or by lying supine or on the left side. The patient admitted mild anorexia for one week prior to admission, but denied fever, pharyngitis, lymph gland enlargement, or known contact with infectious mononucleosis.

Physical examination revealed a small white male in no acute distress at rest. Oral temperature was 101.5 F (38.6 C). The pulse rate was 90 beats per minute and regular. Blood pressure was 140/80 mm Hg. Respiratory rate was 18 per minute. The leaves of the diaphragm were in normal position and moved well with respiratory excursions. There was marked guarding and tenderness to palpation of the left upper quadrant of the abdomen. The spleen was not palpable. Bowel sounds were present. Sequelae of multiple previous episodes of hemarthrosis included

*This report is taken from a paper that appeared in Surgical Clinics of North America, 50: 205, 1970.

†Department of Surgery, University of Chicago.

ankylosis of the left knee, marked limitation of motion of the left ankle, and a flexion deformity of the right elbow.

The hematocrit was 40 per cent, the hemoglobin was 14.0 g per cent, the leukocyte count was 8,250/cu mm, and the platelet count was 725,000/cu mm. The differential included 20 per cent atypical lymphoid cells. Serological studies revealed a non-diagnostic heterophil titer (1:48) with a significantly elevated ox cell lysin level (1:1,280). Differential ox cell lysin study revealed antibodies of the infectious mononucleosis variety in a titer of 1:1,280. The antibodies appeared to be of the convalescent type.[3] These titers failed to change significantly when repeated several times over the next forty-five days. Roentgenograph of the chest was normal. Abdominal film was abnormal because of an unusually large spleen silhouette. Initial spleen scintiphotograph after technetium 99m sulfur colloid injection[4] revealed splenomegaly without displacement or filling defect (Figure 1A). A circulating anticoagulant to Factor VIII was not present by in vitro or in vivo testing.[2]

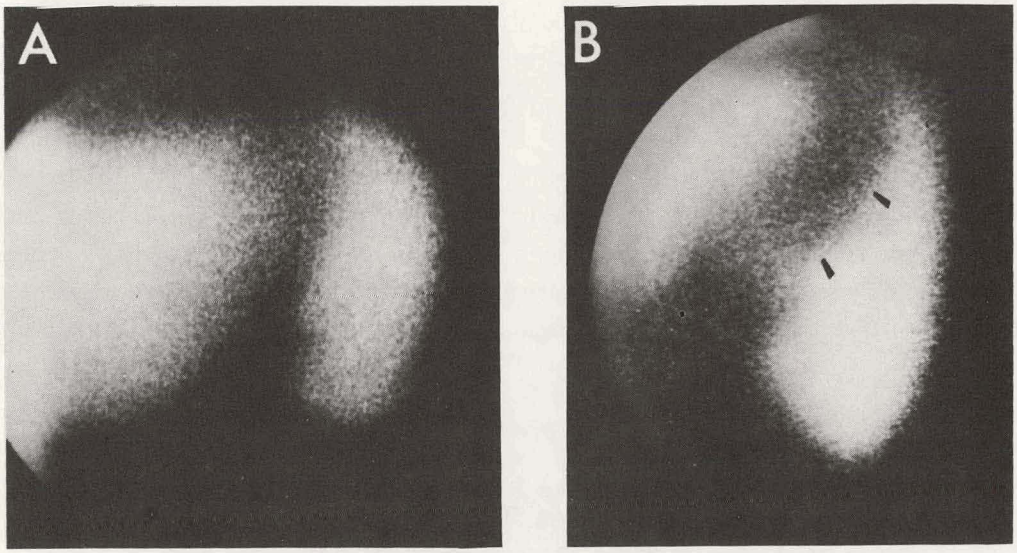

Figure 1. A – Anterior view of the spleen taken with an Anger camera 2-2-68. A dose of 6 mCi technetium 99m sulfur colloid was used as the tracer. In this study, one million counts were collected in about two minutes. Splenomegaly is evident. B – Anterior view of the spleen one week later utilizing the same technique as 1A. A large mass (arrows) is now shown in the upper medial aspect of the organ.

The patient was treated with a double pack of cryoprecipitate (prepared from 500 ml of normal plasma by the general method of Pool et al[5] as modified by the Michael Reese Hospital Blood Bank, Chicago, Illinois) twice daily on the suspicion that intrasplenic bleeding was the basis of his discomfort. The pain subsided and the platelet count returned to 200,000/cu mm by the fifth hospital day. The hematocrit had fallen slowly to 35 per cent by that time. The cryoprecipitate therapy was then discontinued because of the gratifying symptomatic improvement. However, over the next three days off Factor VIII replacement therapy, the hematocrit continued to fall to 31 per cent without evidence for external bleeding, and the pain recurred in the abdomen and left shoulder. Therapy with Factor VIII concentrate was restarted on the eighth day. Intermittent vomiting of bile-stained material occurred. A repeat spleen scintiphotograph

on the ninth day now revealed a large filling defect in the upper medial portion of the spleen which was felt to be consistent with a subcapsular hematoma (Figure 1B). A gastroduodenal examination was performed on the tenth hospital day with minimal manipulation of the patient and without compression views. Extrinsic deformity and anterior, medial, and inferior displacement of the gastric fundus were demonstrated. The perirenal and psoas margins on the left were preserved. The therapy with Factor VIII was intensified (see below), and two units of whole blood were given in preparation for laparotomy on the eleventh hospital day.

At the operation the peritoneal cavity contained approximately 50 cc of unclotted blood. The spleen was markedly enlarged and a large hematoma covered its upper portion and obliterated the gastrolienal ligament. The spleen and the hematoma were delivered into the wound, and the peritoneal attachments of the spleen were divided. The splenic pedicle was manually compressed during the delivery of the spleen and then was serially clamped and divided and ligated with stout nonabsorbable suture material. The peritoneal cavity was irrigated with saline and all bleeding points were carefully oversewn with nonabsorbable suture material. There was no free bleeding at the time of closure. The incision was closed with interrupted monofilament stainless steel wire sutures, and the skin and subcutaneous tissues were closed primarily. Blood loss at the time of operation was negligible.

The spleen plus hematoma weighed 965 g. The firm hematoma at the hilum measured 10 x 10 x 6 cm (Figure 2) and correlated well in position and contour with the defect seen on the second splenic scan (Figure 1B). Histologic sections showed a thin but intact capsule with adjacent hematoma and infiltrating hemorrhage in the hilum. The margins of the hematoma were noted to be undergoing organization, with ingrowth of fibroblasts and capillaries. Close examination of the trabecular arteries and veins showed partial periarteriolar and subendothe-

Figure 2. Resected spleen with hematoma in the location of the mass demonstrated in Figure 1B.

lial infiltration with atypical lymphocytic cells. This finding was felt to be compatible with the diagnosis of infectious mononucleosis.[6]

During the day prior to operation and for the seven days following, the patient received 8 vials (1600-2000 units) of Factor VIII concentrate (Hyland Laboratories, glycine precipitate, "method II") given intravenously after reconstitution every eight hours. This large dosage was sufficient to raise the Factor VIII level above 100 per cent of normal, and, on occasion, the Factor VIII level was still as high as 98 per cent of normal just before the next dose. The Factor VIII level was usually between 40 per cent and 75 per cent of normal before the next dose. Four double packs of cryoprecipitate could be substituted for the eight vials of glycine precipitate without obvious change in the clinical or laboratory results. During this period of intensive treatment with concentrates the plasma fibrinogen level was consistently in excess of 2 g/100 cc.

After the first postoperative week, the Factor VIII dose was reduced to 6 vials every eight hours, but was raised again two days later to 8 vials every eight hours because of mild intermittent epistaxis. The epistaxis continued despite this continued high dosage level. Two and one-half weeks after surgery the Factor VIII therapy was tapered over a four day period and discontinued. The epistaxis ceased soon thereafter.

The patient made an uneventful recovery from the abdominal operation and was discharged on the 28th postoperative day. During the subsequent fifteen months he has required his usual outpatient therapy for hemathroses and intermittent hematuria. There has been no significant alteration in the severity of his bleeding disorder since splenectomy.[7] Despite the intensive therapy with Antihemophilic Factor, there has been no evidence for the appearance of a circulating anticoagulant to Factor VIII, or abnormal liver function studies suggestive of hepatitis.[2]

COMMENT

This is a report of a patient with Hemophilia A who developed a large intrasplenic hematoma following repeated vomiting. Splenic hemorrhage with rupture has necessitated splenectomy in four previously reported patients with documented Hemophilia A.[1,8-10] This is in contrast to earlier teaching which emphasized the known occurrence of splenic rupture in Hemophilia B (Christmas Disease), but not in Hemophilia A.[11] It is interesting to note that in two of these patients,[1,10] as in ours, significant vomiting was apparently the only precipitating event for rupture. Although one of the earlier cases was reported to have clinical and presumably serological evidence for glandular fever (infectious mononucleosis),[9] there was no evidence in any of the previous cases for underlying abnormalities of the spleen which might have made it more susceptible to injury.

The pathological findings of splenomegaly, capsular thinning, and perivascular infiltration of the trabecular vessels by atypical lymphocytes, in association with atypical lymphocytes in the peripheral blood and an elevated ox cell lysin titer suggested to us that involvement of the spleen by infectious mononucleosis might have been an important factor predisposing to rupture in the present case.[6] Although the changes in blood and spleen are consistent with acute infectious mononucleosis, the pattern of unchanging heterophil and ox cell titers is more compatible with the convalescent phase of this disorder. It has been observed that rupture of the spleen as a life-threatening complication of infectious mononucleosis in the patient without coagulation defect is most likely to occur during the third or fourth week of the illness.[6,12] We see no reason to exclude this mechanism of increased splenic susceptibility to injury during the convales-

cent phase as defined by the serologic titers if the histology still documents the presence of the characteristic cellular infiltration in the spleen. Furthermore, one might expect the patient with uncorrected Hemophilia A who develops infectious mononucleosis to have more extensive bleeding difficulty from minor trauma to the enlarged spleen at whatever phase of the illness it occurs.

Although the clinical findings led us to suspect intrasplenic hemorrhage and perhaps slow leakage of blood from a small site of rupture of the splenic capsule, we were reluctant to embark on a major operation in this hemophiliac patient without an accurate preoperative diagnosis. The results of spleen scanning were crucial in establishing the proper preoperative diagnosis and in convincing us to proceed with splenectomy. The excellent correlation between the location of the lesion demonstrated with scintiphotography (Figure 1B) and the hematoma in the surgical specimen (Figure 2) is worthy of reemphasis. The resolving power of the scanning technique when applied to abdominal organs is such that a much smaller lesion, even one of 2 to 3 cm in diameter, could have been detected.[4]

With the advent of Factor VIII concentrates for replacement therapy,[5] necessary dental[13] and other major operations such as appendectomy,[14] splenectomy,[10] and craniotomy for evacuation of post-traumatic subdural hematoma[15] can now be accomplished safely in patients with Hemophilia A. Despite the availability of adequate amounts of concentrates and these gratifying results, mention should be made of two uncommon special clinical situations in which surgery in the hemophiliac is more risky than in the normal patient. One of these is the presence of an acquired circulating anticoagulant to Factor VIII[2,16] which neutralizes the effects of infused concentrates. The other special problem is the development by the untreated patient of extensive organized hematomas, so-called pseudo tumors,[2,17] in the retroperitoneal space or in skeletal muscle masses. These hematomas may have a tendency to enlarge despite adequate replacement therapy as judged by the patient's Factor VIII level. Attempts at surgical drainage of such lesions may only lead to more extensive bleeding. The recent report of more highly concentrated glycine precipitated Factor VIII[18] holds out hope for successful management of even these two difficult problems in hemophilia therapy.

The general principles of Factor VIII replacement therapy are outlined at length by Shulman et al.[2] As indicated in their discussion, smaller doses of Factor VIII concentrate than used in our patient would presumably have been as effective in preventing bleeding complications. Adequate replacement therapy with Factor VIII for at least 10 to 14 days after major surgery is of key importance in avoiding the characteristic problem of late bleeding which has its highest incidence at 6-9 days postoperatively.[9]

Elevated plasma fibrinogen levels are known to occur in patients receiving cryoprecipitated and glycine precipitated Factor VIII concentrates. No ill effects have been attributed to the infusion of fibrinogen in these preparations.[2] The occurrence of epistaxis in our patient at a time when his Factor VIII level was being kept normal, and its subsidence with cessation of the infusions suggest that the high levels of fibrinogen or other substances in the infused concentrate might have interfered with coagulation. This hypothesis has not been tested by repeated hypertransfusion with the Factor VIII concentrates in this or other patients. It is our current practice to use newer Factor VIII concentrates (Courtland Laboratories, Antihemophilic Factor (Human); Hyland Laboratories, Hemofil). Further experience will tell if similar coagulation problems occur with these newer preparations.

In conclusion, major surgery can be undertaken for the same indications in the hemophiliac as in the normal patient, provided that the patient's Factor VIII level can be restored to normal with concentrated replacement materials, and that sufficient amounts of concentrate are available for the necessary duration of protective treatment.

LITERATURE CITED

1. Brook, J., and P. E. Newman. Arch. Int. Med., 115:595, 1965.
2. Shulman, N. R., D. H. Cowan, E. P. Libre, S. P. Watkins, Jr., and V. J. Marger. Ann. Int. Med., 67:856, 1967.
3. Ormiste, V. Personal communication.
4. Gottschalk, A. J. Am. Med. Assoc., 200:630, 1967.
5. Pool, J. G., and A. E. Shannon. New Eng. J. Med., 273:1443, 1965.
6. Smith, E. D., and R. P. Custer. Blood, 1:317, 1946.
7. Gross, J. D., R. C. Hartmann, J. B. Graham, and C. B. Taylor. Bull. Johns Hopkins Hosp., 100:223, 1957.
8. Pitney, W. R. Med. J. Austr., 46:65, 1959.
9. Smith, P. H. Brit. Med. J., 1:296, 1965.
10. Gowda, W., T. Vietti, and J. L. Ternberg. Surgery, 64:1119, 1968.
11. Ratnoff, O. D. Adv. Int. Med., 9:107, 1958.
12. Hoagland, R. J., and H. M. Henson. Ann. Int. Med., 46:1184, 1957.
13. Rayne, J. J. Oral Surg., 26:381, 1968.
14. Schwartz, J. M., B. D. Cohn, N. D. Ritz, and T. Levy. J. Am. Med. Assoc., 198:1175, 1966.
15. Moody, R. A., and S. Mullan. J. Neurosurg, 29:520, 1968.
16. Hougie, C. J. Lab. Clin. Med., 70:384, 1967.
17. Wessler, S., and L. A. Avioli. J. Am. Med. Assoc., 206:2292, 1968.
18. Brinkhous, K. M., E. Shanbrom, A. R. Roberts, W. P. Webster, L. Fekete, and R. H. Wagner. J. Am. Med. Assoc., 205:613, 1968.

ON THE MECHANISM OF ERYTHROPOIETIN-INDUCED DIFFERENTIATION VII. THE RELATIONSHIP BETWEEN STIMULATED DNA SYNTHESIS AND RNA SYNTHESIS*

By

M. Gross† and E. Goldwasser

When primitive cells of the hematopoietic system are exposed to erythropoietin, a series of molecular events is initiated which culminates in the formation of mature erythrocytes. In order to understand the biochemical mechanisms underlying this process of cytodifferentiation we should know the temporal order of these events and their causal relationships to each other. Our in vitro studies with adult rat marrow cells have shown that erythropoietin causes increased RNA synthesis within a few minutes of its addition to the medium.[1,2] Other effects of erythropoietin, such as stimulated iron uptake[3] and increased formation of hemoglobin[4] and of stroma,[5] occur later and are, most likely, not primary effects.

The relationship between erythropoietin action and DNA synthesis still needs to be clarified. In contrast to our earlier findings that erythropoietin had no effect on DNA synthesis in rat marrow cells,[6] Dukes showed that there was an appreciable stimulation of thymidine incorporation in the same system after about three hours of incubation.[7] Since one component of RNA synthesis is increased by fifteen minutes it would appear that, in this system, the effect on DNA synthesis is secondary to an earlier effect, perhaps on a transcriptive step. In addition, we found that inhibition of cell division by colchicine had no effect on erythropoietin-induced stroma synthesis[8] and only partially inhibited increased hemoglobin formation.[9] Paul and Hunter,[10,11] however, studying the effect of erythropoietin on fetal liver cells, found that DNA synthesis was markedly increased within the first hour of incubation, and that inhibition of DNA synthesis by FUDR‡ caused the complete abolition of increased hemoglobin synthesis. From their studies with actinomycin and puromycin these authors suggested that RNA and protein may be formed prior to, and independent of, DNA synthesis.[11] The results in the present paper confirm these suggestions and, taken with those from a previous paper by Hrinda and Goldwasser,[3] show that the action on DNA synthesis is preceded by and dependent upon the synthesis of RNA.

MATERIALS AND METHODS

Rat bone marrow cells were incubated in a medium consisting of 55 per cent NCTC 109, 40 per cent new born calf serum, and 5 per cent rat serum containing carrier iron, as described previously.[2] When FUDR was used as inhibitor, the 109 medium was replaced by a similar, thymidine-free, formulation.

Incorporation of labeled thymidine or deoxycytidine into the trichloracetic acid-insoluble fraction of the cells was used to evaluate DNA synthesis, and incorporation of uridine into the same fraction to measure RNA synthesis. The use of these simplified techniques was justified

*This report is taken from a paper that appeared in J. Biol. Chem., 245:1632, 1970 and forms part of the Ph.D. thesis of Martin Gross, University of Chicago 1969.

†Life Insurance Medical Research Fund Fellow.

‡The abbreviation used is: FUDR, 5-fluorodeoxyuridine.

by our findings that hydroxyurea caused complete inhibition of incorporation of deoxycytidine but not of uridine. Sample preparation and counting of ^{3}H and ^{14}C were described in an earlier paper.[2]

The erythropoietin-induced uptake of iron by marrow cells was measured by counting the washed cell pellet after the cells were incubated in the presence of ^{59}Fe-labeled rat serum, the transferrin of which was 75-100 per cent saturated with iron. Heme was prepared from cell lysates by the method of Fox and Thomson.[12] Since we had previously shown that virtually all of the labeled heme found in cultured marrow cells was in the form of hemoglobin,[13] the heme radioactivity was taken as a measure of hemoglobin synthesis.

NCTC 109 was bought from Microbiological Associates; thymidine-free NCTC 109 from Grand Island Biological; disposable culture dishes from Falcon Plastics; ^{3}H-5-deoxycytidine (0.5 Ci/mmole), ^{3}H-methyl-thymidine (15 Ci/mmole) and ^{3}H-5-uridine (28.3 Ci/mmole) from Nuclear Chicago; ^{14}C-2-uridine (51.5 mCi/mmole) and $^{59}FeCl_3$ (95 mCi/mmole) from New England Nuclear. Cycloheximide was a gift from Upjohn Pharmaceutical Corporation; FUDR was a gift from the Cancer Chemotherapy National Service Center of the National Cancer Institute; puromycin and hydroxyurea were bought from Nutritional Biochemicals Corporation, colchicine from Eli Lilly, and actinomycin D from Merck, Sharp and Dohm. Erythropoietin (Step IV) was a gift from the National Blood Resource Program, National Heart Institute, National Institutes of Health. Its potency was 19 units per mg of protein and it is extremely impure. Similar results, however, are obtained when fractions with much higher potency are used.

RESULTS

Figure 1 demonstrates the effects of FUDR and colchicine on erythropoietin-stimulated DNA synthesis. Both sets of controls (in complete and in thymidine-free medium) show an erythropoietin-induced increase in rate of DNA synthesis up to nine hours, and a sharp decrease thereafter. FUDR caused a complete inhibition of increased DNA synthesis at all three pulse times; colchicine had no effect at the earliest time, but caused progressive inhibition at the later times. These inhibitors also caused appreciable decreases in the rate of thymidine incorporation in cells not treated with erythropoietin. Cells exposed to FUDR showed a 50-65 per cent inhibition at all three pulse times. Colchicine caused a 25 per cent decrease at the two earlier intervals and a 70 per cent decrease at fifteen hours. Similar experiments showed that hydroxyurea (10^{-3} M) also completely inhibited the synthesis of DNA in response to erythropoietin when measured at 3 and 11 hours.

We have already shown that increased RNA synthesis caused by erythropoietin is not due to an effect on the specific activity of the precursor pool;[2] this is also true for the incorporation of deoxycytidine into DNA. When the pool was pre-labeled by incubation with ^{3}H-deoxycytidine for one hour and the external label removed, subsequent incubation in the presence of erythropoietin caused a small but significant increase in the DNA radioactivity, when compared with cells having the same labeled pool but no erythropoietin.

The effects of FUDR, hydroxyurea, and colchicine on erythropoietin-stimulated hemoglobin synthesis and iron uptake were determined in cultures that had been incubated for either 27 or 51 hours, the last 6 hours with ^{59}Fe (Table 1). At the later time both FUDR and hydroxyurea caused complete inhibition of stimulated hemoglobin synthesis and almost complete inhibition of stimulated iron-uptake; the effect of colchicine was slightly less. At the earlier time the in-

Table 1

EFFECTS OF INHIBITORS ON STIMULATED IRON-UPTAKE AND HEMOGLOBIN SYNTHESIS

Cultures in quadruplicate contained 15 x 10^6 nucleated rat bone marrow cells in 1.0 ml of medium. The medium for group A contained thymidine-free NCTC 109. Additions of FUDR (10^{-4} M), hydroxyurea (10^{-3} M) and colchicine (10^{-7} M) were at zero time and erythropoietin (0.10 unit/ml) at 10 minutes. One μCi of ^{59}Fe in 0.05 ml of rat serum was added at 21 or at 45 hours and the cultures were stopped at 27 or 51 hours.

		21 - 27 hours				45 - 51 hours			
		Iron-uptake	Inhibition*	Hemoglobin synthesis	Inhibition	Iron-uptake	Inhibition	Hemoglobin synthesis	Inhibition
	Addition	cpm	%	cpm	%	cpm	%	cpm	%
A	None	6760 (±250)	-	700 (±10)	-	7570 (±30)	-	60 (±3)	-
	Erythropoietin	18130 (±370)	-	4060 (±70)	-	15280 (±150)	-	1730 (±30)	-
	FUDR	5890 (±70)	-	570 (±30)	-	1970 (±30)	-	22 (±1)	-
	Erythropoietin + FUDR	9160 (±120)	71	1140 (±20)	83	2710 (±90)	90	40 (±3)	99
B	None	7440 (±100)	-	1240 (±30)	-	13810 (±360)	-	160 (±7)	-
	Erythropoietin	18000 (±580)	-	7130 (±210)	-	16820 (±230)	-	1190 (±100)	-
	Hydroxyurea	4690 (±80)	-	620 (±30)	-	8270 (±330)	-	46 (±3)	-
	Erythropoietin + hydroxyurea	5880 (±100)	89	940 (±30)	95	8210 (±340)	100	41 (±1)	100
	Colchicine	4420 (±150)	-	710 (±40)	-	650 (±20)	-	19 (±1)	-
	Erythropoietin + colchicine	8680 (±200)	60	2310 (±120)	73	1080 (±20)	86	97 (±5)	92

*Inhibitions expressed are those of the erythropoietin effect. Figures in parentheses are standard deviation of the mean.

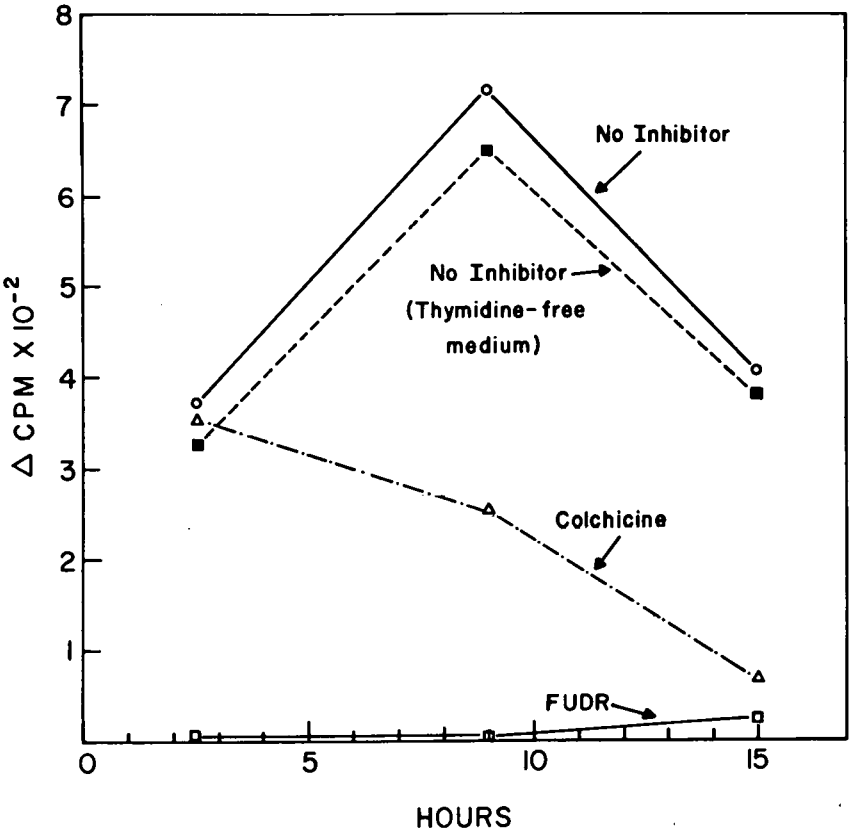

Figure 1. Effects of FUDR and colchicine on erythropoietin-stimulated DNA synthesis. Cultures in quadruplicate contained 15 x 10^6 nucleated rat bone marrow cells in 1.0 ml of medium. Additions of FUDR (10^{-4} M), colchicine (10^{-7} M) were made at zero time and erythropoietin (0.06 units per ml) 10 minutes later. Cultures were pulsed for 2 hours with 1 μCi of ^{3}H-deoxycytidine at indicated times (middle of pulse). Control values were as follows: For the normal medium, 2100, 1190 and 560 cpm at 2.5, 9, and 15 hours respectively. In the thymidine-free medium, the corresponding values were 1680, 1070, and 500 cpm.

inhibition caused by all three inhibitors was somewhat smaller. Stimulation of hemoglobin synthesis was more sensitive to all three inhibitors than was stimulation of iron-uptake. In this experiment, as in the one described in Figure 1, the inhibitors showed a smaller effect on the control than on the stimulated cells.

When the incubation time was shortened to 4 hours (Table 2) the effects of the inhibitors on the same stimulated functions were quite different. Hydroxyurea caused an inhibition of about 50 per cent with respect to both stimulated iron uptake and hemoglobin synthesis; FUDR and colchicine had only a slight inhibitory effect on either of them. It is clear from Figure 1 that FUDR at this time caused complete inhibition of erythropoietin-stimulated DNA synthesis. Although the effects of erythropoietin so early in the culture are small, they are significant. The salient point is that early in the incubation period cells do not require stimulated DNA synthesis or cell division in order to express short term erythropoietin-stimulated iron uptake or hemoglobin synthesis.

Table 2

EFFECTS OF INHIBITORS ON EARLY ERYTHROPOIETIN STIMULATED IRON-UPTAKE AND HEMOGLOBIN SYNTHESIS

Conditions were as in Table 1 except that labeling period was from 0 - 4 hours after which cultures were stopped. Cultures in group B had 0.07 units of erythropoietin per ml.

	Addition	Iron-uptake	Inhibition of erythropoietin effect	Hemoglobin synthesis	Inhibition of erythropoietin effect
		cpm	%	cpm	%
A	None	7470 (±130)	-	1790 (±130)	-
	Erythropoietin	8940 (±290)	-	2310 (±130)	-
	FUDR	7840 (±100)	-	2100 (±20)	-
	Erythropoietin + FUDR	9150 (±150)	11	2590 (±30)	6
B	None	2180 (±60)	-	840 (±10)	-
	Erythropoietin	2600 (±70)	-	1040 (±40)	-
	Hydroxyurea	1910 (±30)	-	670 (±20)	-
	Erythropoietin + hydroxyurea	2110 (±20)	52	760 (±20)	55
	None	2140 (±50)	-	560 (±20)	-
	Erythropoietin	2380 (±80)	-	650 (±20)	-
	Colchicine	2180 (±40)	-	510 (±20)	-
	Colchicine + erythropoietin	2400 (±20)	8	660 (±30)	0

We also determined the effects of these inhibitors on erythropoietin-induced RNA synthesis (Table 3). Hydroxyurea and FUDR had essentially no effect on stimulated uridine incorporation either at 2.5 or 9 hours while colchicine had an inhibitory effect only at the later time. Hydroxyurea caused about 40 per cent inhibition of RNA synthesis in the control (nonstimulated) cells at 2.5 hours and almost 70 per cent inhibition at 9 hours. If FUDR had any significant effect on the control cells it was not inhibitory. Colchicine had no appreciable effect on controls at 2.5 hours but did cause 36 per cent inhibition of RNA synthesis at 9 hours. Despite the effects of the inhibitors on the unstimulated cells, it is clear from these data that the expression of erythropoietin action with respect to RNA formation even as late as nine hours does not require DNA synthesis. Essentially the same results were obtained in a similar experiment using ^{3}H-uridine and pulsing for 15 minutes after 4 hours of incubation. There was no effect of FUDR or colchicine and 26 per cent inhibition of the erythropoietin effect by hydroxyurea.

In a reciprocal type of experiment using inhibitors of RNA or protein synthesis (Table 4), we could show clearly that erythropoietin-induced DNA synthesis had an absolute requirement for RNA and protein formation. Under the same conditions, the control cells showed similar responses to three inhibitors; i.e., 86-90 per cent inhibition of deoxycytidine incorporation.

Table 3

EFFECTS OF INHIBITORS ON STIMULATED RNA SYNTHESIS

Conditions were as in Table 1 except that cultures contained 0.07 units of erythropoietin per ml and were pulsed for 2 hours with 0.50 μCi/ml of ^{14}C-uridine. The times indicated (2.5 hours and 9 hours) are the midpoints of the pulse.

	Addition	2.5 hours	Inhibition of erythropoietin effect	9 hours	Inhibition
		cpm	%	cpm	%
A	None	1320 (±40)	-	1070 (±20)	-
	Erythropoietin	1500 (±30)	-	1330 (±100)	-
	FUDR	1410 (±30)	-	1120 (±30)	-
	Erythropoietin + FUDR	1580 (±30)	6	1390 (±100)	0
B	None	560 (±40)	-	660 (±40)	-
	Erythropoietin	700 (±30)	-	830 (±50)	-
	Hydroxyurea	330 (±15)	-	210 (±10)	-
	Hydroxyurea + erythropoietin	480 (±15)	0	370 (±10)	6
	None	1630 (±40)	-	1440 (±60)	-
	Erythropoietin	1900 (±100)	-	1670 (±40)	-
	Colchicine	1570 (±80)	-	920 (±40)	-
	Erythropoietin + colchicine	1830 (±50)	4	1070 (±40)	35

Table 4

EFFECTS OF INHIBITORS ON STIMULATED DNA SYNTHESIS

Cultures in quadruplicate contained 15 x 10^6 nucleated rat marrow cells in 1.0 ml of medium. The inhibitors were added at zero time and 0.05 units of erythropoietin 10 minutes later. At 5.25 hours 1 μCi/ml of ^{3}H-deoxycytidine was added, and cultures were stopped at 6.75 hours.

Addition	Control	Erythropoietin	Inhibition of erythropoietin effect
	cpm	cpm	%
None	2580 (±200)	4150 (±440)	-
Actinomycin D (8 μg/ml)	350 (±10)	310 (±40)	100
Puromycin (100 μg/ml)	270 (±20)	320 (±40)	99
Cycloheximide (100 μg/ml)	270 (±30)	310 (±20)	99

In a similar experiment at an earlier time (Table 5), using a 40-minute pulse of ^{3}H-thymidine at 2 hours of incubation, we again found complete inhibition of erythropoietin-induced DNA synthesis by cycloheximide, puromycin and actinomycin D.

Table 5

EFFECTS OF INHIBITORS OF EARLY STIMULATED DNA SYNTHESIS

Cultures in quadruplicate contained 25 x 10^6 nucleated rat bone marrow cells in 1.0 ml of medium. Inhibitors were added at zero time and erythropoietin (0.10 units/ml) at 10 minutes. At 1 hour and 40 minutes, 5 μCi/ml of ^{3}H-thymidine was added, and cultures were stopped 40 minutes later.

Addition	Control	Erythropoietin	Inhibition of erythropoietin effect
	cpm	cpm	%
None	19340 (±770)	21890 (±360)	-
Actinomycin D (8 μg/ml)	3120 (±50)	2900 (±70)	100
Puromycin (100 μg/ml)	1380 (±110)	1400 (±80)	99
Cycloheximide (100 μg/ml)	1900 (±30)	1900 (±50)	100

DISCUSSION

Erythropoietin initiates the process by which some unidentified precursor cells develop into mature erythrocytes. The most striking changes occurring during this developmental process, such as synthesis of massive amounts of hemoglobin, loss of nuclear function and, in mammals, loss of the nucleus, are not the immediate consequences of the induction of erythropoiesis. In order to determine the molecular locus of the primary inductive step and the sequence of biochemical events leading to the conversion of primitive cells to red cells we may study changes in function with time or use inhibitors with known specificities.

In previous papers we reported on the time course of erythropoietin stimulation of RNA synthesis.[1,2] Since the earliest change that we have seen in adult marrow cells exposed to erythropoietin is an increase, at 10 to 15 minutes, in synthesis of a very large (150S) nuclear RNA[2] and since both DNA synthesis and protein synthesis are affected only at a later time we have suggested that the primary action of erythropoietin may be on a transcriptive step.

In this paper we have shown by use of FUDR and hydroxyurea that stimulated total RNA synthesis is independent of DNA synthesis for at least the first ten hours of incubation. This is in marked contrast to the observations of Paul and Hunter[11] who found that stimulated RNA synthesis by fetal liver cells was completely inhibited by FUDR. We have no explanation for this difference at present, except to suggest that adult bone marrow cells may be less dependent than fetal liver cells on DNA replication for the expression of erythropoietin action.

The data of Paul and Hunter show an increase in DNA synthesis by fetal liver cells exposed to erythropoietin considerably earlier than we have found to be the case for adult marrow cells[6] (one hour versus three hours). They did not find as rapid an effect on RNA synthesis as we have reported, the earliest effect in fetal liver being seen at about two hours. These differences between the two systems are, in reality not very great. Our studies of stimulation of total RNA synthesis by marrow cells gave results similar to those of Paul and Hunter. Only when the RNA was fractionated on a sucrose gradient did we see the very rapid effect which was confined to the small amount of large-sized RNA.

The effect of erythropoietin on marrow cell DNA synthesis, like that in fetal liver cells, is

abolished by actinomycin D, puromycin, and cycloheximide: In both cases it is clear that erythropoietin acts on RNA and protein synthesis prior to any increase in DNA synthesis.

Ortega and Dukes[14] have shown that inhibition of marrow cell DNA synthesis by cytosine arabinoside has no effect on erythropoietin-stimulated incorporation of glucosamine into the acid-insoluble fraction. The data in Table 2 show that inhibition of DNA synthesis did not affect erythropoietin-stimulated iron uptake or hemoglobin synthesis when measured at four hours although when measurements were made later (Table 1) there was complete inhibition. At present there is no completely satisfactory explanation for these differences. We can suggest that the early erythropoietin effect on hemoglobin synthesis may represent action on cells that are already differentiated to some extent, and may be independent of DNA synthesis. The effect on hemoglobin synthesis at later times may be the result of erythropoietin action on more primitive cells, and their subsequent development may be dependent on DNA synthesis. Experiments testing the effect of erythropoietin on recognizably differentiated cells are in progress.

There are several possible relationships between induced differentiation and stimulated DNA synthesis. Cells that have been committed to the red cell pathway must still undergo 3 or 4 divisions before reaching the mature, non-dividing differentiated stage. If these amplification divisions are inhibited, the induced cells, if they go on to differentiate, may form only 10-15 per cent of the normal amount of hemoglobin. Alternatively, these cells may not manifest any of the characteristic erythroid functions, but they still synthesize a full complement of RNA after erythropoietin has acted. We have found that much of the RNA made by marrow cells after exposure to erythropoietin is retained in the nucleus for at least 3 hours.* It may be that DNA replication and/or mitosis is required for the transfer of some fraction of the newly formed RNA to the cytoplasm where the specific phenotypic functions can be expressed. This latter possibility is essentially the superposition of control of nucleus-to-cytoplasm flow on translational control.

In addition to these possibilities a second type of stimulated DNA synthesis may be considered to be secondary to the inductive step. If erythropoietin acts on a cell that is in equilibrium with a pool of stem cells, induction of differentiation would result in a deficit in that pool which would be made good by increased division of the remaining stem cells. Inhibition of this type of DNA synthesis would be expected to have no direct effect on erythropoietin action until the supply of inducible cells became exhausted. If only a small fraction of the cells was inducible, and if generation of such cells depended on division of stem cells, then inhibition of DNA synthesis would apparently exert a direct effect on erythropoietin action. At present, study of these problems is greatly impeded by our being able to work only with heterogeneous cell populations. When homogeneous populations of stem cells (or erythropoietin-responsive cells if they are different) become available for study we shall be able to resolve some of these difficulties.

LITERATURE CITED

1. Krantz, S. B., and E. Goldwasser. Biochim. Biophys. Acta, 103:325, 1965.
2. Gross, M., and E. Goldwasser. Biochemistry, 8:1795, 1969.
3. Hrinda, M. E., and E. Goldwasser. Biochim. Biophys. Acta, 195:165, 1969.

*Gross, M., and E. Goldwasser, unpublished observations.

4. Krantz, S. B., O. Gallien-Lartigue, and E. Goldwasser. J. Biol. Chem., 238:4085, 1963.

5. Dukes, P. P., F. Takaku, and E. Goldwasser. Endocrinology, 74:960, 1964.

6. Goldwasser, E. In Current Topics in Developmental Biology, Vol. 1, A. Monroy and A. A. Moscona, Eds. New York: Academic Press, 1969, p. 173.

7. Dukes, P. P. Ann. N. Y. Acad. Sci., 149:437, 1968.

8. Dukes, P. P., and E. Goldwasser. Biochim. Biophys. Acta, 108:447, 1965.

9. Gallien-Lartigue, O., and E. Goldwasser. Biochim. Biophys. Acta, 103:319, 1965.

10. Paul, J., and J. Hunter. Nature, 219:1362, 1968.

11. Paul, J., and J. Hunter. J. Mol. Biol., 42:31, 1969.

12. Fox, J. B., and J. S. Thomson. Biochemistry, 3:1323, 1964.

13. Gallien-Lartigue, O., and E. Goldwasser. Science, 145:277, 1964.

14. Ortega, J. A., and P. P. Dukes. Fed. Proc., 28:600, 1969.

MECHANISM OF EXCESSIVE PURINE BIOSYNTHESIS IN HYPOXANTHINE-GUANINE PHOSPHORIBOSYLTRANSFERASE DEFICIENCY*

By

L. B. Sorensen

A substantial proportion of patients with primary gout have a metabolic defect characterized by overproduction of uric acid which is the result of an excessive rate of de novo purine biosynthesis.[1,2] Recently it has been shown that a deficiency of the enzyme hypoxanthine-guanine phosphoribosyltransferase (HG-PRTase) exists in some, though probably in a minority, of these patients.[3,4] A virtually complete deficiency of this enzyme[3] has been demonstrated in children with an X-linked neurological disorder associated with overproduction of uric acid first described by Lesch and Nyhan.[5] In addition, a partial deficiency of HG-PRTase[4] has been observed in hyperuricemic subjects presenting with uric acid lithiasis, monoarticular arthritis, or, rarely, in cases associated with a very low enzyme activity, neurologic dysfunction. HG-PRTase activity was the same in affected members of the same family, but differed from family to family, suggesting that the gouty population with this enzyme deficiency comprises a heterogeneous group of genetic mutations.

HG-PRTase (E.C. 2.4.2.8) converts the free purine bases, hypoxanthine and guanine, to their respective ribonucleotides by reaction with 5-phosphoribosyl-1-pyrophosphate (PRPP). HG-PRTase is presumably necessary for the normal control of purine biosynthesis, although its exact role remains undefined.

To further elucidate the mechanisms involved, I have studied the incorporation of glycine-^{14}C into hypoxanthine, xanthine, and uric acid during treatment with allopurinol (4-hydroxypyrazolo[3,4-d]-pyrimidine) in subjects with normal and deficient HG-PRTase. The data obtained provide evidence that excessive purine synthesis in HG-PRTase deficiency is related to inadequate reutilization and, hence, to increased catabolism of hypoxanthine.

MATERIALS AND METHODS

Included in this study were one normal subject; two brothers with gout characterized by the synthesis of abnormally large quantities of uric acid, but with normal HG-PRTase activity; one gouty patient with a partial deficiency of HG-PRTase; and one patient with the Lesch-Nyhan syndrome. All subjects were maintained on a purine-free diet for five days prior to as well as during the study periods.

Plasma and urinary uric acids were determined by differential spectrophotometry employing purified uricase.[6] Urines were collected at room temperature using toluene as preservative. Urinary hypoxanthine and xanthine were determined by an enzymatic spectrophotometric method.† The principle in this method is based on the conversion of hypoxanthine and xanthine to allantoin by xanthine oxidase and uricase. Since allantoin does not absorb ultraviolet light above 260 mμ,

*This report is taken from a paper that appeared in J. Clin. Invest., 49:968, 1970.

†Sorensen, L. B., F. Kawahara, and D. Chow. Enzymatic spectrophotometric determination of hypoxanthine and xanthine. In preparation.

hypoxanthine and xanthine can be accurately measured by following the decrease in optical density at the wavelengths of maximum absorption by these compounds (at pH 9.3, for hypoxanthine, A_{max} = 257.5 mμ; for xanthine, A_{max} = 280 mμ). Briefly, hypoxanthine and xanthine in urine were determined as follows: (a) 5 ml of urine was acidified to pH 2 with hydrochloric acid and passed through a 0.5 x 15 cm column of Dowex 50 x 8 50-100 mesh in the hydrogen form. (b) The column was rinsed with distilled water and the purines were eluted with 100 ml of 1 M ammonium hydroxide. (c) The eluate was flash evaporated to dryness, and the residue was dissolved in a few drops of 1 N sodium hydroxide and diluted to 25 times the original urine volume with 0.02 M 2-amino-2-methyl-1-propanol buffer at pH 9.3. (d) Four cuvettes were prepared, each containing 3 ml of the purine solution. One unit of uricase (Leo) was added to the second and third cuvettes. Xanthine oxidase was then added to each of these two cuvettes and the absorbance changes were read at 257.5 and 280 mμ, respectively. Sufficient enzyme was added to complete the reactions in 30 min. The percentages of hypoxanthine and xanthine in a mixture of these purines can be calculated from the relative decreases in optical absorption at these two wavelengths. Knowing the relative contributions of hypoxanthine and xanthine to the absorbance at 257.5 and 280 mμ, one can calculate the concentration of hypoxanthine and xanthine from the decrease in absolute absorbance of either wavelength. The sum of hypoxanthine and xanthine was determined by converting the purines in cuvette 4 to uric acid with xanthine oxidase, and measuring the uric acid formed with uricase. The values obtained by the direct and indirect methods agree to within 5 per cent.

The incorporation of glycine into hypoxanthine, xanthine, and uric acid was measured while the patients were maintained on allopurinol (Zyloprim) in doses ranging from 5.3 to 14 mg/kg per day. Glycine-1-^{14}C (SA: 25.8 mc/mmole) was injected intravenously in a dose of 1 μc/kg body weight on the fourth day of allopurinol treatment except in the case of patient A.D. who had been maintained on allopurinol for the previous six months. Urine was collected in 12-hr samples for the first three or four days and thereafter in 24-hr samples for a total of 7 days.

Urinary purines were separated by two-stage ion exchange chromatography using Dowex 50 in the hydrogen form. The method was similar in principle to those used by Weissmann et al,[7] Wyngaarden et al,[8] and Ayvazian and Skupp.[9] The first column, which utilized 8 per cent cross-linked resin of 50-100 mesh, served to isolate urinary purines. An aliquot of urine which contained approximately 25 mg of hypoxanthine plus xanthine was acidified to pH 2 with hydrochloric acid and passed through a 1.8 x 40 cm column of resin. Uric acid, allopurinol, and its oxidation product alloxanthine, were not retained on this column. The column was washed with water and eluted with 500 ml of 1 M ammonium hydroxide. The preparation of the first eluate for the second-stage ion exchange chromatography involved flash evaporation to dryness of the ammonium hydroxide eluate, solubilization of the residue in 100 ml hot water, acidification of the mixture to pH 2 with 1 N sulfuric acid, precipitation of the purines with 20 ml 1 M silver nitrate, and storage at 4° in the dark for 2 or 3 days, to effect complete precipitation. The precipitate was centrifuged and washed 3 times by suspension in 20-ml portions of water. The purines were regenerated by suspending the precipitate in 20 ml hot 0.05 M hydrochloric acid, and separated from the silver chloride precipitate by centrifugation. The silver chloride was washed twice with 10 ml of hot 0.05 M hydrochloric acid. The combined solutions were passed through a filter directly onto a second column, which served to isolate and separate the individual purines by gradient elution. This 2.5 x 30 cm column contained 90 g of 12 per cent cross-linked resin,

200-400 mesh, in the hydrogen form. The sample was washed into the column with 50 ml of water. The gradient elution system used a reservoir flask that contained 3 l of 2 M hydrochloric acid, and a mixing flask that contained 1750 ml of water. Mixing within the lower chamber was accomplished by a magnetic stirrer. The column eluate was collected in 15-ml fractions. The ultraviolet absorption of the effluent fractions was measured at 260 mμ in a Beckman DU spectrophotometer. After collection of 2.5 l of eluate, the upper flask was replaced by a flask containing 6 M hydrochloric acid. The elution pattern is shown in Figure 1. The identity of the compounds comprising the various peaks was established by comparison with the elution sequence

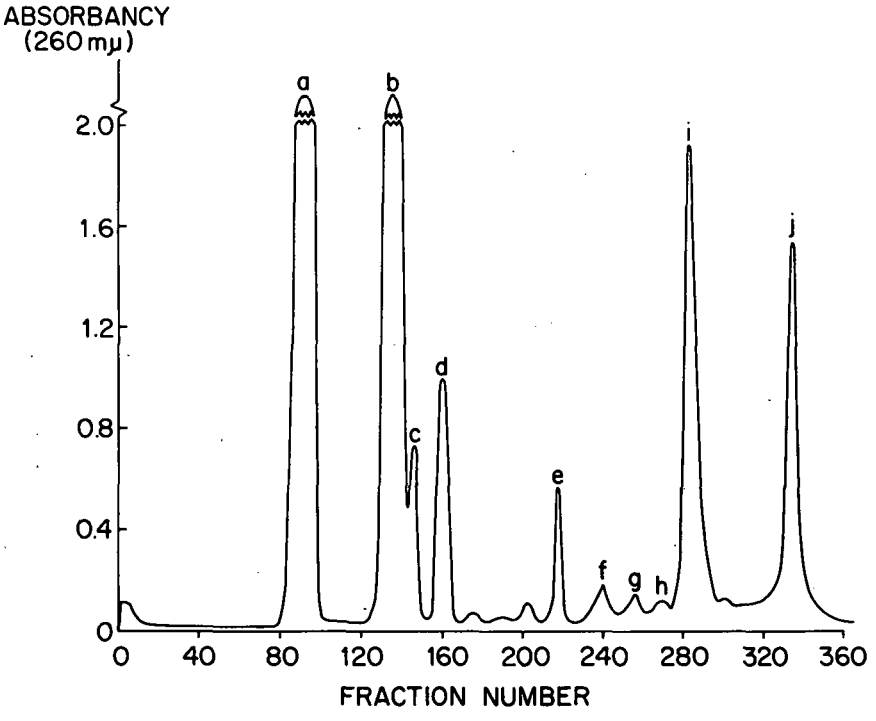

Figure 1. Elution pattern of urinary purines. (a) xanthine; (b) hypoxanthine; (c) 7-methylxanthine; (d) 1-methylxanthine; (e) 1,7-dimethylxanthine; (f) guanine; (g) N^2-methylguanine; (h) 1-methylguanine; (i) 7-methylguanine; and (j) adenine.

of known compounds, by differential spectrophotometry at pH 2 and 9, by enzyme analysis, and by migration of individual purines on paper chromatograms.[7] Despite avoidance of the major dietary sources of methylated purines, i.e., coffee, tea, and chocolate, 1-methylxanthine, 7-methylxanthine, and 1,7-dimethylxanthine were frequently present in small amounts. This finding undoubtedly reflects the widespread occurrence of methylated xanthines in plants,[7] and the fact that the subjects were receiving allopurinol, which inhibits the enzymatic oxidation of several methylated purines, including 1-methylxanthine[10] and 7-methylxanthine.*

The fractions representing the separate peaks of hypoxanthine and xanthine were pooled,

*Sorensen, L. B., F. Kawahara, and D. Chow. Enzymatic spectrophotometric determination of hypoxanthine and xanthine. In preparation.

evaporated to dryness and redissolved in 2.5 ml of dilute sodium hydroxide. Determination of the specific activity of hypoxanthine and xanthine involved measurement of the concentration of purine by enzymatic conversion to uric acid; re-evaporation to dryness of 2 ml of the samples in a desiccator (vacuum, anhydrous calcium chloride); wet combustion of the purine in a vacuum line with collection of evolved carbon dioxide in an ionization chamber;[11] and radioassay of ^{14}C in a vibrating reed electrometer. Specific activities of various purines, notably adenine and 7-methylguanine, were also measured in selected urine samples. Uric acid was isolated from urine and purified as described elsewhere.[11] Radioassay of uric acid-^{14}C was done in a vibrating reed electrometer.

Using methods that have been described previously,[11,12] uric acid pool, uric acid turnover, and incorporation of glycine-1-^{14}C into uric acid were measured in several of the patients during a control period when no drugs were given.

HG-PRTase and adenine phosphoribosyltransferase activities were determined by a radiochemical method.* The incubation mixture contained 50 mM Tris buffer, pH 7.4, 5 mM $MgCl_2$, 1 mM 5-phosphoribosyl-1-pyrophosphate, 0.48 mM purine-8-^{14}C (Schwarz BioResearch, Inc.), and 1.0-1.5 mg of protein from dialyzed erythrocyte hemolysate in a final volume of 250 μl. One-twentieth μc ^{14}C was used for each assay except in patients with the Lesch-Nyhan syndrome for whom, because of the markedly decreased HG-PRTase activity, 5.0-7.5 mg protein and 1 μc of hypoxanthine-^{14}C or guanine-^{14}C were used. After incubation for 10 min at 37°, the reactions were terminated by adding 4 ml of ice-cooled water containing 1 μmole of the corresponding nucleotide. The reaction mixture was passed through a 0.4 x 1.5 cm column of copper-loaded chelating resin (Chelex 100, 200-400 mesh). Nucleotides are not retained and can be washed from the column with a small amount of water. In contrast, the purine bases are strongly bound to the chelating resin. Nucleotide formation was determined by counting ^{14}C contained in the eluate in a liquid scintillation counting system using Bray's solution.[13]

RESULTS

A summary of clinical data, pool and turnover values, and purine phosphoribosyltransferase activities appears in Table 1. All four patients with hyperuricemia had overproduction of uric acid. Patients D.K. and E.K., who were brothers, had normal HG-PRTase activity in red blood cells. Laboratory tests showed that they also had elevated pre-beta lipoproteins, increased serum triglyceride levels, and a diabetic glucose tolerance curve.

A.D. was a 54-year-old man who had his first attack of gouty arthritis at age 22. He had a partial deficiency of HG-PRTase equivalent to 12.5 per cent of normal activity. Three maternal uncles had suffered from gout and all four of his brothers had hyperuricemia, three of them having experienced acute gouty arthritis.

D.T. was an 8-year-old boy with all the clinical features of the Lesch-Nyhan syndrome, including spastic cerebral palsy, choreoathetosis, mental retardation, self-mutilation and recurrent uric acid lithiasis. Hemolysates from this patient contained small but definite amounts of HG-PRTase, clearly evident in time course studies. The respective activities with hypoxanthine and guanine as substrates were about 0.64 per cent and 0.05 per cent of normal. Similar results have been obtained for other patients with the Lesch-Nyhan syndrome studied in this hospital.

*Chow, D., F. Kawahara, T. Saunders, and L. B. Sorensen. Determination of hypoxanthine-guanine phosphoribosyltransferase. In preparation.

Table 1

CLINICAL DATA, URIC ACID POOL AND TURNOVER VALUES, AND ACTIVITIES OF PURINE PHOSPHORIBOSYLTRANSFERASES

Subject	Age	Weight	Gouty arthritis	Tophi	Urate pool size	Turnover	Urine uric acid	Plasma urate	Phosphoribosyltransferase activity		
									Hypoxanthine	Guanine	Adenine
	yr	kg			mg	mg/day	mg	mg/100 ml	mμmole/mg protein/min		
Normal values (26 subj.*)					1,200-1,300	600-700	400 ± 40	< 7	2.14 ± 0.15†	2.49 ± 0.24†	0.431 ± 0.049†
J.G., normal	27	57	-	-	-	-	387	4.0	-	-	-
D.K., gout	33	106	+	+++	3,681	1,508	461	10.6	1.75	2.24	0.487
E.K., gout	30	118	+	0	3,247	1,693	714	8.4	2.22	2.38	0.444
A.D., gout	54	75	+	+	2,397	1,185	790	11.5	0.260	0.320	0.661
D.T., Lesch-Nyhan	8	16	0	0	-	-	840	7.7	0.0137	0.0013	0.839

*Healthy male hospital employees.

†Mean ± standard deviation.

These values are distinctly higher than those reported by Kelley et al who used high voltage electrophoresis for separation of nucleotides and purines.[4]

In accordance with the observations by Seegmiller et al,[3] we found the activity of adenine phosphoribosyltransferase, an enzyme that catalyzes the formation of adenylic acid from adenine and PRPP, to be increased in red blood cells from patients with HG-PRTase deficiency.

The effect of allopurinol upon the excretion of the major purines is shown in Figure 2 and Table 2. This compound is a potent inhibitor of xanthine oxidase, the enzyme that catalyzes the

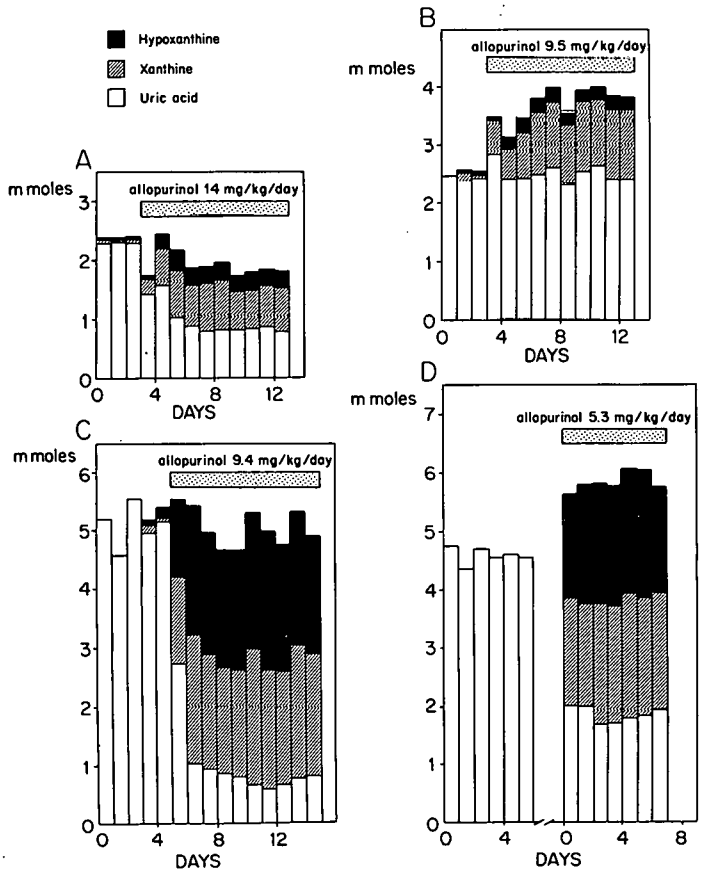

Figure 2. Excretion in urine of oxypurines before and during treatment with allopurinol. A, normal subject (J.G.); B, gout, normal HG-PRTase (D.K.); C, Lesch-Nyhan's syndrome (D.T.); and D, gout, 12.5% of normal activity of HG-PRTase (A.D.).

conversion of hypoxanthine to xanthine and of xanthine to uric acid. Allopurinol reduced the amounts of uric acid in the urine in all subjects except for one patient with gout who had extensive tophaceous involvement. This patient had, however, an eight-fold increase in the excretion of uric acid precursors, indicating that xanthine oxidase was being effectively inhibited. The fact that the specific activity values of ^{14}C in uric acid were never more than half of those in the precursors in this patient suggests that during the period of allopurinol treatment approximately one-half of urinary uric acid originated from tophi (cf. Figure 4).

Allopurinol reduced total urinary oxypurines (defined as the sum of hypoxanthine, xanthine

Table 2

MEAN URINARY OXYPURINE EXCRETION IN A CONTROL PERIOD AND DURING TREATMENT WITH ALLOPURINOL*

Subject	Hypoxanthine		Xanthine		Uric acid		Total oxypurine	
	Control	Allopurinol	Control	Allopurinol	Control	Allopurinol	Control	Allopurinol
	μmoles/day							
J.G.	45	278	46	727	2,301	825	2,392	1,830
D.K.	51	232	120	1,133	2,384	2,476	2,555	3,841
E.K.	42	357	116	1,131	3,967	1,730	4,125	3,218
A.D.	87	2,003	133	1,976	4,701	1,855	4,921	5,834
D.T.	184	2,126	68	2,051	5,000	732	5,252	4,909

*Mean values of 7 determinations beginning at least 3 days after institution of allopurinol therapy.

and uric acid) in the normal subject from 2.39 mmoles/day in the control period to 1.83 mmoles/day during the treatment period. Similarly in the gouty subject E.K., who had normal HG-PRTase activity, the pre-treatment value of 4.13 mmoles of oxypurine per day fell to 3.22 mmoles/day while he was on allopurinol in a dose of 10 mg/kg/day. On the other hand, patients who were deficient in HG-PRTase showed an increase in the precursors of uric acid commensurate with the reduction in urinary uric acid, so that the total excretion of urinary oxypurines remained constant or even increased slightly. The modest rise in total purines in patient A.D. (Figure 2, D) is probably related to the more efficient clearing by the kidney of hypoxanthine and xanthine as compared to uric acid, leading to excretion in the urine of purine that would normally be excreted into the gastrointestinal tract.

During allopurinol treatment the molar ratios of hypoxanthine to xanthine in subjects with a deficiency of HG-PRTase differed strikingly from those ratios in subjects with normal enzyme activity. Xanthine predominated over hypoxanthine in the urine from the normal subject and from the 2 patients with gout who had normal HG-PRTase activity. The molar ratios of xanthine to hypoxanthine were 2.61, 4.90 and 3.11 respectively (Table 2). These data suggest that the principal pathway of uric acid production in these individuals is via xanthine that has been formed from guanine rather than from hypoxanthine.

Patients with HG-PRTase deficiency excreted more hypoxanthine than xanthine. The molar ratio of hypoxanthine to xanthine was 1.01 for the adult with partial HG-PRTase deficiency and 1.04 for the boy with the Lesch-Nyhan syndrome (Table 2). When correction was made for the differences in body weight, the patient with the Lesch-Nyhan syndrome had urinary hypoxanthine values that were forty times higher than the mean values for three patients with normal HG-PRTase activity. These observations imply that hypoxanthine is the major source of the excessive uric acid production in HG-PRTase deficiency.

The patterns of labeling of hypoxanthine, xanthine, and uric acid are shown in Figures 3 through 6. In each instance the specific activity is expressed as dpm/mmole purine adjusted to a glycine-^{14}C dose of 1 μc/kg body weight.

For hypoxanthine the isotope concentration reached a maximum within the first 6 hr in all four patients, then fell rapidly over the next 20 hr. In patients with HG-PRTase deficiency the initial labeling of hypoxanthine was 5 and 2-1/2 times higher than normal. The shape of the specific activity curves for hypoxanthine between days one and seven was different in deficiency

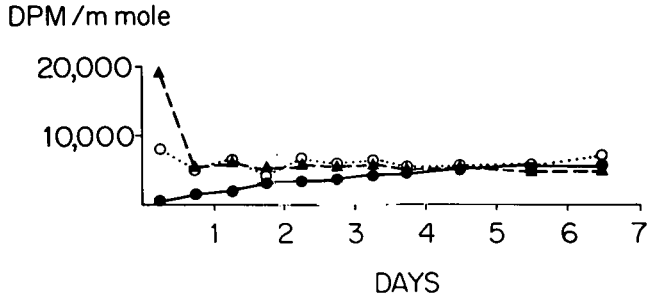

Figure 3. Specific activities of urinary purines after injection of 1 μc/kg body weight of glycine-^{14}C into a normal subject (J.G.). Glycine-^{14}C was injected on the fourth day of allopurinol administration. ▲- - - ▲, hypoxanthine; o · · · o, xanthine; ●——●, uric acid.

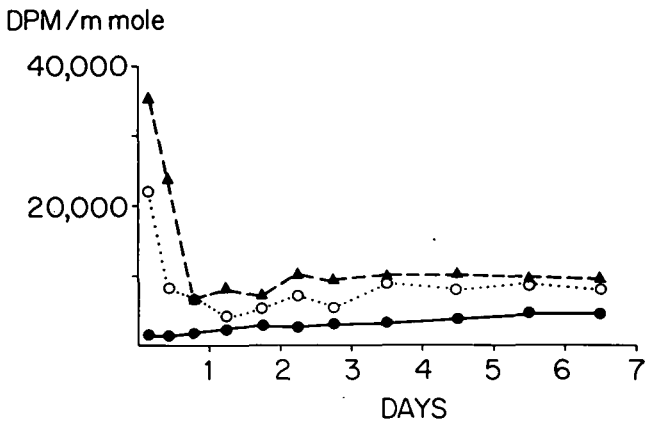

Figure 4. Specific activities of urinary purines after injection of 1 μc/kg body weight of glycine-^{14}C into a gouty subject with normal HG-PRTase activity (D.K.). Glycine-^{14}C was injected on the fourth day of allopurinol administration. Symbols as in Figure 3.

states of HG-PRTase and in states of normal enzyme activity. In the latter case the isotope concentration was almost stationary between day 1 and day 7. In enzyme deficiency states there was evidence of a small second peak which appeared between 24 and 48 hr; ^{14}C concentration then gradually decreased to less than half the value of the second peak over the next 5 days.

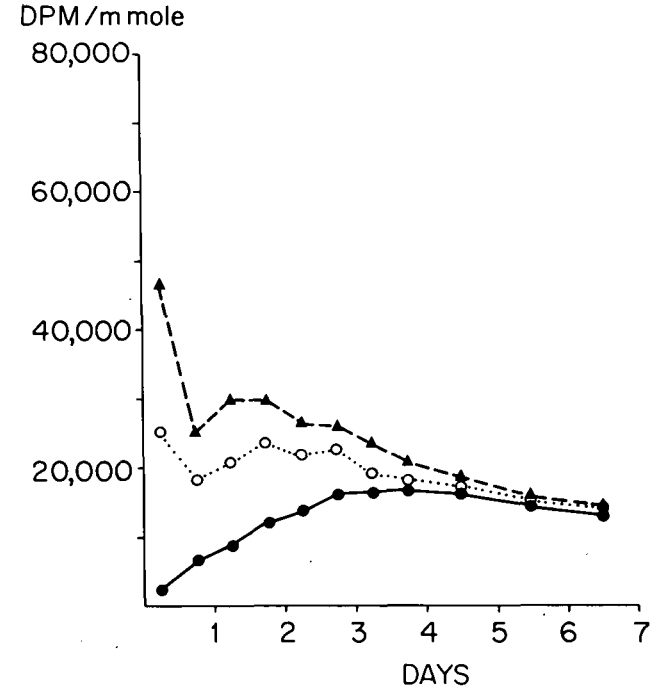

Figure 5. Specific activities of urinary purines after injection of 1 μc/kg body weight of glycine-^{14}C into a gouty subject with 12.5% of normal activity of HG-PRTase (A.D.). The patient was maintained on allopurinol for six months prior to injection of glycine-^{14}C. Symbols as in Figure 3.

Xanthine was also maximally labeled within the first 6 hr in all patients studied. The xanthine specific activity values were at first considerably less than those of hypoxanthine, but later tended to approximate and parallel them.

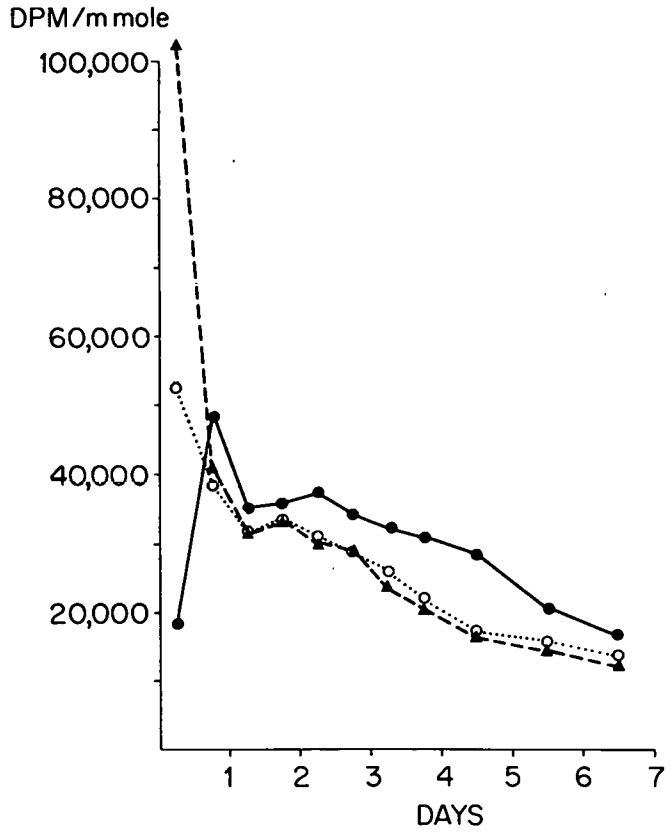

Figure 6. Specific activities of urinary purines after injection of 1 μc/kg body weight of glycine-^{14}C into a patient with the Lesch-Nyhan syndrome (D.T.). Glycine-^{14}C was injected on the fourth day of allopurinol administration. Symbols as in Figure 3.

The patterns of incorporation of ^{14}C into uric acid were similar in all patients but the one with the Lesch-Nyhan syndrome. Initially there was only slight labeling of uric acid. Specific activities then gradually rose to maximal values after 3 to 6 days. During the latter part of the studies uric acid specific activity values approached those of its precursors in two cases, while in a third case (D.K.), the concentration of uric acid remained lower, presumably because non-isotopic uric acid in tophi contributed to the dilution of labeled uric acid in the soluble pool. The boy with the Lesch-Nyhan syndrome showed maximal labeling of uric acid within the first 24 hr. Subsequently the concentration of ^{14}C in uric acid fell gradually, but more slowly than in hypoxanthine and xanthine, so that the specific activity in uric acid became slightly higher. This latter observation may be related to the fact that the kidney clears hypoxanthine and xanthine more rapidly than uric acid.

The concentration of ^{14}C in urinary hypoxanthine from the same four subjects has been plotted logarithmically versus time in Figure 7. Within the period of study each curve appears

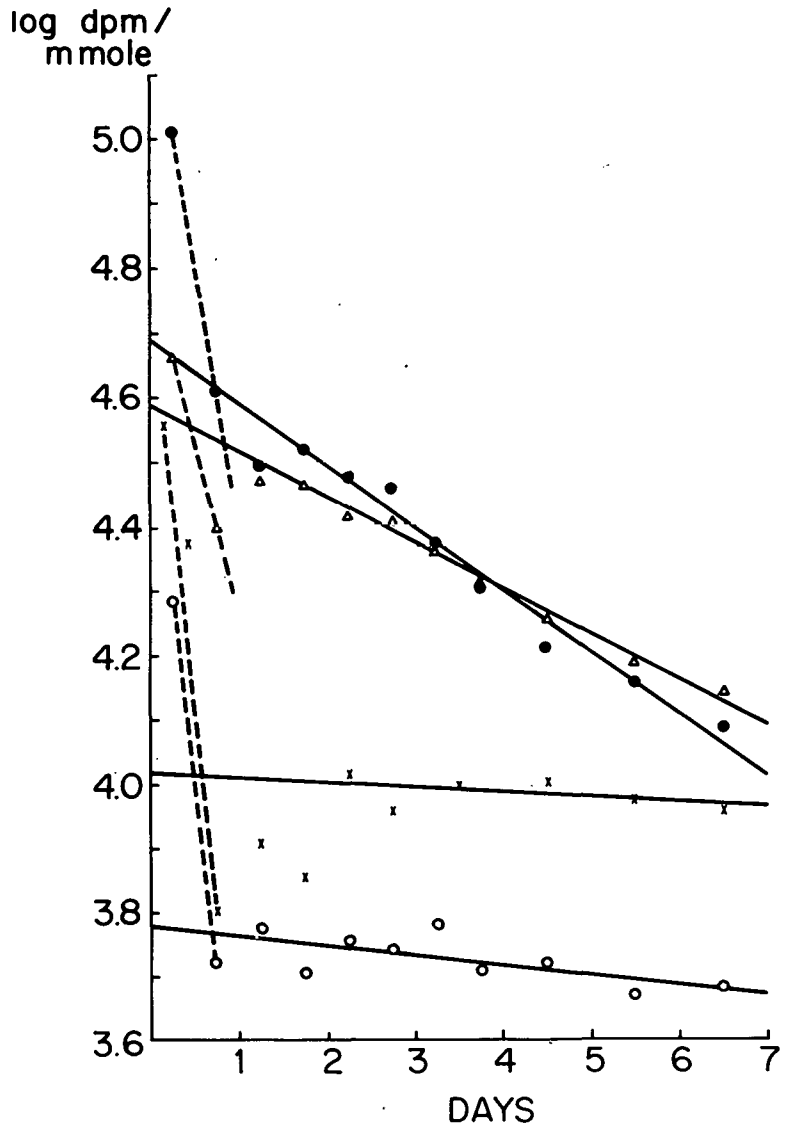

Figure 7. Logarithmic plots of the isotope concentration in hypoxanthine versus time. ●——●, the Lesch-Nyhan syndrome; △——△, gout, 12.5% of normal HG-PRTase activity; x——x, gout, normal HG-PRTase activity; o——o, normal subject.

to be biphasic, consisting of a rapid and a slow component. The major process contributing to the initial, rapid component is assumed to be the conversion of labeled glycine to hypoxanthine via inosinic acid and adenine nucleotides. The slope of this component is determined by the turnover of free nucleotides and the admixture of nonlabeled hypoxanthine arising from the breakdown of tissue nucleic acids. The slower component presumably represents the turnover of the adenine moiety of nucleic acids. The most significant difference between subjects with deficient and normal HG-PRTase is in the slopes of isotope decline in the second component. The rate constants of this process were calculated from observations between 42 and 156 hr. These data fitted a first order kinetic system quite well, but the probability that the slower component comprises a multicompartmental system should be strongly entertained. A standard

formula for comparison of the slopes of two regression lines was used to evaluate the significance of the difference between the slopes.[14] The rate constants and the results of statistical analysis are given in Table 3.

The very slow decline of the second slope observed in patients with normal HG-PRTase activity indicates that under normal conditions hypoxanthine is continually reutilized. This finding corroborates similar evidence obtained in studies of xanthinuric patients.[15,16] On the other hand, a deficiency of HG-PRTase prevents adequate recycling of hypoxanthine, and thereby leads to increased catabolism of hypoxanthine.

Table 3

SLOPES OF REGRESSION LINES FOR ISOTOPE DECLINE IN HYPOXANTHINE AND SIGNIFICANCE LEVELS OF THE DIFFERENCES BETWEEN THE SLOPES

Subject	K*	SE†
J.G.	- 0.0363	0.0151
D.K.	- 0.0173	0.0140
A.D.	- 0.1634	0.0069
D.T.	- 0.2222	0.0151
Slopes compared	**P‡**	**t**
D.T. vs J.G.	< 0.001	8.98
A.D. vs J.G.	< 0.001	7.59
D.T. vs A.D.	< 0.005	3.53
D.K. vs J.G.	> 0.4	0.855

*Δ specific activity of hypoxanthine/day.

†Standard error.

‡P value from t test for paired samples. Significance values based on two-tailed distribution.

In order to determine the extent to which hypoxanthine is derived by cleavage of newly formed IMP the isotope concentration in adenine was determined in the first urine sample after injection of glycine-^{14}C, and again on the fifth day. Comparison of the specific activities of hypoxanthine and adenine (Table 4) suggests that adenine derivatives are the principal source of hypoxanthine and that IMP cleavage plays a minor role in the genesis of hypoxanthine. Cleavage of even a minute fraction of newly formed IMP-^{14}C would be expected to yield higher initial concentration of ^{14}C in hypoxanthine compared to adenine, because ^{14}C in the adenine pool is diluted at an early stage by unlabeled adenine arising from tissue nucleic acids.

Table 4 also gives specific activity values of 7-methylguanine. Early labeling of this compound was observed in all patients studied. Similar findings have been reported by Wyngaarden et al.[8]

^{14}C was not incorporated into scattered samples of methylated xanthines, indicating the exogenous origin of these compounds.

The effect of allopurinol on the rate of de novo purine biosynthesis was measured by follow-

Table 4

SPECIFIC ACTIVITIES OF URINARY PURINES FROM FOUR SUBJECTS AFTER INTRAVENOUS INJECTION OF GLYCINE-1-^{14}C IN A DOSE OF 1 μc/kg BODY WEIGHT

Subject	Time	Hypoxanthine	Adenine	Xanthine	7-Methylguanine
	Day	dpm/mmole			
J.G.	0.25	19,300	14,300	7,900	5,200
	4.5	5,200	5,600	5,400	2,600
D.K.	0.15	35,700	31,200	22,100	10,200
	4.5	10,100	10,900	7,700	6,200
A.D.	0.25	46,400	42,900	25,000	11,800
	4.5	18,300	17,100	16,900	7,400
D.T.	0.25	102,000	71,800	52,500	13,300
	4.5	16,200	17,200	17,300	5,400

ing the incorporation of isotopic glycine into urinary hypoxanthine, xanthine and uric acid (Table 5). The seven-day incorporation value for ^{14}C in the normal subject was 0.0581 per cent of the administered isotope. Comparative control values in normal subjects ranged from 0.15 to 0.20 per cent. Similarly, 0.12 per cent of injected glycine-^{14}C was recovered in oxypurines from the gouty subject D.K. during the allopurinol study, while in a 7-day period when no drug was given, his brother E.K. who had a similar degree of overproduction of uric acid, excreted 0.250 per cent of injected isotope in uric acid. Thus in two subjects with normal HG-PRTase activity allopurinol reduced the de novo purine synthesis to less than half the pretreatment rate.

The boy with the Lesch-Nyhan syndrome had comparable incorporation values in the con-

Table 5

INCORPORATION OF GLYCINE-^{14}C INTO URINARY PURINES (7 DAYS)

Subject	Control study uric acid*	Allopurinol study			
		Hypoxanthine	Xanthine	Uric acid*	Total oxypurine
	% of dose	% of dose			
Normal value	0.150-0.200				
J.G.		0.009	0.024	0.025	0.058
E.K.	0.250				
D.K.		0.007	0.027	0.087	0.121
A.D.	0.781	0.191	0.153	0.143	0.487
D.T.	2.770	1.172	1.101	0.535	2.718

*Corrected for extrarenal elimination of uric acid.

trol and allopurinol studies, indicating failure of allopurinol to suppress purine biosynthesis in this condition. The response to allopurinol was equivocal in the patient who had 12.5 per cent of normal HG-PRTase activity in that allopurinol decreased the incorporation of glycine into the major purines by 38 per cent, while the excretion of total oxypurine rose slightly.

DISCUSSION

Possible modes by which HG-PRTase deficiency leads to accelerated purine synthesis have been discussed by Kelley et al.[4] These include: (a) decreased concentration of inosinic and guanylic acids, leading to reduced feedback inhibition of PRPP amidotransferase, the rate-limiting enzyme of de novo synthesis; (b) decreased utilization of PRPP for direct synthesis of GMP and IMP, making this substrate potentially available for purine biosynthesis de novo; (c) activation of PRPP amidotransferase by increased concentration of hypoxanthine or guanine.

Balis has postulated that HG-PRTase completes the sequence of reactions in a cyclic interconversion of adenine and hypoxanthine derivatives, and that deficiency of this enzyme causes depletion of intracellular nucleotides due to increased catabolism of inosinic acid to inosine and hypoxanthine.[17] The biochemical bases of accelerated purine biosynthesis have been investigated in cultured skin fibroblasts obtained from patients with HG-PRTase deficiency.[18,19] These studies have yielded the following information: (a) enzyme-deficient cells had greatly increased concentration of PRPP although the rate of synthesis of this compound was not increased; (b) there were no significant differences between normal and deficient fibroblasts with respect to the concentrations of guanosine triphosphate or of total adenine ribonucleotides; (c) an excess of hypoxanthine or guanine caused a stimulation of the rate of the early reactions of purine synthesis de novo.

The major objective of the present investigation was to acquire information from appropriate in vivo studies with respect to the source of excessive uric acid formation in HG-PRTase deficiency. Such information was obtained by comparing the effect of allopurinol on urinary oxypurines in subjects with normal and deficient HG-PRTase, and by following the incorporation of glycine-1-^{14}C into the major purines. In the presence of normal enzyme activity allopurinol treatment resulted in proportionately greater increases in the excretion of xanthine compared to hypoxanthine. The mean molar ratio of xanthine to hypoxanthine for three subjects with normal HG-PRTase was 3.36 to 1. A similar preponderance of xanthine over hypoxanthine has been observed in previous studies on the effect of allopurinol on purine excretion,[20,21] and in patients with xanthinuria, a congenital absence of xanthine oxidase.[9,16] These data suggest that the principal pathway of uric acid production is normally through xanthine that has been formed from guanine rather than from hypoxanthine. Patients with HG-PRTase deficiency excreted more hypoxanthine than xanthine. When correction was made for the difference in body weight, the boy with the Lesch-Nyhan syndrome had urinary hypoxanthine values that were forty times higher than the mean value for three subjects with normal HG-PRTase activity, while an adult with a partial deficiency of the enzyme equivalent to 12.5 per cent of normal activity had a tenfold increase in urinary hypoxanthine compared to normal. The patterns of ^{14}C-labeling of the oxypurines in HG-PRTase deficiency reflect the role of hypoxanthine as precursor of xanthine. These findings imply that hypoxanthine is the major source of the excessive uric acid production in HG-PRTase deficiency.

The slow dilution in specific activity of hypoxanthine after the first 24 hr in subjects with

normal HG-PRTase activity is evidence for continual reutilization of hypoxanthine in normal purine metabolism. Similar conclusions have been reached from studies of purine metabolism in patients with xanthinuria. A xanthinuric patient had a daily turnover of xanthine of 276 mg, 79 per cent of which was excreted in the urine. In the same patient the turnover of hypoxanthine was 960 mg daily, of which only 5.7 per cent appeared in the urine.[16] Moreover, hypoxanthine and adenine were utilized to a much greater extent than were xanthine and guanine. Only 1 per cent of intravenously injected adenine-^{14}C was recovered in the urine after 24 hr[9] and 28 per cent of hypoxanthine-^{14}C after 21 days.[16] The recoveries of guanine and xanthine were 74 per cent in 2 weeks and 75 per cent in 3 weeks, respectively.[9,16] These data indicate quite clearly that hypoxanthine is an active intermediary metabolite that is being continually recycled, presumably through synthesis to inosinic acid which is in turn converted to 5'-adenine and guanine nucleotides. On the other hand, xanthine and guanine are only slightly reutilized. Thus, the principal role of HG-PRTase appears to be the conservation of hypoxanthine rather than guanine.

The incorporation of glycine into hypoxanthine in patients with HG-PRTase deficiency was quite different from that observed in subjects with normal enzyme activity. Following a small second peak of isotope enrichment on day 2 there was a fairly rapid decline in ^{14}C-concentration. The rate constants for this diluting process were 0.22 day^{-1} for a boy with the Lesch-Nyhan syndrome and 0.16 day^{-1} for an adult with partial deficiency. This finding indicates a greater than normal loss of ^{14}C from the hypoxanthine pool and dilution of isotope by newly formed unlabeled hypoxanthine arising from the turnover of the complex pools of adenine and hypoxanthine derivatives.

The deficiency of HG-PRTase provides a logical biochemical rationale for the loss of hypoxanthine. Failure of normal reutilization of hypoxanthine for the direct synthesis of IMP leaves less of this nucleotide available for conversion to AMP and GMP. These purine nucleotides are natural feedback inhibitors of PRPP amidotransferase, the enzyme responsible for the rate-controlling step of purine synthesis. A relaxation of the cooperative feedback inhibition serves as a stimulus for the increased de novo synthesis. It would appear that an insufficient concentration of AMP is as important as any shortage of GMP in slackening a regulatory feedback mechanism in HG-PRTase deficiency. Consistent with this proposition is the finding by Seegmiller et al[22] that adenine decreased purine biosynthesis de novo by 45 per cent without significantly altering the turnover of uric acid in a patient who had only 1 per cent of the normal activity of HG-PRTase. Adenine is readily converted to its nucleotide by adenine PRTase in both normal subjects and patients with HG-PRTase deficiency. An increased formation of AMP through the reutilization pathway results in a concurrent depression in its generation from IMP formed de novo.

In subjects with normal HG-PRTase de novo purine biosynthesis is depressed in situations where the reutilization of hypoxanthine is augmented as a consequence of increased concentration of this purine, e.g., in xanthinuria and in patients treated with allopurinol. The present data can be synthesized into a scheme of cyclic interconversions of adenine and hypoxanthine derivatives proposed by Balis.[17] This scheme involves the following sequence of reactions: AMP to adenosine, to inosine, to hypoxanthine, to IMP and back to AMP (Figure 8). Lack of HG-PRTase prevents this cycle from functioning.

A decreased reutilization of hypoxanthine could conceivably result from a genetically determined increase in xanthine oxidase which would favor the oxidative catabolism of hypoxanthine

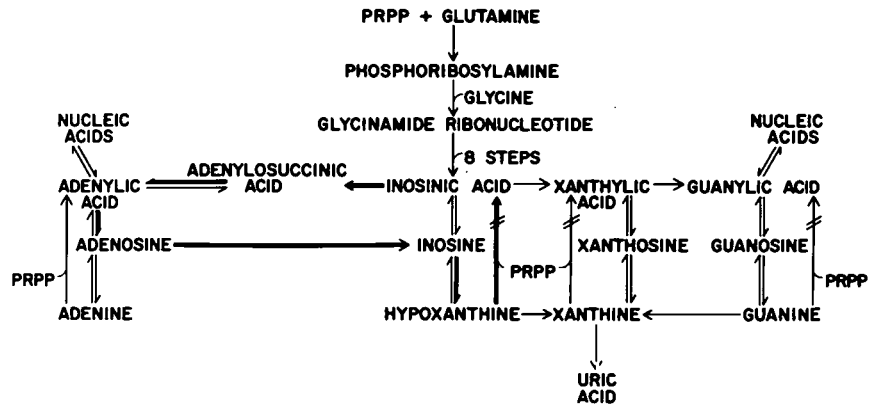

Figure 8. Simplified scheme of de novo purine biosynthesis, reutilization pathways and purine interconversions. The heavy arrows indicate the cyclic interconversion of adenine and hypoxanthine derivatives. The blocked reactions in HG-PRTase deficiency are shown by the parallel lines intersecting the arrows.

to uric acid. Recently Carcassi et al[23] have reported increased activity of xanthine oxidase in liver biopsy material from patients with primary gout. Since xanthine oxidase is an inducible enzyme[24] such an increase could also be a secondary phenomenon.

The rapid labeling of urinary adenine observed in the present studies provides evidence that a portion of glycine-^{14}C is quickly converted into AMP. A comparison of the specific activities of adenine and hypoxanthine five days after the injection of glycine-^{14}C suggests that hypoxanthine is derived principally from adenine derivatives and that cleavage of IMP to hypoxanthine via inosine does not contribute in any great measure to the formation of uric acid in either normal man or in patients with HG-PRTase deficiency. The labeling patterns of adenine and hypoxanthine are quite similar to those observed in several of the patients studied by Wyngaarden et al,[8] although the interpretations of the data vary in some respects.

Early labeling of 7-methylguanine was seen in all subjects studied, corroborating similar evidence presented by Wyngaarden et al.[8] 7-Methylguanine is known to be a constituent of transfer RNA and ribosomal RNA.[25] It is also known that methylation of nucleic acid occurs at the macromolecular level. The early labeling of 7-methylguanine is an indication that certain species of RNA turn over at a rapid rate.

The early and accelerated appearance of glycine-^{14}C into uric acid in some patients with primary gout has in the past been interpreted to mean the existence of a "shunt" pathway whereby newly synthesized purine bases were converted to uric acid without prior incorporation into nucleic acids. The present data do not lend support to such a proposition.

Allopurinol produced a significant decrease in the rate of purine biosynthesis de novo in subjects with normal HG-PRTase activity. This effect was demonstrated by measuring the cumulative incorporation of glycine-^{14}C into hypoxanthine, xanthine, and uric acid during allopurinol treatment and by summating the daily excretion of the three oxypurines before and during allopurinol therapy. The latter parameter was not valid for a patient with extensive tophaceous involvement, who actually increased the excretion of oxypurine while on allopurinol. Nevertheless, the drug substantially reduced biosynthesis de novo in this patient as evidenced by decreased incorporation of glycine-^{14}C into uric acid and its precursors.

Allopurinol did not suppress the incorporation of glycine-^{14}C into the major purines, nor did it reduce total oxypurine excretion in the patient with the Lesch-Nyhan syndrome. The patient who had 12.5 per cent of the normal activity of HG-PRTase had a modest reduction of glycine-^{14}C incorporation into oxypurines during the period of treatment with allopurinol. Whether this difference is a valid measure of a reduction of purine biosynthesis de novo or whether it reflects variations in the pool size and turnover of glycine, is open to question. In this connection it is of interest that azathioprine (Imuran) effectively inhibited de novo purine synthesis in the same patient.[12] Since this inhibition is effectuated by nucleotide derivatives acting at the rate-limiting step catalyzed by PRPP amidotransferase,[26] it follows that azathioprine or one of its intermediary metabolites, e.g., 6-mercaptopurine, has been converted to the nucleotide form. In patients with the Lesch-Nyhan syndrome, azathioprine has no discernible effect on purine biosynthesis.[27]

Possible mechanisms by which allopurinol inhibits de novo purine synthesis have been discussed by Kelley et al.[28] The inhibitory effect requires the presence of HG-PRTase activity. The finding that allopurinol increased the incorporation of labeled hypoxanthine into soluble nucleotides and nucleic acids in mice,[29] suggests that the effect of allopurinol on de novo purine synthesis is related to higher concentration of hypoxanthine, which in turn—in the presence of adequate HG-PRTase activity—increases the formation of IMP via the reutilization pathway.

The activity of HG-PRTase in hemolysates from the boy with the Lesch-Nyhan syndrome was at least 10 times higher than the values reported by Kelley et al.[4] Whether this discrepancy reflects differences in the assay technique or whether it means that some patients with the Lesch-Nyhan syndrome have small, but detectable HG-PRTase activity remains to be resolved. In this connection it is of interest that Fujimoto and Seegmiller[30] found skin fibroblasts from patients with the Lesch-Nyhan syndrome to contain HG-PRTase activity that was around 3 per cent of normal, although the activity in erythrocyte hemolysates was less than 0.04 per cent of normal values.

LITERATURE CITED

1. Seegmiller, J. E., A. I. Grayzel, L. Laster, and L. Liddle. J. Clin. Invest., 40:1304, 1961.
2. Sorensen, L. B. Arch. Int. Med., 109:379, 1962.
3. Seegmiller, J. E., F. M. Rosenbloom, and W. N. Kelley. Science, 155:1682, 1967.
4. Kelley, W. N., M. L. Greene, F. M. Rosenbloom, J. F. Henderson, and J. E. Seegmiller. Ann. Intern. Med., 70:155, 1969.
5. Lesch, M., and W. L. Nyhan. Amer. J. Med., 36:561, 1964.
6. Praetorius, E. Scand. J. Clin. Lab. Invest., 1:222, 1949.
7. Weissmann, B., P. A. Bromberg, and A. B. Gutman. J. Biol. Chem., 224:407, 1956.
8. Wyngaarden, J. B., A. E. Blair, and L. Hilley. J. Clin. Invest., 37:579, 1958.
9. Ayvazian, J. H., and S. Skupp. J. Clin. Invest., 44:1248, 1965.
10. Bergmann, F., H. Kwietny, G. Levin, and D. J. Brown. J. Amer. Chem. Soc., 82:598, 1960.
11. Sorensen, L. B. Scand. J. Clin. Lab. Invest., 12 (Suppl. 54):1, 1960.

12. Sorensen, L. B. Proc. Nat. Acad. Sci. U.S., 55:571, 1966.

13. Bray, G. A. Anal. Biochem., 1:279, 1960.

14. Brownlee, K. A. Statistical Theory and Methodology in Science and Engineering. New York: John Wiley & Sons, 1960, p. 288.

15. Ayvazian, J. H., and S. Skupp. J. Clin. Invest., 45:1859, 1966.

16. Bradford, M. J., I. R. Krakoff, R. Leeper, and M. E. Balis. J. Clin. Invest., 47:1325, 1968.

17. Balis, M. E. Fed. Proc., 27:1067, 1968.

18. Rosenbloom, F. M., J. F. Henderson, I. C. Caldwell, W. N. Kelley, and J. E. Seegmiller. J. Biol. Chem., 243:1166, 1968.

19. Rosenbloom, F. M., J. F. Henderson, W. N. Kelley, and J. E. Seegmiller. Biochim. Biophys. Acta, 166:358, 1068.

20. Yü, T.-F., and A. B. Gutman. Amer. J. Med., 37:885, 1964.

21. Sweetman, L., and W. L. Nyhan. Nature, 215:859, 1967.

22. Seegmiller, J. E., J. R. Klinenberg, and R. W. E. Watts. J. Clin. Invest., 47:1193, 1968.

23. Carcassi, A., R. Marcolongo, Jr., E. Marinello, G. Riario-Sforza, and C. Boggiano. Arthritis Rheumat., 12:17, 1969.

24. Stirpe, F., and E. Della Corte. Biochem. J., 94:309, 1965.

25. Borek, E., and P. R. Srinivasan. Annu. Rev. Biochem., 35:275, 1966.

26. McCollister, R. J., W. R. Gilbert, Jr., D. M. Ashton, and J. B. Wyngaarden. J. Biol. Chem., 239:1560, 1964.

27. Kelley, W. N., F. M. Rosenbloom, and J. E. Seegmiller. J. Clin. Invest., 46:1518, 1967.

28. Kelley, W. N., F. M. Rosenbloom, J. Miller, and J. E. Seegmiller. N. Engl. J. Med., 278: 287, 1968.

29. Pomales, R., S. Bieber, R. Friedman, and G. H. Hitchings. Biochim. Biophys. Acta, 72:119, 1963.

30. Gujimoto, W. Y., and J. E. Seegmiller. J. Clin. Invest., 48:27a, 1969.

ADRENOCORTICOTROPIN STIMULATION OF 2-KETOGLUTARATE OXIDATION BY ISOLATED RAT EPIDIDYMAL ADIPOSE TISSUE: MEDIATION BY CYCLIC-AMP AND RELATIONSHIP TO LIPID METABOLISM*

By

J. L. Skosey†

Cyclic AMP‡ mediates the effects of a number of hormones. In isolated adipose tissue, ACTH stimulates adenyl cyclase, resulting in enhanced conversion of ATP to cyclic AMP. Cyclic AMP in turn stimulates the lipase system of adipose tissue, and lipolysis of adipose tissue triglycerides is enhanced.[1] I observed previously that ACTH stimulated the oxidation of 2-ketoglutarate-1,2-^{14}C to $^{14}CO_2$.[2] In this study, I investigated the possibility that cyclic AMP mediated the stimulatory effect of ACTH upon 2-ketoglutarate oxidation by isolated adipose tissue.

In further experiments, I considered the possibility that enhanced 2-ketoglutarate oxidation was secondary to one of the effects of ACTH upon lipid metabolism. Besides enhancing lipolysis, ACTH stimulates triglyceride synthesis[3,4] and inhibits fatty acid synthesis.[5,6] Fatty acids released by the lipolytic effect of ACTH could act as uncoupling agents and thereby stimulate oxidative processes.[7] Tissue stores of high energy compounds are depleted as they are utilized for triglyceride synthesis. The depletion of high energy stores could serve as a stimulus for oxidation to replete the stores via oxidative phosphorylation.[8] The results indicate that ACTH does not stimulate 2-ketoglutarate oxidation as an indirect consequence of either of these effects upon lipid metabolism.

EXPERIMENTAL PROCEDURE

Special preparations. Dr. C. H. Li generously supplied α_p-ACTH. A second sample of porcine ACTH was purchased from Calbiochem. N^6-2'-O-dibutyryl cyclic-3',5'-adenosine monophosphate was obtained from C. F. Boehringer, 2-ketoglutarate-1-^{14}C (lot 78052) from Calbiochem, and D-glucose-1-^3H (Code TRA 285, batch 1) from Amersham-Searle. Phentolamine mesylate (Regitine®) was the product of the Ciba Pharmaceutical Company. I obtained caffeine, 2-desoxy-D-glucose, and 2,4-dinitrophenol from commercial sources.

Incubation media. The basic medium was Krebs-Ringer bicarbonate buffer[9] containing gelatin (2 mg per ml). Glucose, 2-ketoglutaric acid, glucose-1-^3H and 2-ketoglutarate-1-^{14}C were added as indicated in the tables and figures. It was possible to measure simultaneously 2-ketoglutarate-1-^{14}C oxidation to $^{14}CO_2$ and lipogenesis (incorporation of ^3H from glucose-1-^3H into total lipid and fatty acid) when the medium contained both labeled precursors. Caffeine and phentolamine mesylate were dissolved directly in the incubation medium, DNP was first dissolved in a small volume of absolute ethanol,[10] and ACTH from a concentrated stock solution in 0.9 per cent NaCl-0.2% gelatin (1-10 μl of stock solution per ml of incubation medium).

*This report is taken from a paper that appeared in J. Biol. Chem., 245:510, 1970. The work was supported in part by a U. S. Public Health Service General Research Support Grant.

†Postdoctoral Fellow of the Arthritis Foundation.

‡The abbreviations used are: ACTH, adrenocorticotropin; cyclic AMP, cyclic-3',5'-adenosine monophosphate; DBCAMP, N^6-2'-O-dibutyryl cyclic-3',5'-adenosine monophosphate, DNP, 2,4-dinitrophenol; 2DG, 2-desoxy-D-glucose; GLC, glucose; NS, non-significant Student's t($p > 0.05$).

Incubation procedure. Epididymal fat pads removed from decapitated 100-160 g Sprague-Dawley male albino rats (weight range in any single experiment less than 30 g) were placed in 20 ml serum bottles containing 2 ml of medium and a 10 x 44 mm test tube. One fat pad from each animal served as a contra lateral control. The bottles were capped with rubber stoppers coated with a thin film of stopcock grease, gassed for 10 min through a 21 gauge needle (using a second 21 gauge needle as a vent) with humidified 95 per cent O_2 - 5 per cent CO_2 and placed in a Dubnoff shaker for 1 hr at 37° and 80 cycles per minute. Incubation was stopped by injection of 0.5 ml of hyamine solution (1 volume 1 M hyamine in methyl alcohol and 3 volumes toluene) into the test tube, and 0.5 ml 6 N H_2SO_4 into the medium. Zero time controls (gassed but not placed on the shaker) were included with each incubation.

Estimation of incorporation of radioactivity. Agitation of the bottles for 2 hrs at room temperature resulted in complete collection of the $^{14}CO_2$ (evolved from the acidified medium) into the hyamine. The contents of the test tube were transferred quantitatively to a calibrated counting vial, and 7.5 ml of phosphor solution (4.8 mg diphenoxazole per ml toluene) and toluene to a volume of 15 ml were added. The tissue was homogenized in 10 ml of acidified isopropanol heptane,[11] 6 ml each of heptane and water were added, the mixture was shaken vigorously, and allowed to layer. A 3 or 5 ml aliquot of the upper phase was transferred to a counting vial containing 10 ml of phosphor solution (6 mg 2,5-diphenyloxazole per ml toluene) for counting. Preliminary experiments demonstrated that the upper phase contained essentially all of the lipid radioactivity. No ^{14}C from 2-ketoglutarate-1-^{14}C was detected in the total lipid fraction. For determination of incorporation of ^3H into fatty acid, 3 ml of the upper phase was transferred to a calibrated screw-capped culture tube and dried under N_2. The residue was then twice dissolved in 1 ml of absolute ethanol and dried under N_2. 2 ml of absolute ethanol and 3 ml of 5 N KOH were added to each tube which was then capped and autoclaved for 30 min to hydrolyze the lipid. After allowing the tubes to cool to room temperature, 40 per cent ethanol was added to bring the volume to 5 ml, if necessary. 3 ml of 6 N H_2SO_4, 6 ml absolute ethanol, and 8 ml heptane were added in sequence to the tubes which were then capped, shaken, and centrifuged to facilitate separation into two phases. 5 ml of upper phase was transferred to a counting vial and 10 ml of phosphor solution (as above) was added for counting. Counting of aliquots of medium in Bray's mixture, and of appropriate standards prepared with either ^3H- or ^{14}C-labeled toluene, allowed expression of incorporation as mμatoms of precursor radioactivity.

Medium glycerol was determined by an enzymatic method.[12]

After calculation of means and standard errors, application of Student's t test yielded the appropriate p value. A p value of greater than 0.05 was considered non-significant (NS).

RESULTS AND DISCUSSION

ACTH Stimulation of 2-Ketoglutarate Oxidation by Isolated Adipose Tissue

In a previous study, ACTH stimulated the production of $^{14}CO_2$ from glutamate-1-^{14}C and 2-ketoglutarate-1,2-^{14}C by isolated adipose tissue.[2] In agreement with these findings, ACTH stimulated the production of $^{14}CO_2$ from 2-ketoglutarate-1-^{14}C (Table 1). In some experiments, at the lowest concentration of ACTH used (0.1 μg per ml), the hormone effect was minimal and not statistically significant. The data suggest that the effectiveness of the hormone diminishes when the concentration of medium glucose is increased, with 2-ketoglutarate concentration remaining constant. The hormone is consistently active at a concentration of 0.3 and 1 μg per ml.

Table 1

EFFECT OF ACTH UPON 2-KETOGLUTARATE OXIDATION BY ISOLATED ADIPOSE TISSUE

The incubation medium contained 2-ketoglutarate-1-^{14}C and glucose at the concentrations indicated. a_p-ACTH was used. See Experimental Procedure for the technics of incubation and estimation of $^{14}CO_2$ production.

2-Ketoglutarate concentration	Glucose concentration	ACTH concentration	$^{14}CO_2$ produced, mean ± S.E.		
			Control (n)[a]	+ACTH (p)[b]	Difference (p)[b]
mM	mg/ml	μg/ml	mμmoles/100 mg tissue/hr		%
0.05	0	0.1	2.13 ± 0.15 (6)	3.60 ± 0.41 (<0.005)	68.1 ± 11.1 (<0.005)
0.1	0.5	0.1	2.12 ± 0.32 (6)	3.29 ± 0.27 (<0.001)	64.3 ± 13.8 (<0.01)
1	0.5	0.1	8.30 ± 1.20 (8)	13.1 ± 0.92 (<0.005)	101 ± 50.7 (>0.05)
0.05	3	0.1	2.32 ± 0.14 (6)	2.87 ± 0.32 (>0.05)	24.0 ± 12.6 (>0.05)
0.1	3	0.1	1.90 ± 0.21 (6)	2.46 ± 0.25 (<0.001)	30.2 ± 4.4 (<0.001)
0.1	0	0.3	4.41 ± 0.59 (6)	9.71 ± 1.13 (<0.005)	131 ± 25.1 (<0.005)
0.1	1	0.3	3.93 ± 0.45 (6)	6.80 ± 1.12 (<0.02)	71.6 ± 12.7 (<0.005)
0.1	3	0.3	2.10 ± 0.19 (9)	3.64 ± 0.25 (<0.001)	81.0 ± 13.7 (<0.001)
1	3	0.3	6.58 ± 0.68 (9)	10.1 ± 0.65 (<0.005)	68.7 ± 22.7 (<0.02)
0.1	1.5	1.0	2.88 ± 0.49 (6)	9.90 ± 0.76 (<0.001)	275 ± 42.5 (<0.005)

[a]Number of tissue pairs.

[b]Significance of difference between control and experimental groups.

$^{14}CO_2$ can be produced from 2-ketoglutarate-1-^{14}C in two pathways utilized for 2-ketoglutarate metabolism.[13] When 2-ketoglutarate is metabolized via the "forward reaction" of the Krebs cycle to succinate, carbon-1 is evolved as CO_2. 2-Ketoglutarate can also be metabolized via the "backward reaction" of the Krebs cycle to citrate which can be cleaved to yield oxalacetate and acetyl-CoA. CO_2 is formed from the carbon atom originally in position 1 of 2-ketoglutarate as oxalacetate is converted to pyruvate. Carbons 2-5 of 2-ketoglutarate can be incorporated into fatty acid as 2-ketoglutarate is metabolized via the "backward reaction."[13] ACTH suppressed incorporation of ^{14}C from glutamate-U-^{14}C into fatty acid.[2] This suggests that ACTH stimulated $^{14}CO_2$ production from 2-ketoglutarate-1-^{14}C by enhancing oxidation of 2-ketoglutarate to succinate.

ACTH action could block the formation of 2-ketoglutarate from unlabeled endogenous precursors. If this were the case, the contribution of medium 2-ketoglutarate-1-^{14}C to the available 2-ketoglutarate pool would be proportionately greater. The specific activity of evolved $^{14}CO_2$ would likewise increase, offering a possible explanation for the observed effect of ACTH upon 2-ketoglutarate metabolism. This explanation is, however, unlikely. Substances likely to be converted to 2-ketoglutarate include glucose and other intermediates of the Embden-Meyerhof pathway, fatty acids, and amino acids, in particular glutamic acid. $^{14}CO_2$ is produced from glucose-6-^{14}C as glucose is metabolized via the Krebs cycle. ACTH stimulates this conversion.[3] Acetate is an intermediate in a pathway by which both glucose and fatty acid can enter the Krebs cycle. ACTH does not alter, or slightly stimulates, $^{14}CO_2$ production from acetate-1-^{14}C.[2,5] Glutamate-1-^{14}C can be converted to 2-ketoglutarate-1-^{14}C which is then oxidized, resulting in $^{14}CO_2$ production. $^{14}CO_2$ production from glutamate-1-^{14}C is enhanced by ACTH.[2] Thus, ACTH enhances, rather than blocks, the conversion of a number of substances which could possibly contribute to the 2-ketoglutarate pool.

Cyclic-AMP Mediation of ACTH-Stimulated 2-Ketoglutarate Oxidation

The "lipolytic hormones" (including ACTH, the catecholamines, glucagon, and thyrotropin) enhance adipose tissue adenyl cyclase activity, resulting in an increase in the tissue level of cyclic-AMP. Cyclic-AMP then stimulates the adipose tissue lipase system, enhancing the lipolysis of adipose tissue triglycerides. Cyclic AMP also mediates the effects of these hormones upon a number of other tissues.[1] In this study, the possibility that an ACTH-induced rise in tissue cyclic AMP mediated the hormone stimulation of 2-ketoglutarate oxidation was considered.

Sutherland et al[1] suggested four criteria to be fulfilled before an effect of a hormone could be considered to be mediated by a rise in tissue cyclic AMP level. First, the hormone should stimulate adenyl cyclase in broken cell suspensions. Second, tissue cyclic AMP should rise prior to the effect of the hormone in question, and should rise in proportion to hormone concentration. Third, drugs that inhibit phosphodiesterase activity should potentiate the hormone action. Fourth, the effect of the hormone should be mimicked by the addition of exogenous cyclic AMP or one of its derivatives. ACTH stimulates adenyl cyclase in broken cell suspensions of adipose tissue, and effects a prompt increase in the level of cyclic AMP in intact tissue. Thus, the first two criteria are fulfilled for any effect of ACTH upon adipose tissue.[1] Experiments using caffeine, a phosphodiesterase inhibitor, and the cyclic AMP derivative DBCAMP were done to determine if the remaining criteria could be fulfilled. The effects of glucose and of phentolamine upon the actions of ACTH and of DBCAMP were also explored.

Effect of caffeine upon 2-ketoglutarate oxidation. Caffeine inhibits cyclic AMP phosphodiesterase.[14] In the presence of glucose (3 mg per ml), ACTH (0.1 μg per ml) minimally stimulated 2-ketoglutarate oxidation by 30 and 24 per cent in two experiments (Figure 1). Caffeine alone (0.5 mM) had no significant effect, although caffeine potentiated the effect of ACTH (Figure 1). The two agents in combination stimulated 2-ketoglutarate oxidation by 139 per cent and caffeine enhanced 2-ketoglutarate oxidation by 70 per cent in ACTH-stimulated tissues. Although caffeine at 1 mM and 3 mM concentrations did not alter 2-ketoglutarate oxidation, the drug at 10 mM concentration stimulated 2-ketoglutarate oxidation by 154 per cent (Figure 2).

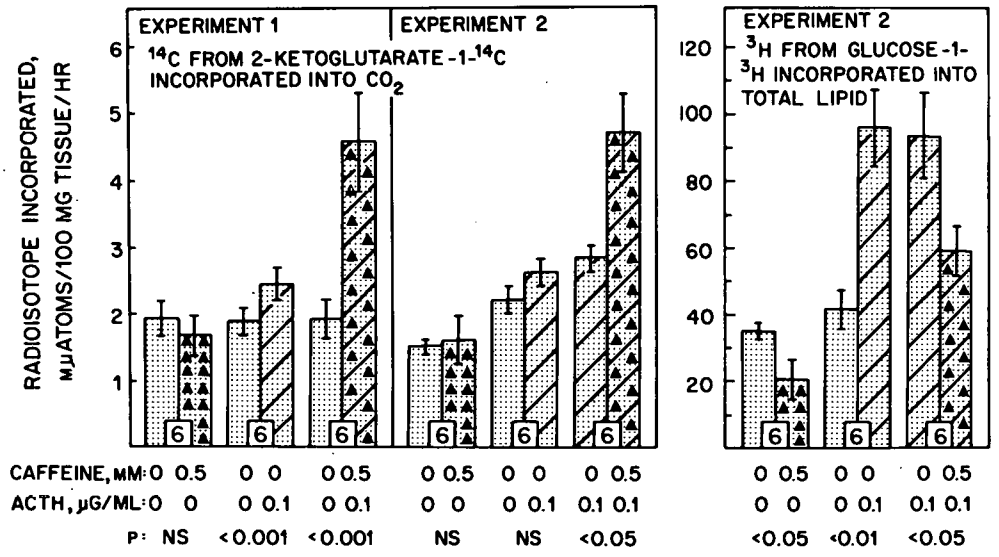

Figure 1. Effect of ACTH and caffeine upon 2-ketoglutarate oxidation and lipogenesis by isolated adipose tissue. The incubation medium contained 2-ketoglutarate-1-^{14}C (0.1 mM) in both experiments, glucose (3 mg per ml) in experiment 1 and glucose-1-^{3}H (3 mg per ml) in experiment 2. Caffeine (▲), α_p-ACTH (hatched bars), or caffeine plus α_p-ACTH (▲ and hatched bars) were present at the indicated concentrations. The height of the bars indicates the mean incorporation into each group of paired tissues; the length of the vertical lines, two standard errors of the mean. The number at the base of each pair of bars indicates the number of tissue pairs. Tissues were incubated and $^{14}CO_2$ and ^{3}H-lipid estimated as described in Experimental Procedure.

Effect of DBCAMP upon 2-ketoglutarate oxidation (Table 2). DBCAMP is more effective than its parent compound, cyclic AMP, in stimulating adipose tissue lipolysis. The enhanced activity of the acyl derivative has been attributed to its ability to readily penetrate the adipose cell, and to its resistance to cyclic-AMP phosphodiesterase.[15] DBCAMP, inconsistently at 1 mM concentration, but definitely at concentrations of 3 and 10 mM, stimulated 2-ketoglutarate oxidation. In contrast to ACTH, altering the concentration of glucose did not appear to alter the stimulatory effect of DBCAMP (Table 2, expt. 2).

Effect of glucose upon ACTH- and DBCAMP-stimulated 2-ketoglutarate oxidation (Figure 3). As noted above, the presence of glucose in the incubation medium diminished the stimulation of 2-ketoglutarate oxidation by ACTH, but not by DBCAMP. Thus, it appeared that glucose could be

Table 2

EFFECT OF N^6-2'-O-DIBUTYRYL CYCLIC-3',5'-ADENOSINE MONOPHOSPHATE (DBCAMP) UPON 2-KETOGLUTARATE OXIDATION BY ISOLATED ADIPOSE TISSUE

The incubation medium contained 2-ketoglutarate-1-^{14}C (0.1 mM) in all experiments, and glucose at the concentrations indicated. See Experimental Procedure for the technics of incubation and estimation of $^{14}CO_2$ and ^3H-total lipid production.

Experiment	Glucose concentration	DBCAMP concentration	$^{14}CO_2$ produced, mean ± S.E.		
			Control (n)[a]	+DBCAMP (p)[b]	Difference (p)[b]
	mg/ml	mM	mμmoles/100 mg tissue/hr		%
1	3	1	2.25 ± 0.13 (6)	2.89 ± 0.08 (<0.005)	+30.0 ± 5.5 (<0.005)
2a	3	1	0.46 ± 0.06 (6)	0.66 ± 0.06 (<0.05)	+51.7 ± 21.1 (>0.05)
2b	1	1	0.51 ± 0.04 (6)	0.75 ± 0.13 (>0.05)	+47.9 ± 23.8 (>0.05)
2c	0.33	1	0.55 ± 0.11 (6)	0.83 ± 0.12 (>0.05)	+61.6 ± 14.7 (<0.05)
3a	1.5	0.3	2.07 ± 0.30 (5)	2.32 ± 0.23 (>0.05)	+15.9 ± 11.6 (>0.05)
3b	1.5	1	2.43 ± 0.14 (6)	2.90 ± 0.30 (>0.05)	+19.9 ± 10.3 (>0.05)
3c	1.5	3	3.00 ± 0.46 (6)	4.94 ± 0.49 (<0.02)	+80.8 ± 26.8 (<0.05)
4a	1.5	0.1	2.46 ± 0.23 (6)	2.61 ± 0.29 (>0.05)	+5.8 ± 6.4 (>0.05)
4b	1.5	1	2.49 ± 0.20 (6)	2.46 ± 0.31 (>0.05)	-0.8 ± 9.5 (>0.05)
4c	1.5	10	2.29 ± 0.45 (6)	4.27 ± 0.51 (<0.001)	+104 ± 25.7 (<0.01)
5a	1.5	1	1.80 ± 0.48 (6)	2.04 ± 0.43 (>0.05)	+22.2 ± 33.6 (>0.05)
5b	1.5	3	2.04 ± 0.18 (6)	4.78 ± 0.68 (<0.01)	+139 ± 34.8 (<0.02)
5c	1.5	10	1.89 ± 0.13 (6)	4.62 ± 0.42 (<0.001)	+148 ± 25.2 (<0.005)

[a]Number of tissue pairs.

[b]Significance of difference between control and experimental groups.

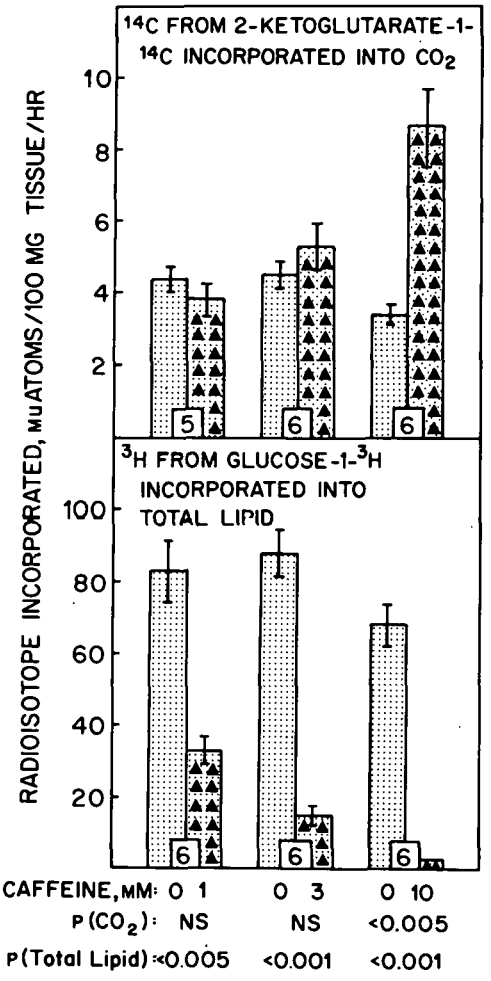

Figure 2. Effect of caffeine upon 2-ketoglutarate oxidation and lipogenesis by isolated adipose tissue. The incubation medium contained 2-ketoglutarate-1-^{14}C (0.1 mM) and glucose-1-^{3}H (1.5 mg per ml). Caffeine (▲) was present at the indicated concentrations. See Figure 1 for further explanation of figure.

interfering with ACTH stimulation of adenyl cyclase. Corbin and Butcher* have found that glucose in high concentration (3 mg per ml) suppressed epinephrine stimulation of a rise in adipose tissue cyclic-AMP levels. The results of experiments testing the effect of glucose upon ACTH- and DBCAMP-stimulated 2-ketoglutarate oxidation were in accord with their finding. Glucose alone (3 mg per ml) did not alter 2-ketoglutarate oxidation, but suppressed 2-ketoglutarate oxidation by tissues stimulated by ACTH (0.3 and 0.1 μg per ml) by 27 and 22 per cent, respectively. Glucose did not alter 2-ketoglutarate oxidation by tissues stimulated with DBCAMP (1 and 3 mM). Glucose suppresses ACTH stimulation of free fatty acid release and this has been attributed to an increased rate of re-esterification of released fatty acids.[16] Diminished ACTH stimulation of cyclic AMP production may also contribute to the glucose suppression of ACTH-stimulated lipolysis. The availability of glucose may also alter the pattern of metabolism in adipose

*Corbin, J. D., and R. W. Butcher, personal communication.

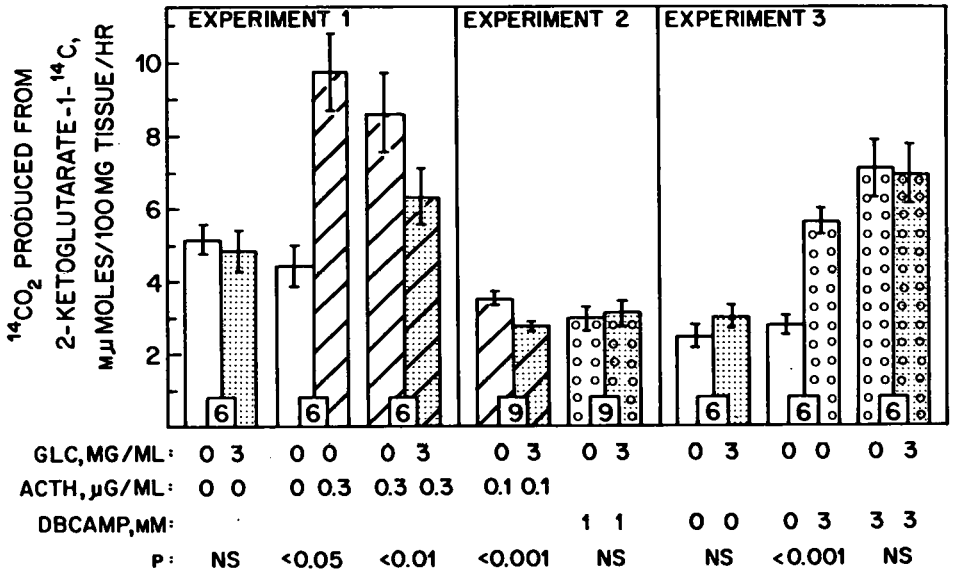

Figure 3. Effect of glucose upon ACTH and N^8-2'-O-dibutyryl cyclic adenosine monophosphate (DBCAMP) stimulation of 2-ketoglutarate oxidation by isolated adipose tissue. The incubation medium contained 2-ketoglutarate-1-^{14}C (0.1 mM) in all experiments. Glucose (GLC, stippled bars), α_p-ACTH (hatched bars), DBCAMP (o), α_p-ACTH plus glucose (hatched and stippled bars), or DBCAMP plus glucose (o and stippled bars) were present at the indicated concentrations. See Figure 1 for further explanation of the figure.

tissue which is under the influence of ACTH. As less glucose is available to adipose tissue, the metabolism of substrates such as fatty acids via the Krebs cycle may be favored.

Effect of phentolamine upon ACTH-stimulated 2-ketoglutarate oxidation. Aulich, Stock and Westerman[17] found that the α-adrenergic blocking agent phentolamine blocked the lipolytic effect of ACTH by interfering with the action of cyclic-AMP. Phentolamine also blocked the stimulation of 2-ketoglutarate oxidation by ACTH (Table 3). With a glucose-free incubation medium, ACTH (0.1 μg per ml) stimulated 2-ketoglutarate oxidation by 77 per cent. ACTH in combination with phentolamine (1 or 0.1 mM) had no significant effect upon 2-ketoglutarate oxidation (i.e., stimulated by only 14 or 10 per cent). In a confirming experiment (Table 3, expt. 2), ACTH (0.1 μg per ml) stimulated 2-ketoglutarate oxidation by 64 per cent. Phentolamine (1 mM) suppressed 2-ketoglutarate oxidation by 19 per cent in tissues incubated with ACTH.

In one instance (Table 3, expt. 2a), phentolamine alone significantly stimulated 2-ketoglutarate oxidation. To explore this observation, paired tissues were incubated in the presence of phentolamine, ranging in concentration from 0.33 to 3 mM (Figure 4). The highest concentration of phentolamine definitely stimulated 2-ketoglutarate oxidation by 136 per cent.

Relationship of Effects of ACTH upon Adipose Tissue Lipogenesis and 2-Ketoglutarate Oxidation

ACTH stimulates both triglyceride synthesis and oxygen consumption in isolated adipose tissue.[8] Adipose tissue triglyceride synthesis requires ATP for the formation of glycerol-1-phosphate from glucose and for fatty acid activation.[18] The decrease in tissue stores of high-energy compounds could serve as a stimulus of oxidation to regenerate high-energy stores via

Table 3

EFFECT OF ACTH AND PHENTOLAMINE UPON 2-KETOGLUTARATE OXIDATION AND LIPOGENESIS BY ISOLATED ADIPOSE TISSUE

The incubation medium contained 2-ketoglutarate-1-^{14}C (0.1 mM) in both experiments, no glucose in experiment 1, and glucose-1-^{3}H (0.5 mg per ml) in experiment 2. The experimental medium contained ACTH and/or phentolamine as indicated. In experiment 2c, the control medium contained ACTH, 0.1 μg per ml. α_D-ACTH was used. See Experimental Procedure for the technics of incubation and estimation of $^{14}CO_2$ and ^{3}H-total lipid production.

Experiment	Addition to experimental medium		Radioisotope incorporated, mean ± S.E.		
	ACTH	Phentolamine	Control (n)[a]	Experimental (p)[b]	Difference (p)[b]
	μg/ml	mM	mμatoms/100 mg tissue/hr		%
^{14}C from 2-ketoglutarate-1-^{14}C incorporated into CO_2					
1a	0.1	0	2.30 ± 0.32 (4)	3.90 ± 0.12 (<0.01)	+76.7 ± 17.6 (<0.05)
1b	0	1	2.20 ± 0.48 (3)	2.46 ± 0.14 (>0.05)	+21.0 ± 22.8 (>0.05)
1c	0.1	1	2.62 ± 0.35 (4)	2.98 ± 0.24 (>0.05)	+14.3 ± 13.9 (>0.05)
1d	0	0.1	2.30 ± 0.27 (3)	2.24 ± 0.13 (>0.05)	+0.5 ± 15.1 (>0.05)
1e	0.1	0.1	3.58 ± 0.32 (4)	3.92 ± 0.49 (>0.05)	+10.0 ± 11.4 (>0.05)
2a	0	1	2.31 ± 0.75 (6)	3.06 ± 0.32 (>0.05)	+52.9 ± 20.8 (<0.05)
2b	0.1	0	2.12 ± 0.32 (6)	3.29 ± 0.27 (<0.02)	+64.3 ± 13.8 (<0.01)
2c	0.1[c]	1	3.68 ± 0.32 (6)[c]	2.93 ± 0.23 (>0.05)	-19.0 ± 6.4 (<0.05)
^{3}H from glucose-1-^{3}H incorporated into total lipid					
2a	0	1	13.8 ± 3.2 (6)	11.1 ± 1.3 (>0.05)	-0.3 ± 19.2 (<0.05)
2b	0.1	0	13.8 ± 2.7 (6)	36.0 ± 3.0 (<0.001)	+152 ± 31.0 (<0.005)
2c	0.1[c]	1	42.2 ± 2.2 (6)[c]	17.9 ± 2.8 (<0.001)	-58.3 ± 4.9 (<0.001)

[a]Number of tissue pairs.

[b]Significance of difference between control and experimental groups.

[c]The control medium contained ACTH, 0.1 μg per ml, in experiment 2c.

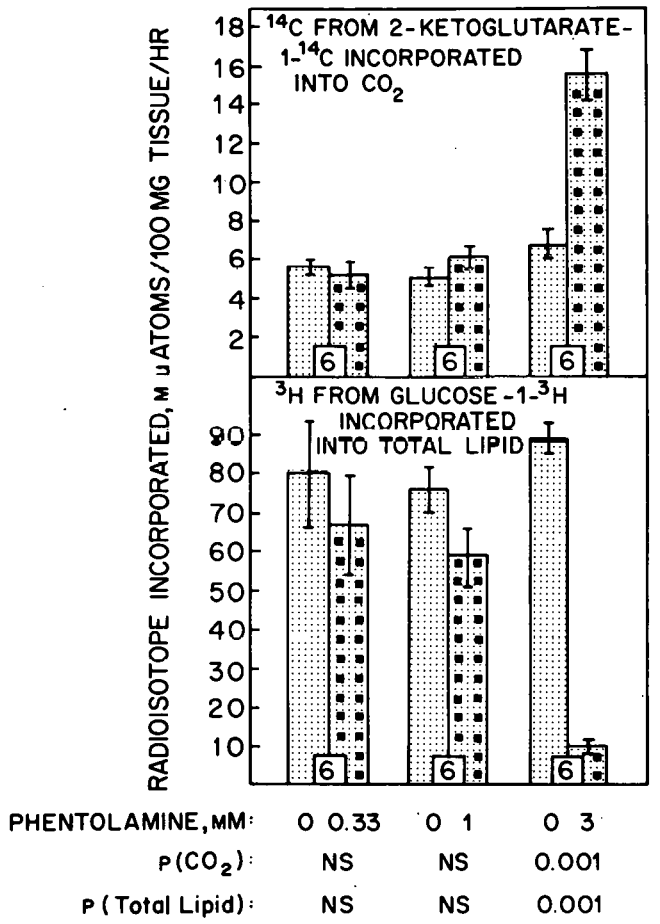

Figure 4. Effect of phentolamine upon 2-ketoglutarate oxidation and lipogenesis by isolated adipose tissue. The incubation medium contained 2-ketoglutarate-1-^{14}C (0.1 mM) and glucose-1-^{3}H (1.5 mg per ml). Phentolamine (■) was present at the indicated concentrations. See Figure 1 for further explanation of the figure.

oxidative phosphorylation.[8] In this study the incorporation of ^{3}H from glucose-1-^{3}H into adipose tissue total lipid served as a measure of lipogenesis. Approximately 40 per cent of the ^{3}H incorporated into total lipid was found in fatty acid following saponification of the total lipid fraction (Figure 5). ACTH stimulated total lipid synthesis, but inhibited incorporation of label into fatty acid (Figure 5). The stimulation of total lipid synthesis by ACTH probably reflects the stimulatory effect of the hormone upon fatty acid esterification.[3,4] Three types of experiments suggested that enhanced 2-ketoglutarate oxidation in the presence of ACTH did not occur in response to a need to regenerate high energy compounds utilized for triglyceride synthesis. First, the effects of some agents upon lipogenesis were opposite from their effects upon 2-ketoglutarate oxidation. Second, DNP, which presumably depleted high-energy stores by blocking oxidative phosphorylation, did not enhance 2-ketoglutarate oxidation to the same degree as ACTH. Third, ACTH and DBCAMP each stimulated 2-ketoglutarate oxidation in the presence of 2-desoxy-D-glucose (2DG) which inhibited lipogenesis.

Dissociation of 2-ketoglutarate oxidation from lipogenesis. As noted above, caffeine (0.5

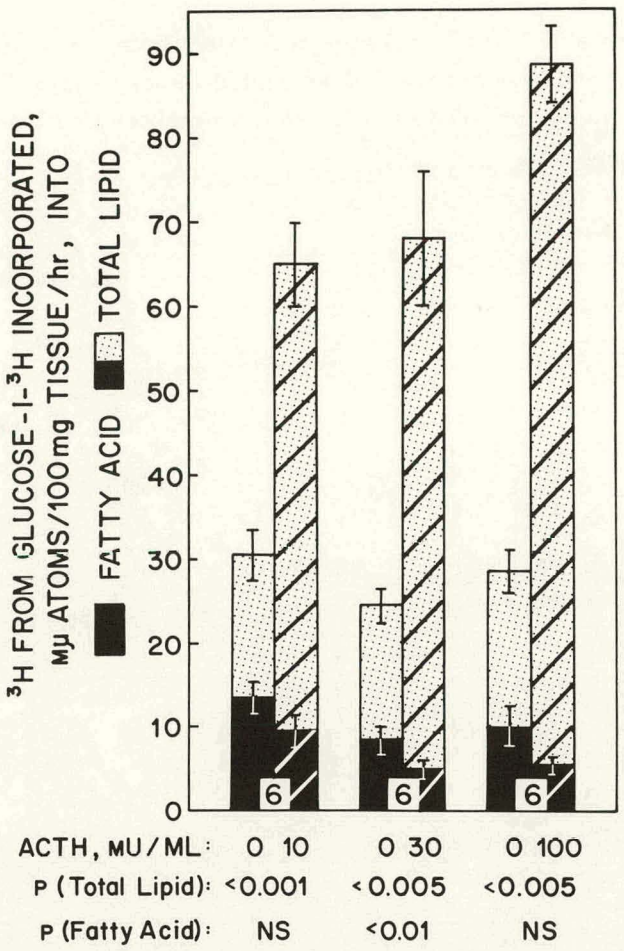

Figure 5. Effect of ACTH upon lipogenesis by isolated adipose tissue. The incubation medium contained 2-ketoglutarate (0.1 mM) and glucose-1-^{3}H (1.5 mg per ml). ACTH (Calbiochem) (cross-hatched bars) was present at the indicated concentrations. The total height of each bar represents incorporation into total lipid, the black portion represents incorporation into fatty acid. See Figure 1 for further explanation of the figure.

mM) potentiated the effect of ACTH upon 2-ketoglutarate oxidation. ACTH alone (0.1 μg per ml) stimulated lipogenesis by 157 per cent (Figure 1). In contrast to its potentiating effect upon ACTH-stimulated 2-ketoglutarate oxidation, caffeine suppressed lipogenesis by ACTH-stimulated tissues by 32 per cent.

Caffeine alone inhibits lipogenesis.[6] In this study, the degree of inhibition was proportional to drug concentration between 1 and 10 mM (Figure 2). At 10 mM concentration, caffeine almost completely abolished lipogenesis, while its greatest stimulatory effect was upon 2-ketoglutarate oxidation.

Blecher[19] found that DBCAMP in low concentrations (0.075-0.3 mM) stimulated incorporation of label from glucose-U-^{14}C into total lipid of adipose cells. Higher concentrations (0.75-3 mM) inhibited incorporation of glucose carbon into total lipids. DBCAMP had a similar effect upon the incorporation of label from glucose-1-^{3}H into total lipid of adipose tissue (Figure 6). Although without a significant effect at a concentration of 0.1 mM, DBCAMP stimulated lipo-

genesis at concentrations of 0.3 and 1 mM (the peak effect being at 0.3 mM), had no significant effect at 3 mM, and inhibited lipogenesis at a concentration of 10 mM. DBCAMP (3 and 10 mM) stimulated 2-ketoglutarate oxidation. The nucleotide was most effective at a concentration (10 mM) that inhibited lipogenesis.

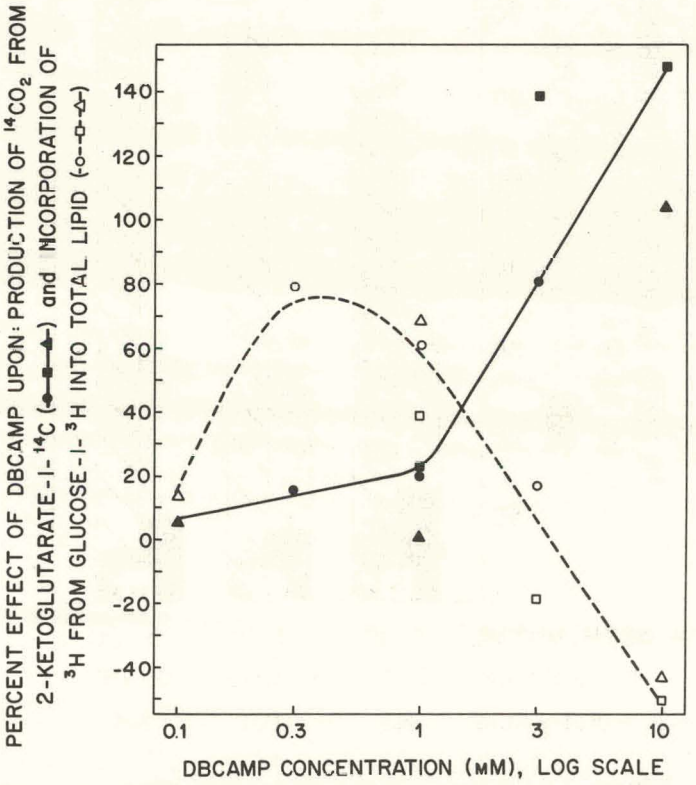

Figure 6. Effect of DBCAMP upon 2-ketoglutarate oxidation and lipogenesis. The incubation medium contained 2-ketoglutarate-1-^{14}C (0.1 mM) and glucose-1-^{3}H (1.5 mg per ml). The open symbols represent the effect of DBCAMP upon lipogenesis, closed symbols the effect upon 2-ketoglutarate oxidation. Negative effects indicate inhibition. Data from tissues incubated in the same experiment are represented by symbols of the same shape. Each point represents the mean of values from 6 paired tissues.

The effect of DBCAMP upon lipid synthesis differed from that of ACTH in yet another way. Although ACTH inhibited incorporation of ^{3}H from glucose-1-^{3}H into fatty acid at all concentrations tested, the lower concentrations of DBCAMP, which stimulated total lipid synthesis, also enhanced incorporation of label into fatty acid (Figure 7). The disparity between the effects of ACTH and of caffeine and DBCAMP suggests that ACTH stimulation of adipose tissue lipogenesis is not mediated by cyclic AMP. This conclusion, however, is not in accord with current concepts of ACTH action and requires further evaluation.

Phentolamine (1 mM) suppressed both 2-ketoglutarate oxidation and lipogenesis in tissues incubated with ACTH (Table 3). Phentolamine alone in higher concentration (3 mM) suppressed lipogenesis by 90 per cent while, as noted above, stimulating 2-ketoglutarate oxidation by 136 per cent (Figure 4). The mechanisms of the drug effects upon 2-ketoglutarate oxidation and lipo-

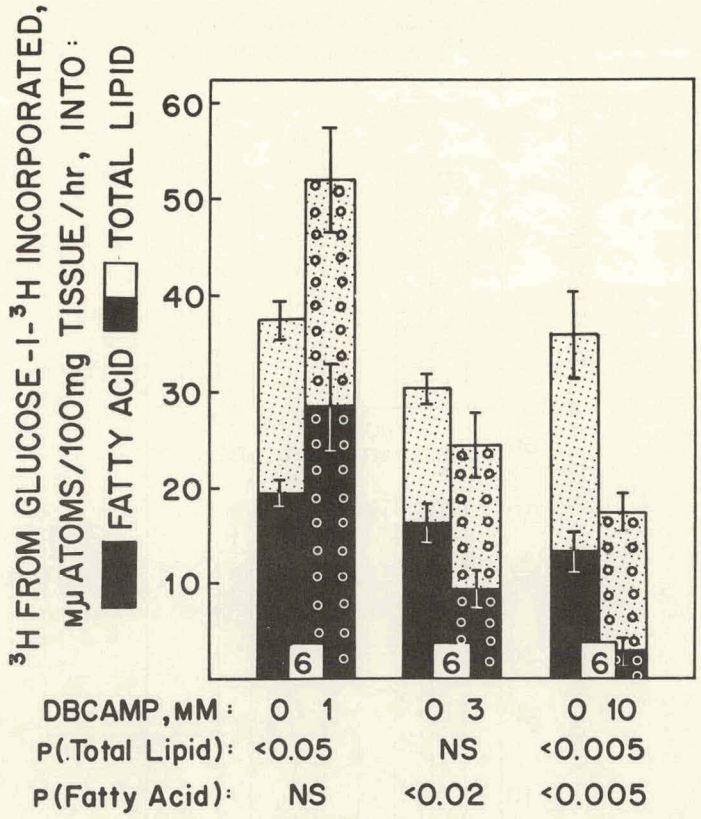

Figure 7. Effect of DBCAMP upon lipogenesis by isolated adipose tissue. The incubation medium contained 2-ketoglutarate-1-^{14}C (0.1 mM) and glucose-1-^{3}H (1.5 mg per ml). DBCAMP (o) was present at the indicated concentrations. See Figures 1 and 5 for further explanation of the figure.

genesis are not clear, but the finding offers another example of the dissociation of effects upon the two processes.

Effect of DNP upon 2-ketoglutarate oxidation and lipogenesis (Figure 8). Experiments with DNP provided a second line of evidence that enhanced 2-ketoglutarate oxidation was not simply a secondary response to depressed levels of high energy compounds. DNP suppressed lipogenesis, presumably by uncoupling oxidative phosphorylation and blocking the formation of high energy compounds necessary for triglyceride synthesis. Concentrations of DNP ranging from 0.1 to 1 mM had increasing inhibitory effects upon lipogenesis. Although DNP did stimulate 2-ketoglutarate oxidation (by 30-35 per cent), the effect at 0.1 mM was equal to that at 1.0 mM, a concentration which virtually abolished lipogenesis (i.e., inhibited by 98 per cent). Even when lipogenesis was maximally suppressed (and oxidative phosphorylation presumably maximally inhibited), the stimulatory effect of DNP upon 2-ketoglutarate oxidation did not approach the maximal stimulation observed with ACTH (Table 1), DBCAMP (Table 2), caffeine (Figure 2), or ACTH plus caffeine (Figure 1).

Effect of 2DG upon ACTH- and DBCAMP-stimulated 2-ketoglutarate oxidation and lipogenesis (Figure 9). 2DG competitively inhibits glucokinase[20] and thus interferes with glucose utilization. When the medium concentration of glucose-1-^{3}H was 1 mg per ml, 2DG, 1 mg per ml,

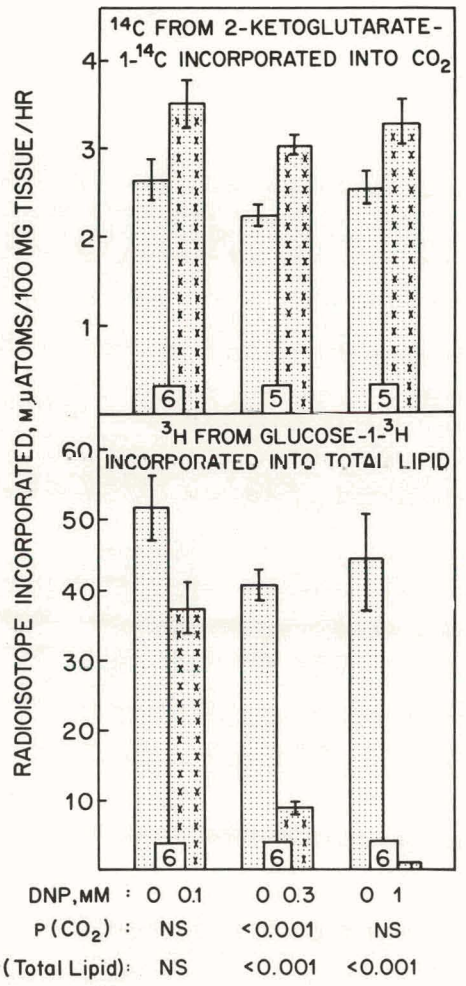

Figure 8. Effect of 2,4-dinitrophenol (DNP) upon 2-ketoglutarate oxidation and lipogenesis by isolated adipose tissue. The incubation medium contained 2-ketoglutarate-1-^{14}C (0.1 mM) and glucose-1-^{3}H (1.5 mg per ml). DNP (x) was present at the indicated concentrations. See Figure 1 for further explanation of the figure.

inhibited incorporation of label into total lipid by 48 per cent but did not alter 2-ketoglutarate oxidation. ACTH, 0.3 μg per ml, stimulated both 2-ketoglutarate oxidation (by 72 per cent) and lipogenesis (by 169 per cent). In the presence of ACTH, 2DG inhibited lipogenesis by 79 per cent but did not affect 2-ketoglutarate oxidation.

With the medium glucose-1-^{3}H concentration 0.5 mg per ml, and in the presence of 2DG, 1 mg per ml, DBCAMP, 1 mM, stimulated both 2-ketoglutarate oxidation (by 79 per cent) and lipogenesis (by 56 per cent). 2DG suppressed lipogenesis by DBCAMP-stimulated tissues, but did not alter 2-ketoglutarate oxidation in tissues incubated with DBCAMP. Thus, 2DG suppressed lipogenesis in tissues incubated without the addition of hormone or nucleotide, in tissues incubated with ACTH, and in tissues incubated with DBCAMP. 2DG did not alter 2-ketoglutarate oxidation under any of these conditions.

Data from the three types of experiments cited above indicated that the stimulatory effect of ACTH upon 2-ketoglutarate oxidation did not depend upon enhanced lipogenesis. It is possible,

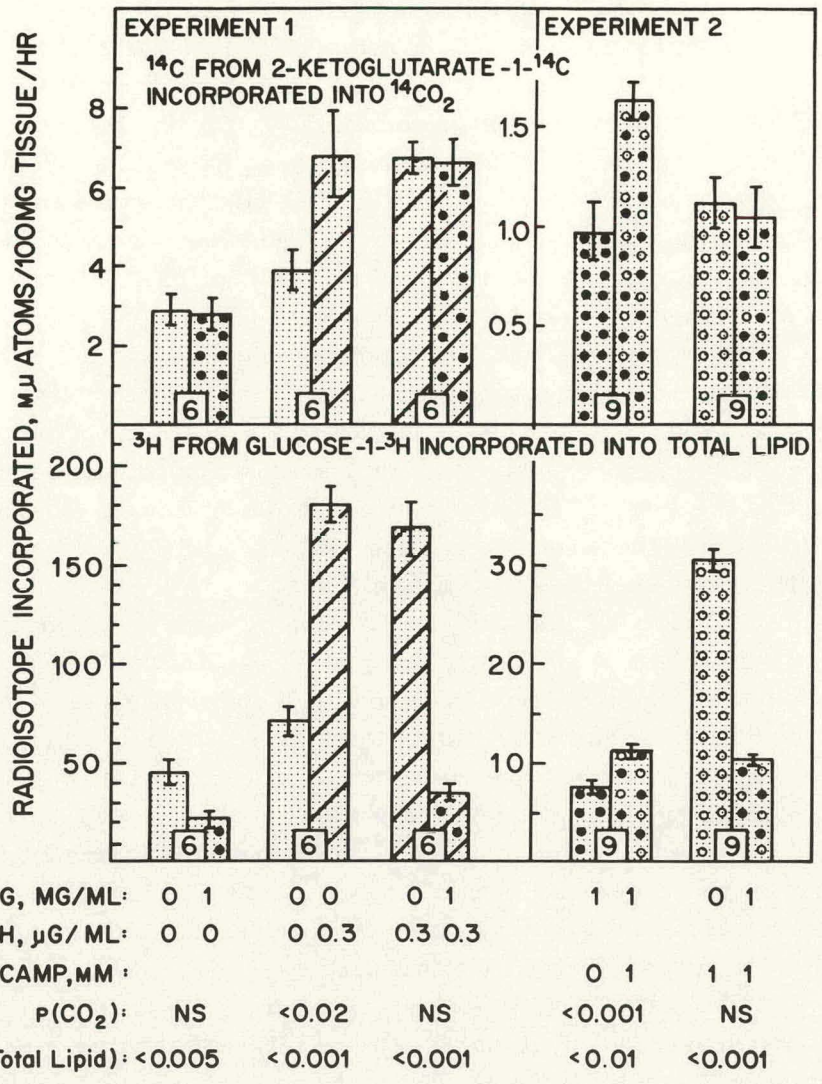

Figure 9. Effect of 2-desoxy-D-glucose (2DG) upon ACTH and N^6-2'-O-dibutyryl cyclic adenosine monophosphate (DBCAMP) stimulation of 2-ketoglutarate oxidation and lipogenesis by isolated adipose tissue. The incubation medium contained 2-ketoglutarate-1-^{14}C (0.1 mM) and glucose-1-^{3}H (1 mg per ml in experiment 1, 0.5 mg per ml in experiment 2). 2DG (●), ACTH (hatched bars), ACTH plus 2DG (hatched bars and ●), DBCAMP (o), and DBCAMP plus 2DG (o and ●) were present at the indicated concentrations. See Figure 1 for further explanation of the figure.

however, that enhanced 2-ketoglutarate oxidation (or enhanced Krebs cycle oxidation reflected by increased 2-ketoglutarate oxidation) served as a source of high energy compounds which were then utilized for triglyceride synthesis.

Relationship of Effects of ACTH upon Lipolysis and 2-Ketoglutarate Oxidation

The cell membrane contains adenyl cyclase and is presumably the site of cyclic-AMP synthesis.[1] 2-Ketoglutarate oxidation occurs in the mitochondria. Cyclic-AMP or a product of cyclic-AMP action could alter mitochondrial metabolism and result in enhanced 2-ketoglutarate

oxidation. Hirschfield and Koritz[21] found that fatty acids caused swelling (increased permeability) of rat adrenal mitochondria and stimulated pregnenolone synthesis. Fatty acids, released by the lipolytic effect of ACTH (acting through cyclic AMP) could enhance adipose mitochondrial permeability to 2-ketoglutarate or to a co-factor necessary for its utilization, and thus enhance the oxidation of 2-ketoglutarate. Since 2-ketoglutarate is an intermediate in the Krebs "cycle," the primary effect could be upon the metabolism of some other intermediate with the observed effect upon 2-ketoglutarate metabolism a secondary phenomenon. The possibility that stimulation of 2-ketoglutarate oxidation resulted from an accumulation of fatty acid released by the lipolytic action of ACTH was considered.

Epinephrine, another "lipolytic hormone," under conditions which prevent tissue accumulation of an excess of fatty acid, stimulates adipose tissue oxygen consumption. Hagen and Ball[7] suggested that this increase in oxygen uptake may be partly due to an uncoupling of oxidative phosphorylation by fatty acids. Free fatty acids, released by the lipolytic effect of ACTH, could, by this mechanism, contribute to the stimulatory effect of the hormone upon 2-ketoglutarate oxidation. Judging from the limited effect of the uncoupling agent DNP upon 2-ketoglutarate oxidation (Figure 8), this contribution must be relatively small.

In the absence of albumin or other fatty acid acceptors in the incubation medium, the fatty acids released by the lipolytic effect of ACTH will either be re-esterified or accumulate within the cell.[8] Adipose tissue requires glucose as a source of glyceride glycerol for fatty acid esterification.[3] 2DG, by inhibiting glucose utilization, would be expected to interfere with fatty acid esterification resulting in a further increase in tissue fatty acid levels. Thus, any effect of ACTH due to a rise in tissue fatty acid level should be more pronounced in the presence of ACTH and 2DG in combination. In the first experiment depicted in Figure 9, glycerol released into the medium was measured as an index of lipolysis. The addition of 2DG to the incubation medium resulted in a 22 per cent decrease in glycerol released in the presence of ACTH from 242 ± 14 to 189 ± 15 mμmoles per 100 mg tissue per hour (mean ± S.E.). 2DG inhibited total lipid synthesis from glucose-1-^{3}H by 79 per cent in the same tissues (Figure 9), leaving a large excess of fatty acid unesterified. As noted above, 2DG did not alter 2-ketoglutarate oxidation in the presence of ACTH (Figure 9). These findings suggest that the effect of ACTH upon 2-ketoglutarate oxidation does not result from the increase in tissue free fatty acid level induced by the hormone.

The exact mechanism by which ACTH, acting through cyclic AMP, stimulates 2-ketoglutarate oxidation was not elucidated by these studies. Further studies with DNP suggested that the mechanism is in part analogous to the mechanism of the lipolytic effect of epinephrine. Fassina[10] found that DNP inhibited norepinephrine stimulated lipolysis. He suggested that DNP action depleted the tissue of ATP necessary as a substrate for adenyl cyclase[2] and for lipase activation.[22] The level of cyclic AMP, in adipose tissue maximally stimulated with epinephrine, is low (approximately 10,000 picomoles per g dry weight)[23] in comparison to the level of ATP in unstimulated tissue (approximately 300,000 picomoles per g dry weight).[24] Fassina therefore suggested that of the two possibilities, lipase activation was more affected by ATP deficiency. DNP altered the effect of ACTH upon 2-ketoglutarate oxidation as it did the effect of epinephrine upon lipolysis (Figure 10). ACTH, 1 μg per ml, stimulated 2-ketoglutarate oxidation by 275 per cent. In the presence of ACTH, DNP, 1 mM, suppressed 2-ketoglutarate oxidation by 55 per cent. DBCAMP, 3 mM, stimulated 2-ketoglutarate oxidation by 71 per cent. DNP suppressed 2-ketoglutarate oxi-

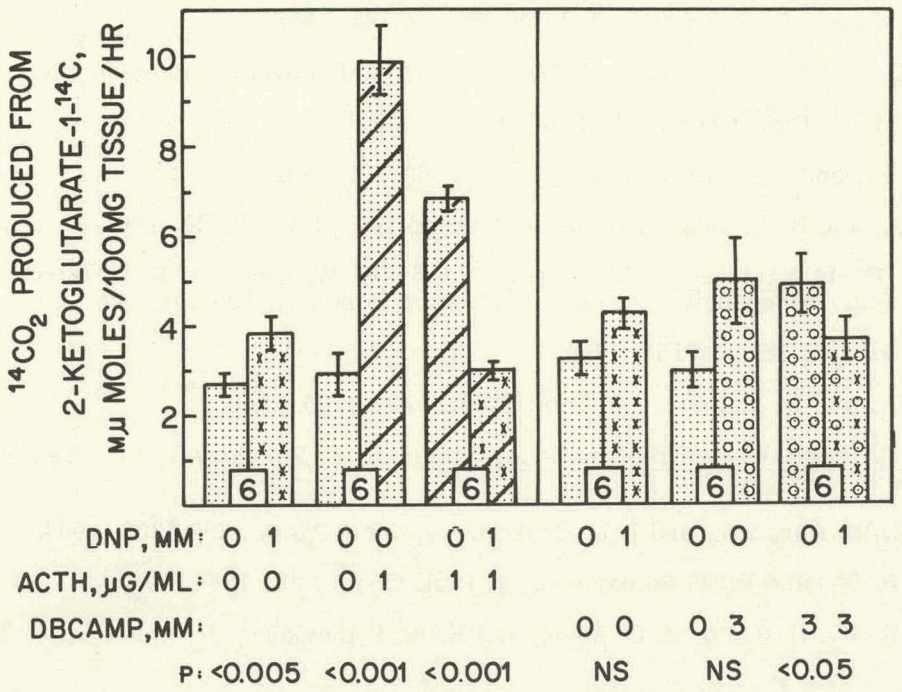

Figure 10. Effect of 2,4-dinitrophenol (DNP) upon ACTH and N^6-2'-O-dibutyryl-cyclic adenosine monophosphate (DBCAMP) stimulation of 2-ketoglutarate oxidation by isolated adipose tissue. The incubation medium contained 2-ketoglutarate-1-^{14}C (0.1 mM) and glucose (1.5 mg per ml). DNP (x), ACTH (hatched bars), ACTH plus DNP (hatched bars and x), DBCAMP (o), and DBCAMP plus DNP (o and x) were present at the indicated concentrations. See Figure 1 for further explanation of the figure.

dation by DBCAMP stimulated tissues by 25 per cent. These results are compatible with the possibility that the stimulatory effect of ACTH and of DBCAMP upon 2-ketoglutarate oxidation requires ATP or some other high energy compound which is deficient in tissues incubated with DNP.

A number of metabolites such as lactate, pyruvate, and ketone bodies inhibit the lipolytic effect of ACTH.[25] Enhanced Krebs cycle oxidation may assist in the removal of some of these metabolites and their inhibitory effects upon lipolysis.

ACKNOWLEDGMENTS

Miss Evelyn Damgaard provided expert technical assistance for this study. Mrs. Genevieve LaPinska assisted in preparation of the manuscript. Dr. L. B. Sorensen provided laboratory space and facilities. I thank him and Drs. R. H. Palmer and F. Kawahara for critical discussion of this work.

LITERATURE CITED

1. Sutherland, E. W., G. A. Robison, and R. W. Butcher. Circulation, 37:279, 1968.
2. Skosey, J. L. J. Biol. Chem., 241:5108, 1966
3. Lynn, W. S., R. M. MacLeod, and R. H. Brown. J. Biol. Chem., 235:1904, 1960.

4. Vaughan, M., and D. Steinberg. J. Lipid Res., 4:193, 1963.

5. Orth, R. D., W. D. Odell, and R. H. Williams. Am. J. Physiol., 198:640, 1960.

6. Vaughan, M. J. Biol. Chem., 236:2196, 1961.

7. Hagen, J. H., and E. G. Ball. Endocrinology, 69:752, 1961.

8. Ball, E. G., and R. L. Jungas. Proc. Nat. Acad. Sci. U.S., 47:932, 1961.

9. Cohen, P. P. In Manometric Techniques, Ed. 3. W. W. Umbreit, R. H. Burris, and S. F. Stauffer, Eds. Minneapolis: Burgess Publishing Company, 1957, p. 149.

10. Fassina, G. Life Sci., 5:2151, 1966.

11. Dole, V. P., and H. Meinertz. J. Biol. Chem., 235:2595, 1960.

12. Wieland, O. In Methods of Enzymatic Analysis. H. F. Bergmeyer, Ed. New York: Academic Press, 1963, p. 211.

13. Madsen, J., S. Abraham, and I. L. Chaikoff. J. Biol. Chem., 239:1305, 1964.

14. Butcher, R. W., and E. W. Sutherland. J. Biol. Chem., 237:1244, 1962.

15. Butcher, R. W., R. J. Ho, H. C. Meng, and E. W. Sutherland. J. Biol. Chem., 240:4515, 1965.

16. Steinberg, D., M. Vaughan, and S. Margolis. J. Biol. Chem., 235:PC38, 1960.

17. Aulich, A., K. Stock, and E. Westerman. Life Sci., 6:929, 1967.

18. Steinberg, D., M. Vaughan, and S. Margolis. J. Biol. Chem., 236:1631, 1961.

19. Blecher, M. Biochem. Biophys. Res. Commun., 27:560, 1967.

20. Parry, M. J., and D. G. Walker. Biochem. J., 99:266, 1966.

21. Hirshfield, I. N., and S. B. Koritz. Biochemistry, 3:1994, 1964.

22. Rizack, M. A. J. Biol. Chem., 239:392, 1964.

23. Butcher, R. W., C. E. Baird, and E. W. Sutherland. J. Biol. Chem., 243:1705, 1968.

24. Ohta, M., R. J. Jarrett, and J. B. Field. J. Lab. Clin. Med., 67:1013, 1966.

25. Carlson, Lars A. In Protein and Polypeptide Hormones, Part I. M. Margoulies, Ed. Amsterdam: Excerpta Medica Foundation, International Congress Series No. 161.

PERSISTENT IMPAIRMENT OF HAIR GROWTH AFTER SINGLE LARGE DOSES OF X-RAYS*

By

F. D. Malkinson,† M. L. Griem, and R. Marianovic

Hair matrix cells constitute physiologically unique populations, in which periods of exceedingly active cell proliferation alternate regularly with periods of total reproductive inactivity. Hair growth is cyclic, and progresses through three stages: anagen, the period of active matrix cell proliferation; catagen, a short-lived involutional stage; and telogen, the resting phase characterized by complete absence of cell division. Hair matrix cells provide a useful indicator system for in vivo studies on the effects of ionizing radiation or of a wide variety of pharmacologic agents on rapidly dividing or nonproliferative cell populations.[1] Radiation or pharmacologically induced changes in hair matrix cells may provide information useful for the evaluation of cellular responses in other tissues or organs, and, perhaps in malignant tumors.

Previous studies in mice[2] have shown that single doses of 200, 400, 600, or 800 rads impair anagen hair growth, as measured by dose-dependent reductions of 8 to 13 per cent in overall hair lengths. Irradiation of telogen hairs with single doses of 500, 1000, or 1500 rads resulted in dose-dependent reductions of 5 to 13 per cent in the lengths of the immediately succeeding "generation" of anagen hairs. For telogen hairs, a 2-1/2 fold greater dose of x-rays was required to produce growth retardation equivalent to that observed in anagen hairs.

The current study was planned to assess the duration of effects on telogen follicles of single, larger doses of ionizing radiation. Our goal was to determine whether more severe injury to resting follicles would permanently impair subsequent hair formation and growth.

METHOD

CF No. 1 female mice, three months old, were used in these experiments. A three square centimeter area was plucked on the back above each thigh in all animals. Plucking of telogen hairs immediately induces the anagen phase of the growth cycle. Since anagen lasts for about 19 days in this strain of mouse, preliminary plucking and "cycling" insured the presence of telogen hairs when radiation was subsequently administered on the 24th day after plucking. In the animals treated with 1500 rads, hairs were plucked immediately after irradiation to induce anagen. Telogen hair samples were removed from control and treatment sites 24 days after irradiation (first plucking) and, again, 24 days later (2nd plucking). In animals receiving 2000 and 2500 rads, hairs were plucked two months after irradiation to induce anagen. Telogen hair samples (first plucking) were taken from control and treatment sites four weeks later—three months after irradiation—and ten months after irradiation (2nd plucking).

---

*This report is taken from a paper that appeared in Radiation Research, 43:83, 1970. The work was supported by grants from the U. S. Public Health Service Division of Radiological Health and the U. S. Atomic Energy Agency.

†Section of Dermatology, Department of Medicine, Presbyterian-St. Luke's Hospital, and the Departments of Medicine and Dermatology, The University of Illinois College of Medicine.

Radiation was delivered with a Machlett OEG - 60 tube operated at 50 kV and 30 mA with 2 mm Al filtration added. This produced a surface dose of 402 rads/min at a focal skin distance of 11 cm, and a beam quality of 1.2 cm half-value depth in tissue. A single 2 cm portal was irradiated on the right back above the thigh. Single surface doses of 1500, 2000, and 2500 rads were administered to separate groups of mice. The animals were adequately shielded and treated individually without anesthesia.

For subsequent hair length measurements all irradiated animals served as their own controls.

Several hundred hairs from each final sample were floated on a shallow layer of water in a glass Petri dish. The hairs were examined with a binocular dissection microscope which permitted ready identification of the four types of mouse hair.[3] Except for some thinning of the shaft, no dystrophic or other morphologic alterations were noted in hair removed from irradiated areas. Twenty to twenty-five intact awl-type telogen hairs were removed from the Petri dish with a small forceps and placed parallel to each other in rows on a standard 3.5 x 4.0 inch lantern-slide glass plate. A 4 x 1 cm strip of translucent graph paper was placed along the lower right corner of the plate. A second identical glass plate was taped firmly to the first, and the resulting slide was projected onto a screen, giving a 15 to 17-fold image enlargement.

The magnified images of all intact hairs were "traced" with pencil on paper placed over the screen, and their lengths subsequently measured with a flexible rule. Actual hair lengths were calculated by correcting the measured magnified lengths according to the magnification factor of the projected unit scale or graph paper.

In normal unirradiated animals variations in awl-type telogen hair lengths between contralateral sites were less than 2 per cent, and usually less than 1 per cent.

Statistical analysis of experimental data included computation of the standard deviation of the mean and the standard error of the mean.

Microscopic studies of skin specimens were carried out 15 months post-irradiation. Hairs were plucked from treatment and control sites, and 15 days later each mouse received a peritoneal injection of 20 μCi of tritiated thymidine (specific activity: 14.0 Ci/millimole). Serial skin biopsies were begun one hour later and continued at hourly intervals for 22 hours. All biopsy specimens were taken with a 3 mm dermal punch without anesthesia. Not more than 6 biopsies each from control and treatment sites were taken from any one animal.

Skin biopsies were fixed in buffered formalin and sectioned at 4 microns. Autoradiographs were prepared with Ilford K_2 emulsion. These were developed after three weeks exposure at 4° C.

Not less than 100 mitoses were scored for each hourly interval studied.

RESULTS

The results of the hair measurement studies are presented in Table 1. When telogen hairs were exposed to single doses of radiation, hair growth, as measured by overall hair length, was significantly reduced in the next succeeding hair generation. In the animals receiving 1500 rads, a 12 per cent reduction in length was found in hair induced to grow immediately post-irradiation and plucked 24 days later.[2] Hair length measurements in the next or second hair generation 48 days post-irradiation showed complete recovery from radiation effects.

In the animals treated with higher doses of radiation only 3 of 12 mice receiving 2500 rads

Table 1

REDUCTIONS OF HAIR LENGTH IN MICE RECEIVING RADIATION IN EARLY TELOGEN

Dose (rads)	Animals	Average length (mm) control	Average length (mm) irradiated		% growth retardation		Standard error of mean % retardation
			1st plucking	2nd plucking	1st plucking	2nd plucking	
1500	10	7.80	6.88[a]	7.55	12	3	0.564, 2.1
2000-2500	15	7.41	5.41	4.98	27	33	1.14, 1.62

[a]Previously reported.[2]

survived the study period. Consequently the animals receiving 2000 and 2500 rads have been treated as a single experimental group. All of these mice showed some post-irradiation hair loss three weeks after treatment. This gradually increased in severity until four weeks later when moderate to severe post-irradiation alopecia was seen in all animals. The severity of hair loss was comparable in animals irradiated at both 2000 and 2500 rads. After another week the remaining hairs were plucked. Four weeks later substantial hair regrowth had occurred, although only about 2/3 of the irradiated follicles appeared to survive. At this time—three months after irradiation—hair lengths of telogen samples were reduced 27 per cent below those from the control sites. Hair shafts from the treatment sites showed some thinning as well as marked shortening (Figure 1). Hairs were again removed from these animals ten months post-irradiation, at which time overall hair lengths were reduced 33 per cent in the treatment areas, and hair shafts remained abnormally thin. Student's t test revealed a significant difference between the lengths of the 3-month post-treatment hairs (reduced 27 per cent) and the 10-month post-treatment hairs (reduced 33 per cent).

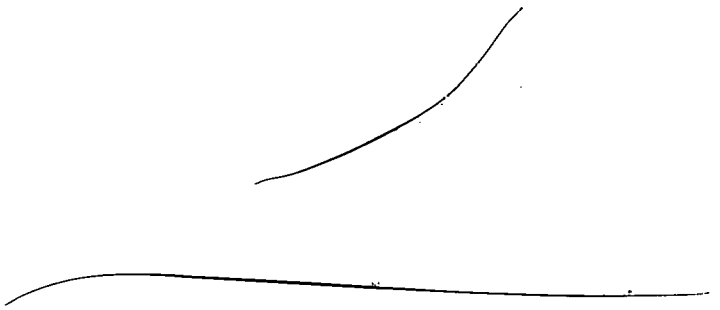

Figure 1. Thinning and shortening of hair 3 months after treatment of telogen follicles with a single dose of 2000 rads. Lower hair was removed from contralateral control site (magnification X15).

Full replacement of surviving hairs plucked from treatment sites was substantially retarded at all times up to 14 months post-treatment. Replacement of hair was complete within 2-1/2 weeks in the plucked control areas, but took four weeks or longer in the irradiated areas (Figures 2a,2b). Loss of a substantial number of animals precluded extensive histologic studies of hair regrowth but repeated gross observations suggested that growth was particularly slowed in the pre-eruptive stages of anagen.

Comparison of growth rates in normal hairs removed from control sites at different times revealed no significant change in hair length. The average lengths of normal awl hairs differed by only 0.02 millimeters between 3 and 13 months. Biopsy sections and autoradiographs revealed that the duration of the matrix cell cycle was not significantly altered in the treatment sites 15 months after irradiation (Figure 3a,3b). The mitotic index on the irradiated side was 0.68 per cent, which is a substantial reduction from the 1.51 per cent recorded on the control side. Undue emphasis should not be accorded to such index determinations, however, since the total population of hair matrix cells is not well defined in histologic preparations. Hair matrix populations vary in size considerably from one hair type to another, and the relative radiosensitivity of the various hair types has not been precisely determined. Isolation of single follicles by re-

A

B

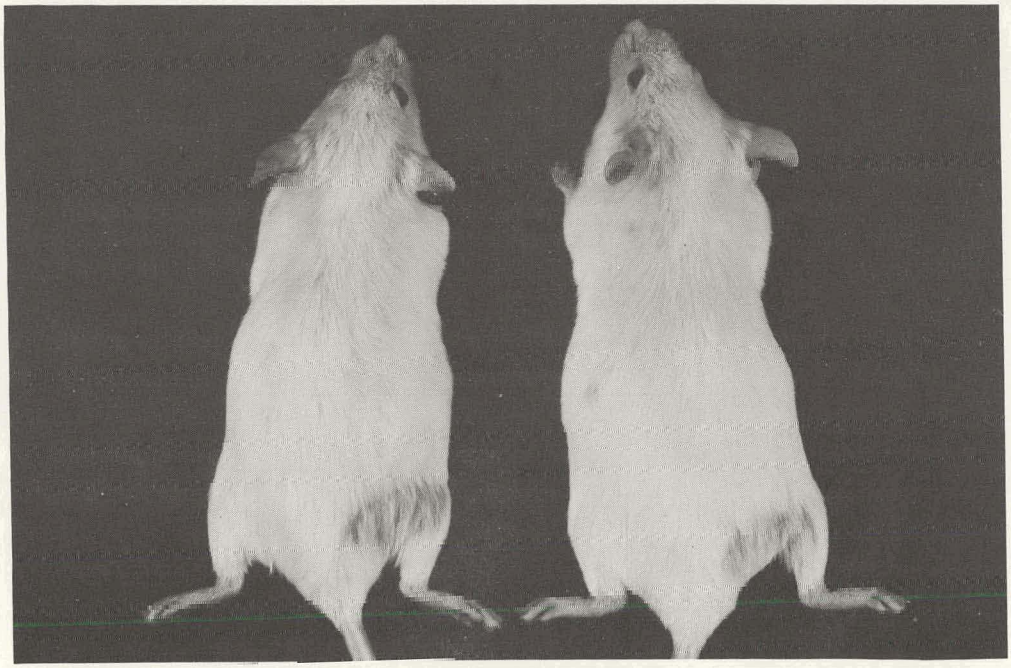

Figure 2. A. Retarded hair replacement at sites of irradiation (right legs) 16 days after plucking of treatment sites and contralateral control areas. Photograph taken 14 months after administration of 2000 rads. B. Same animals as in Figure 2A. Photograph taken 14 days later, or 30 days after plucking. No additional regrowth of hair was seen in the treatment sites after the 30-day period.

A

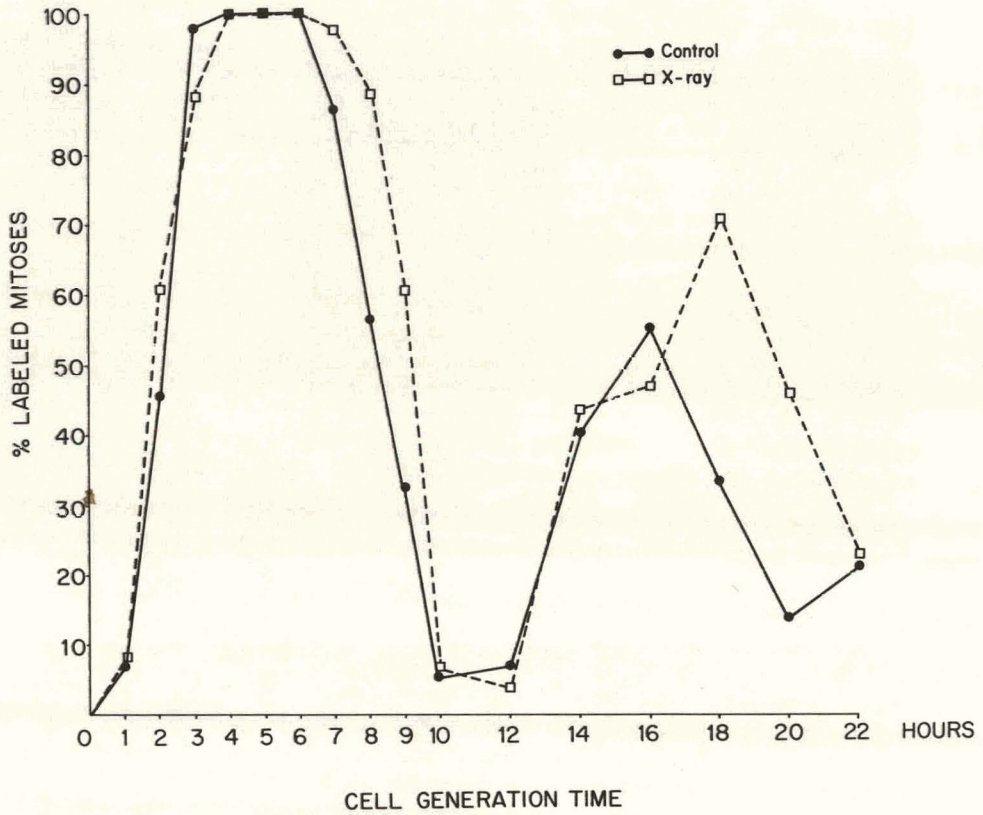

B

Control side	Irradiated side
T_{G_2} + 1/2 M ~ 2 hours	T_{G_2} + 1/2 M ~ 2 hours
T_S ~ 6 hours	T_S ~ 7 hours 30'
T_{G_1} + 1/2 M ~ 5 hours 30'	T_{G_1} + 1/2 M ~ 5 hours 00'
T_C ~ 13 hours 30'	T_C ~ 14 hours 30'

Figure 3. A. Labeled mitoses curves from irradiated and control sites. Biopsies taken 15 months post-radiation. B. Duration of hair matrix cell nuclear cycle and its subdivisions for control and irradiated sides. Computed from labeled mitoses curves, Figure 3A.

cently developed techniques should provide for more precise mitotic and/or labeling index determinations in the future.

DISCUSSION

Acute exposure to ionizing radiation produces a variety of changes in hair. Morphologic abnormalities,[4] depigmentation,[5] and impaired incorporation of isotope-labeled amino acids or other compounds into hair[6] may all follow irradiation. Moderate single doses of radiation temporarily reduce growth rates in both anagen and telogen hairs.[2] The present study indicates that single large doses of radiation delivered to telogen hairs permanently reduce the growth rates of all succeeding hair generations, at least within the observation period of ten months. Radiation effects vary from immediate, one-generation post-irradiation length reductions of 5 per cent after 500 rads[2] to the sustained length reductions of 27 per cent to 33 per cent following exposure to 2000 to 2500 rads observed in the current study. Only in the higher dose ranges are hair replacement rates visibly slowed. The severity and duration of these changes are clearly dose-dependent.

In the past, responses to radiation have been studied far more intensively in mitotically active cells than in resting cell populations. Impaired growth of anagen hairs following irradiation of predecessor telogen hairs demonstrates that nondividing (probably G_0) matrix cells are susceptible to radiation damage. Since onset of matrix cell division does not follow until 72 hours after plucking,[7] telogen matrix cells apparently sustain and "store" radiation damage, which is then expressed in succeeding cell generations following appropriate mitotic stimuli. Since there is, as yet, no experimental evidence for the migration of epithelial or connective tissue cells from one hair follicle or papilla to another, the destruction or survival of a follicle after irradiation, as well as the degree of recovery from injury, depends entirely on cell responses in situ.

From the studies reported here certain questions arise concerning possible alterations in cell kinetics and the mode of persistence of radiation effects. An essentially normal matrix cell cycle in the sites treated with high doses of radiation indicates that a prolonged cell cycle is not primarily responsible for the abnormally small hairs or slowed regrowth rates: It seems more likely that these changes result from an overall reduction in size of the stem cell pool. The number of matrix cells undergoing differentiation and maturation is presumably depleted in proportion to the smaller size of the proliferative cell population. This proposal receives support from the substantially reduced mitotic index for irradiated matrix cells. The prolonged duration of hair changes found in these studies and the increased shortening of hairs between the 3-month and 10-month periods post-treatment also suggest that some of the long-term alterations observed in epithelial cell populations may be the consequence of progressive radiation injury to the fine vasculature of the hair papillae. Persistent cellular damage such as chromosomal aberrations in epithelial or connective tissue cells may also be a contributory factor. Studies are currently planned to investigate these possibilities.

LITERATURE CITED

1. Griem, M. L., and F. D. Malkinson. In Frontiers of Radiation Therapy and Oncology, Vol. 4. J. M. Vaeth, Ed. New York: S. Karger, 1969, pp. 24-45.

2. Malkinson, F. D., and M. L. Griem. Arch. Dermatol., 94:491, 1966.

3. Dry, F. W. J. Genetics, 16:287, 1926.

4. Williams, A. W. Brit. J. Dermatol., 18:63, 1906.

5. Chase, H. B. J. Morph., 84:57, 1949.

6. Malkinson, F. D., and M. L. Griem. Radiation Res., 33:554, 1968.

7. Johnson, E. In Biology of the Skin and Hair Growth. A. G. Lyne and B. F. Short, Eds. Sydney: Angus and Robertson, Ltd., 1965, pp. 491-505.

BIOLUMINESCENCE AND RADIATION RESPONSE OF PHOTOBACTERIUM FISCHERI H-2*

By

I. A. Lerch

It is the purpose of this paper to extend the discussions on the interactions of radiation with microbiological targets to a system amenable to in vivo surveys of cellular function. The intense bioluminescence of Photobacterium fischeri H-2† provides a simple means for monitoring an asynchronous suspension of cells at varying intervals after irradiation. Clues to the mechanisms of radiation damage may be derived from measurements of the radiation-altered cellular luminescence. Ideally, any monitored cellular expression should be biochemically defined and easily measured. Although bacterial luminescence certainly satisfies the latter requirement, it is far from being a fully understood phenomenon. Enough of the central features of the luciferase enzyme system have been studied by Hastings, Gibson et al,[1-4] however, to permit a general radiobiological study.

MATERIALS AND METHODS

Bacterial cell preparation. Photobacterium fischeri H-2 is a rod shaped flagellate of marine origin approximately 0.5 micron x 2.0 micron which emits a brilliant blue-green bioluminescence that peaks at a wavelength of 490 nm. The agar and nutrient broth that constitute the growth media are as prescribed by Farghaly[5] plus 5.0 g/L pancreatic digest of casein‡ and 0.5 g/L yeast extract.§ Inocula taken from agar subcultures were grown in saline nutrient broth at 25° C with either mechanical agitation or simple gas infusion for attainment of air equilibration in a stoppered one-liter Ehrlenmeyer flask. Sample suspensions were not gassed during or after irradiation. The estimated time periods between withdrawal of aliquots from the gassed population to the end of the radiation exposure were about one minute for low doses (5 K rads to 50 K rads) and up to 5 minutes for high doses (above 70 K rads). Growth was monitored by measuring the optical density at 600 nm of a sample suspension in a test tube spectrophotometer. One milliliter and 2.6 ml aliquots of suspension were introduced into sterile plastic test tubes¶ which were placed in a masonite phantom for exposure to an unanalyzed 20 MeV pulsed electron beam. Bioluminescence of the suspension was measured pre- and post-irradiation. Dilutions for plating were accomplished with 1.25 M PO_4 buffer adjusted to a pH of 7. Oxygen concentration of the suspensions was monitored with the Beckman 39065 polarographic oxygen sensor coupled with the Model 777 oxygen analyzer. During each irradiation experiment, the growth of the sus-

*This report is taken from a paper that appeared in Radiation Research, 43:161, 1970.

†Cells so designated by K. Nealson, Department of Microbiology, University of Chicago, who procured them from the laboratory of J. W. Hastings, Biological Laboratories, Harvard University.

‡Bacto-tryptone from Difco Laboratories, Detroit, Michigan.

§Bacto-yeast extract from Difco Laboratories.

¶Falcon plastic 12 mm x 75 mm capped test tubes Model No. 2003.

pension was monitored to determine the asynchronous growth phase and provide control measurements for the survival curves.

Linear accelerator and dosimetry. The characteristics of the linear accelerator have been reported in detail by Skaggs et al,[6] Wood and Skaggs* and Skaggs and Lanzl.† The beam was tuned to an energy of 20 MeV and extracted from the linear section of the accelerator without magnetic analysis. The modulating pulse was monitored with a toroidal coil pulse transformer coupled to an oscilloscope equipped with a Polaroid camera. The pulse was nominally tuned to a rectangular configuration with variable amplitude from 8 to 360 mA and with variable duration from 0.5 to 1.5 μsec. The pulse repetition frequency for all irradiations was 60 Hz. The dose rate per pulse to the experimental interspace was calibrated for each experiment with EG & G glass capillary encapsulated CaF_2 TLD microrods. In order to determine the standard deviations due to pulse inconsistencies and dose gradient at the target, multiple exposures of groups of three such microrods in test tubes were made at varying intervals from the irradiation port under simulated experimental conditions. The experimental exposures were not measured with TLD but doses were determined by counting the number of calibrated pulses delivered to the target. The pulses were monitored for constancy during irradiation with the oscilloscope coupled pulse transformer mentioned above. The microrods were calibrated with respect to the scanning pencil beam ion chamber which, in turn, had been calibrated with Faraday cup measurements and chemical dosimetry.‡ The doses per pulse thus obtained varied from 10 rads to 6,000 rads depending upon tuning conditions and distance from the irradiation port and all dose rates to include dose nonuniformities are recorded on the appropriate figures. All dose rates presented in this report are determined for the 0.5 to 1.5 μsec pulses. The RF duty cycle is unknown hence no effort was made to estimate the instantaneous dose rate associated with the carrier wave pulse. Periodic determinations of the pulse isodose distributions at the various intervals from the irradiation port were made with Adlux film in an appropriate phantom under conditions of reduced beam intensity. The film measurements were consistent with the TLD measurements.

Bioluminescence measurements. The purpose of the experimental electronics was to measure the post-irradiation bioluminescent output of a given aliquot of cellular suspension as a function of time. Samples, 2.6 ml to 3.0 ml, were introduced into glass scintillation vials which were placed into our EG & G TLD reader equipped with a special adapter head. The phototube current was then monitored either with a strip chart recorder or the circuit illustrated in Figure 1. The output of the phototube was fed into an operational amplifier with a diode feedback loop thus yielding a log signal which was amplified and put into an x-y plotter for visual display. The remaining circuitry measured the slope of the semi-log decay curve§ for the purpose of studying the glow curve kinetics. A ramp generator was included as the time drive for the x-y plotter. Calibration of the apparatus was arbitrary but maintained constant with respect to a light standard in our laboratory. The units of light intensity used in the strip chart recordings

*G. T. Wood, and L. S. Skaggs, ACRH Semiannual Report to the AEC, ACRH-7:69, 1957.

†L. S. Skaggs, and L. H. Lanzl. Presented at the 9th International Congress of Radiology, July 1959, Munich, Germany. ACRH Semiannual Report to the AEC, ACRH-12:31, 1959.

‡The ion chamber calibrations were done by M. Rozenfeld, Argonne Cancer Research Hospital.

§See pp. 147-48[7] for a discussion of this differentiator circuit.

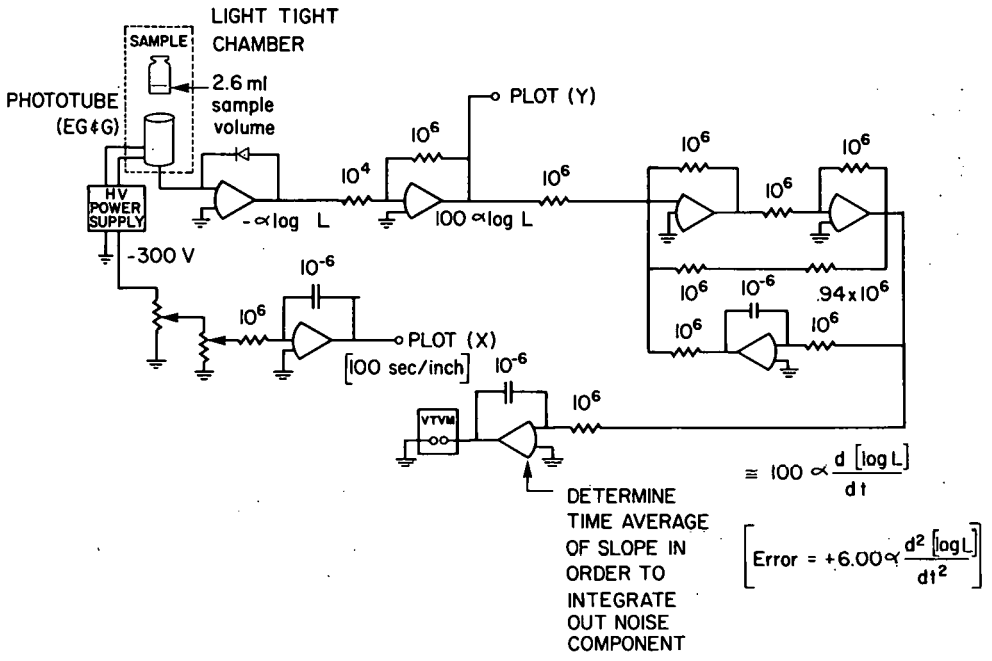

Figure 1. Schematic representation of the experimental electronics used to obtain semi-log time dependent plots of bioluminescent intensity. Sample volumes varied from 2 to 3 ml.

are simply volts of signal input to the measuring instrument. The log units employed in the x-y recordings are weighted by the electronic calibration factor α introduced by the diode feedback network.

RESULTS

Glow curve kinetics. If an aliquot of a suspension of cells in nutrient broth is introduced into a scintillation vial, mechanically agitated, and then inserted into a light detection chamber, the glow curve of Figure 2 is obtained. The luminescence intensity builds to a plateau, drops slightly, and then falls sharply to an almost constant (gradually declining) residual level between 10 per cent and 50 per cent of the peak intensities. The duration of the initial plateau is extended by increased mechanical agitation and higher oxygen concentration but diminishes with increasing cellular concentration.

Bioluminescent survival. Bioluminescent survival is defined as the fraction of luminescence exhibited by an irradiated suspension with respect to the control luminescence. The measurements of luminescence are made upon equilibration of the samples approximately 1 to 2 hours after irradiation at which time the luminescence intensities remain constant (this is defined as the ultimate decay level). Figure 3 is a semi-log time-dependent plot of ultimate decay levels as a function of dose for a late exponential phase suspension. It should be noted that not only does the time duration of the bioluminescence plateau increase with dose, but the luminescent intensity depreciates at the plateau and residual levels with the peaking phenomenon disappearing altogether at the higher doses.

Glow curve of the irradiated suspension. Figure 4 is an overlay of a time-dependent semi-log plot derived from an experiment with an immature (i.e., exponential phase) cellular suspen-

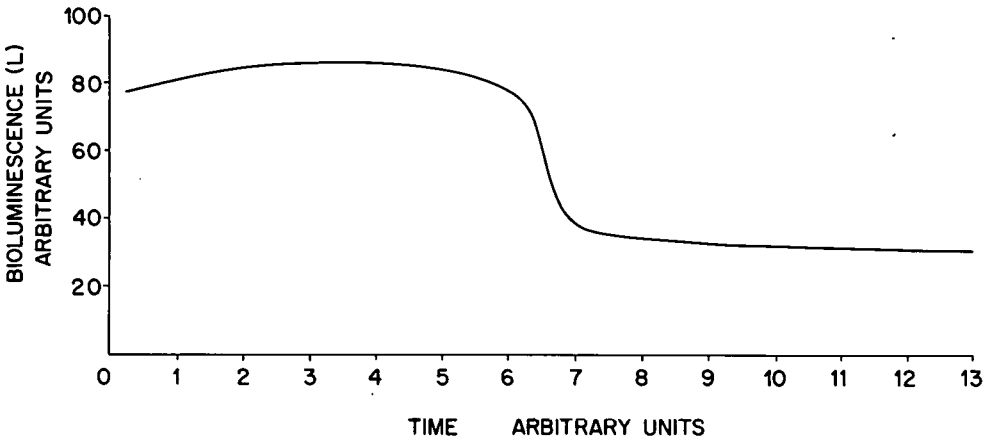

Figure 2. Representative glow curve of an oxygenated or air equilibrated suspension of asynchronously growing or stationary phase cells. The scale values are arbitrary and dependent on growth phase, concentration of oxygen dissolved in the suspension and the degree of mechanical agitation prior to measurement.

sion. It will be noted that the plot has 2 sections. The first section is the immediate postirradiative function derived one minute or less after exposure and illustrates the kinetics of bioluminescence decay. The second section of the plot is a record of the ultimate decay levels of the residual bioluminescence measured approximately 1.5 hours after irradiation and exemplifies

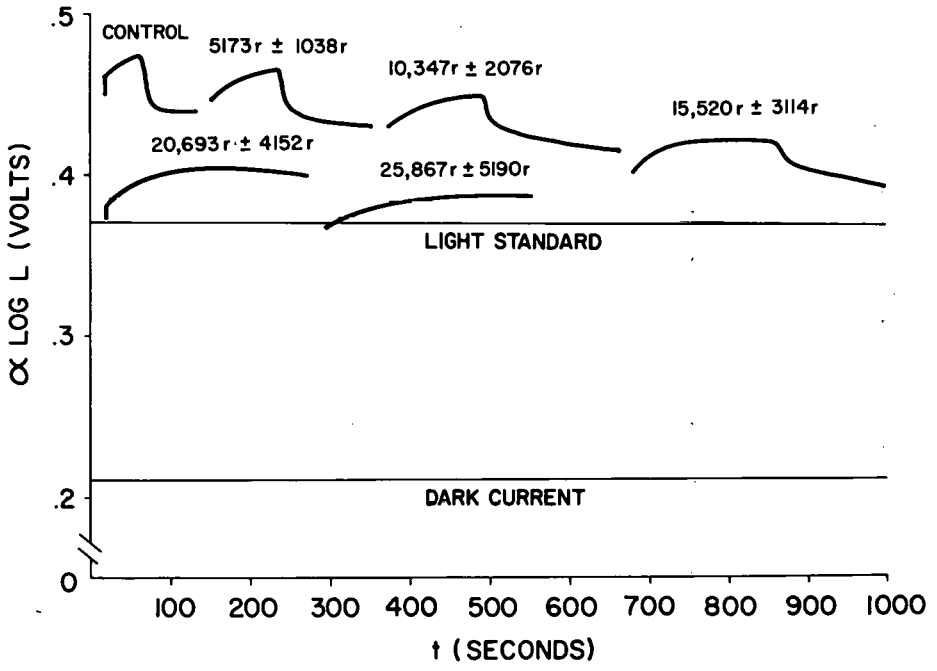

Figure 3. Semi-log time dependent bioluminescence plots of irradiated "late" exponential phase asynchronous suspensions. Samples were irradiated with an unanalyzed 20 MeV electron beam with 0.65 μsec 360 mA peak modulated pulses. The dose rate was $9.95 \pm 2.00 \times 10^8$ rads/sec averaged over the pulse.

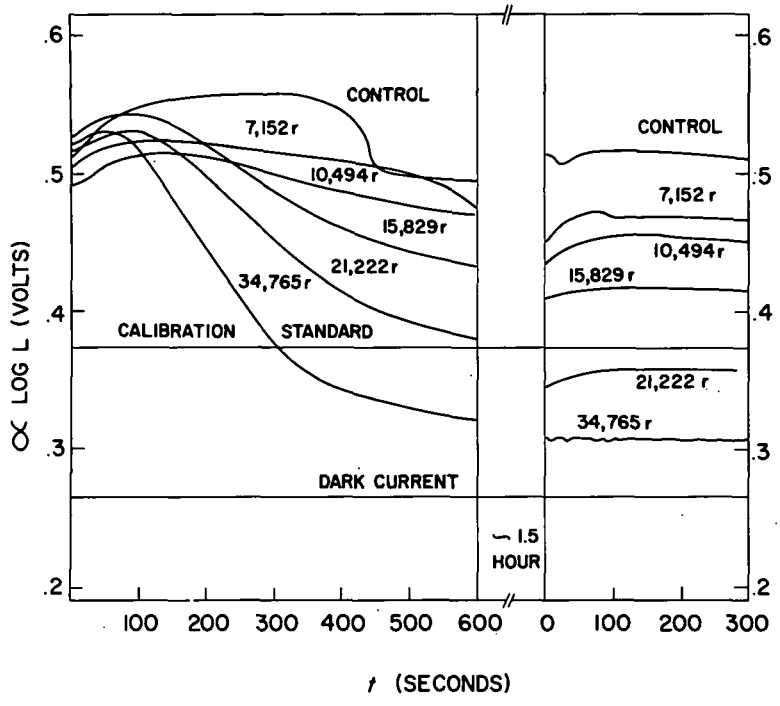

Figure 4. Immediate postirradiation semi-log time dependent glow curves for varying exposures. The second section was recorded approximately 90 min after the termination of the initial measuring interval. Samples were irradiated with an unanalyzed 20 MeV electron beam with 1.1 μsec pulses at a dose rate of 5.86 x 10^7 rads/sec averaged over the pulse.

the type of data employed for determining bioluminescence survival. After each measurement, the x-y recorder was reset so that a cumulative record of glow curves was obtained for purposes of intercomparison. Each plot is labeled with the dose delivered to the sample. The survival curve derived from the second section of this plot has the following exponential regression parameters (but is not presented in graphic form here):

Extrapolation number (n) = 1.94

D_o = 4,127 rads

Standard error of estimate* (S_e) = 0.23

Figure 5 is a linear plot of the function β (to be defined in the Discussion section) and the electronically measured slope of the immediate postirradiative semi-log decay plots (measured in the interval between bioluminescence peaking and leveling to ultimate decay intensities) as a function of dose. These functions are reasonably linear and will be considered in detail. The measured slope is determined in units of mv/second which is then divided by the electronic calibration factor a introduced by the log amplifier in the measuring circuit.

Clonogenic versus bioluminescent survival. The results of the experiment reported above describe the behavior of those cells able to emit luminescence after exposure to irradiation. Classical experiments determine the cell's capacity to divide and form viable clones. Compari-

*This is the standard error of estimate for the fitted semi-log expression.

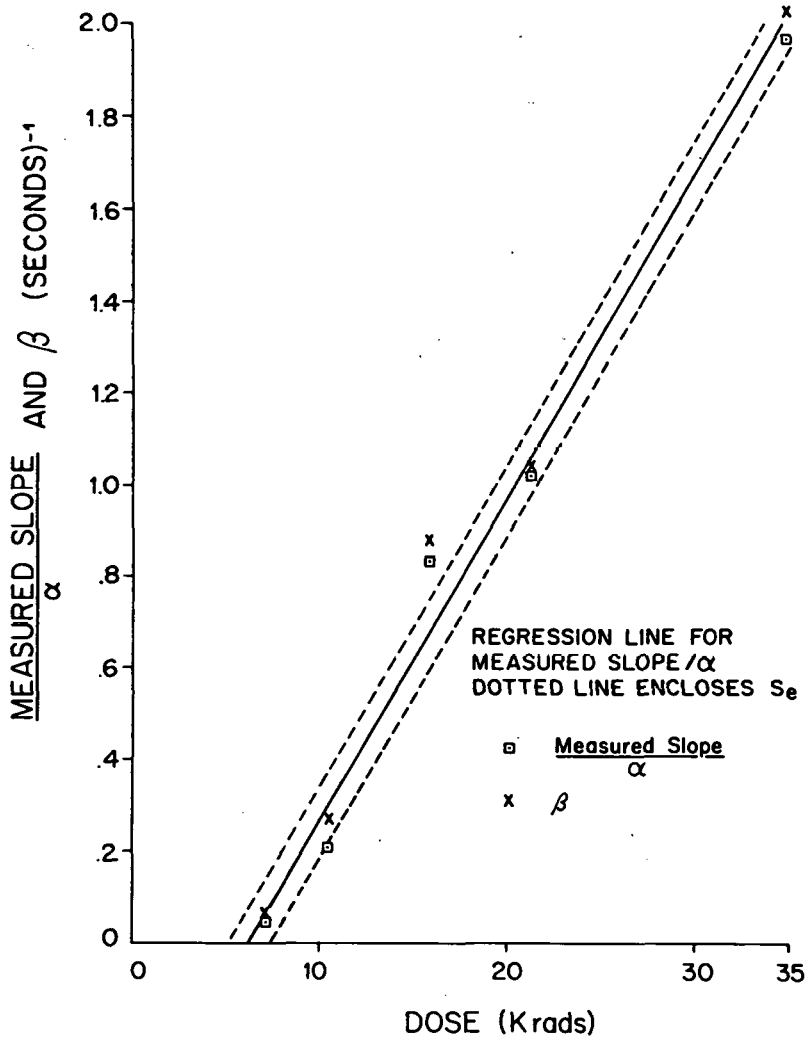

Figure 5. Electronically measured slope and β as a function of dose for the experiment represented in Figure 4. The measured slope is obtained from the electronic circuitry of Figure 1 for the semi-log decay curves of Figure 4. The function β is defined in the text by expression 4 and is obtained experimentally from the relation, measured slope = $\frac{N_d}{N_o}\beta$.

son of the results of these two techniques should then be expected to provide information that would enable the experimenter to differentiate between reproductive damage and general physiological damage as expressed in cellular bioluminescence. Figure 6 represents data obtained from a single experiment during which a stationary phase suspension of air equilibrated cells was exposed to varying doses of radiation. The ultimate bioluminescent intensities were measured after an adequate decay interval of approximately 2 hours. The ratio of the clonogenic survival slope to the bioluminescent survival slope was 2.33.

DISCUSSION

Glow curve. The dependence of the glow curve kinetics on the degree of mechanical exci-

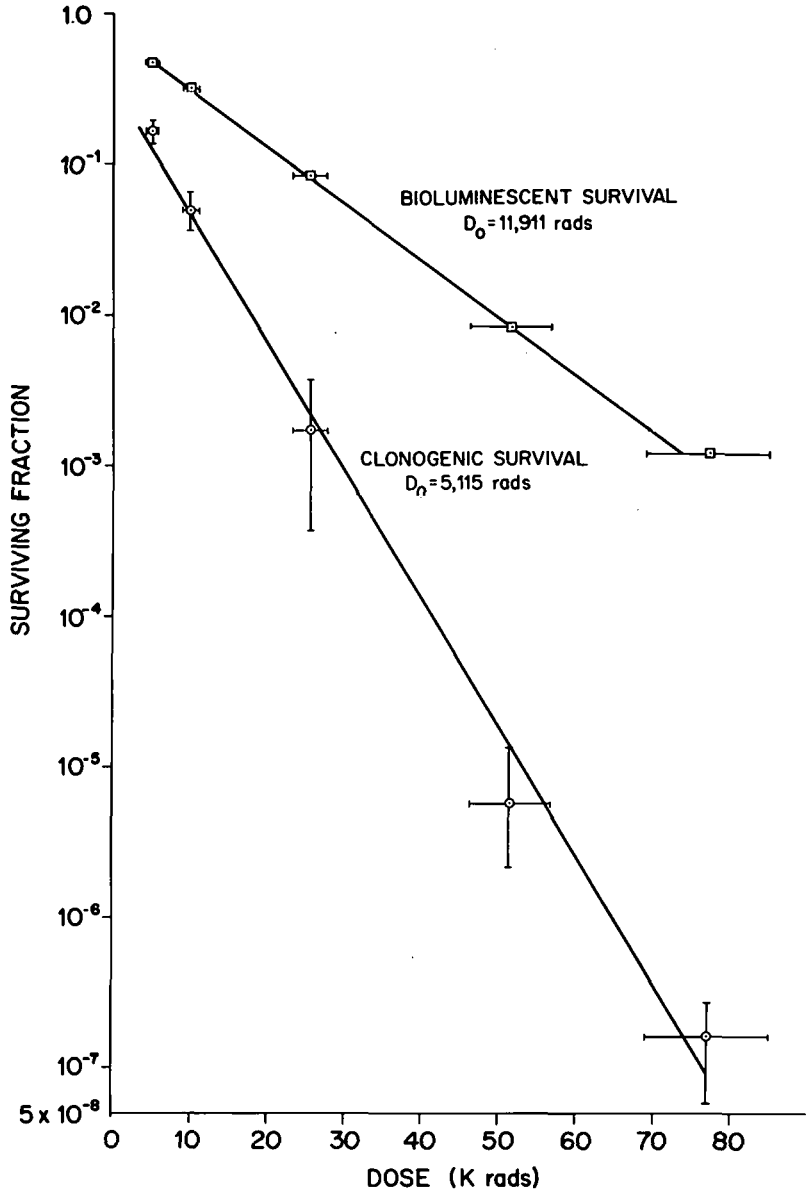

Figure 6. Clonogenic and bioluminescent survival for air equilibrated suspensions. Samples were irradiated with an unanalyzed 20 MeV electron beam with 1.25 μsec 8.4 mA peak modulated pulses. The dose rate was 6.87 ± 0.71 x 10^7 rads/sec averaged over the pulse.

tation and the relation between cellular concentration and the time duration of the bioluminescence plateau are consistent with a model proposed by Vladimirov for luminescence from homogenates.[8] The initial intensification of luminescence is taken to indicate the accumulation of an oxidized product. The production of luminescence occurs when the oxidized product combines with another reactant. Hence, immediately subsequent to mechanical agitation of the suspension, the cells are brought into proximity with the dissolved oxygen. As the increased flux of oxygen penetrates into the cell interior, the oxidized product accumulates promoting increased luminescence. If the rate of formation of the oxidized product is slightly greater or less than the

light producing reaction, the glow curve will increase slightly or decline. If the oxidized product suddenly stops accumulating, as would occur if any of the reactants were exhausted (e.g., oxygen would be used up if the supply is restricted during measurement), the luminescence will fall as the oxidized product is used up. The residual level of luminescence would then be a consequence of the light produced by a small surface layer of cells which have access to atmospheric oxygen in the scintillation vial. An increase in the concentration of oxygen available to the cellular suspension or a drop in cellular concentration could account for changes in the time duration for the luminescence plateau observed in Figure 3 by altering the total amount of oxygen available to the cells over the measurement interval. This scheme is consistent with the biochemical picture drawn by Hastings and Gibson[1-4] derived from an in vitro luciferase enzyme system of P. fischeri. In their picture of bioluminescence, Hastings and Gibson have proposed the oxidation of a reduced luciferase enzyme intermediate to produce a long-lived bioluminescent intermediate. This oxidized product then leads to the production of high quantum yield luminescence in an aldehyde mediated reaction pathway.

Immediate postirradiation glow curve kinetics. It would be of value to be able to differentiate between the case in which damaged cells "turn off" luminescence or simply glow with diminished intensity. The former possibility associates the reduction of luminescence with a cataclysmic event which totally blocks one or more critical biochemical functions and could be a reflection of actual cell death. A kinetic model formed from either of these postulates should implicate the appropriate mechanism for cell damage when compared with the results reported in Figure 4.

As may be seen from the data given in Figures 3, 4 and 6, the ultimate bioluminescent survival levels describe the normal exponential function associated with the expression of radiation damage by simple microbial systems. This feature must be incorporated into any model of population kinetics seeking to relate the time decay of postirradiation luminescence as a function of dose. The assumption will be made that radiation damaged cells fully extinguish their luminescence. If this assumption is correct, then the plots of Figure 4 will serve to substantiate the following arguments.

Let N be the number of cells glowing at time t, N_d be the number of damaged cells capable of glowing immediately after exposure which will eventually lose all luminescence and N_o be the number of cells in the suspension which is irradiated. N_d will be a function only of dose and $N_o - N_d$ will represent those cells giving rise to the ultimate decay levels of luminescence. Hence, the number of cells still glowing at time t after irradiation which will be extinguished is $N - (N_o - N_d)$. Simple population kinetics may be used to relate the change in the number of cells glowing at time t after irradiation to the population $N - (N_o - N_d)$ as follows:

$$dN = - \beta [N - (N_o - N_d)] dt \quad (1)$$

where β is the rate constant regulating the decay of luminescence. Expression 1 may be rearranged and integrated to yield the following:

$$N = N_o - N_d (1 - e^{-\beta t}) \quad (2)$$

The experimental circuitry of Figure 1 essentially monitors the logarithmic form of expression 2. By taking the logarithm of expression 2 and making a two term Maclaurin expansion of the result, a relation may be derived which describes the semi-log time-dependent decay of postirradiation luminescence as follows:

$$\ln N_{t \to o} \cong \ln N_o - \frac{N_d}{N_o} \beta t \tag{3}$$

Hence, the model based on population kinetics predicts that the initial decay of luminescence will be exponential, as is indeed the case. However, the decay is modulated by the magnitude of the damaged fraction (which is a function of dose). The damaged fraction is equal to 1—the surviving fraction which is a slowly varying function of dose whereas, from Figure 5, the slopes of the decay curves vary linearly as dose. This latter fact is illustrated in Table 1. Hence, the assumption that radiation damaged cells fully extinguish their luminescence according to simple population kinetics, is untenable. The rate constant β must be a linear function of dose (see Figure 5). It would thus appear that the postirradiation cellular luminescence is a direct function of dose such that many cells are capable of luminescence but at reduced intensities. This strongly suggests that the enzyme system itself is the target.

Table 1

BIOLUMINESCENCE DECAY CURVE PARAMETERS AS A FUNCTION OF DOSE

Dose (rads)	Measured slope (mv/sec)	$\frac{N_d}{N_o}$	β
7,152	1.56	0.74	0.06
10,494	6.94	0.78	0.27
15,829	28.18	0.96	0.88
21,222	34.75	0.99	1.04
34,765	67.00	0.99	2.02

Additional radiobiological parameters may be defined by writing the rate constant as a linear function of dose,

$$\beta = CR + A \tag{4}$$

where R is dose and C and A are constants dependent only on radiosensitivity. By referring to expression 2 it may be seen that the fraction $\frac{[N - (N_o - N_d)]}{N_d}$ represents the quotient of the damaged cell population still glowing at time t after receiving a dose R. When this fraction falls to 1/e at the time t_e, from 2 and 4 the following expression is derived:

$$R = \frac{1}{Ct_e} - \frac{A}{C} \tag{5}$$

From Figure 5, it has been determined that $1/C = 14.3$ K rad-seconds and t_e varies between 100 to 300 seconds. The ratio A/C was 5.3 K rads. Since the ratio $1/Ct_e$ is relatively small, A/C may be defined as the dose necessary to reduce the fraction of the damaged cell population still glowing to 1/e in the time t_e. This dose (5,295 rads) for Figures 4 and 5 was of the same order of magnitude as the dose D_o (4,127 rads). Table 2 summarized the computed regression parameters for this experiment.

Clonogenic versus bioluminescent survival. The enhanced radiosensitivity of the cellular reproductive function with respect to bioluminescence is probably a reflection of the relative biochemical importance of these two processes. The number of biochemical targets afforded by

Table 2

LINEAR REGRESSION PARAMETERS FOR THE EXPRESSION X = CR + A WHERE X = β AND (MEASURED SLOPE)/α

X $(sec)^{-1}$	C $(K\ rad\text{-}sec)^{-1}$	A $(sec)^{-1}$	R_e[b] (rads)	S_e $(sec)^{-1}$
(Measured slope)/α	0.07	-0.44	6,271	0.084
β	0.07	-0.37	5,295	0.087

[b] $R_e = \frac{1}{Ct_e} - \frac{A}{C}$

the property of bioluminescence is limited in contrast to the large number of interdependent biochemical functions essential to the reproducing cell.

ACKNOWLEDGMENTS

I should like to thank Professor L. Skaggs for his support and criticisms, K. Nealson for introducing me to this organism, and H. Forsthoff, L. Claus and other members of the operating staff of the linear accelerator, Argonne Cancer Research Hospital, for their technical assistance.

This investigation was supported in part by United States Public Health Service Training Grant CA513206 and Argonne Cancer Research Hospital Project No. 14, Government Contract AT(11-1)-69.

LITERATURE CITED

1. Hastings, J. W., Q. H. Gibson, and C. Greenwood. Proc. Natl. Acad. Sci. U.S., 52:1529, 1964.
2. Hastings, J. W., Q. H. Gibson, and C. Greenwood. Photochem. Photobiol., 4:1227, 1965.
3. Gibson, Q. H., J. W. Hastings, G. Weber, W. Duane, and J. Massa. In Flavins and Flavoproteins. E. C. Slater, Ed. Amsterdam: Elsevier Publishing Company, 1966, pp. 341-66.
4. Hastings, J. W., and Q. H. Gibson. J. Biol. Chem., 242:720, 1967.
5. Farghaly, A. H. M. J. Cellular Comp. Physiol., 36:165, 1950.
6. Skaggs, L. S., J. C. Nygard, and L. H. Lanzl. Radiology, 64:117, 1955.
7. Jackson, A. S. Analog Computation. New York: McGraw-Hill, 1960.
8. Valdimirov, Y. A. NASA Technical Translation, F-456, 1967.

THE AMINO ACID SEQUENCE IN THE VICINITY OF THE COVALENTLY BOUND ADENYLIC ACID IN GLUTAMINE SYNTHETASE FROM ESCHERICHIA COLI*

By

R. L. Heinrikson†‡ and H. S. Kingdon‡

Under certain conditions of growth, the Escherichia coli glutamine synthetase is modified by the introduction into the enzyme molecule of covalently bound adenylic acid. This mechanism for modification of the preformed enzyme was discovered independently in this country by Kingdon and Stadtman[1,2] and in Germany by Holzer and his co-workers.[3,4] An enzyme was described by Kingdon et al[5] and by Wulff et al[6] which catalyzes the adenylylation of the glutamine synthetase in the presence of magnesium ions and glutamine, using ATP as the adenylic acid donor. Another enzyme, which catalyzes deadenylylation, has been studied by Shapiro and Stadtman,[7] Shapiro,[8] and by Heilmeyer et al.[9] Kingdon et al[5] showed that glutamine synthetase can be adenylylated to the extent of 12 5'-adenylyl groups per enzyme molecule. Since E. coli glutamine synthetase has been shown to have a molecular weight of 600,000, with 12 identical subunits,[10] this corresponds to one 5'-adenylic acid per subunit. The 5'-adenylyl group in naturally occurring glutamine synthetase was identified by Shapiro et al[11] and Shapiro and Stadtman[12] have shown that this moiety is attached to the enzyme by a phosphodiester link to a tyrosine hydroxyl.

The present communication describes the isolation of a tryptic peptide containing covalently bound adenylic acid from fully adenylylated E. coli glutamine synthetase, and also reports the amino acid sequence in the vicinity of the AMP.

EXPERIMENTAL PROCEDURE

Materials. E. coli, strain W, was grown as described by Kingdon and Stadtman[2] on a glycerol-glutamate medium designed to yield glutamine synthetase with a high degree of substitution with adenylic acid (synthetase II).

Glutamine synthetase was prepared from frozen lots of E. coli W by the procedure of Woolfolk et al.[10] A yield of 450 mg (0.75 μmole) of apparently homogenous enzyme was obtained from 1.5 kg of wet cells. A portion of the purified enzyme subjected to polyacrylamide gel electrophoresis at pH 8.5[13] gave a single band. The ratio of the absorbance at 260 mμ to that at 280 mμ was 0.77, indicating an adenylate content of 9 moles per mole of enzyme.[5] The specific enzyme activity of this preparation was consistent with that expected for pure enzyme labeled to a comparable degree with AMP.[2,5]

ATP: glutamine synthetase adenylyltransferase was partially purified as described by Mecke et al[14] from the same cells as the glutamine synthetase.

The introduction of ^{14}C-labeled AMP into the glutamine synthetase preparation was accom-

*This report is taken from a paper that appeared in J. Biol. Chem., 245:138, 1970; the work was supported in part by a grant from the National Science Foundation.

†Department of Biochemistry, University of Chicago.

‡Recipient of a Career Development Award from the U. S. Public Health Service.

plished by methods reported earlier.[5] Glutamine synthetase, 450 mg; ATP: glutamine synthetase adenylyltransferase, 177 mg; and 8-^{14}C-adenosine-5'-triphosphate (Amersham/Searle, 50 μC; 250 μmoles) were incubated for 90 min at 37° in a total volume of 50 ml in the presence of 10 mM Tris buffer, pH 7.6, 50 mM $MgCl_2$, and 1 mM L-glutamine. After incubation, the reaction mixture was cooled to 0°, and the ^{14}C-adenylyl-glutamine synthetase was repurified by repeated acid-ammonium sulfate precipitations, identical to Step VI in the standard enzyme preparation.[10] The recovery of labeled protein after 2 reprecipitations was nearly quantitative (438 mg) and the specific radioactivity of the product was 480,000 cpm per μmole, consistent with the introduction of 3 to 4 labeled adenylyl groups per mole of enzyme. Polyacrylamide gel electrophoresis of the ^{14}C-adenylyl-glutamine synthetase revealed a single band and this material provided the source of the adenylyl peptide.

Trypsin (type XI, diphenyl carbamyl chloride treated, crystallized, dialyzed salt free and lyophilized; Lot 78B-8170), carboxypeptidases A and B (treated with diisopropyl fluorophosphate), and dimethylaminonaphthalene-5-sulfonyl chloride were obtained from Sigma. Iodoacetic acid was purchased from Matheson and was used without further purification. Urea was recrystallized and deionized according to the procedures of Benesch et al.[15] Pyridine, ethyl acetate and phenylisothiocyanate (Matheson) were distilled before use. Trifluoroacetic acid was obtained from Aldrich. All other reagents were of the purest commercially available grade.

Protein determinations. Protein was determined colorimetrically by a modification of the biuret reaction[16] with crystallized bovine albumin as a reference standard. Effluent fractions from column chromatographic procedures were monitored spectrophotometrically for protein content by measuring the absorbance of the solutions at 260 mμ and 280 mμ.

Amino acid analyses. Amino acids were determined by automated ion exchange chromatography according to Spackman et al[17] with a Bio Cal BC-200 analyzer equipped with a microcuvette flow cell system and an electronic scale expander. These optional systems permitted quantitation of as little as 3 to 5 nanomoles of amino acid with an accuracy of ± 5 per cent. Peptide samples were hydrolyzed in 6 N HCL in vacuo for 22 hours at 110 ± 0.2°, special precautions being observed in the preparation and hydrolysis of samples.[18,19]

Electrophoretic separation of peptides. Fractionation of peptides by high voltage paper electrophoresis at pH 6.5 was performed in a Gilson Electrophorator (Model D), following the general techniques outlined by Dreyer and Bynum.[20] Peptide samples, together with leucine, aspartic acid and lysine markers, were spotted on sheets of Whatman #3 chromatographic paper 57 cm in length, and electrophoresis was carried out in pyridine-acetate buffer, pH 6.5 (pyridine: acetic acid:H_2O; 25:1:225) for 45 min at 3000 v (53 v per cm). The positions of the amino acids and peptides were detected by immersing the dry electrophoretograms in a solution of ninhydrin-$CdCl_2$ reagent.[20] After drying for 15 to 30 min at room temperature, the papers were placed in a forced-air oven at 70° for 5 to 10 min to complete the color development. As little as 5 nanomoles of peptide could be visualized easily by this technique.

Radioactivity measurements. The radioactivity of solutions containing ^{14}C-labeled proteins and peptides was measured by counting 5- to 100 μl samples dried on aluminum planchets (1-1/4 inch) in a Nuclear-Chicago gas flow counter (Model 181A) with an efficiency of about 35 per cent. The radioactivity of peptides separated by high voltage paper electrophoresis was measured in a Packard Tricarb scintillation counter (Model 574). Ninhydrin-positive spots from electrophoretograms were excised and immersed in vials (2.5 x 5 cm) containing 15 ml of the scintillation liquid

(0.5 per cent 2,5-diphenyloxazole and 0.025 per cent p-bis-2'-(5'-phenyloxazoyl) benzene in toluene). This procedure has an efficiency of approximately 65 per cent for compounds containing ^{14}C.

Preparation of reduced and carboxymethylated enzyme. Approximately 100 mg of lyophilized ^{14}C-adenylyl-glutamine synthetase (80,000 total counts per min) were reduced and carboxymethylated as described by Crestfield et al.[18] Separation of the modified protein from the other components of the reaction mixture was achieved by gel filtration of the solution on a column (4 x 52 cm) of Sephadex G-25 with 50 per cent acetic acid as eluent. Protein appeared in the effluent at 310 ml and continued to emerge for 120 ml. The combined fractions containing protein were rotary-evaporated to a volume of 15 to 20 ml and the solution was lyophilized. Overall recovery of protein was about 75 per cent. Amino acid analysis of a 3 mg sample of reduced, carboxymethylated ^{14}C-adenylyl-glutamine synthetase subjected to hydrolysis in 6N HCl at 110° for 24 hours was in close agreement with the composition reported earlier.[11] All of the cystine appeared as S-carboxymethyl cysteine and there was no indication that alkylation of methionine, histidine, or lysine residues had occurred.

Hydrolysis of reduced and carboxymethylated enzyme with trypsin. A suspension of 55 mg (42,000 total cpm) of reduced, carboxymethylated ^{14}C-adenylyl-glutamine synthetase in 5 ml of 0.5 mM Tris buffer, pH 8.0, was cooled to 0° and the pH was brought to 11.5 by the dropwise addition of chilled 1 M NaOH. After stirring for 5 to 10 minutes nearly all of the protein dissolved and the pH was immediately readjusted to 8.0 with cold 1 M HCl. The protein remained in solution under these conditions and precipitated only at pH values less than 7. The solution was placed in a vessel maintained at 40° in a pH-stat titrimeter (Radiometer Automatic Titrator, type TTT1) and 0.05 ml of trypsin (0.27 mg in 1 mM HCl) was added. The pH was kept at 8.0 by the addition, with the calibrated microsyringe, of 0.1 N NaOH. Hydrolysis proceeded rapidly, and within 2 hrs 80 per cent of the theoretical amount of base required for the complete neutralization of the protons liberated during hydrolysis had been consumed. This calculation was based upon the number of lysine and arginine residues per mole of enzyme.[11] A second 0.05 ml portion of trypsin was added and the reaction was allowed to proceed overnight at room temperature.

The digestion mixture was rotary-evaporated to dryness and dissolved in 2 ml of 0.1 M NH_4HCO_3. Insoluble material was removed by centrifugation and discarded. The supernatant solution, containing 95 per cent of the original radioactivity, was passed through a column (1.5 x 193 cm) of Sephadex G-25 (fine) eluted with 0.1 M NH_4HCO_3 (cf. Figure 1). Effluent fractions were collected at a flow rate of 15 ml per hr, and the fractionation was monitored by determination of the absorbancy at 260 mμ and 280 mμ, and by measurement of radioactivity. As may be seen in Figure 1, radioactivity emerged in two peaks, each of which coincided with peaks having high A_{260}:A_{280} ratios. The major component (peak A) contained the adenylyl peptide and accounted for about 80 per cent of the radioactivity of the sample added to the column. The elution behavior of peak B suggested that it was of low molecular weight. High voltage paper electrophoresis of a portion of the pooled fractions comprising this peak revealed that the radioactivity was not coincident with ninhydrin-positive material. This would indicate that peak B may consist in part of ^{14}C-adenine liberated by mild acid hydrolysis of the labile adenine-ribose bond.[12]

Isolation of the ^{14}C-adenylyl peptide. The fractions containing peak A (Figure 1) were combined and lyophilized repeatedly to remove NH_4HCO_3. The lyophilized material (32,000 cpm) was dissolved in 3 ml of 0.1 M acetic acid and the clear solution was added to a column (0.9 x 60 cm)

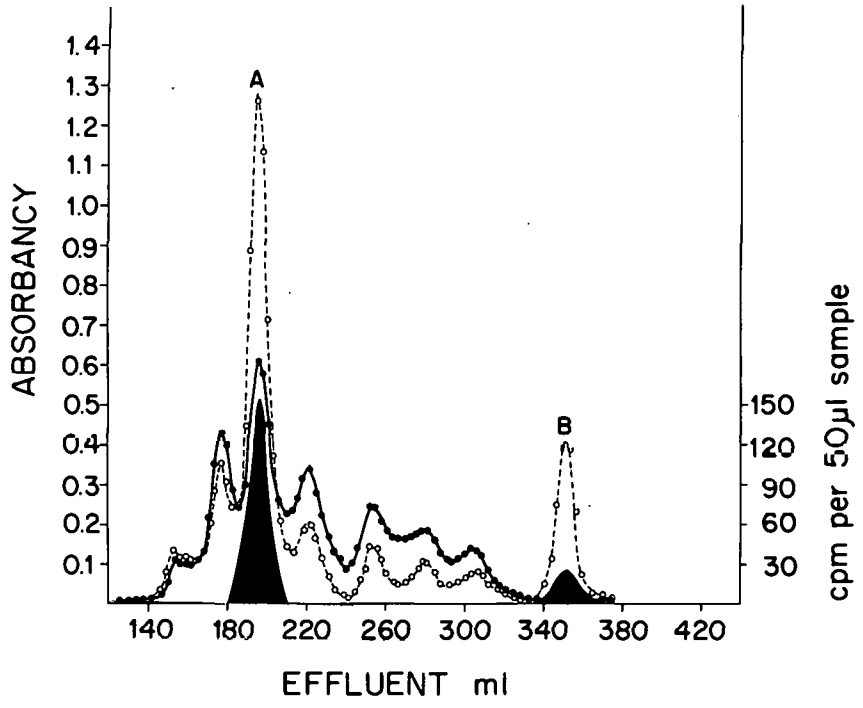

Figure 1. Gel filtration of a tryptic digest of reduced and carboxymethylated ^{14}C-adenylyl glutamine synthetase on a column (1.5 x 193 cm) of Sephadex G-25 (fine) eluted with 0.1 M NH_4CO_3. Fractions of 3.5 ml were collected at a flow rate of 15 ml per hour. ●——●, absorbancy at 280 mμ; o- - -o, absorbancy at 260 mμ. Shaded areas indicate radioactivity.

of Dowex AG-1-X2 acetate (200 to 400 mesh) equilibrated with the same solvent. Peptides were eluted from the column with a linear gradient of increasing acetic acid concentration. The mixing chamber contained 250 ml of 0.1 M acetic acid and the reservoir contained an equal volume of 0.6 M acetic acid. Fractions of 5 ml were collected at a flow rate of 15 ml per hour and these were analyzed for absorbancy at 260 mμ and radioactivity. As shown in Figure 2, the ^{14}C-adenylyl peptide emerges late in the elution scheme, well separated from other ultraviolet-absorbing peptides. The yield of the adenylyl peptide obtained in this step was more than 90 per cent, and the overall yield, starting from reduced and carboxymethylated ^{14}C adenylyl glutamine synthetase, was 70 per cent. A portion of the combined radioactive fractions subjected to paper electrophoresis at pH 6.5 gave a single ninhydrin-positive spot coincident with radioactivity. The electrophoretic mobility of the adenylyl peptide indicated a net charge of -4 and amino acid analysis revealed it to be a dodecapeptide (12 amino acid residues).

Sequential analysis. Stepwise degradation of the adenylyl peptide was performed by the method of Edman[21] as modified by Gray.[22] Amino acid analysis of the peptide was carried out after each stage of the degradative procedure. In some cases, end group analyses were performed by reaction of the peptides with DNS-Cl*.[22] The DNS-amino acids were separated and identified by two-dimensional thin layer chromatography on polyamide layers (Gallard-Schlesinger) as described by Woods and Wang.[23]

*DNS- = dimethylaminonaphthalene-5-sulfonyl-.

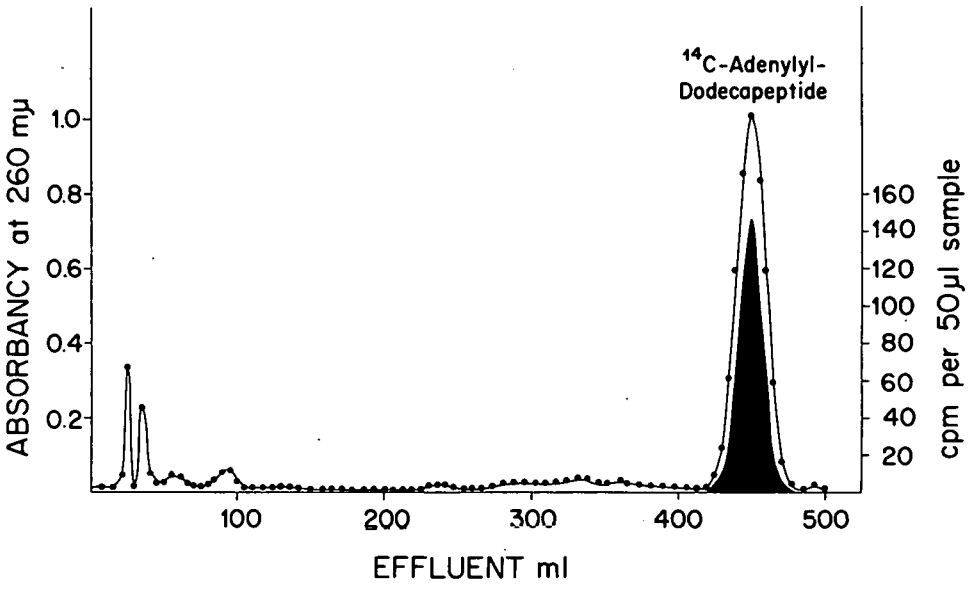

Figure 2. Chromatography on Dowex AG 1-X2 of the radioactive material recovered from Sephadex (Peak A, Figure 1). The column (0.9 x 60 cm) was equilibrated with 0.1 M acetic acid and sample elution was performed with an increasing linear gradient of acetic acid concentration. The mixing chamber contained 250 ml of 0.1 M acetic acid and the reservoir contained an equal volume of 0.6 M acetic acid. Fractions of 5 ml were collected at a flow rate of 15 ml per hour. The shaded area indicates radioactivity.

RESULTS

A peptide containing covalently bound ^{14}C-AMP was isolated in 70 per cent yield from a tryptic digest of reduced and carboxymethylated ^{14}C-adenylyl glutamine synthetase by gel filtration on Sephadex (Figure 1), and ion exchange chromatography on Dowex AG 1-X2 (Figure 2). Paper electrophoresis of the purified adenylyl peptide at pH 6.5 gave a single ninhydrin positive spot coincident with radioactivity, and the electrophoretic mobility of the peptide relative to that of aspartic acid indicated a formal charge of -4. Amino acid analysis revealed it to be a dodecapeptide with the following composition: Asp, 2.04; Glu, 2.00; Pro, 2.06; Gly, 0.94; Ala, 1.00; Leu, 2.12; Tyr, 0.90; Lys, 0.96. No other amino acids were present in amounts exceeding 0.04 residue. The tryptic ^{14}C-adenylyl dodecapeptide is similar in composition to the decapeptide obtained after digestion of adenylylated glutamine synthetase with pepsin and pronase,[12] except that it contains one less residue of proline and an additional residue each of alanine, leucine and lysine.

The composition and electrophoretic behavior of the peptide indicate the absence of amidated residues. Four negative charges and one positive charge are donated respectively by the β and γ carboxyl groups of the 4 aspartic and glutamic acid residues and the ϵ-amino group of lysine. The fifth negative charge is on the phosphoryl oxygen of the AMP moiety.

Sequence Analysis

The amino acid sequence of the tryptic adenylyl dodecapeptide and the steps employed to establish this structure are summarized in Figure 3. Details of the degradative procedures are described in the following paragraphs.

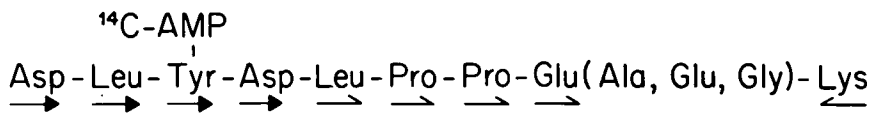

Figure 3. Sequence of amino acids in the region of the covalently bound adenylic acid in E. coli glutamine synthetase. The methods employed to establish sequences are denoted as follows: ——>, Edman degradation; —~>, reaction with DNS-Cl; <——, hydrolysis with carboxypeptidase B.

Edman degradation. Eight consecutive stages of the Edman degradation were performed to establish the sequence of the amino acid residues in the N-terminal region of the peptide chain. Portions of the residual peptides were subjected to amino acid analysis after each stage and the amino acids identified by difference.[24] In each amino acid analysis presented below, the missing amino acid is underlined. The results obtained by the subtractive method for the first four amino acid residues were confirmed by reaction of a portion of the residual peptide with DNS-Cl and identification of the amino terminal DNS-amino acids (Figure 3).

First step (85 per cent): Asp, 1.15; Leu, 2.12; Tyr, 0.90; Pro, 2.06; Glu, 2.00; Gly, 0.94; Ala, 1.00; Lys, 1.06. Paper electrophoresis of this peptide gave a single ninhydrin positive spot corresponding to a peptide with a formal charge of -3. The peptide, however, no longer coincided with radioactivity, which appeared in the neutral band. These results suggested that at some stage of the degradative procedure, part of the ^{14}C-adenylyl moiety had been cleaved from the original peptide. Since the altered electrophoretic mobility of the peptide was consistent with the removal of one residue of aspartic acid, it seemed likely that cleavage of the acid-labile adenine-ribose bond[12] might have occurred during the cyclization step in trifluoracetic acid. To test this hypothesis, 5 mg of 5'-AMP were dissolved in 1.0 ml of TFA* and the solution was incubated at 55° for 10 minutes. The TFA was removed under vacuum and the residue was dissolved in 1 ml of n-butanol saturated with water. A portion of this solution, together with adenine, adenosine and 5'-AMP markers, was spotted on a sheet of Whatman #1 paper and subjected to ascending chromatography in n-butanol saturated with water. Inspection of the chromatogram under ultraviolet light clearly revealed that the AMP had been completely converted to adenine. Another portion of the TFA-treated nucleotide was chromatographed on Whatman #1 together with ribose and ribose-5-phosphate markers. The ascending solvent system was ethyl acetate: pyridine: H_2O (40:10:5). Spots were detected by spraying the dried paper with a solution containing 0.8 g of phthalic acid, 0.5 ml of aniline and 50 ml of n-butanol saturated with water, and then drying the chromatogram in an oven at 80° for 10 to 15 minutes.

The only substance identified in the TFA-treated nucleotide was ribose-5-phosphate. These findings suggest that during the Edman procedure the ^{14}C-adenylyl peptide is quantitatively converted to ^{14}C-adenine and a peptide in which ribose is linked via a phosphodiester bond to tyrosine.

Second step (88 per cent): Asp, 1.06; Leu, 1.20; Tyr, 0.91; Pro, 2.10; Glu, 2.05; Gly, 0.89; Ala, 0.98.

Third step (80 per cent): Asp, 1.02; Leu, 1.18; Tyr, 0.21; Pro, 2.02; Glu, 2.10; Gly, 0.94; Ala, 0.96.

*TFA = trifluoroacetic acid.

Fourth step (78 per cent): Asp, 0.28; Leu, 1.10; Tyr, 0.20; Pro, 2.15; Glu, 1.94; Gly, 1.01; Ala, 1.06.

Fifth step (75 per cent): Asp, 0.25; Leu, 0.30; Tyr, 0.20; Pro, 1.97; Glu, 2.04; Gly, 1.01; Ala, 0.99.

Sixth step (70 per cent): Asp, 0.26; Leu, 0.32; Tyr, 0.15; Pro, 1.33; Glu, 2.01; Gly, 0.98; Ala, 1.05.

Seventh step (68 per cent): Asp, 0.20; Leu, 0.25; Tyr, 0.18; Pro, 0.62; Glu, 2.09; Gly, 0.97; Ala, 1.10.

Eighth step (65 per cent): Asp, 0.22; Leu, 0.27; Tyr, 0.16; Pro, 0.55; Glu, 1.42; Gly, 0.98; Ala, 1.05.

Treatment with carboxypeptidases A and B. Lysine was placed at the carboxyl terminus of the ^{14}C-adenylyl peptide on the basis of the specificity of trypsin. Proof for this assignment was obtained by hydrolysis of the peptide with carboxypeptidase B. A solution of the peptide (0.02 μmoles) and 10 μg of carboxypeptidase B in a total volume of 200 μl of 0.2 M N-ethylmorpholine acetate buffer, pH 8.5 was incubated for 2 hours at 37°. Short column amino acid analysis of 50 μl of the reaction mixture gave 0.0048 μmole of lysine, indicating a release of over 95 per cent of the C-terminal lysine. Analysis of a blank control containing no peptide revealed no basic amino acids.

After 2 hours of reaction with carboxypeptidase B, 10 μg of carboxypeptidase A were added and aliquots were removed for long column amino acid analysis at 45, 90 and 180 min reaction at 37°. No further release of amino acids was observed. Similar reaction mixtures were prepared containing the synthetic peptides gly-gly-ala, ala-gly-gly and gly-gly-leu. In 3 hours at 37°, carboxypeptidase A catalyzed the nearly quantitative removal of both C-terminal alamine and C-terminal leucine but was almost totally inactive toward a glycine residue in this position. These findings are in keeping with the known specificity of carboxypeptidase a.[25] Thus it would appear as if the penultimate residue in the adenylyl peptide is glycine or glutamic acid and not alanine.

DISCUSSION

The E. coli glutamine synthetase is subject to a unique form of metabolic regulation which can be summarized by the following equations:

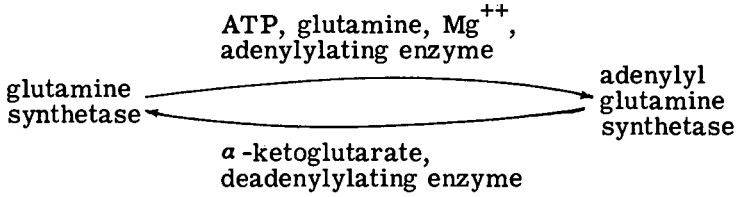

From these equations, and from corroborating in vivo experiments,[2] it is apparent that this mechanism provides the organism with a method of rapid, reversible change in the net glutamine synthesizing capacity of the cell. Nitrogen surfeit favors the adenylylated form; nitrogen starvation favors the un-adenylylated form.[4] Since the adenylalated form has a lower specific activity in the presence of Mg^{++},[25] and since it is more sensitive to feedback inhibition by a number of feedback inhibitors[1,5] than is the unadenylylated form, it seems likely that there is less gluta-synthesizing capacity under conditions of nitrogen surfeit. In vivo experiments have shown that

when the environment of the organism is suddenly changed from nitrogen surfeit to nitrogen starvation the return to the more active enzyme is very rapid.[2]

A recent review by Holzer deals with the broad topic of regulation of enzymes by enzyme-catalyzed chemical modifications, including the glutamine synthetase example.[26]

The present report delineates the amino acid sequence of the glutamine synthetase in the region of the covalently bound adenylic acid. The partial sequence of a tryptic, adenylylated dodecapeptide isolated from the enzyme is asp-leu-tyr-asp-leu-pro-pro-glu(ala,glu,gly)-lys.

$$^{14}\text{C-AMP}$$

Since after quantitative removal of lysine by carboxypeptidase B, no further amino acids were released from the peptide by carboxypeptidase A, one would expect the penultimate residue to be either glutamic acid or glycine. The fact that a single AMP-containing peptide was obtained by tryptic digestion further strengthens the argument that all 12 subunits of the enzyme are identical.[10] It should be emphasized, however, that both in the identification of tyrosine as the AMP-binding moiety by Shapiro and Stadtman[12] and in the current study, radioactive AMP was introduced into the glutamine synthetase beginning with an enzyme preparation that already contained some AMP. If, therefore, early-labeled AMP sites were different from late-labeled AMP sites, the current studies could still have overlooked 1 or 2 non-identical subunits among the 12. This possibility is being investigated further.

ACKNOWLEDGMENTS

The authors wish to thank Drs. I. C. Gunsalus and Lowell Heger of the University of Illinois, Urbana, Illinois, for making their fermentation facilities available for growth of E. coli; they are also indebted to Dr. Jordan Tang, Oklahoma Medical Research Foundation, Oklahoma City, Oklahoma, for valuable discussions. The expert technical assistance of Mrs. Phyllis Rosenblum is gratefully acknowledged.

LITERATURE CITED

1. Kingdon, H. S., and E. R. Stadtman. Biochem. Biophys. Res. Commun., 27:470, 1967.
2. Kingdon, H. S., and E. R. Stadtman. J. Bacteriol., 94:949, 1967.
3. Heilmeyer, L., D. Mecke, and H. Holzer. European J. Biochem., 2:399, 1967.
4. Holzer, H., H. Schutt, F. Masek, and D. Mecke. Proc. Natl. Acad. Sci. U.S., 60:721, 1968.
5. Kingdon, H. S., B. M. Shapiro, and E. R. Stadtman. Proc. Natl. Acad. Sci. U.S., 58:1703, 1967.
6. Wulff, K., D. Mecke, and H. Holzer. Biochem. Biophys. Res. Commun., 28:740, 1967.
7. Shapiro, B. M., and E. R. Stadtman. Biochem. Biophys. Res. Commun., 30:32, 1968.
8. Shapiro, B. M., Biochemistry, 8:659, 1969.
9. Heilmeyer, L., Jr., F. Battig, and H. Holzer. European J. Biochem., 9:259, 1969.
10. Woolfolk, C. A., B. M. Shapiro, and E. R. Stadtman. Arch. Biochem. Biophys., 116:177, 1966.
11. Shapiro, B. M., H. S. Kingdon, and E. R. Stadtman. Proc. Natl. Acad. Sci. U.S., 58:642, 1967.
12. Shapiro, B. M., and E. R. Stadtman. J. Biol. Chem., 243:3769, 1968.
13. Davis, B. J. Ann. N. Y. Acad. Sci., 121:404, 1964.

14. Mecke, D., K. Wulff, K. Liess, and H. Holzer. Biochem. Biophys. Res. Commun., 24:452, 1966.

15. Benesch, R. E., H. A. Lardy, and R. Benesch. J. Biol. Chem., 216:663, 1955.

16. Zamenhof, S. In Methods in Enzymology, Vol. 3. S. P. Colowick and N. O. Kaplan, Eds. New York: Academic Press, 1957, p. 702.

17. Spackman, D. H., W. H. Stein, and S. Moore. Anal. Chem., 30:1190, 1958.

18. Crestfield, A. M., S. Moore, and W. H. Stein. J. Biol. Chem., 238:622, 1963.

19. Moore, S., and W. H. Stein. In Methods in Enzymology, Vol. 6. S. P. Colowick and N. O. Kaplan, Eds. New York: Academic Press, 1963, p. 819.

20. Dreyer, W. J., and E. Bynum. In Methods in Enzymology, Vol. 11. S. P. Colowick, N. O. Kaplan, and C. W. H. Hirs, Eds. New York: Academic Press, 1967, p. 32.

21. Edman, P. Acta Chem Scand., 4:277, 283, 1950.

22. Gray, W. R. In Methods in Enzymology, Vol. 11. S. P. Colowick, N. O. Kaplan, and C. W. H. Hirs, Eds. New York: Academic Press, 1967, p. 469.

23. Woods, K. R., and K.-T. Wang. Biochem. Biophys. Acta, 133:369, 1967.

24. Konigsberg, W. In Methods in Enzymology, Vol. 11. S. P. Colowick, N. O. Kaplan, and C. W. H. Hirs, Eds. New York: Academic Press, 1967, p. 461.

25. Ambler, R. P. In Methods in Enzymology, Vol. 11. S. P. Colowick, N. O. Kaplan, and C. W. H. Hirs, Eds. New York: Academic Press, 1967, p. 155.

26. Holzer, H. Adv. Enzymol., 32:297, 1969.

BIOCHEMICAL CORRELATES OF CARDIAC HYPERTROPHY. III. CHANGES IN DNA CONTENT; THE RELATIVE CONTRIBUTIONS OF POLYPLOIDY AND MITOTIC ACTIVITY*

By

D. Grove,† K. G. Nair,‡ and R. Zak§

Hypertrophy is usually defined as a diffuse enlargement of individual cells of a tissue, whereas hyperplasia refers to an increase in cell numbers. Measurement of tissue DNA is one method of distinguishing between the two processes, since the total DNA in the organ should remain unchanged in hypertrophy but should increase with hyperplasia. In experimentally-induced work overload of the left ventricle, such as is produced by aortic banding, hypertrophy should result in a fall of the DNA concentration per milligram of heart tissue since the increase in heart weight would dilute the constant DNA content. An unchanged or increased DNA concentration would indicate DNA synthesis and the formation of new nuclei and probably of new cells.

Information on such changes in DNA content in cardiac hypertrophy is conflicting. Some investigators report a decrease in the concentration of DNA (mg DNA per unit weight of tissue) with no change in total DNA content of the heart;[1-4] others describe a moderate decline in DNA concentration with increase in total DNA content;[5,6] and a third group claims that there is no change in DNA concentration and that the total increase in DNA content is proportional to the increase in cell mass.[1,3,7-9,11,19] Finally, a fourth group has described a definite increase in both DNA concentration and total DNA content of the heart during cardiac hypertrophy.[12-14]

This and the following paper describe studies on the changes in myocardial DNA during the first twelve days after aortic constriction which were undertaken with the aim of determining the nature and cellular origin of these changes during hypertrophy.

We confirm that cardiac DNA content rises significantly after acutely produced cardiac hypertrophy. Possible causes for this increase are: (1) increased mitotic activity in muscular elements; (2) increased mitotic activity in nonmuscular elements; (3) polyploidization of existing nuclei; (4) infiltration by inflammatory cells; (5) changes in cytoplasmic DNA, i.e., mitochondrial DNA. The first four processes are considered in this paper.

MATERIALS AND METHODS

Supravalvular aortic stenosis was produced in female Sprague-Dawley rats weighing 200 to 220 g (12 to 13 weeks old) as described by Nair et al.[15] Both normal and sham-operated litter mates served as controls. Rats were killed at intervals of 2 to 12 days after operation. Hearts were excised, trimmed to remove connective tissue and the atria, blotted thoroughly to remove

*This report is taken from a paper that appeared in Circulation Res., 25:463, 1969. The work was supported in part by grants from U. S. Public Health Service, the National Heart Institute, and the Chicago Heart Association.

†Predoctoral trainee of the National Heart Institute, Department of Medicine, University of Chicago.

‡Recipient of U. S. Public Health Service Career Development Award.

§Departments of Medicine and Biochemistry, University of Chicago.

excess blood, and weighed. The left ventricle and septum were dissected from the right ventricle and prepared for biochemical or histological analysis.

Least-square regression lines of heart weight versus body weight in sham-operated controls were drawn. The extent of hypertrophy was determined by comparing the observed heart weight with the value indicated by the appropriate plot for a control animal of the same age and weight.

The DNA content of the left ventricle was determined 1 to 12 days after operation by grinding a 50 to 100 mg piece in 0.5 N PCA with a small quantity of sea sand (Reagent Grade, Merck) in a mortar and pestle. Nucleic acids were extracted as previously described.[15] DNA determinations were done in duplicate by the diphenylamine method of Burton.[17]

Sections for microspectrophotometry and for the counting of polyploid nuclei were prepared as follows: The left ventricle was opened by a longitudinal cut, fixed 24 hours in phosphate-buffer neutral formalin (pH 6.9), dehydrated, and embedded in paraffin. Sections fourteen microns thick were cut at a right angle to the midpoint of the long axis of the ventricle, stained by Feulgen's method, and mounted under oil of refractive index 1.568, which rendered the cytoplasm virtually invisible. Nuclear light absorbance was measured by the two-wavelength microspectrophotometric method[18] using a microspectrophotometer built by Dr. Hewson Swift.* Microscopic fields in which nuclei were to be scored for polyploidy corresponded to points on a preselected grid. For each heart studied, 1,000 or more muscle cell nuclei in fields containing muscle bundles oriented parallel to the plane of the section were scored visually as diploid (2c) or polyploid (4c or more). Only muscle cell nuclei were scored for polyploidy. The nuclei of nonmuscular elements presented a technical problem and were not scored.

The accuracy with which muscle nuclei could be identified in Feulgen-stained sections was estimated as follows: Sections stained with Harris' hematoxylin and eosin B, and Feulgen-stained sections, were prepared from each of six hearts. Two thousand nuclei were counted and classified as muscle or connective tissue cell nuclei in each section. The correlation coefficient was determined for the regression line relating the relative frequencies of muscle nuclei found in the two counts.

Whether polyploid muscle nuclei were distributed in sections according to the predictions of the Poisson distribution was tested by means of chi-square. Sections from ten hearts were used. The total number of polyploid nuclei observed was divided by the total number of fields (area of each field = 0.0202 mm^2) to give the value of the Poisson lambda. From this value the expected frequency of fields containing 0, 1, 2, or 3 or more polyploid nuclei, based on the total number of fields observed, was calculated, and compared by chi-square with the frequencies observed.

Mitotic indices (number of mitoses observed per 10,000 nuclei) were determined by counting 25,000 or 50,000 total nuclei per heart in sections from left ventricular muscle of several hypertrophied and control hearts. Mitotic figures from metaphase to early telophase were scored as mitoses. When necessary, sections were remounted under oil of unmatched refractive index to facilitate identification of cell types.

Sections stained with hematoxylin and eosin were used to evaluate the possibility of infiltration of inflammatory cells.

*Department of Biology, University of Chicago.

RESULTS

From three to twelve days following aortic banding, there was a considerable increase in total cardiac DNA content. See Table 1 and Figure 1. The DNA concentration per mg of heart tissue remained similar to control values although an increase or decrease was occasionally observed.

Table 1

CHANGES IN DNA CONCENTRATION AND TOTAL DNA CONTENT IN LEFT VENTRICLE AFTER AORTIC CONSTRICTION

Experiment	No. of rats	DNA*			
		μg/mg tissue	P	μg/ventricle	P
Short-Term Hypertrophy					
Sham-operated	40	1.38 ± 0.03		$6.7 \times 10^2 \pm 10$	
Aortic constriction					
Moderate hypertrophy (19%)†	30	1.41 ± 0.04	< 0.5	$8.0 \times 10^2 \pm 19$	< 0.001
Gross hypertrophy (44%)	10	1.51 ± 0.05	< 0.5	$10.3 \times 10^2 \pm 30$	< 0.001
Chronic Hypertrophy					
Sham-operated	18	1.22 ± 0.03		$7.0 \times 10^2 \pm 16$	
Aortic constriction					
Moderate hypertrophy (31%)	8	1.02 ± 0.02	< 0.2	$7.6 \times 10^2 \pm 23$	< 0.05
Gross hypertrophy (55%)	6	0.86 ± 0.03	< 0.1	$7.6 \times 10^2 \pm 28$	< 0.05

All rats banded at three months. Short-term hypertrophy: animals sacrificed 3 to 12 days after banding. Chronic hypertrophy: animals sacrificed 2 to 4 months after banding.

*Mean values ± SE are given. P = probability of chance occurrence.

†The percentage of hypertrophy was determined by comparison of wet weights of banded hearts with those of sham-operated litter mates of similar body weight.

When the changes in total ventricular DNA and DNA concentration are plotted against the change in heart weight following aortic constriction, two results are apparent: (1) There is no consistent fall in DNA concentration. (2) Total ventricular DNA increases significantly above the values obtained for the control hearts (Figure 1).

In chronically hypertrophied hearts 2 to 4 months after aortic constriction the total DNA in the left ventricle is 10 per cent higher than in sham-operated controls of the same age. Increase in DNA content in chronic hypertrophy is, however, significantly less than in hearts of similar size in short-term experiments. The reduction in DNA content between the two periods under study was about 25 per cent. Although there also is a tendency toward the decrease in DNA concentration per mg of heart tissue in chronic hypertrophy, and especially in gross hypertrophy, the changes are not statistically significant.

Polyploidy. We wished to determine the degree of polyploidy specifically in muscle cell nuclei. We were able to select muscle cell nuclei accurately for the study of polyploidy in Feulgen-stained sections. The correlation coefficient for the regression of "percentage of mus-

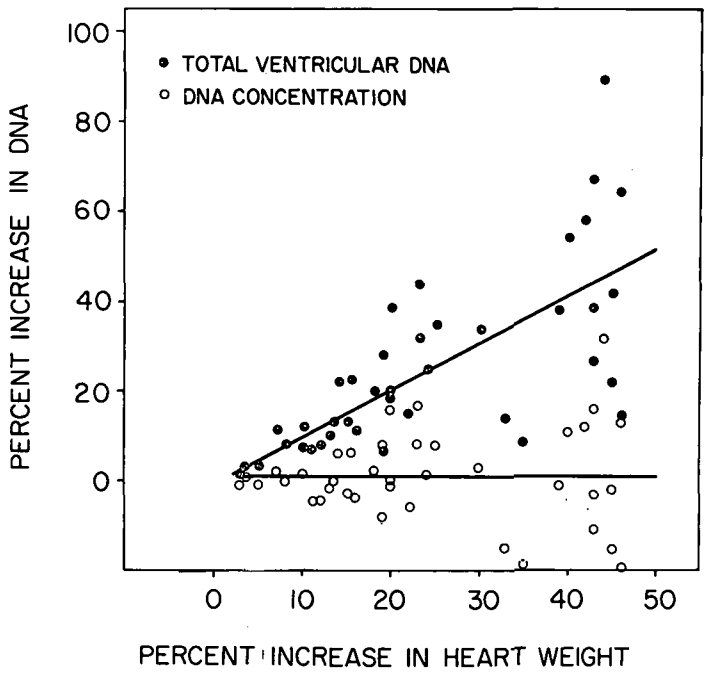

Figure 1. Relation of changes in DNA concentration, and total ventricular DNA, to changes in heart weight after aortic constriction. Data are expressed as percentage of increase over sham-operated controls. Determinations were made 2 to 12 days after banding.

cle nuclei in Feulgen-stained sections" upon "percentage of muscle nuclei in hematoxylin and eosin-stained sections" was 0.98.

The histogram of absorbance values for Feulgen-stained heart muscle cells was polymodal (Figure 2) indicating the presence of diploid and polyploid nuclei. Several nuclei of high, but indeterminate, degrees of polyploidy were also observed. Absorbance measurements included in this figure were made on nuclei of one hypertrophied and two normal hearts, stained together. Measurements of liver parenchymal nuclei are included for comparison (Figure 2).

The frequencies of polyploid nuclei were determined from clearly identified heart muscle cells in sections from animals of the following ages: (1) 6 weeks old, two unoperated controls; (2) 12 to 13 weeks old, one sham-operated control, three normal unoperated controls, four banded animals with cardiac hypertrophy ranging from 27 to 67 per cent above control animals. Animals were killed one to three weeks after operation. (3) 17 to 18 weeks old, one sham-operated, three normal controls and four animals with 32 to 51 per cent cardiac hypertrophy killed ten days after aortic constriction.

Hypertrophy was accompanied by an increase in the frequency of polyploid nuclei of the muscle cells (Figure 3). Hypertrophied hearts of 12- to 13-week-old rats showed 4.2 ± 0.11 (SEM) per cent polyploid muscle nuclei compared to 1.89 ± 0.08 in controls. In the 17- to 18-week-old group, hypertrophied hearts had 3.9 ± 0.2 per cent polyploid muscle nuclei, compared to control hearts with 1.56 ± 0.06. The increases are statistically significant. When "percentage of polyploid nuclei" is plotted as a function of "percentage of hypertrophy," the correlation coefficient, r, is + 0.91. The correlation coefficient is shown to be significantly different from zero by the Z-test ($p < 10^{-7}$, n = 16; see Figure 4). Thus, there is a rather regular correlation

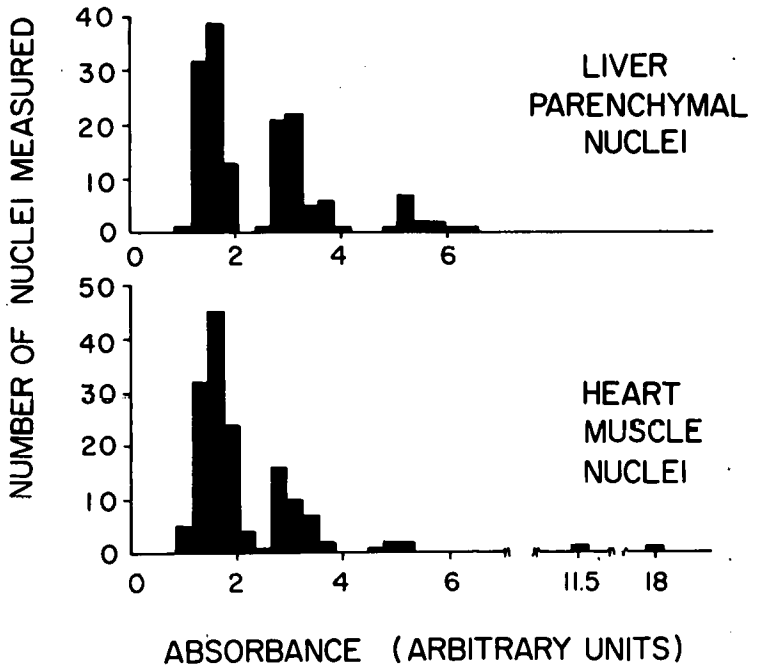

Figure 2. Absorbance values for Feulgen-stained rat liver cells and heart muscle cell nuclei.

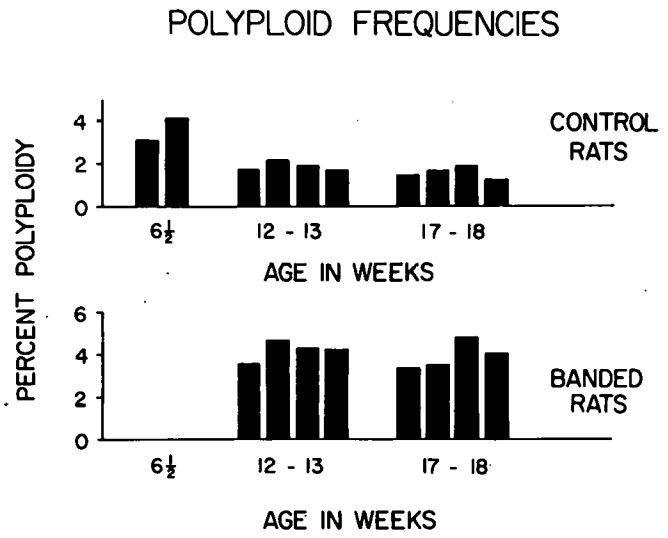

Figure 3. Polyploidy frequencies in heart muscle cell nuclei in banded and control rats. Rats 12 to 13 weeks old were killed 1 to 3 weeks after operation. Rats 17 to 18 weeks old were sacrificed 10 days after banding.

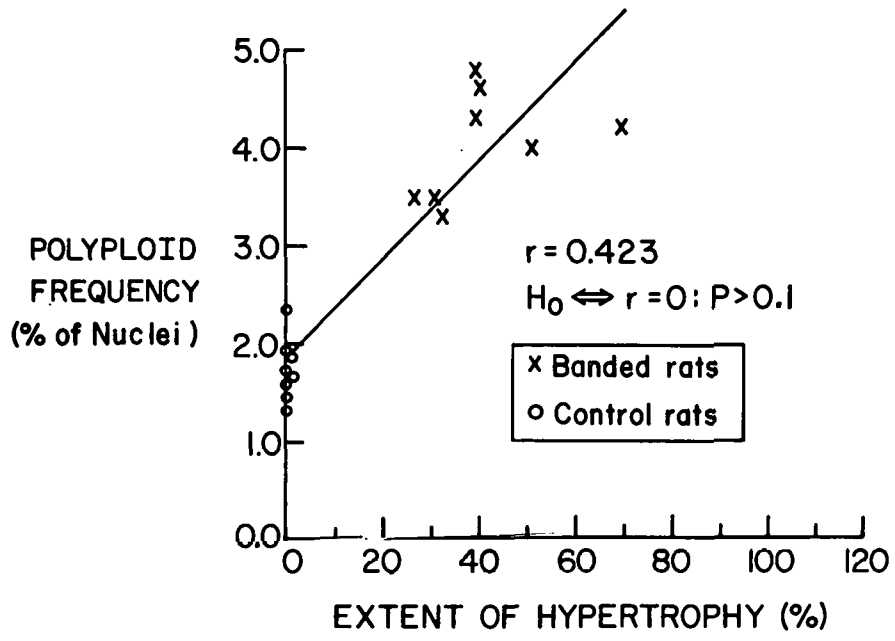

Figure 4. The relative frequency of polyploid muscle nuclei as a function of the extent of hypertrophy. The correlation coefficient, r, is significantly larger than zero: for the null hypothesis (H_0) that r = 0, $p < 10^{-6}$.

between the degree of hypertrophy and the relative frequency of polyploid muscle cell nuclei in these experiments. The distribution of polyploid nuclei in microscope fields does not differ significantly from that predicted by a fitted Poisson distribution, when compared by chi-square with two degrees of freedom (Table 2).

Infiltration by inflammatory cells. Inflammatory cells (so-called round cells) made up 0.2 to 0.3 per cent of the nuclear population in both control and hypertrophied heart. Significant infiltration of inflammatory cells was not observed in the hypertrophied hearts.

Table 2

OBSERVED DISTRIBUTION OF POLYPLOID MUSCLE CELL NUCLEI COMPARED WITH THE DISTRIBUTION PREDICTED BY THE POISSON DISTRIBUTION

Number of polyploid nuclei per field i	Number of fields observed to contain i polyploid nuclei f_i	Total number of polyploid nuclei in class i $i \times f_i$	Poisson predictions of numbers of fields containing i nuclei f_p	$(f_i - f_p)^2/f_p$
0	1686	0	1677.2928	0.04520
1	330	330	347.1663	0.84882
2	44	88	35.9283	1.81340
3 or more	3	9	2.6126	0.05745
	2063	427	2063.0000	$\chi^2 = 2.76487$
	$\lambda = 427/2063 = 0.20698$		$p > 0.20$, 2 DF	

Mitotic indices. The mitotic indices of hypertrophic hearts averaged ten times higher than those of controls (Table 3). Almost without exception the mitoses were found in cells other than muscle cells. In only one instance out of eighty-six was a mitosis observed in a cell that could not be distinguished from muscle cells. The increase in mitotic index in hypertrophied hearts was statistically significant. The correlation coefficient of the regression line of the mitotic index as a function of degree of hypertrophy was + 0.90 (Figure 5).

Table 3

MITOTIC INDICES OF CONTROL AND HYPERTROPHIED HEARTS

Mitotic index (Mitoses per 10,000 nuclei)	
Control group (n = 7)	Banded group (n = 7)
0.00	1.00
0.19	2.39
0.19	2.40
0.38	2.40
0.40	2.93
0.40	3.97
0.40	4.74
AVG: 0.28	AVG: 2.80
SEM: 0.06	SEM: 0.46

By t test: $p < 0.0025$ (one tail). The experimental animals were studied two days after aortic banding.

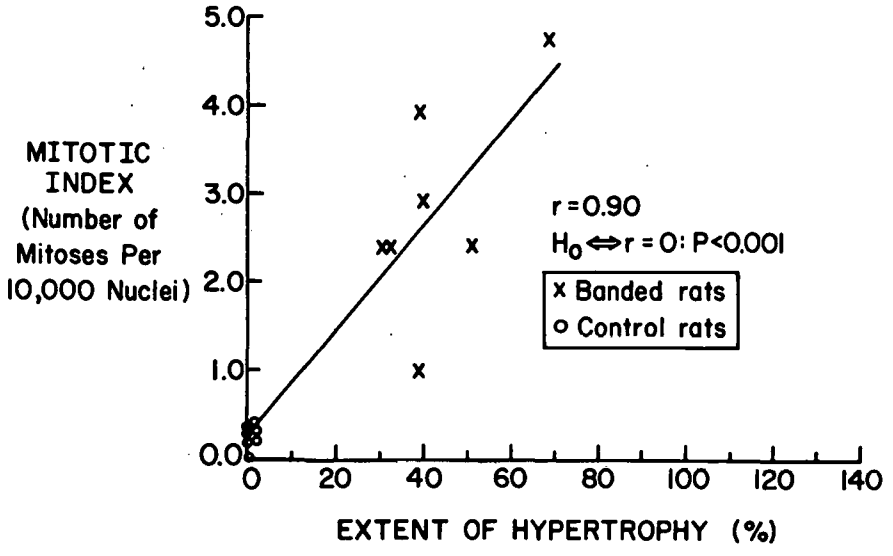

Figure 5. The mitotic index as a function of the extent of hypertrophy. The correlation coefficient, r, is significantly larger than zero: for the null hypothesis that $r = 0$, $p < 10^{-7}$.

DISCUSSION

DNA content in hypertrophy. Our results clearly indicate that the total DNA content of cardiac tissue rises during the acute phase of cardiac hypertrophy. Otherwise there would have been a "dilution effect," i.e., the DNA concentration would have fallen with increasing hypertrophy. Instead, DNA concentration did not change significantly.

The results obtained by different investigators are summarized in Table 4. It is evident that the data pertaining to changes in DNA concentration should be analyzed according to the duration and intensity of the hypertrophy. The age and maturity of the cardiac tissues must also be taken into account. During the acute phase of cardiac hypertrophy the DNA content appears to change proportionally to the increase in heart weight so that there is no increase in DNA concentration although the total DNA content is increased. RNA concentration in this period is markedly increased. The very large increase in DNA concentration noted by Gluck and collaborators[14] may result partly from their use of very young, rapidly growing animals.

Four months or more after constriction of the aorta the situation differs. RNA, if still increased, is barely above control levels. Most reports agree that the DNA concentration in chronically hypertrophied hearts is below control values while total DNA content is still increased, although to a less extent than a short-term hypertrophy.

That cardiac hypertrophy is accompanied by a more or less proportional increase in the DNA concentration has also been reported by other laboratories in different situations such as DOCA-induced hypertension[12] and in nutritional anemia.[7-9] A change in total DNA, however, was not detected in the hearts of anemic animals.[4]

Mechanism of DNA increase. The mechanism of increase in DNA content has been the subject of systematic study in our laboratory. No evidence for infiltration by inflammatory cells was noted and therefore increase in DNA content through such a process is eliminated.

The frequency of polyploid nuclei was the next subject of study.[29] In autopsy specimens from human hearts Sandritter and Scomazzoni,[21] as well as Kompman, Paddags and Sandritter[22] found that normal human hearts have an appreciable population of polyploid nuclei and that the frequency of nuclei with a high degree of polyploidy (8c, 16c and 32c) increases markedly with myocardial hypertrophy. In hypertrophied rabbit hearts, Arutyunov[23] showed that both the DNA concentration and the DNA content per nucleus increased 7 to 10 days after operation. In rats, the DNA content per nucleus was reported by Chernuch et al[25] to remain stable for 4 to 7 days after banding, to decrease by 15 per cent at 21 days, and then to increase by 22 per cent three months after aortic banding. Capers,[24] however, found no change in DNA content of the nuclei of enlarged human hearts. Perhaps these differences are due to variations in the technique of estimation. We have employed the rigorous criteria of microspectrophotometry, using the method of Hewson Swift.[18] We observed more than a doubling of the frequency of polyploid nuclei. This increase, however, can account for no more than 1 per cent of the increase in DNA concentration of the myocardium. In the present study no evidence was found for variation in the DNA content of individual diploid or tetraploid nuclei with hypertrophy. Therefore, although polyploidy increases in our model, it is quantitatively of little significance.

The development of polyploidy and its significance are as yet unclear. Sandritter and collaborators consider polyploidy as a step in what is termed an amitotic process of nuclear division.[21,22] Beam and King[26] suggested a mechanism whereby successive mitoses in single liver cells produce cells with two stable polyploid nuclei. If such a mechanism were responsible for

Table 4

DNA CHANGES IN SHORT-TERM AND CHRONIC MYOCARDIAL HYPERTROPHY

Reference	Animal	Part of the heart	Time after operation	Type of operation	Wet wt. change (%)	RNA change (conc.) (%)	DNA change (%)	
							(Conc.)	(Total)
Short-Term Hypertrophy								
1	Rabbit	LV	8 days	AA	N.G.	+ 46	+18NS	+
3	Rabbit	LV	7 days	AA	+84	+ 30	- 2NS	+80
14	Puppy	LV	4 days	AA	N.G.	+164	+70	+
10	Rat	LV	5 days	AA	+30	+100	+15NS	+50
19	Rat	LV + RV	7 days	AA	30-50	+ 30	+ NS	+30
11	Rat	LV	4 days	AA	+23	+ 17	- 4NS	+18
This paper	Rat	LV	3-12 days	AA	+30	+ 32	+ 2NS	+32
Chronic Hypertrophy								
1	Rabbit	LV	4 mo.	AA	+25	- 10NS	-25	0
2	Rabbit	LV	6 mo.	AA	+51	+ 6	-20	+21
3	Rabbit	LV	6 mo.	AA	+100	+ 2NS	-72	-44
13	Dog	LV	2.5 yr.	AA	+53	+ 35	+30	+98
5	Dog	LV	2.5 yr.	AA	+48	- 11NS	-15	+26
6	Rat	LV + RV	5-7 mo.	AbA	N.G.	0	-	+
This paper	Rat	LV	3-4 mo.	AA	+28	- 10	-13	+12

Abbreviations used: LV - left ventricle; LV + RV - left and right ventricle; AA - constriction of ascending aorta; AbA - constriction of abdominal aorta; NS - not significant; N.G. - not given by authors.

the production of polyploid muscle nuclei, these nuclei should appear in pairs. That they were distributed in a manner not significantly different from the predictions of a "fitted" Poisson distribution suggests that most of them are produced by random DNA replication in single nuclei, and not by the double mitosis proposed by Beam and King.

The correlation coefficients for the changes in mitotic index and percentage of polyploid muscle nuclei with hypertrophy are both positive, and significantly different from zero (Figures 4 and 5). Whether polyploidization of the muscle nucleus population can increase indefinitely with extreme degrees of hypertrophy in rat hearts remains to be learned, although Sandritter and Scomazzoni[21] found very extensive polyploidization in pathologically hypertrophied human hearts.

Mitotic index. Mitotic figures are conspicuously absent from the adult human heart, whereas they are abundant in the heart of the newborn rat[28] (D. Grove, unpublished observation). The observations of Klinge and Stocker[28] indicate that in the rat, maturity of heart muscle cells in terms of lack of mitotic activity is manifest by three months of age. Our studies were done on mature female rats in the acute phase of cardiac hypertrophy. Mitotic indices (number of mitoses per 10,000 nuclei), as determined by systematic counting of 25,000 or 50,000 nuclei per left ventricle, were on the average ten times higher than the corresponding indices in control rats. In no instance could we find a mitotic figure in a muscle cell. The mitotic activity was restricted to nuclei of nonmuscular elements such as connective tissue cells in the interstitium, and nuclei of blood vessels. Thus the bulk of DNA synthesis is associated with mitotic activity in the less differentiated elements of the cardiac tissue. This process will be discussed in more detail in the accompanying publication.

ACKNOWLEDGMENTS

We are deeply indebted to Professor Murray Rabinowitz and Professor Hewson Swift for their guidance and criticisms in the writing of this paper. We also wish to acknowledge the excellent technical help given by Mrs. Wu.

LITERATURE CITED

1. Rossie, G. F., and M. A. Dianzani Mor. Sperimentale, 108:385, 1958.
2. Nowy, H., H. D. Frings, and K. Rey. Experientia, 15:70, 1959.
3. Meerson, F. Z., and G. P. Ramenskaya. Vopr. Med. Khim., 6:598, 1960 (in Russian).
4. Sumner, R. G., and H. D. McIntosh. Circulation Res., 12:170, 1963.
5. Kleitke, B., and H. Sydow. Acta Biol. Med. Ger., 14:447, 1965.
6. Grimm, A. F., R. Kubota, and W. V. Whitehorn. Circulation Res., 19:55, 1966.
7. Widdowson, E. M., and R. A. McCance. Brit. J. Exptl. Pathol., 36:175, 1955.
8. Norman, T. D., and W. J. Carter. Clin. Res., 8:45, 1960.
9. Korecky, B., and I. W. French. Circulation Res., 21:635, 1967.
10. Moroz, L. A. Circulation Res., 21:449, 1967.
11. Morkin, E., and T. P. Ashford. Am. J. Physiol., 215:1409, 1968.
12. Koplitz, R. M., and R. E. Priest. Fed. Proc., 21:198, 1962.

13. Meerson, F. Z., T. D. Beloshapkina, E. F. Lushnikov, E. M. Leikina, G. M. Markovskaya, and G. V. Chernyshova. Vest. Akad. Med. Nauk USSR, 18:27, 1963.

14. Gluck, L., N. S. Talner, H. Stern, T. H. Gardner, and M. U. Kulovich. Science, 144:1244, 1964.

15. Nair, K. G., A. F. Cutilletta, R. Zak, T. Koide, and M. Rabinowitz. Circulation Res., 23: 451, 1968.

16. Diem, K. (editor). Documenta Geigy. New York: Scientific Tables, 1962.

17. Burton. K. Biochem. J., 62:315, 1956.

18. Swift, H., and E. Rasch. In Physical Techniques in Biology Research. G. Oster and A. W. Pollister. New York: Academic Press, 1956, p. 354.

19. Fanburg, B. L., and B. I. Posner. Circulation Res., 23:123, 1968.

20. Zak, R., Grove, D., and M. Rabinowitz. Am. J. Physiol., 216:647, 1969.

21. Sandritter, W., and G. Scomazzoni. Nature, 202:100, 1964.

22. Kompmann, M., I. Paddags, and W. Sandritter. Arch. Pathol., 82:303, 1966.

23. Arutyunov, V. D. Fed. Proc., 25:353, 1966.

24. Capers, T. H. Am. Heart J., 68:102, 1965.

25. Chernukh, A. M., P. N. Alexandrov, G. M. Alekhina, M. S. Pshennikova, and F. Z. Meerson. Dokl. Akad. Sci. USSR, 178:255, 1968.

26. Beam, H. W., and N. C. King. Anat. Res., 83:281, 1942.

27. Linzbach, A. J. In Handbuch d. Algemeinen Pathologie, VI. F. Buchler, E. Letterez, and F. Roulet, Eds. Berlin: Springer-Verlag, 1955, p. 180.

28. Klinge, O., and E. Stocker. Experientia, 24:167, 1968.

29. Grove, D., R. Zak, and K. G. Nair. Clin. Res., 16:231, 1968.

BIOCHEMICAL CORRELATES OF CARDIAC HYPERTROPHY. IV. OBSERVATIONS ON THE CELLULAR ORGANIZATION OF GROWTH DURING MYOCARDIAL HYPERTROPHY*

By

D. Grove,† R. Zak,‡ K. G. Nair,§ and V. Aschenbrenner

In the preceding paper[1] we reported that in hearts hypertrophying in response to experimentally produced aortic constriction the DNA content increases proportionally to the increase in heart weight in the early phase of hypertrophy (i.e., cardiac enlargement without regard to possible hyperplasia). In the chronic phase of hypertrophy, the DNA content falls below the level present in the acute phase but is still higher than in control animals. Although we found that polyploid frequencies in muscle nuclei more than doubled, the large increase in DNA content in hypertrophied hearts could not be accounted for by the increased polyploidy. No mitotic activity was observed in differentiated muscle cells but the mitotic index in nonmuscular elements was greatly increased.

These results indicate strongly that cell proliferation is predominantly if not exclusively limited to nonmuscular cells at least in this model of rapidly developing cardiac hypertrophy. Similar results and conclusions have been obtained by Crane and Dutta,[2] Meerson and Alekhina[3] and Morkin and Ashford.[4]

The increased cardiac muscle mass after aortic constriction therefore results in the development of larger muscle cells, in which the ratio of the volume of the cytoplasm to the volume of nucleus is increased. Meerson has suggested that the decrease in DNA relative to cell volume may cause a deficiency in transcriptive capacity and therefore lead to decreased cardiac function.[5] There is as yet, however, no evidence that deficiency of sites for transcription in nuclear DNA can limit the process of normal protein synthesis and cell function. Yaffe and Feldman's observation that messenger RNA for muscle proteins has a relatively long life is evidence against this view.[6] Furthermore, the possible existence of the mechanism of gene amplification in differentiated cells as suggested by Pelc[7] and demonstrated for cistrons for ribosomal RNA in frogs[8] could overcome possible deficiencies in transcription sites.

In the present paper we examine further the processes of DNA synthesis and cell proliferation in the adult rat heart during rapid growth induced by an increased work load. A change in tissue architecture is discussed on the basis of results obtained by autoradiography, quantitative histological methods, detailed statistical analysis of nuclear populations in heart muscle, and chemical determination of hydroxyproline content.

---

*This report is taken from a paper that appeared in Circulation Res., 25:473, 1969. The work was supported in part by grants from the U. S. Public Health Service, the National Heart Institute, and the Chicago Heart Association.

†Predoctoral trainee of the National Heart Institute, Department of Medicine, University of Chicago.

‡Departments of Medicine and Biochemistry, University of Chicago.

§Recipient of a U. S. Public Health Service Career Development Award.

MATERIALS AND METHODS

Supravalvular aortic stenosis was produced in female Sprague-Dawley rats weighing 200 to 220 g as described by Nair et al.[9] Normal and sham-operated litter mates served as controls. The details of the preparation of the tissue specimens for biochemical and histological analysis are given in a previous paper.[1]

Autoradiography. The autoradiographic techniques were based on those developed by Messier and Leblond[10] and Joftes.[11]

Two hundred microcuries of tritiated thymidine (sp. act. 6 μc/mole) were injected intraperitoneally 48 hours after operation. Animals were sacrificed 24 hours later by decapitation under ether anesthesia, their hearts were removed and fixed, and mounted in paraffin blocks. Four-micron sections were cut and mounted on glass slides. They were then dipped in Kodak NTB-2 liquid emulsion at 42° C, dried in absolute darkness for 1 hour, and exposed for 1 to 3 weeks at 4° C in light-proof boxes containing Drierite. Sections were developed for 2 minutes and 45 seconds in Kodak D-19 developer at 19 ± 1/2° C, stopped by dipping in water for 10 seconds, and fixed in Kodak Acid Fixer (prepared in distilled water) for 2 minutes. Slides were washed and stained with hematoxylin and eosin B, or with cold azure B, pH 4. They were dehydrated and mounted under oil of refractive index 1.540. The frequencies of labeled nuclei were determined by counting, in each heart, 100 labeled nuclei or 500 fields, whichever came first.

Autoradiographic grain counting. Grains in autoradiographs were evaluated in a probabilistic manner. An eyepiece insert was prepared for the microscope, which made it possible to determine various standard areas in each field. The possible standard areas (all either square or rectangular in shape) were 5, 10, 15, 25, 50, 75, 100, 200, or 400 units, and for the whole field, 12,000 units (equal to about 0.015 mm^2 with the ocular used). For each autoradiograph to be counted, 20 random fields were selected, and all the grains in each field, whether apparently associated with labeled nuclei or not, were counted. For the total number of grains thus counted, the average number of grains associated with each of the standard field areas could be calculated. Each of these numbers was considered to approximate the Poisson parameter lambda, from which the background (random) likelihood of finding any number of grains in each standard area could be determined. The grains were then counted, and the number of grains, the smallest of the standard areas able to circumscribe all the grains associated with the nucleus, and the cell type, were determined for each apparently labeled nucleus that was observed. After a number of nuclei in randomly selected fields had been counted, a table listing the number of events required to exceed Poisson predictions of probabilities for various values of lambda was consulted, and all nuclei having as many grains or more than the number listed for a probability of 10^{-4} at the appropriate lambda value were considered labeled.

Staining. Hearts to be studied by microscopic methods were prepared in a standard manner. Animals were sacrificed by a blow on the head, their hearts excised, trimmed to remove the atria and external connective tissue, and weighed. After weighing, the ventricles were fixed in phosphate-buffer 12 per cent formaldehyde, pH 6.9, for 24 hours. They were then cut in half by a slice at a right angle to the long axis of the left ventricle, approximately at the midpoint of the axis, and fixed 24 hours longer in fresh formalin. They were dehydrated, cleared in xylene, and mounted in paraffin blocks. Sections were always oriented at a right angle to the long axis of the left ventricle, and taken as close to the midpoint of the axis as possible.

Measurement of section thicknesses. Nuclear densities (number of nuclei per volume of tissue), were determined by measuring average section thicknesses. Using an ocular micrometer, the thicknesses of sections were determined by measuring the thickness of folds in the sections, i.e., parts of the section oriented at a right angle to the plane of the section. Sections without folds were not used for these determinations. Section thickness was considered to be satisfactorily determined when the standard error of the mean of the measurements was less than 2 per cent of the mean. In most cases, about twenty measurements were required to satisfy this criterion. Sections without folds were not used for determination of nuclear densities. Fields to be studied were selected in a rigorously randomized manner.

Preparation of nuclear DNA. The excised heart was washed free of blood, ground with sea sand (Merck) and extracted with equal volumes of 6 per cent 4-amino salicylate and phenol-cresol mixture (500 g phenol crystals, 70 ml redistilled cresol, 55 ml water, 0.5 g 8-hydroxyquinoline). DNA was precipitated with 2 volumes of ethanol, removed with a glass rod and washed with 75 per cent ethanol. It was dissolved in standard sodium citrate and digested overnight at 37° in a dialysis bag with RNAse (400 μg/ml) and pronase (500 μg/ml) which had previously been heated to 80° for 10 minutes at pH 5.0. The nuclear DNA was then separated from mitochondrial DNA after denaturation and renaturation by CsCl equilibrium centrifugation precipitated by trichloroacetic acid and its radioactivity was measured in a liquid scintillation counter.[12,13]

Estimation of ^{3}H-thymidine pool specific activity. Excised hearts washed with saline were ground with sea sand and extracted with 5 per cent trichloroacetic acid. The pyrimidine derivatives were separated from degradation products by charcoal absorption and the radioactivity in the supernatant was measured in a liquid scintillation counter.[12]

Hydroxyproline containing proteins were measured in the residue remaining after digestion in 0.1 N NaOH at 0°. The residue was hydrolyzed in 6 N HCl in a sealed tube for 20 hours at 110°. Hydroxyproline was determined using p-dimethylamino-benzaldehyde.[14]

RESULTS

Incorporation of ^{3}H-thymidine into cardiac nuclear DNA. ^{3}H-thymidine incorporation into purified nuclear DNA was greatly increased after banding the aorta. This conforms with our previous observation that total cardiac DNA increased by 20 to 40 per cent, following aortic constriction.[1] In the first group the increase in heart weight was 8 per cent, in the second 36 per cent as compared with sham-operated litter mates. Fifty microcuries of ^{3}H-thymidine per 100 g of body weight were injected on the second and third day after operation; the second injection was divided into three doses, three hours apart, in order to cover a longer period of the synthetic phase. Incorporation into nuclear DNA isolated from hearts enlarged by 8 per cent was more than doubled, and incorporation into hearts enlarged by 36 per cent was increased six times (Table 1).

The specific radioactivity of thymidine pool. To be sure that differences in incorporation of ^{3}H-thymidine into DNA did not reflect changes in precursor pool specific activity, the total radioactivity in trichloroacetic acid extracts of hearts and the radioactivity absorbed by charcoal (nucleosides and nucleotides) were measured in control hearts and in hearts after aortic constriction (Figure 1). ^{3}H-thymidine given intraperitoneally rapidly entered into heart muscle and reached a maximum concentration within 15 min after injection. ^{3}H-thymidine was rapidly converted into noncyclic metabolites that are not absorbed by charcoal. The calculated half-life of

Table 1

INCORPORATION OF ^{3}H-THYMIDINE INTO THE NUCLEAR DNA ISOLATED FROM HEARTS OF SHAM-OPERATED AND BANDED RATS

Sham-operated cpm/μg DNA	Banded	
	Increase in heart weight (%)	cpm/μg DNA
117	8	432
147	36	1152

^{3}H-thymidine (50 μc per 100 g b. wt.) was administered intraperitoneally to two groups of 4 animals on the second and third day after operation. Rats were sacrificed 12 hours after the second injection.

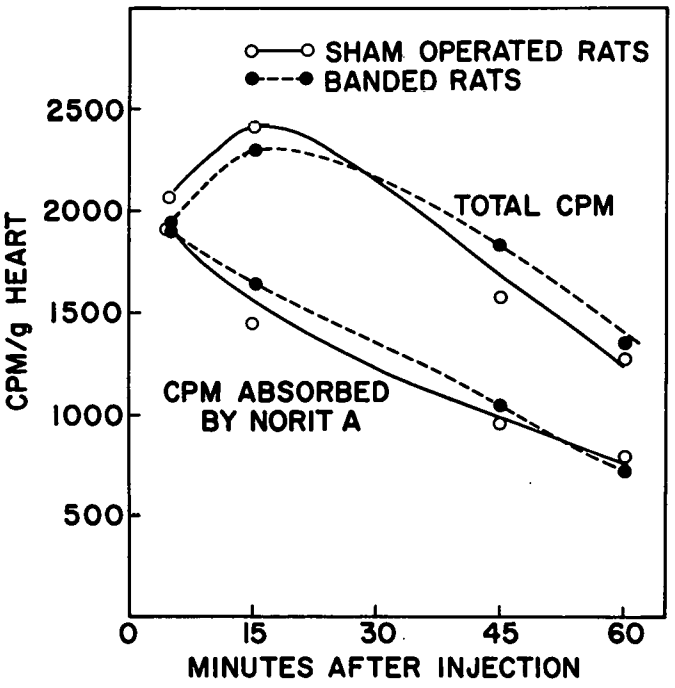

Figure 1. Radioactivity in TCA extracts of hearts from rats with aortic constriction and their sham-operated litter mates. ^{3}H-thymidine absorbed by Norit A represents labeled cyclic thymidine derivatives. Each point is average of 2 determinations. ^{3}H-thymidine (5 μc) was injected per 100 g body wt, three days after aortic constriction.

the labeled thymidine pool was approximately 25 minutes. No difference in the pattern of accumulation or decay of radioactivity was found between hearts of control and banded animals. It is recognized that the immediate precursor in the synthesis of DNA, thymidine triphosphate, was not measured. However, the results indicate that the increased incorporation of thymidine into DNA is not due to changes in the specific activity of the precursor pool.

Autoradiography. Two days after banding, hypertrophied hearts had a higher concentration of labeled nuclei than did sham-operated hearts. Sections from three hypertrophied and three

sham-operated hearts were studied by autoradiography; the sections from hypertrophied hearts had an average of 33 labeled nuclei per square millimeter of area, while those from sham-operated hearts averaged 6.5 labeled nuclei per square millimeter of section. Thus nuclei incorporating tritiated thymidine were about 5 times more common in hypertrophied than in sham-operated hearts. Autoradiographs were developed at slightly varying times after the application of the emulsion, and meaningful comparison of grain counts in different specimens was therefore impossible. In one instance the left ventricle of a hypertrophied heart was compared to the right ventricle of the same heart in the same section. In this case the average number of grains per nucleus (12.0 in the right ventricle, 9.5 in the left) did not differ significantly ($p > 0.25$ by the Wilcoxon test,[15]) and the rate of ^{3}H-thymidine incorporation per labeled nucleus was not increased in the hypertrophied ventricle.

Labeling by ^{3}H-thymidine was primarily confined to the nuclei outside muscle cells (Figure 2A). Only rarely was a labeled muscle nucleus found (Figure 2B). No labeled muscle nuclei were observed in the sham-operated hearts.

Quantitative histology. For each heart used, several sections were studied with random selection of fields. Nuclei were classified as of muscular, connective tissue, round cell, and unknown origin. In general, any nucleus that clearly lacked the morphology typical of the muscle cell, or was not surrounded by myofibril-containing eosinophilic material, was considered to be of connective tissue origin. "Round cells" were considered to be inflammatory cells, and were classified separately. "Unknown" nuclei were those that could not be classified with confidence.

In hypertrophied heart, muscle nuclei comprised a smaller proportion and connective tissue nuclei comprised a larger proportion of the total nuclear population than in control hearts (Table 2). The muscle of control hearts at 12 to 13 or 17 to 18 weeks of age contained 24 to 28 per cent of the nuclei whereas the muscle of hypertrophied hearts at 12 to 13 weeks of age contained only 17.6 per cent of the nuclei. These differences are statistically significant. A younger (6-1/2 week) control heart had virtually the same ratio of muscle to connective tissue nuclei as the older control hearts.

Nuclear densities. "Nuclear densities" were defined as number of nuclei per unit volume, and were calculated from the formula:

$$\text{nuclei per unit volume of tissue} = \frac{\text{number of nuclei observed in n fields}}{\text{n x section thickness x field area}}$$

In hypertrophied hearts the density of muscle nuclei was significantly reduced when compared with the densities of muscle nuclei in control hearts of the 12 to 13 and 17 to 18 week old groups (Tables 2 and 3). Neither the density of connective tissue nuclei nor that of the total nuclear population was significantly altered in hypertrophied hearts. In the single case studied, a 6-1/2 week old control heart had greater densities of both muscle and connective tissue nuclei than did any of the older hearts.

Nuclei per heart. It was assumed that alterations in cardiac volume due to fixation, were identical in control and hypertrophic hearts and that such alterations were essentially negligible. On this basis, the numbers of the various types of nuclei per heart were calculated for each heart on the basis of the heart weight determined at sacrifice and the assumption that in life the myocardial density is 1.10 (Table 4). It follows from this calculation that the total number of muscle nuclei was not increased in the hypertrophied hearts, and may have been decreased, while the total number of connective tissue nuclei had apparently increased, especially in com-

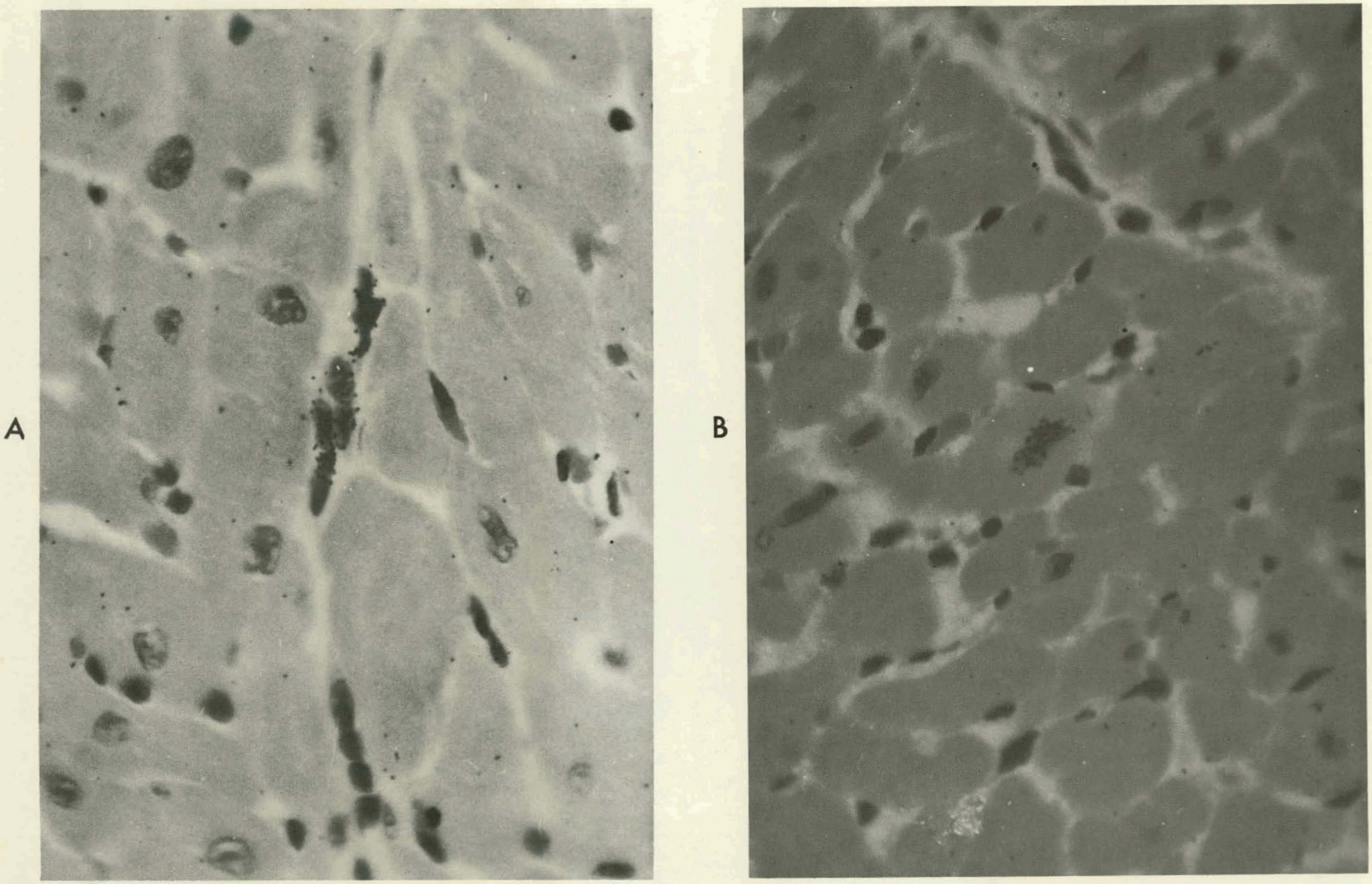

Figure 2. A: Several ^{3}H-thymidine labeled connective tissue nuclei.
B: A muscle nucleus labeled with ^{3}H-thymidine (magnification 1100X).

Table 2

THE FREQUENCIES OF TYPES OF NUCLEI IN CONTROL AND BANDED HEARTS

Animals	N		Muscle nuclei (%)	Connective tissue nuclei (%)	Round cells (%)	Unknown (%)
12 to 13 week controls	4	Avg	25.3[a]	74.9[d]	0.3	0.5
		SEM	0.5	0.5	-	-
12 to 13 week banded	4	Avg	17.6[b]	82.0[e]	0.3	0.2
		SEM	0.5	0.5	-	-
17 to 18 week controls	4	Avg	26.6[c]	72.9[f]	0.2	0.3
		SEM	0.6	0.5	-	-
6-1/2 week control	1	Avg	28.2	71.5	0.3	0.0

Comparisons by "t" test

a versus b $P < 0.001$

b versus c $P < 0.001$

d versus e $P < 0.005$

e versus f $P < 0.005$

Table 3

CONCENTRATIONS OF NUCLEI PER μl OF TISSUE IN CONTROL AND BANDED HEARTS

Group	n	Number of nuclei per microliter of tissue		
		Muscle nuclei	Connective tissue nuclei	All nuclei
Banded 12 to 13 weeks	4	122,000[a]	569,000	693,000
Control 12 to 13 weeks	4	192,000[b]	564,000	762,000
Control 17 to 18 weeks	4	198,000[c]	545,000	765,000
Control 6-1/2 weeks	1	291,000	735,000	1,030,000

Comparisons by "t" test.

a versus b $P < 0.005$

a versus c $P < 0.02$

Table 4

THE NUMBER OF NUCLEI IN RAT LEFT VENTRICLE

Group	n	Nuclei per heart x 10^{-8}		
		Muscle nuclei	Connective tissue nuclei	All nuclei
Banded 12 to 13 weeks	4	1.13	5.30	6.45
Control 12 to 13 weeks	4	1.47*	4.28	5.81
Control 17 to 18 weeks	4	1.71†	4.71	6.45
Control 6-1/2 weeks	1	1.81	4.54	6.35

*In comparison with the banded groups $P < 0.05$.

†In comparison with the banded groups $P < 0.01$.

parison with the control hearts of the same chronological age (12 to 13 weeks). Each nucleus was assumed to contain 6.2 $\mu\mu$g DNA.

Nuclear distribution. It was of interest to determine whether the addition of connective tissue nuclei during hypertrophic growth was proportional to the number of such nuclei present at each point before banding, i.e., whether new connective tissue nuclei appeared in a uniform or a nonrandom distribution.

The hypothesis was made that the new growth was uniform. It was tested statistically by comparing, by the F test,[16] the variances about their means of the ratios (muscle nuclei/connective tissue nuclei) in individual microscopic fields of sections from hypertrophied and control hearts (see Appendix A). Thus, instead of a comparison of these ratios themselves, comparison was made of their distributions in control and hypertrophic hearts.

If the F test should demonstrate that the variance was significantly larger in hypertrophied than in control hearts, it would follow that connective tissue nuclei were less uniformly distributed after hypertrophy than before. Conversely, a significantly smaller variance after hypertrophy would imply an even more uniform distribution of connective tissue nuclei than in controls.

If in fact, such a test indicates that connective tissue nuclei have a less uniform distribution, it must follow that muscle cell nuclei are also more irregularly distributed. Since, however, no evidence was found for significant proliferation of muscle cell nuclei, any change in distribution was considered to be secondary to alteration in the growth pattern of connective tissue nuclei. Comparisons of these variances are presented in Table 5. The variance was significantly greater in hypertrophied hearts than in any group of control hearts considered separately, and also significantly greater than all controls considered as a single group. None of the control groups differed significantly from any of the other controls.

Hydroxyproline assays. Hydroxyproline concentration in the left ventricle was initially decreased on the second day following aortic constriction but rose by the eleventh day to above control values (Table 6). The total hydroxyproline content (μg/heart) was initially unchanged from control values but also rose above control levels on the eleventh day.

Table 5

COMPARISON BY "F" TEST OF THE DISTRIBUTIONS OF CONNECTIVE TISSUE AND MUSCLE NUCLEI IN CONTROL AND BANDED ANIMALS

Group	s^2	n		Group			
				Control 12-13 weeks	Control 17-18 weeks	Control 6-1/2 weeks	All controls
Banded 12 to 13 weeks	0.178639	183	F	1.993	2.127	1.920	2.038
			P	<0.002	<0.002	<0.05	<0.002
Control 12 to 13 weeks	0.089624	116	F		1.067	1.038	1.022
			P		>0.2	>0.2	>0.2
Control 17 to 18 weeks	0.083968	121	F			1.108	1.044
			P			>0.2	>0.2
Control 6-1/2 weeks	0.093030	31	F				1.061
			P				>0.2
All controls	0.087651	268					

The null hypothesis is that for any two groups compared $s_1^2 = s_2^2$. That the variance of the banded group is larger than that of any other group of hearts suggests that new connective tissue nuclei do not appear in strict proportion to the number of connective tissue nuclei already present at each point before banding.

Table 6

HYDROXYPROLINE CONTENT OF CONTROL AND BANDED HEARTS

Group	(n)	Hydroxyproline μg/100 mg wet weight	Hydroxyproline μg/heart
Sham-operated (2 days)	(19)	41.9 ± 1.3	267 ± 10
P (by t test: one tail)		< 0.01	N.S.
Banded (2 days)	(22)	37.0 ± 1.3	274 ± 7
Sham-operated (11 days)	(8)	47.0 ± 2.9	361 ± 21
P (by t test: one tail)		< 0.005	< 0.005
Banded (11 days)	(8)	65.2 ± 4.2	603 ± 35

DISCUSSION

The data presented in this paper provide additional evidence that there is little or no division of cardiac muscle cells following a stimulus to cardiac growth, although total cardiac DNA synthesis is markedly increased. Incorporation of tritiated thymidine into nuclear DNA of hypertrophied hearts was more than six times that of controls two days after banding. Although it is probable that mitochondrial DNA[17,18] also is replicating at this stage, the separation of nuclear and mitochondrial DNA by CsCl gradient centrifugation eliminates the contribution of extranuclear DNA. The size of the thymidine pool as estimated above apparently did not change during the experimental procedure, therefore pool size changes of thymidine triphosphate probably did not account for the increased thymidine incorporation in the hypertrophied hearts.

Radioautography clearly showed that the incorporated tritiated thymidine was almost exclusively associated with nuclei of the connective tissue. The rare muscle nucleus that contained radioactivity may possibly represent a polyploid cell.

Additional evidence that there was no significant proliferation of muscle cells comes from the quantitative determination of cell types. Muscle nuclei made up a smaller fraction of the total number of nuclei in the hypertrophied hearts. The decreased proportion of muscle nuclei was probably secondary to both a decrease in number of muscle nuclei and to an increase in the number of connective tissue nuclei. The decrease in absolute number of muscle nuclei in hypertrophy was statistically significant. Although the observed increase in number of connective tissue nuclei was not statistically significant, the increase is likely to be real. The significant increase in total ventricular DNA content, coupled with the increase in ratio of connective tissue to muscle nuclei, clearly demonstrates that an increase in total number of connective tissue cells must have occurred.

Thus, in our system proliferation of muscle cells during hypertrophic growth lags far behind the proliferation of connective tissue nuclei, and probably occurs to a very limited extent, if at all. Similarly, in diaphragm[12] increases in DNA content with hypertrophy are also associated with

proliferation of connective tissue elements. These results will be discussed with reference to (1) ability of muscle cells to multiply; (2) connective tissue hyperplasia; (3) relevance to other types of cardiac hypertrophy.

Ability of muscle cells to multiply. The cardiac muscle cell apparently loses its ability to divide fairly early in its life. Not all authors are agreed on the exact time at which this ability is lost, and more particularly there is lack of agreement concerning the morphologic and biochemical conditions in the cell which necessitate the end of mitotic activity. Skeletal and cardiac muscle may not be exactly alike in this respect. Stackdale and Holtzer[19] have shown that in developing skeletal muscle DNA synthesis and mitotic cell divisions are incompatible with contractile activity; once the dividing, mononucleated myoblasts fuse to form multinucleated myotubes DNA synthesis ceased in the myotubular nuclei. The results in the differentiating heart are less conclusive. In some studies no mitotic figures are reported in cells containing myofibrils.[20-22] Recently, Manasek has shown[23] by electron microscopy that both contractile and undifferentiated cells are able to divide, confirming the previous light microscopic studies of Mark and Strasser[24] and DeHaan.[25] Thus the differentiation of the heart muscle seems to have features somewhat different from those of skeletal muscle, although these differences may not be basic. As Holtzer and associates[26] state: "in skeletal muscle the decision to synthesize contractile proteins is coupled with the decision to withdraw from the mitotic cycle. In cardiac muscle it may take another division or two before the decision to withdraw from the mitotic cycle takes effect."

It is generally agreed that the number of mitoses in the heart decreases rapidly after birth.[27-32] Although the nuclear density in the growing heart decreases, the total number of nuclei in adult mammalian heart muscle is twice the early postnatal value.[33] Hort[33] supports the thesis that amitotic divisions are the source of new nuclei, but a recent electron microscopic study of postnatal growing heart by Shafiq et al[34] reports that colchicine arrests mitoses in undifferentiated myoblasts and other "free" cells, but not in the already formed muscle fibers. The presence of undifferentiated presumptive muscle cells in developing heart was also described by Wainrach and Sotello.[20] Although the abundant satellite cells in developing skeletal muscle may possibly be myogenic cells (e.g.[34]), such subsarcolemmal satellite cells are not found in developing heart muscle.

In view of the progressive decline in mitotic rates and nuclear densities with age, heart muscle might be considered biochemically adult when DNA synthesis effectively stops. In rats 48 days after birth no more DNA synthesis could be detected.[28] In mice 5 weeks after birth fewer than 0.1 per cent of the nuclei are labeled and those are of endocardial, endothelial, and connective tissue.[29]

Despite the fact that DNA synthesis in the adult heart is at very low levels, some incorporation of labeled thymidine into DNA is always measurable both chemically[4] (this paper) and by radioautography.[7,32] The number of labeled nuclei exceeds the number of observed mitoses by a factor of 10.[7,32] This discrepancy is interpreted by Pelc[7] as evidence for a small amount of "metabolic" DNA, while Klinge[32] explains this observation by "collapsed" mitoses that do not lead to cytoplasmic divisions.

Evidence presented in this paper and by others[2-4] indicates that DNA synthesis is not resumed in differentiated heart muscle cells in the case of cardiac hypertrophy, a situation similar to that of skeletal muscle (e.g.[12,18]). Reports of DNA synthesis in muscle cells of hypertrophying left ventricles of banded rats[35] and in atria (but not ventricles) in hearts with ventric-

ular infarction[36] are in contrast to the above finding. Improved techniques such as thin section radioautography or evaluation with the electron microscope will be necessary to make the identification of cell types less ambiguous and results more conclusive.

Connective tissue hyperplasia. In contrast to the apparent inactivity of the muscle nuclei during hypertrophy, the connective tissue nuclei become quite active, both in terms of mitotic activity and uptake of tritiated thymidine. Increased proliferation of connective tissue nuclei is associated with increased synthesis of collagen. Enhanced synthesis of DNA was noticed on the second day after banding and reached a peak on the seventh day.[3,4] No change was detected in the collagen content of the myocardium on the second day, but by the eleventh postoperative day it had increased by approximately 67 per cent. Thus the new connective tissue nuclei and collagen are produced at about the same time. Increased collagen content has been shown to accompany cardiac enlargement produced by other methods: narrowing of the aorta in rats[37] and pulmonary artery in cats,[38] administration of isoprenaline, long-term adaptation to hypoxia, and physical stress.[37] Exceptions were cardiomegaly produced by anemia, where collagen content did not change, and the effects of thyroxine administration, where the collagen content increased only moderately.[37]

As to the localization of collagen production, no attempt was made to distinguish between the synthesis of collagen in connective tissue of the interstitium and in the blood vessels. There are different opinions about changes of number of capillaries in hypertrophying heart. No change was reported by Roberts and Wearn,[39] while Linzbach[40] found that the ratio of capillaries to the cross-sectional area of the muscle fibers is relatively constant during hypertrophy except in the advanced stages. The thickness of blood vessel wall is said to increase.[41]

A statistical analysis of the spatial distribution of connective tissue nuclei demonstrated that the distribution was different after hypertrophy. If muscle cell nuclei are considered as a fixed matrix in space, then connective tissue nuclei are arranged more irregularly in this matrix after hypertrophy than before it. Alternatively, new connective tissue nuclei are not produced in proportion to the number already present at each point before hypertrophic growth starts.

Our observations are consistent with the hypothesis that acute constriction of the aorta may lead to focal or scattered necrosis with subsequent replacement by connective tissue.

Relevance to other types of cardiac hypertrophy. The observations made in this paper refer to rapidly produced cardiac hypertrophy. It is not known whether the generalization that division of cardiac muscle cells does not occur in cardiac hypertrophy in the adult applies to all pathological or experimental situations. To date however, in contrast to skeletal muscle, no evidence for cardiac muscle regeneration has ever been obtained. It is likely that it does not occur under ordinary physiological and pathological situations. That does not necessarily mean that the potential for muscle cell proliferation has been lost but only that it is not stimulated under the pathological and experimental conditions so far examined.

Clinical cardiac hypertrophy is likely to have a more gradual onset than is produced by experimental aortic constriction. The abrupt hyperplasia of connective tissue cells observed in this study may be related to the rapid appearance of hypertrophy, and may be modified in other types of more slowly developing cardiac enlargement.

The cardiac hypertrophy occurring in congenital lesions in the young may differ from the model studied here. The potential for muscle cell division is retained in embryonic and young

muscle cells, and it may be that stimuli for cardiac growth lead to cell division under these circumstances. More work must be done to clarify this part.

APPENDIX A

In order to test whether changes in the distribution of connective tissue nuclei, relative to the distribution of muscle cell nuclei, had occurred, it was necessary to devise a variable whose variance would not be greatly affected by the change in the ratio of muscle to connective tissue nuclei that was found with hypertrophy. This was accomplished as follows:

Given a section of tissue in which $\underline{P}$ total nuclei including $\underline{M}$ muscle nuclei and $\underline{C}$ connective tissue nuclei, are counted in $\underline{N}$ total fields, $M + C = P$. If in each field scored, $\underline{m_i}$ $(i = 1,2 \ldots N)$ muscle and $\underline{c_i}$ connective tissue nuclei are counted,

$$\sum_{i=1}^{N} m_i + \sum_{i=1}^{N} c_i = M + C = P$$

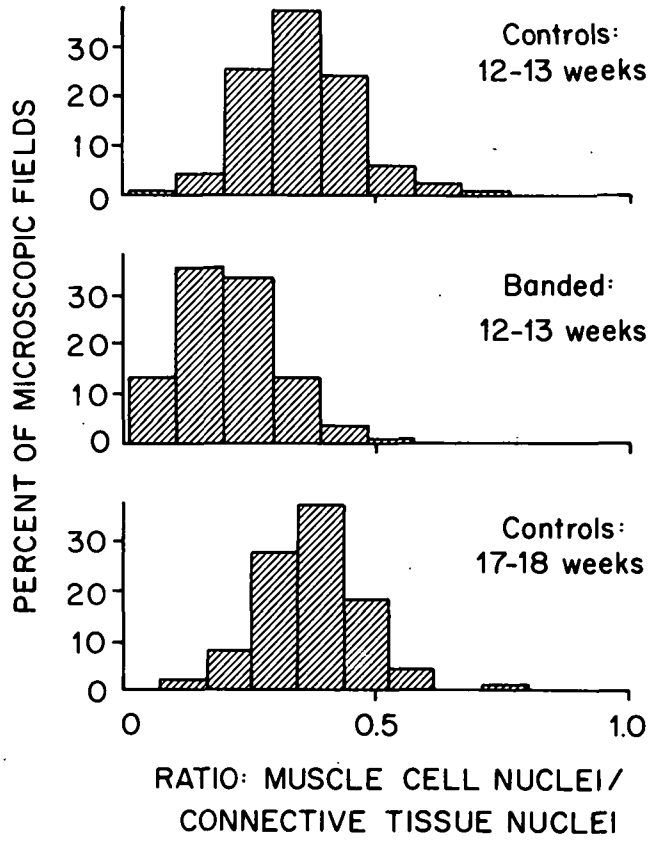

Figure 3. The ratio of muscle nuclei to connective tissue nuclei in control and hypertrophic hearts.

Define the average ratio of muscle to connective tissue nuclei for the section (or heart), $R = M/C$. For each field $\underline{r_i} = m_i/c_i$, and for a large number of fields

$$\left(\sum_{i=1}^{N} r_i\right) \Big/ N = \bar{r}_i \approx R, \text{ and } \bar{r}_i/R \approx 1$$

One may call r_i/R a "normalized" variable. It is seen that r_i/R has an average value close to 1, regardless of the average value M/C, and that the variance of r_i/R,

$$s^2_{r_i/R} = \sum_{i=1}^{N} \frac{\left((r_i/R) - \left(\sum_{i=1}^{N} r_{i/NR}\right)\right)^2}{N - 1}$$

provides a mean of comparing the shapes of the distributions of r_i/R in different sections or different hearts. In the material studied in these experiments, typical values for R were 0.35 for control hearts, and 0.21 for hypertrophic hearts. In Figure 3 are plotted the values of m_i/c_i for microscope fields in sections from control and hypertrophic hearts, and in Figure 4 are

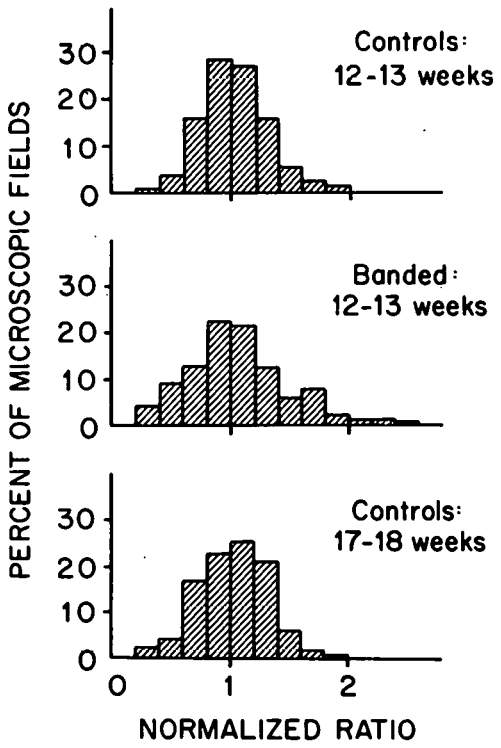

Figure 4. Plot of the value of the "normalized" variable, r_i/R, in control and hypertrophic hearts. The distribution of the variable r_i/R in banded animals is not significantly different from the normal ($P > 0.05$ by χ^2).

plotted the values r_i/R for the same hearts. Clearly, the variance $s^2_{r_i/R}$ is larger in the case of the hypertrophic hearts. This change in variance with hypertrophy is detected by the F test, and suggests a nonuniform growth of connective tissue.

ACKNOWLEDGMENTS

We thank Dr. Murray Rabinowitz for his extremely valuable discussions and suggestions and Dr. Hewson Swift for his help and encouragement. We also thank Mrs. Grace Wu for her excellent technical assistance.

LITERATURE CITED

1. Grove, D., K. G. Nair, and R. Zak. Circulation Res., 25:483, 1969.
2. Crane, W. A. J., and L. P. Dutta. J. Pathol. Bacteriol., 86:83, 1963.
3. Meerson, F. Z., and G. M. Alekhina. Dokl. Akad. Sci. USSR, 173:122, 1967.
4. Morkin, E., and T. P. Ashford. Am. J. Physiol., 215:1409, 1968.
5. Meerson, F. Z., G. M. Alekhina, P. N. Aleksandrov, and A. G. Bazardjan. Am. J. Cardiol., 22:337, 1968.
6. Yaffe, D., and M. Feldman. Devel. Biol., 9:347, 1964.
7. Pelc, S. R. J. Cell Biol., 22:21, 1964.
8. Brown, D. D., and I. B. Dawid. Science, 160:272, 1968.
9. Nair, K. G., A. F. Cutilletta, R. Zak, T. Koide, and M. Rabinowitz. Circulation Res., 23: 451, 1968.
10. Messier, R. B., and C. P. LeBlond. Am. J. Anat., 106:247, 1960.
11. Joftes, D. L. Lab. Invest., 8:131, 1959.
12. Zak, R., Grove, D., and M. Rabinowitz. Am. J. Physiol., 216:647, 1969.
13. Gross, N. J., G. S. Getz, and M. Rabinowitz. J. Biol. Chem., 244:1552, 1969.
14. Newman, R. E., and M. A. Logan. J. Biol. Chem., 184:299, 1950.
15. Diem, K. (editor). Documenta Geigy. New York: Scientific Tables, 1962.
16. Bliss, C. I. Statistics in Biology. New York: McGraw-Hill, 1967.
17. Rabinowitz, M., J. Sinclair, L. DeSalle, R. Haselkorn, and H. H. Swift. Proc. Natl. Acad. Sci. U.S., 53:1126, 1965.
18. Rabinowitz, M. Bull. Soc. Chim. Biol., 50:311, 1968.
19. Stackdale, F. L., and H. Holtzer. Exptl. Cell. Res., 24:508, 1962.
20. Wainrach, S., and J. R. Sotello. Z. Zellforsch., 55:622, 1961.
21. Rumery, R. E., and R. J. Blandau. Acta Anat., 58:116, 1964.
22. Rumery, R. E., and W. O. Rieke. Anat. Res., 158:501, 1967.
23. Manasek, F. J. J. Cell Biol., 37:191, 1968.
24. Mark, G. E., and F. F. Strasser. Exptl. Cell Res., 44:217, 1966.
25. DeHaan, R. Devel. Biol., 16:216, 1967.
26. Ishikawa, H., R. Bischoff, and H. Holtzer. J. Cell Biol., 38:538, 1968.
27. Grohmann, D. Z. Zellforsch., 55:104, 1961.

28. Enesco, M., and C. P. LeBlond. J. Embryol. Exptl. Morphol., 10:530, 1962.

29. Petersen, R. O., and R. Baserga. Exptl. Cell Res., 40:340, 1965.

30. Rumyantsev, P. P. Arkh. Anat. Histol. Embryol., 47:59, 1964; Fed. Proc., 24:T899, 1965.

31. Overy, H. R., and R. E. Priest. Lab. Invest., 15:1100, 1966.

32. Klinge, O., and E. Stocker. Experientia, 24:167, 1968.

33. Hort, W. Virchows Arch. Pathol. Anat., 323:223, 1953.

34. Shafiq, S. A., M. A. Goricki, and A. Mauro. J. Anat., 103:135, 1968.

35. Wegner, G., and E. Molbert. Virchows Arch. Pathol. Anat., 341:54, 1966.

36. Rumyantsev, R. P., and V. O. Mirakjan. Experientia, 24:1234, 1968.

37. Bartosova, D., M. Chvapil, B. Korecky, O. Poupa, K. Rakusan, Z. Turek, and M. Vitez. J. Physiol., 200:285, 1969.

38. Buccino, R. A., E. Harris, J. F. Spann, and E. H. Sonnenblick. Am. J. Physiol., 216:425, 1969.

39. Roberts, J. R., and J. T. Wearn. Am. Heart J., 21:617, 1941.

40. Linzbach, A. J. Am. J. Cardiol., 5:370, 1960.

41. Meerson, F. Z., T. D. Beloshapkina, E. F. Lushnikov, E. M. Leikina, G. N. Markovskaya, and G. V. Chernyshova. Vest. Akad. Med. Nauk USSR, 18:27, 1963; Fed. Proc., 23:T667, 1964.

DEGRADATION AND REASSEMBLY OF A HUMAN SERUM HIGH DENSITY LIPOPROTEIN: EVIDENCE FOR DIFFERENCES IN LIPID AFFINITY AMONG 3 CLASSES OF POLYPEPTIDE CHAINS*

By

A. Scanu,† E. Cump, J. Toth, S. Koga,‡ E. Stiller,§ and L. Albers

Earlier studies from this laboratory showed that the protein moiety of human serum high density lipoprotein (HDL),¶ prepared in an essentially lipid-free form (apo HDL) by treatment with organic solvents (Scanu et al,[1] Scanu[2]) retains its capacity to bind lipids both in vitro (Scanu and Hughes[3]) and in vivo (Scanu[4]). In subsequent work (Scanu,[5] Sodhi and Gould[6]), it was shown that there was a direct interaction between apo HDL and phopholipids or phospholipids and free cholesterol, whereas the uptake of neutral lipids (cholesterol esters and triglycerides) was minimal (Sodhi and Gould[6]). More recently, the problem of the reassembly of HDL from its constituents was further analyzed by Hirz and Scanu,[7] who, by subjecting mixtures of apo HDL and HDL lipids to sonic irradiation at 40° C, were able to restore a complex closely resembling a native high density lipoprotein. Stimulated by such observations and by the recent discovery that apo HDL is made of chemically distinct polypeptide chains (Shore and Shore,[8] Scanu et al[9]) we planned to investigate, in greater detail, the mechanism of HDL reassembly with the hope of learning more about HDL structure. An account of such investigations is the object of the present report. It will also include studies on the partial degradation of HDL since the data obtained are complementary to those on reassembly.

MATERIALS AND METHODS

Preparation of HDL_2 and apo HDL_2. HDL_2 was separated from freshly drawn sera of healthy male, 24-hour fasted, Caucasian human donors (Rh-, group A) as described previously.[2] Apo HDL_2, in an essentially lipid-free form, was prepared by extraction of HDL with 3:2 ethanol:ether at -10° C.[2]

Fractionation of apo HDL_2 by gel filtration. Apo HDL_2, dissolved in Tris buffer, 0.01 M pH 8.4, 8 M urea was separated in Sephadex-G200 columns at 15° C according to the conditions described previously.[9] Fractions III, IV and V, each of which contains a chemically distinct class of polypeptides[9]—I and II appear to represent mixtures of these—were dialyzed against Tris buffer, 0.01 M pH 8.4, 10^{-3} EDTA, to remove the urea, and then concentrated by vacuum dialysis at

* This report is taken from a paper that appeared in Biochemistry, 9:1327, 1970. The work was supported in part by grants from the National Institutes of Health, Life Insurance Medical Research Fund and the Chicago and Illinois Heart Associations.

† Recipient of Research Career Development Award from the U. S. Public Health Service.

‡ Department of Medicine, University of Chicago. Post-doctoral research fellow, Chicago and Illinois Heart Association.

§ Post-doctoral research fellow, United States Public Health Service.

¶ The abbreviations used in the text are as follows: HDL_2 = serum high density lipoprotein of d 1.063-1.125; apo HDL_2 = protein moiety of HDL_2 after extraction with ethanol-ether; L = whole lipid extract from HDL_2; III, IV and V refer to the three classes of proteins separated from apo HDL_2 by gel filtration.[9]

4° C to a final concentration of 1-2 mg/ml. The lack of cross-contamination among these three fractions was checked by polyacrylamide gel electrophoresis in 8 M urea and, occasionally, by immunoprecipitation and amino acid analysis. The details of these techniques are given elsewhere.[9]

Preparation and storage of HDL_2 lipids. The 3:2 ethanol:ether extracts from HDL_2 were cleared of any precipitate by centrifugation at 4° C (3,000 rpm, Sorvall refrigerated centrifuge) and then brought to dryness by flash evaporation. The dry materials were dissolved in hexane (10-20 mg/ml) and stored at -20° C under N_2. In certain experiments the phospholipids of HDL_2 were separated from the non-polar lipids by column chromatography as described before.[2] Further separation of individual phospholipids or neutral lipids was carried out by thin layer chromatography (see below).

Re-assembly experiments. After evaporation of the hexane phase by N_2, the lipids were suspended in 0.02 M EDTA, pH 7.4, to a final concentration of 10-50 mg/ml and the suspensions were sonicated briefly in a Branson Sonifier (Heat Systems Co., Melville, L. I., N. Y.) (75 watts, 15 seconds, 40° C) to obtain an even lipid dispersion. Aliquots of the desired lipid concentration were diluted to a final volume of 8 ml with 0.02 M EDTA, pH 7.6, and transferred into an aluminum cooling cell, 2-3/4 inches long x 3/4 inch diameter (Heat Systems Co.) designed for fast dissipation of heat. To the lipid emulsion was then added sufficient dry apo HDL to obtain the final lipid-protein weight ratio of 1:1. Protein or lipid above this ratio remained unbound (see Results). After a gentle hand shaking of the final mixture to insure mixing of the constituents, sonication was carried out in a Branson Sonifier using the standard microtip assembly at 40° C for a total period of 3 minutes (3 one-minute sonication periods with 3 two-minute intervals). Bubbling of N_2 through the mixture during sonication was initially employed to prevent possible peroxidation, but was, however, found to be unnecessary, and was omitted in subsequent studies. Sonic irradiation of separate preparations of HDL_2, apo HDL_2 or HDL_2 lipids was carried out under the same conditions as those for lipid-protein mixtures. Aliquots of the resulting products were dialyzed against NaCl-$NaBr_2$ d 1.21 g/ml solutions and then analyzed in a Spinco Mod E Analytical Ultracentrifuge.

Fractionation of lipid-protein mixtures after sonic irradiation. Three fractions (1 ml) were separated by preparative ultracentrifugation (Spinco 40.3 rotor, 40,000 rpm, 15° C, 36 hours): < 1.063, 1.063-1.21 and > 1.21. Density adjustments were made with solid NaCl and NaBr as previously described.[9] In some instances the $d < 1.063$ fraction was further separated into $d < 1.006$ and d 1.006-1.063 fractions by preparative ultracentrifugation.

Analyses of sonicated mixtures after ultracentrifugal fractionation. A. Before delipidation. Each fraction was studied by analytical polyacrylamide gel electrophoresis in 8 M urea[9] and then analyzed for protein and lipid composition by analytical ultracentrifugation and electron microscopy. The fractions were also tested by immunodiffusion techniques (Ouchterlony and immunoelectrophoresis) with antisera prepared in the rabbit against human apo HDL, and its Sephadex fractions III, IV and V.[9] Circular dichroic spectra of all of these products were also recorded.

B. After delipidation. All fractions were delipidated by 3:2 ethanol:ether[2] except that the extraction procedure was, in most instances, carried out in smaller (10 ml) conical centrifuge tubes when handling specimens with a protein content of 0.5 to 1 mg/ml. The lipid extracts were analyzed by a combination of thin layer chromatography and chemical procedures (see below).

The lipid-free proteins were, after analysis by polyacrylamide gel electrophoresis, hydrolyzed by 6N HCl (see, for conditions, Scanu et al[9]) and the amino acid content of the hydrolysates was determined in a Beckman Mod 120C Amino Acid Analyzer equipped with a scale expander. Tryptophan and cystine were determined as described previously.[2]

Studies of HDL_2 after degradation by ethyl ether. To insure reproducibility the following conditions were carefully followed. Fifty ml capacity Pyrex round bottom centrifuge tubes were partially filled with 30 ml ethyl ether and kept at 4° C. HDL_2 containing 10 mg protein in 2 ml 0.15 M NaCl, 0.001 M EDTA was added dropwise, and the tubes were then filled completely with ethyl ether. After stoppering, the tubes were rotated in a Multi-Purpose Rotator Model 150V (Scientific Industries, Inc., Springfield, Mass.) at approximately 15-20 revolutions per minute for 12 hours at 4° C. This was followed by a centrifugation step (3,000 rpm at 4° C) to allow for a clear separation between the aqueous and other phases. The latter was removed by aspiration and the yellow-clear lipoprotein solution was washed twice with ethyl ether at 4° C. After the two washings, any trace of organic solvent was removed by N_2. The resulting product was analyzed at d 1.21 g/ml in a Spinco Mod E Analytical Ultracentrifuge and then fractionated by preparative ultracentrifugation into 3 fractions: d < 1.063, d 1.063-1.21 and d > 1.21. These fractions were then analyzed before and after complete delipidation as indicated for the fractions obtained from the experiments of reassembly.

Separation of HDL_2 and ether-treated HDL_2 by gel filtration. The experiments were carried out at 10° C in Sephadex G-200 columns (2 x 100 cm) using 0.1 M Tris pH 8.4, 0.001 M EDTA as the equilibrating and eluting buffer. An ascending flow of 10-12 ml/hr was used with monitoring of effluent at 280 mm in an ISCO recorder (Instrumentation Specialties Co., Inc., Lincoln, Neb.). The peaks were concentrated by vacuum dialysis at 4° C and then either analyzed or rechromatographed under the same conditions.

Fractionation of HDL_2 was also carried out by filtration through Sephadex 4B (Pharmacia, Uppsala, Sweden) columns, 2.5 x 40 cm, using 0.05 M Tris, pH 7.4, 10^{-3} EDTA at a flow rate of about 10 ml/hr.

Analytical procedures. Flotational studies were carried out in a Spinco Mod E Analytical Ultracentrifuge using a Spinco An-D rotor and double sector cells to allow for the simultaneous analysis of solvent and lipoprotein solution. Runs were carried out at 42,040 rpm, 20° C. Flotational rates were determined from Schlieren photographs magnified (x 20) in a Nikon Mod 6C (Nikon Co., Japan) microcomparator.

Electron microscopy was performed in an RCA EMU-3G unit using a pointed filament, an accelerating voltage of 50 KV, a 50 U objective aperture, and a maximum instrument magnification of X30,000. Magnification was determined by reference to a carbon grating replica of 2160 lines/mm. Particle sizes were determined directly from negatives on a Nikon microcomparator. Before microscopy the samples were extensively dialyzed against 0.01 M phosphate buffer, pH 8.6, 10^{-3} M EDTA. Ultra-thin, carbon coated, fenestrated formvar grids were employed. The negative stain was 2 per cent phosphotungstic acid in 0.001 M phosphate buffer, pH 7.0.

Studies by the technique of circular dichroism were carried out in a Cary Mod 6001 spectropolarimeter with circular dichroism attachment, as described previously.[10]

Immunological testing of the various lipoprotein fractions was carried out by double diffusion techniques in agarose gels.[2] The antisera used against HDL, apo HDL, fractions III, IV and V were prepared in the laboratory.[9]

The technique for the determination of total protein, total cholesterol and phospholipids were as described previously.[2] Separation of free and ester cholesterol was carried out by silica gel thin layer chromatography and so was the separation of the various phospholipid fractions.[2] These fractions, after identification by iodine vapor, were scraped off the thin layer plates and quantified chemically.

All organic solvents were freshly distilled before use.

RESULTS

Studies on re-assembly of apo HDL_2 and subfractions. Apo HDL_2 + L. After sonic irradiation (total sonication time: 3 minutes) the mixture, which was frankly turbid, became clear yellow, similar in appearance to native HDL_2. As shown previously with HDL_3,[7] turbidity persisted when HDL_2-L was sonicated in the absence of apo HDL_2. Such a solubilizing effect by apo HDL_2 was not observed with human serum albumin, α_1- and α_2-globulin, γ-globulin, cytochrome c, lysozyme and myoglobin at least in terms of the commercial preparations used (Nutritional Biochemicals, Cleveland, Ohio; Mann Research Laboratories, Orangeburg, N. J.).

In the analytical ultracentrifuge the sonicated apo HDL_2 + L mixture examined at d 1.21 g/ml at 20° C exhibited a main component (about 80 per cent of total) of $F_{1.21}$ = 2.0, and two minor components, one in the low-density range ($F_{1.21}$ = 20) and the other of density greater than 1.21. Similar results were obtained by preparative ultracentrifugation. In terms of protein content, 70-80 per cent of the starting material was in the top 1 ml of the d 1.063-1.21 and gave a single component in the analytical ultracentrifuge (Figure 1C); 10-15 per cent was in the d > 1.21 fraction, and about 5 per cent in the top of the d < 1.063 fraction. The chemical composition of these fractions was distinct (Table 1) indicating not only differences in protein-lipid but also in cholesterol-phospholipid ratios—see top 1 ml of d < 1.063 and d > 1.21. These two fractions, however, had similar cholesterol free:ester ratio and the phospholipid distribution (phosphatidylcholine, sphingomyelin, phosphatidylethanolamine and serine, lysophosphatidylcholine) described for HDL.[2] The d 1.21 bottom 1 ml had only a small amount of lipids, almost exclusively lecithin, with traces of cholesterol.

By polyacrylamide gel electrophoresis in 8 M urea, the d 1.063 fraction did not penetrate

Table 1

PROPERTIES OF THREE ULTRACENTRIFUGAL FRACTIONS FROM A SONICATED MIXTURE OF apo HDL_2 + L

Ultracentrifugal fractions (1 ml) density (g/ml)	Appearance	Protein	Lipid			
			Phospholipid	Cholesterol		Triglycerides
				Ester	Free	
		% weight[a]				
< 1.063	sl.turbid	18.2	30.8	33.0	6.8	11.2
1.063 - 1.21	clear	52.8	33.2	10.0	2.0	2.0
> 1.21	clear	96.0	4.0	-	-	-

[a]Values are the average of two determinations.

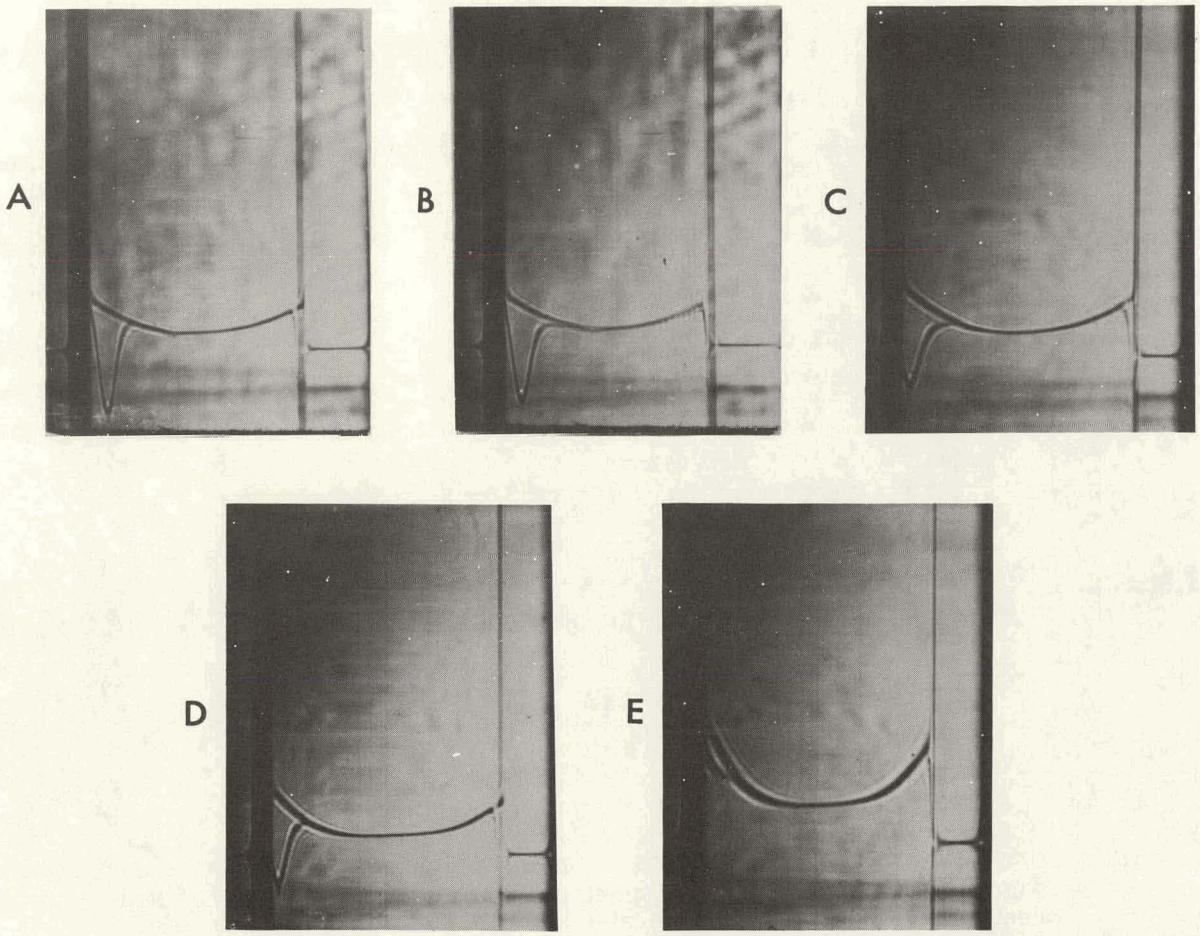

Figure 1. Schlieren optics ultracentrifugal patterns of various HDL_2 products before and after re-assembly. A. HDL_2 4 mg/ml; B. HDL_2 sonicated, 4 mg/ml; C. Apo HDL_2 + L (d 1.063-1.21) 3.2 mg/ml protein; D. III + L (d 1.063-1.21) 1.7 mg/ml; E. IV + L (d 1.063-1.21) 0.46 mg/ml. All specimens were dialyzed against d 1.21 $NaCl$-$NaBr_2$ solutions before analysis. Speed, 42,040 rpm; AN-D rotor with double sector cells; t°, 20° C. All pictures were taken 40 minutes after rotor had reached full speed. Flotation is from left to right.

the gel. After delipidation with ethanol ether (Figure 2A,a), however, several bands with distinct mobility were observed. The d 1.21 top (2A,b) showed two major bands of about equal intensity. The d 1.21 bottom exhibited only a major band (Figure 2A,b) while a faster component was either absent or only seen in trace amounts. The results were identical before and after delipidation. When these band patterns are compared with that of apo HDL_2, previously described,[9] and represented in Figure 3, it can be concluded that the polypeptide chains corresponding to Sephadex peaks III and IV are about equally represented in the d 1.21 top, peak III was the almost exclusive component of the d 1.21 bottom, and d 1.063 top contained traces of III but was predominantly IV and V. The correspondence of the observed bands with the Sephadex fractions previously described was supported by immunological studies using specific antisera and also by the result of the amino acid analyses.

Electron microscopy showed that there was a significant difference in number and average

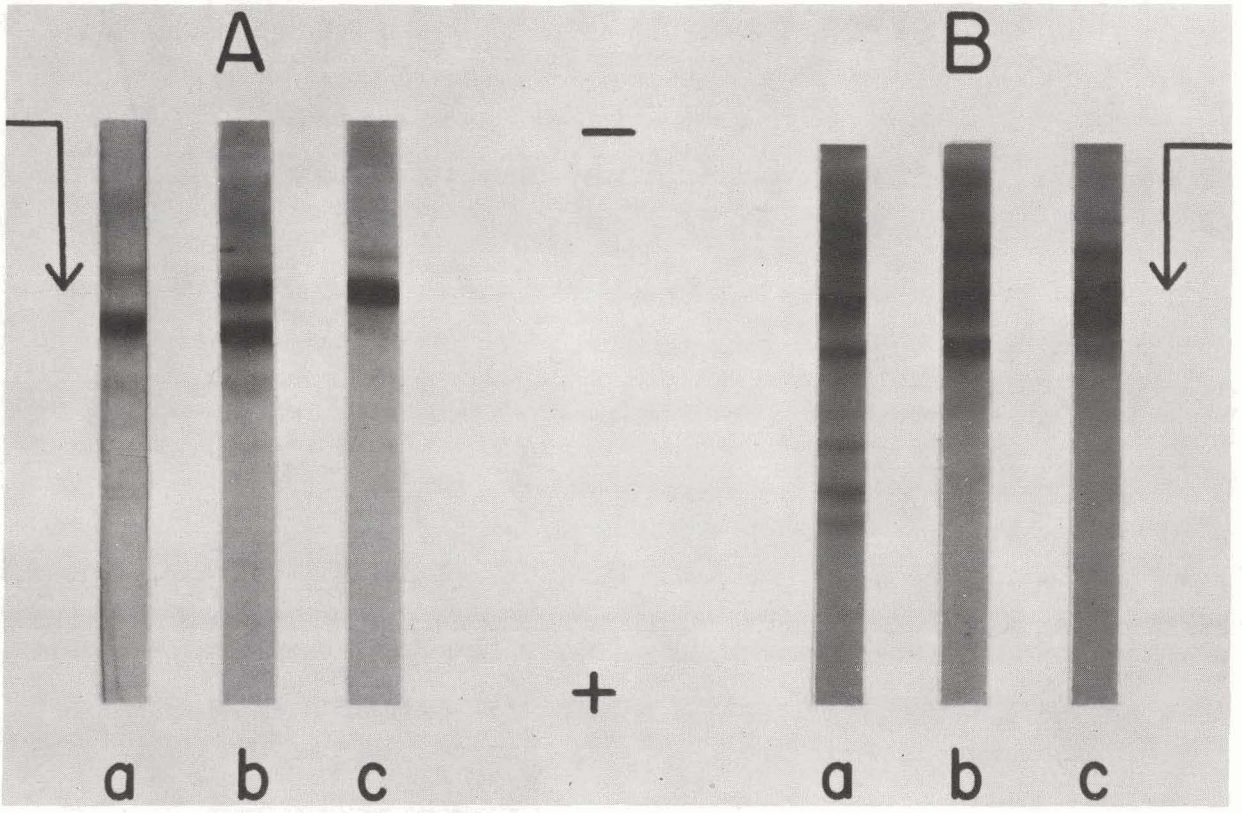

Figure 2. Polyacrylamide gel electrophoresis (8 M urea) of three ultracentrifugal fractions from sonicated apo HDL_2 + L mixtures. A = after 3 minutes sonication; B = after 6 minutes. a = d < 1.063; b = 1.063-1.21; c = > 1.21. All fractions were studied after extraction with 3:2 ethanol ether. The electrophoretic conditions were described before.[9]

particle size among the three ultracentrifugal fractions studied only before delipidation (Table 2). The d < 1.063 contained the largest particles (range 150-400 Å; number average 250 Å) and d > 1.21 the smallest (range 50-120 Å; number average 70 Å). The d 1.21 top had particles in the size range of 65-180 Å; number average 110 Å (Figure 4,B). These particles were slightly larger than those observed with HDL_2 (Table 2 and Figure 4,A) but about equal in size to sonicated HDL_2 (Table 4, see also later).

Further similarity between HDL_2 and the d 1.063-1.20 top from sonicated apo HDL_2 + L mixture was observed by the technique of circular dichroism. The two products gave indistinguishable patterns (0.01 M Tris, pH 8.4, 10^{-3} M EDTA, 27° C) and, as previously described,[10] exhibited two negative bands at 222 and 208 nm and a positive peak at 198 nm. The molar ellipticity values in 10^{-4} deg-cm^2/decimole were $[\theta]_{222}$ = 2.0-2.2, $[\theta]_{208}$ = 1.9-2.1 $[\theta]_{198}$ = 3.8-4.2. When the spectra were recorded as a function of temperature in the range of 20° and 80° C, the course of the thermal transition of both HDL_2 and the reconstituted lipoprotein, based on the changes of the 222 nm band, was similar and markedly distinct from apo HDL_2 (Figure 5). In all of the above experiments, protein and lipid in the sonicated mixtures were in the weight ratio of 1:1. If apo HDL_2 exceeded this ratio, it was recovered in the d > 1.21 bottom as a mixture of III and IV (no V was detected). In turn, any excess lipid was recovered in the d < 1.006 top fraction.

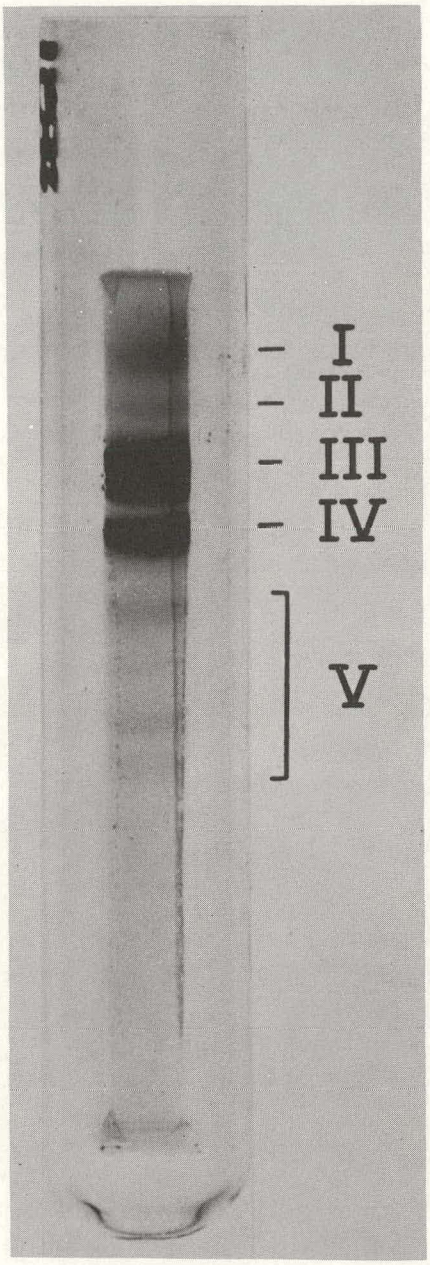

Figure 3. Polyacrylamide gel electrophoresis in 8 M urea of apo HDL_2. The correspondence of these bands with fractions obtained by gel filtration is indicated.[9]

The effect of the length of sonication time on the re-assembly experiments was also examined. At 1 minute sonication the apo HDL_2 + L mixture, although significantly clearer than the starting one, was still opalescent. This was due to unbound lipids that floated at $d < 1.006$ and led to lower recoveries of d 1.21 top and bottom fractions. The polyacrylamide gel pattern of the d 1.21 top exhibited both peaks III and IV, whereas the bottom 1.21 ml had essentially only III. With longer periods of sonication (above three minutes) the protein-lipid mixtures remained

Table 2

ELECTRON MICROSCOPIC FINDINGS IN THE RE-LIPIDATED PRODUCTS FROM apo HDL_2 AND ITS SUBFRACTIONS III AND IV

Materials		Particle size, Å	
		Range	Number average
HDL_2		60-135	90
HDL_2 sonicated		70-170	110
Apo HDL_2 + L	d < 1.063	150-400	250
	d 1.063-1.21	65-180	110
	d > 1.21	50-120	70
III + L	d < 1.063	120-410	200
	d 1.063-1.21	60-160	120
	d > 1.21	40-140	90
IV + L	d < 1.063	180-600	300
	d 1.063-1.21	70-280	180
	d > 1.21	50-150	100

perfectly clear: there was a tendency for IV to decrease in relation to III in the d 1.21 top and to progressively increase in the d < 1.063 fraction. Concomitantly, more III sank into the d 1.21 bottom. The patterns remained unchanged when the same products were analyzed after 1 to 2 weeks at 4° C. Patterns after 6 minutes sonication are shown in Figure 2B. Additional bands preceding III, probably representing aggregation, were seen.

Re-lipidation of apo HDL_2 with non-HDL lipids. The experiments were carried out with purified preparations of phosphatidylcholine (egg) (Sylvana Co., Millburn, N. J.), cholesterol free, cholesterol oleate and triolein (Applied Science Laboratories, State College, Pa.). Sonication of apo HDL_2 with phosphatidylcholine (1:1 weight ratio) for 3 minutes at either 4° or 40° C led to formation of a protein-phospholipid complex floating at d 1.24 with properties very similar to those described for a corresponding product prepared in the laboratory by a different re-lipidation technique.[5] III and IV were the polypeptide chains of this complex. Apo HDL_2 produced also solubilization (sonication 3 minutes, 40° C) of aqueous suspensions of phosphatidylcholine, cholesterol free and ester and triolein added in proportions similar to their counterparts in HDL_2. The high density lipoprotein recovered in the d 1.21 top ml had again III and IV as its protein constituents. A more detailed investigation of this and other systems containing varying mixtures of artificial lipids will be reported elsewhere.

Re-lipidation of III, IV and V. Sonic irradiation of these fractions was carried out in the presence of whole lipid extracts from HDL_2 under the experimental conditions described in Methods. Fractions III or IV produced a complete solubilization of the HDL_2 lipid suspension. The solubilization time was more rapid (within 2 minutes) with fraction IV than with fraction III (within 3 minutes). In all protein-lipid weight ratios used (0.1-2:1), Fraction V failed to produce complete clearing of the lipid suspension; this appeared slightly opalescent in contrast to the starting mixture which was frankly turbid. The lipid-protein composition of the top ml of the d 1.063-

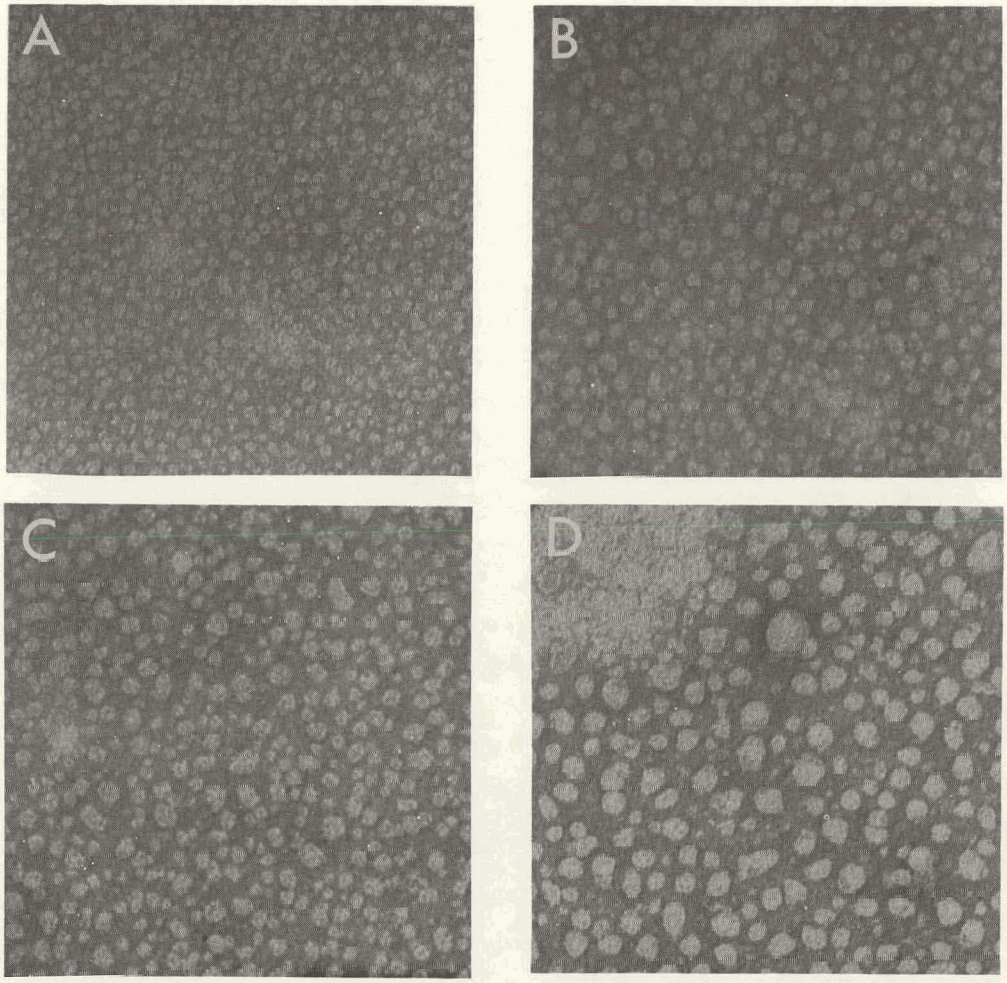

Figure 4. Electron micrographs of HDL_2 (A); apo HDL_2 + L, d 1.21 top (B); III + L, d 1.21 top (C); IV + L, d 1.21 top (D). For experimental conditions, see text. Final magnification = 120,000 X.

1.21 fractions obtained from the relipidation of III and IV and V are shown in Table 3. Clear differences in protein-lipid ratio and lipid distribution were noted between fractions III and IV, the latter having more lipid with a prevalence of neutral lipids. On the other hand, no material floating between d 1.063 and 1.21 was noted with sonicated fraction V + L mixtures. About 90 per cent of fraction V was recovered in the d 1.063 top of $S_{f(1.063)}$ 4-6 (per cent weight composition: protein, 20; phospholipid, 24; cholesterol esters, 39; cholesterol free, 7; glyceride, 10); the remainder was in the d 1.21 bottom. In the sonicated mixtures containing either III or IV, about 1-2 per cent was recovered in the d 1.063 top ml (because of low yield no accurate chemical analysis was performed). The remaining 10-20 per cent was in the d 1.21 bottom ml and contained 3-4 per cent lipid.

By polyacrylamide gel electrophoresis, the re-lipidated fractions III and IV maintained their distinct mobilities (see, Scanu et al[9] and Figure 3). This was also the case of the ultracentrifugal d 1.21 top and bottom fractions whether studied before or after delipidation with ethanol-ether. In the d 1.063 top ml, only a minute amount of either III or IV was observed after delipidation. In terms of the sonicated V + L mixtures, the top < 1.063 fraction, when analyzed before delipi-

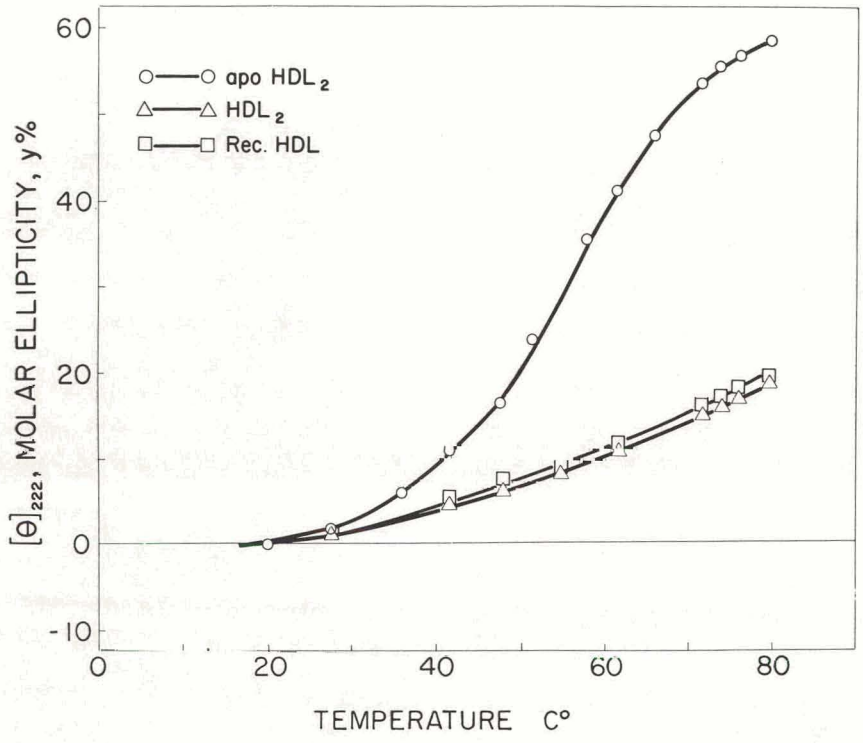

Figure 5. Thermal dependence of denaturation of HDL_2, apo HDL_2 and reconstituted HDL as assessed by circular dichroic analyses. The graph is a representation of the per cent change of the 222 nm band as a function of temperature.

Table 3

LIPID-PROTEIN COMPOSITION OF THREE ULTRACENTRIFUGAL FRACTIONS FROM SONICATED MIXTURES OF apo HDL_2 SUBFRACTIONS AND LIPIDS

Apo HDL_2 sub-fractions	d 1.063-1.21 (top 1 ml)				
	Protein	Lipid			
		Phospholipid	Cholesterol ester	Cholesterol free	Glyceride
	% weight[a]				
III	50.1	30.0	11.8	2.0	6.2
IV	45.0	27.8	17.2	4.0	6.0
V	-[b]	-	-	-	-

[a]The values are the average of two determinations.

[b]None detected.

dation, failed to penetrate the gel. After treatment with 3:2 ethanol-ether the characteristic four band pattern of peak V (see Figure 3) was observed. The same pattern was found in the d < 1.063 bottom when V was added in excess to the system.

In the analytical ultracentrifuge the d 1.21 top from sonicated III + L mixtures exhibited a

single flotational component with $F_{1.21}$ = 2.0-2.2 (Figure 1D). On the other hand, the corresponding fraction from IV + L mixture gave a broad floating component (Figure 1E) with $F_{1.21}$ values between 1.0 and 6. No studies on the analytical ultracentrifuge were conducted with the IV + L mixture after fractionation in the preparative ultracentrifuge.

Electron microscopy revealed a significant difference in size distribution between reassembled products from III and IV (Table 2), the former exhibiting a striking similarity with apo HDL_2 + L. Electron micrography of these products (d 1.21 top) are shown in Figure 4.

Graded re-lipidation of III and IV. These experiments were designed to determine whether the high density lipoprotein species obtained from the re-assembly experiments with III or IV, are capable of further incorporating IV, or III, respectively. The experimental design was as follows: III or IV were sonicated in the presence of HDL_2 lipids (weight ratio 1:1) for 3 minutes at 40° C. After cooling to 4° C, either III or IV was added without sonication (weight ratio, III:IV, 1:1) and the resulting mixtures $(III + L)_{son}$ + or $(IV + L)_{son}$ + III kept at 4° C for 12 hours. They were then separated in the preparative ultracentrifuge at d < 1.063, 1.063-1.21 and > 1.21 and the fractions obtained were analyzed as indicated previously. In some experiments, peak V was also used. The results of such experiments (Table 5) indicate that when a lipoprotein complex is formed by the sonication procedure, further addition of protein, although in small amounts, is possible with very little energy requirement. Examination of Table 4 again indicates the tendency by III, IV and V to distribute specifically in given ultracentrifugal fractions. If the initial sonication step was omitted, however, no significant incorporation of either cholesterol esters or triglycerides was observed.

Table 4

GRADED RE-LIPIDATION OF FRACTIONS III AND IV FROM apo HDL_2

Constituents in the mixture[a]			Polypeptides in ultracentrifugally-separated fractions[c]		
A	B	C	d < 1.063	1.063-1.20	> 1.21
III	Lipids[b]	IV	III, IV	III, IV	III
III	Lipids	V	III, V	III, V	III
IV	Lipids	III	IV	IV, III	III
IV	Lipids	V	IV, V	IV, V	-

[a] A+B were sonicated for 3 minutes at 40° C. The resulting product $(A+B)_{son}$ was then mixed with C without sonication and the mixture kept for 12 hours at 4° C before separation in the preparative ultracentrifuge. Identification of proteins after delipidation was carried out by polyacrylamide gel electrophoresis in 8 M urea and by amino acid analysis.

[b] The lipids were a total extract from HDL_2.

[c] Underlined components were only present in small amounts with respect to the major component.

Effect of sonication of HDL_2. As observed previously with HDL_3,[7] sonication (3 minutes) did not change the appearance or spectral properties (ultraviolet absorption spectroscopy and circular dichroism) of HDL_2 although differences in average size distribution were observed by electron microscopy (Table 2). When HDL_2, before and after sonication, was separated into

Table 5

LIPID-PROTEIN COMPOSITION OF ULTRACENTRIFUGAL FRACTIONS FROM ETHYL ETHER-TREATED HDL_2[a]

Product density (g/ml)	Protein	Lipids		
		Phospholipid	Total cholesterol	Triglycerides
	% weight			
< 1.063	20.0	35.6	30.4[b]	14.0
1.063-1.21	51.6	29.5	15.5[c]	3.4
> 1.21	96.0	4.0	-	-

[a] All percentages based on weight.

[b] % cholesterol esters: 78.6.

[c] % cholesterol esters: 82.0.

d < 1.063, 1.063-1.21 and > 1.21 fractions, more significant differences between the two products were noted. The d < 1.063 fraction was only found in sonicated HDL_2 (10-15 per cent of the starting material) and gave a IV-V pattern after delipidation, fraction V being predominant. In the d 1.21 top fraction, both fractions III and IV were present in apparently similar proportions as in apo HDL_2 (Figure 3) with no V. About 10-20 per cent of the starting material was recovered in the d 1.21 bottom with sonicated HDL_2, in contrast to 1-2 per cent observed with HDL_2; the sonicated specimen had peak III almost exclusively. The differences in distribution of electrophoretic band patterns in HDL_2 before and after sonication were corroborated by amino acid analysis. When the time dependence of sonication on HDL_2 was studied (1 to 5 minutes at 40° C), it was found that by prolonging sonic irradiation, although the solutions remained perfectly clear, there was a tendency for the d < 1.006 fraction to increase (the peptides were predominantly IV and V), and for III to increase in the d 1.21 bottom. These reactions were not reversed after a maximum observation period of 2 weeks during which the specimens were kept at 4° C.

Effect of sonication on apo HDL_2. Sonic irradiation under the standard conditions described in Methods appeared to favor solubilization of apo HDL_2. Solutions of apo HDL_2 (2-5 mg in 10^{-2} M Tris, pH 8.6, 10^{-3} M EDTA), compared before and after sonication, showed no significant differences at least in terms of the parameters employed (ultraviolet absorption spectroscopy, circular dichroism and polyacrylamide gel electrophoresis). The observations were the same regardless of the time of sonication (1 to 5 minutes) at 40° C.

Studies on degradation of HDL_2. Effect of ethyl ether on HDL_2. Under the experimental conditions employed, ether extracted only about 2 per cent of lipids, both cholesterol and phospholipids. When the resulting ether-treated product was fractionated by ultracentrifugation, marked structural consequences were noted. In contrast to untreated HDL_2 which, upon recentrifugation, was essentially all recovered in the d 1.21 top (about 1-2 per cent of protein was found in the d 1.21 bottom), ether treatment caused about 50 per cent decrease of the d 1.063-1.21 fraction, appearance of a fraction floating at d 1.063 (about 10 per cent of the starting material) and a significant portion (30-40 per cent) essentially free of lipids, in the d 1.21 bottom. As indicated by the chemical analysis (Table 5) the floating fractions at 1.063 and 1.21 differed not only in protein-lipid ratio but also in lipid distribution, the lipid fraction showing a greater

percentage of cholesterol than the heavier one.

By polyacrylamide gel electrophoresis, the ultracentrifugal fractions examined after further delipidation by ethanol-ether, showed again significant changes. As shown in Figure 6, the d 1.063 top was characterized by the presence of IV and V (III was not constantly seen), the d 1.21 top by III and IV in about equivalent amounts, whereas d > 1.21 contained almost exclusively

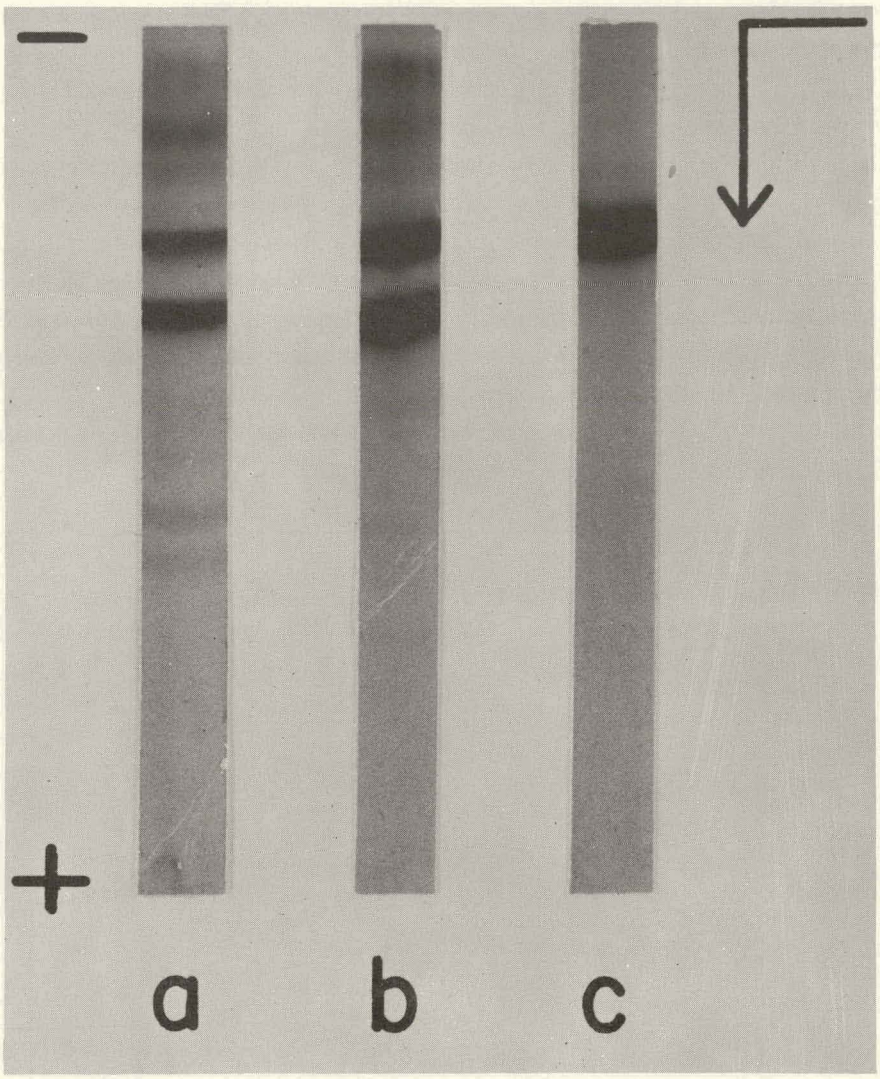

Figure 6. Polyacrylamide gel electrophoresis of ultracentrifugal fractions from HDL_2 treated with ethyl ether. Before analysis all fractions were extracted with 3:2 ethanol:ether. The conditions of electrophoresis were the same as in Figure 2. a = d < 1.063; b = d 1.063-1.21, c = d > 1.21.

peak III. The interpretation of the band pattern was again consistent with the results of the immunological studies and amino acid analysis. By prolonging ether extraction up to 48 hours the effects on HDL_2 were only slightly changed. These consisted of a further decrease of the d > 1.21 top fraction with a proportional increase of d < 1.063 and d > 1.21. Polyacrylamide gel

electrophoresis indicated the following patterns: predominance of IV + V in d < 1.063; predominance of IV over III in d > 1.21 and almost exclusive presence of III in d > 1.21 bottom.

Separation of HDL_2 before and after ether treatment by gel filtration. By Sephadex G-200, HDL_2, before ether treatment, exhibited two distinct components, the major one (A) partially eluted in the void volume and a second one (B) representing about 5 per cent of all eluted material (Figure 6). A third peak, representing about 1 per cent of the total eluted protein was seen occasionally but not identified. Recoveries were in the order of 90 per cent. Fraction A had essentially the same chemical composition as HDL_2 whereas B contained only 4 per cent phospholipids and trace of cholesterol. After delipidation, the proteins of A exhibited, by polyacrylamide gel electrophoresis, the band patterns of peaks III and IV in approximately the same distribution as in apo HDL_2. On the other hand, B showed exclusively a peak III band pattern. The interpretation of the polyacrylamide gel pattern was corroborated by immunology and amino acid analysis.

Fractionation of HDL_2, that had been extracted with ether, by Sephadex G-200, produced a decrease of A with a relative increase of peak B (Figure 7). This exhibited the same characteristics as the corresponding product obtained by gel filtration of untreated HDL_2. Either treatment thus appeared to increase the amount of lipid-poor apoprotein, an observation in keeping with the results obtained by ultracentrifugation.

Sepharose 2B experiments (these were limited to HDL_2) gave results very similar to those with Sephadex G-200 and therefore were not pursued further.

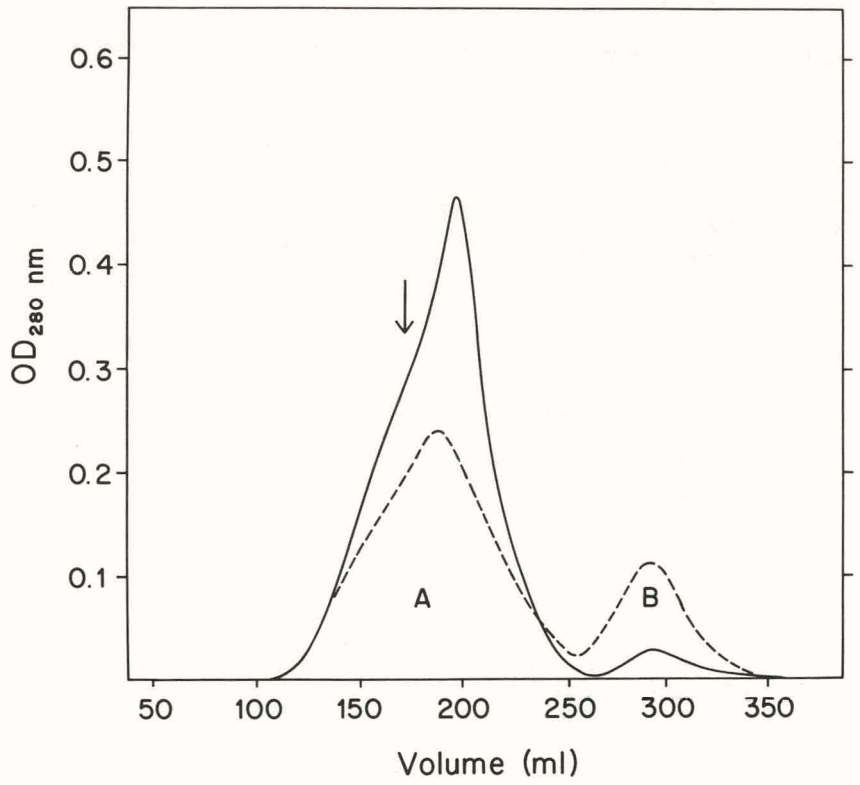

Figure 7. Fractionation of HDL_2 by Sephadex G-200. Column dimensions, 2 x 100 cm; eluting buffer, 0.1 M Tris, pH 8.4, 0.01 M EDTA; ascending flow rate, 10-12 ml/hour; temperature, 10° C. The arrow indicates the void volume.

DISCUSSION

Previous work from this laboratory has shown that when the lipid moiety of human serum HDL_3 is sonicated in the presence of lipid-free HDL_3 protein, the resulting mixture, initially turbid, becomes clear due to the formation of a water-soluble lipid-protein complex which as a whole closely resembled the starting lipoprotein.[7] The current studies have now extended such observations to HDL_2 protein, and demonstrated in addition, that three distinct lipoprotein species are produced in a proportion largely dependent on the conditions of sonication. The analysis of such lipoproteins indicated that the two classes floating in the d 1.063 and 1.21 top had all the lipid components of HDL_2, whereas the heavier fraction (d > 1.21) composed of about 95 per cent protein, contained essentially only phospholipids. It is further interesting that each lipoprotein species could also be distinguished on the basis of their protein moiety (see Figure 8). For instance, with 3 minutes sonication, IV and V were the predominant polypeptides of the

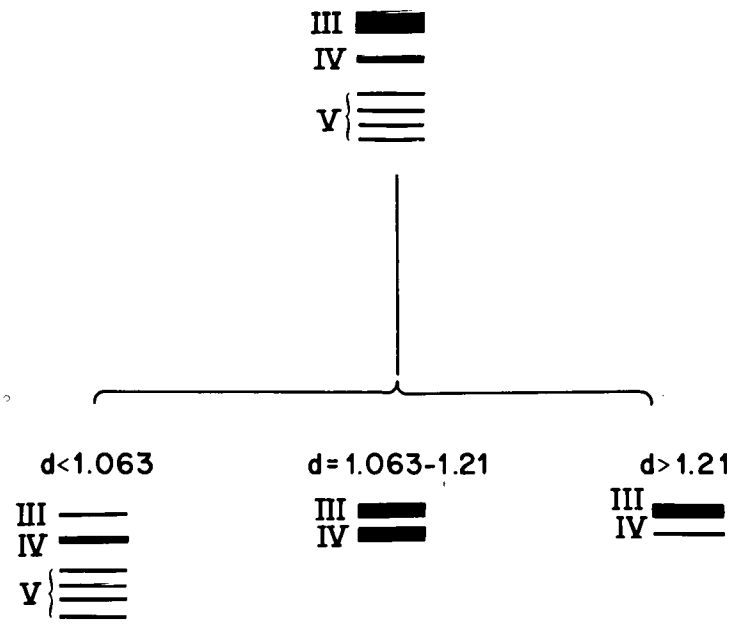

Figure 8. Scheme of fractionation of polypeptide chains of apo HDL_2 achieved in the re-assembly experiments employing apo HDL_2 + L.

d 1.063 top, III and IV those of the d 1.21 top whereas the d 1.21 bottom contained III almost exclusively. Upon increasing the time of sonication there was a tendency for III to increase in the d 1.21 bottom, with the largest percentage of IV in the d 1.063 top. It is thus apparent that the 3 classes of polypeptide chains previously described in apo HDL_2[9] have a different affinity for lipids, a conclusion that receives support from the re-assembly experiments using individual III, IV and V. In every instance the results of such studies showed that (1) non-polar lipids (free cholesterol, ester cholesterol and glycerides) could be incorporated into distinct lipid-protein complexes as indicated by chemical, ultra-centrifugal and electron microscopic data; (2) the process required the presence of both protein and phospholipids in the system and (3) energy, provided in the form of thermal and sonic irradiation. The energy for the incorporation of neutral lipids into the water-soluble lipid-protein complex contrasts with low energy requirement

observed with the reaction involving only protein and phospholipids.[5] We interpret this observation to mean that non-polar lipids must overcome some resistance to penetration by the protein-phospholipid polar surface of the lipoprotein to occupy a core location away from the aqueous environment. This observation may not necessarily apply to circulating plasma where current evidence suggests that cholesterol esters in HDL derive from an intramolecular process through the activity of the enzyme lecithin-cholesterol acyl transferase.[11]

Of interest were the experiments on HDL_2 degradation showing that ether treatment causes dissociation of this lipoprotein into species similar to those formed during the re-assembly experiments. It was surprising that ether, which extracted little lipid from HDL_2, had a profound structural effect on the HDL_2 causing it to dissociate into products distinct in protein-lipid ratio, lipid distribution, and nature of the protein moiety. Such results, which are in general agreement with those by Hayashi et al,[12] suggest that HDL_2, as we isolate it in the ultracentrifuge, is in fact a mixture of distinct lipid-protein complexes, although they give little insight as to how they are assembled. Some speculative thoughts appear, however, permissible on the basis of the re-assembly studies. The idea, for instance, that III is an essential and specific constituent of HDL_2 appears supported by the following findings: (1) it represents 70-80 per cent of whole apo HDL_2;[9] (2) the re-assembled III + L produced a high density lipoprotein closely resembling that of native HDL in all the physical and chemical parameters examined. (3) III appeared size limiting since in its absence lipoprotein particles formed during re-assembly were of a significantly larger diameter than in HDL_2. In contrast, upon sonication with lipids, IV formed a rather unusual high density lipoprotein, markedly heterogeneous in size and density (see Figures 1 and 4 and Table 2), or had the tendency to dissociate from ether-treated or sonicated HDL_2 as a protein-lipid complex of $d < 1.063$. In no instance was IV, in contrast to III, either encountered or a predominant component of the d 1.21 bottom. This was also the case with V which, like IV, had, upon removal from HDL_2, a preferred association with a low density lipid-protein complex.

Based on the experimental evidence obtained in the current studies, we would favor the hypothesis that III is the "structural" protein constituent of HDL_2 contributing, with phospholipids, to the surface coat of this lipoprotein which has as a non-polar core, cholesterol esters and triglycerides. On the other hand, IV and V would be "functional" elements, probably involved in the interaction of HDL_2 with the other plasma lipoproteins. As far as IV is concerned, this alleged functional role is not clear. With regard to V, its derivation from exchange processes between high and very low density lipoproteins is suggested by the fact that this polypeptide class is present in both lipoproteins (to be published). It is of interest to point out that either IV or V could be added to the reassembled sonicated III + L complex to give a final lipoprotein very similar in protein distribution to that observed in ultracentrifugally isolated HDL_2. Support for the structural role of III in HDL comes also from the observation that the reassembled IV + L, by itself distinct from any described high density lipoproteins, binds III only to a limited extent, at least in the absence of external energy source (sonication and temperature). If proteins of type III are in fact essential structural elements of HDL_2, able by their special arrangement at the surface of the molecule to control the overall size of the lipoprotein, then marked structural alteration of the latter would be expected upon partial or total removal of these polypeptide chains. Corroboration for such speculations comes from the degradation experiments: an increase in the time of either sonication or ether extraction produced a progressive loss of III from HDL_2 and a parallel increase of a low-density complex, probably originating from the reduction of polar

groups and the coalescence of lipids into relatively more hydrophobic particles with preferential affinity for IV or V. Regardless of the exact nature of this phenomenon, the molecular details of which obviously remain to be established, one is impressed by the high degree of structural re-organization possible in HDL, which allows for lipid to remain "soluble" in an aqueous environment. A better understanding of these phenomena is likely to derive from the isolation and characterization (now in progress) of the various polypeptide chain members of III, IV, and V, and from the definition of their specific binding properties for lipids.

We would like to stress that the re-assembly technique developed in the current studies, or any similar methodology, appears to provide a very useful tool for the study of the structure and function of plasma high density lipoprotein and even allows for some fractionation of its polypeptide chains. Since the natural lipids of HDL may be replaced effectively by artificial mixtures, it would be possible in the future to introduce appropriate markers to define whether native high density lipoproteins and their re-assembled counterpart have identical biological behavior. One must be aware, however, of some of the drawbacks of the sonication method in re-assembly studies. Our results have clearly indicated that sonic irradiation, under the experimental conditions employed, causes some modifications of intact HDL_2 as expressed by a slight increase of its median particle size (see Table 2) and some protein loss (10-15 per cent) from the complex. We are not presently in a position to define the extent of the structural differences between "native" and sonicated products precisely or even to assess whether the term "native" can be properly applied to a lipoprotein after its isolation from plasma. If we rely, however, on the chemical, immunological, ultracentrifugal and circular dichroic data obtained in the current studies and on the NMR results to be reported elsewhere (Leslie, R. B. and Scanu, A., to be published) then we may conclude that the two products (intact and re-assembled) are at least strikingly similar. It remains for future studies (chemical modification of intact and re-assembled complexes, response to proteolytic and lipolytic enzymes, deuterium exchange studies, etc.) to determine how close such structural similarity is and whether the correlation also extends to their functional behavior (i.e., participation in the activity of the enzymes lipoprotein lipase and lecithin-cholesterol acyl transferase). The information obtained should improve our understanding of the role of high density lipoproteins in fat transport.

ACKNOWLEDGMENT

The authors thank Mr. Jerry Grofman from the Department of Biophysics of the University of Chicago for valuable assistance during the electron microscopic studies.

LITERATURE CITED

1. Scanu, A., L. A. Lewis, and M. Bumpus. Arch. Biochem. Biophys., 74:390, 1958.
2. Scanu, A. J. Lipid Res., 7:295, 1966.
3. Scanu, A., and W. L. Hughes. J. Biol. Chem., 235:2876, 1960.
4. Scanu, A. Adv. Lipid Res., 3:63, 1965.
5. Scanu, A. J. Biol. Chem., 242:711, 1967.
6. Sodhi, H. A., and R. G. Gould. J. Biol. Chem., 242:1205, 1967.

7. Hirz, R., and A. Scanu. Proceedings 3rd Great Lakes Meeting, American Chemical Society (June 5-6, 1969), p. 24, and Proceedings 158th National Meeting, American Chemical Society (Sept. 7-12, 1969), abst. #191.

8. Shore, B., and V. Shore. Biochemistry, 7:2773, 1968.

9. Scanu, A., J. Toth, C. Edelstein, S. Koga, and E. Stiller. Biochemistry, 8:3309, 1969.

10. Scanu, A., and R. Hirz. Proc. Nat. Acad. Sci. U.S., 59:898, 1968.

11. Glomset, J. A., E. T. Janssen, R. Kennedy, and J. Dobbins. J. Lipid Res., 7:639, 1966.

12. Hayashi, S., F. Lindgren, and A. Nichols. J. Am. Chem. Soc., 81:3793, 1959.

X-RAY SENSITOMETER FOR SCREEN-FILM COMBINATIONS USED IN MEDICAL RADIOGRAPHY*

By

A. G. Haus and K. Rossmann

A radiographic image is a two-dimensional distribution of photographic densities on film which is produced by a two-dimensional distribution of x-ray exposures. For the evaluation of the imaging capability of radiographic film or film-screen combinations it is important to know the density increments resulting from known exposure increments, or in other words, to describe the sensitometric properties of a given film or film-screen combination. It is customary[1,2] to describe a film or film-screen combination sensitometrically by means of the so-called characteristic curve or H & D curve,† an example of which is shown in Figure 1. For the sake of convenience, density is usually plotted as a function of the logarithm of relative exposure.

In principle, the series of relative exposures necessary to cover the full density range of the film can be obtained either by varying the exposure time and keeping the x-ray intensity constant (time-scale sensitometry), or by varying the x-ray intensity and keeping the exposure time constant (intensity-scale sensitometry). The method of measurement to be chosen depends on the system whose sensitometric properties are to be measured and on the manner in which the system is to be used. In the case of radiographic film exposed to direct x-rays without intensifying screens, either method can be used and will give the same result. Usually time-scale sensitometry is employed in this case, because it can readily be carried out by means of a modification of the Hurter and Driffield wheel shown in Figure 2. The wheel acts essentially as a series of rotating apertures of different lengths which permit simultaneous exposure of different parts of a film strip at various exposure times.

When radiographic film is used with intensifying screens the film is mainly exposed by light from the screens. In this case time-scale and intensity-scale sensitometry will, in general, result in different characteristic curves. Therefore, that sensitometric technique should be used which most nearly simulates the actual conditions under which the screen-film combination is exposed. During a typical radiographic exposure the exposure time does not vary over the area of the film. Rather, the radiation intensity is modulated by the x-ray absorption in different parts of the subject. Therefore, intensity-scale sensitometry should be used for screen-film combinations.

The simplest method of varying the radiation intensity in the film plane by well-known increments during the sensitometric exposure is one which makes use of the decrease in intensity as the film is moved away from the radiation source (inverse square law). Although this can be carried out manually in various ways, precision, reproducibility and efficiency are improved by

*This report is taken from a paper that appeared in Radiology, 94:673, 1970. The work was supported in part by a grant from the U. S. Public Health Service.

†After Hurter and Driffield who, in 1890, first used this curve.

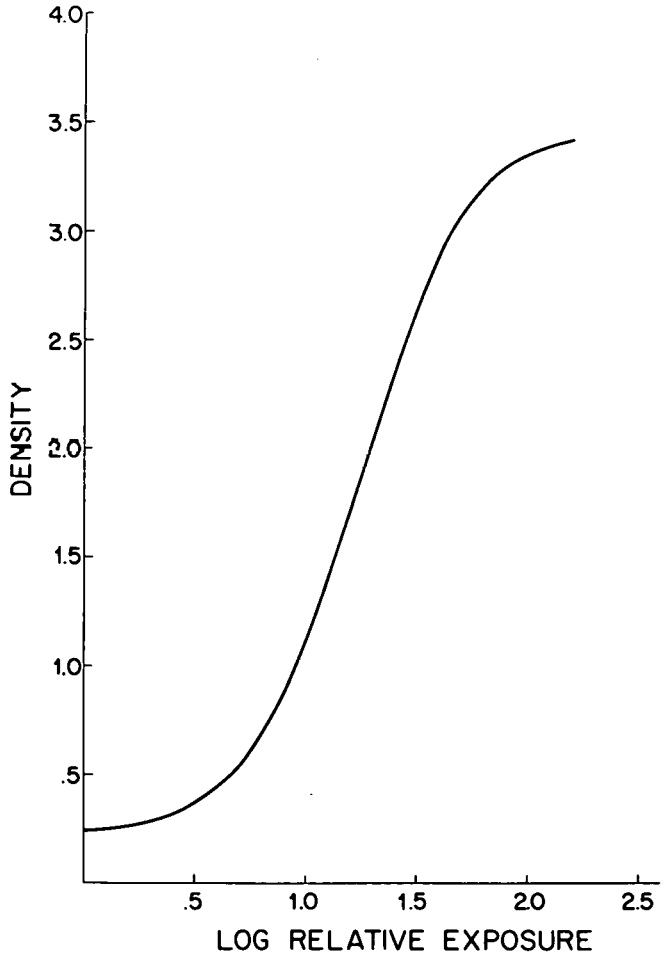

Figure 1. Characteristic curve of a typical radiographic film-screen combination.

automation as first shown by H. M. Cleare of the Eastman Kodak Research Laboratories.*

Based on the foregoing considerations an automatic, intensity-scale x-ray sensitometer was designed as shown in Figure 3. Its basic components are:

1. an x-ray source continuously emitting constant radiation intensity at diagnostic kilovoltages,
2. a shutter permitting accurate and reproducible exposure timing,
3. a device providing automatic, stepwise increase of focus-film distance to produce known, constant increments of exposure,
4. a special cassette and cassette moving device.

The x-ray source is a conventional 250 KVP General Electric Maxitron therapy x-ray tube. Several modifications were made so that output stability could be maintained. These include a line voltage stabilizer and more precise operator control meters for observing kilovoltage, primary line voltage and tube current setting. At 80 KVP the fluctuation in kilovoltage is no greater than ± 1/2 KVP at constant tube current.

*H. M. Cleare, private communication.

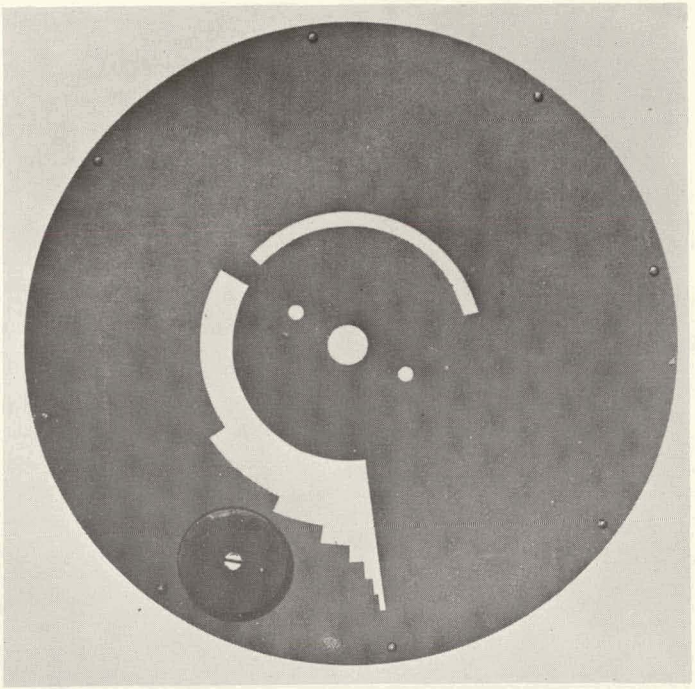

Figure 2. Lead sector wheel for time-scale sensitometer. (Based on Hurter and Driffield sector wheel.)

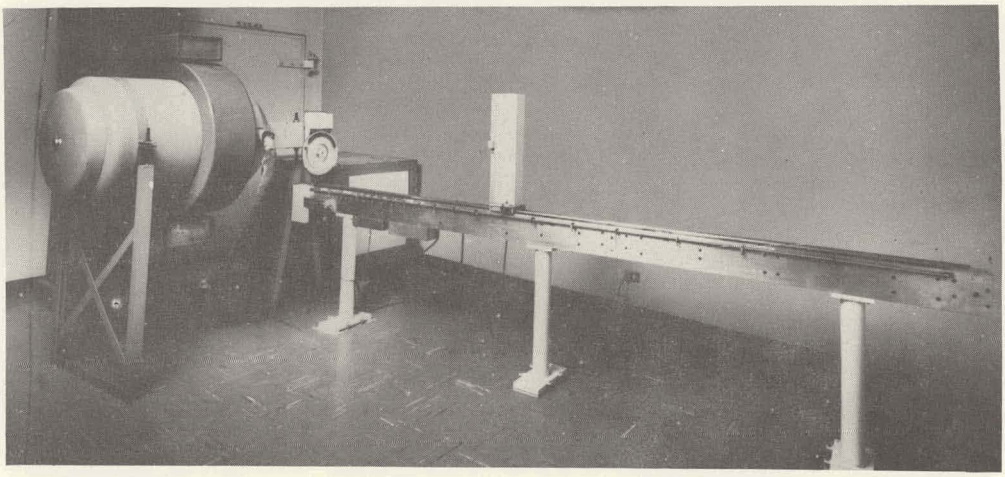

Figure 3. Intensity-scale x-ray sensitometer.

The timing shutter is shown in more detail in Figure 4. Two superimposed lead lined sector wheels which can be turned relative to each other define the selection of apertures marked off in degrees. With the sector wheels set at a given degree opening, the shutter is rotated at a constant rate of 18 RPM by a synchronous motor which results in a certain exposure time. The range of exposures for practical work is from 0.05 seconds (5.4°) to 1.48 seconds (160°). Behind the aperture defined by the sector wheel are two springs controlled by solenoids allowing two lead shutters to open and close. The action of the timing shutter is synchronized with the

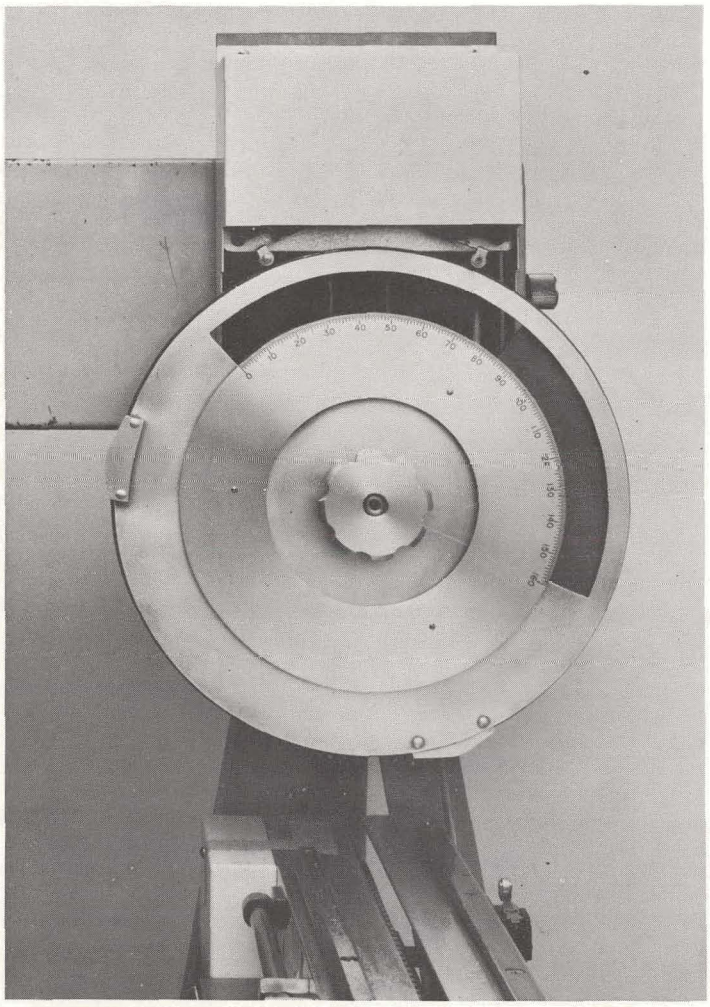

Figure 4. Timing shutter mechanism.

rotation of the wheel and the movement of the cassette carriage by two microswitches located above the sector wheels; its purpose is to avoid film exposure while the cassette carriage is moving. Behind the lead shutters is a diaphragm that limits the beam size. The size of this diaphragm was designed with three purposes in mind:

a) The film sees the entire focal spot at all distances,

b) the beam size is large enough at the shortest focal spot-film distance to give a uniform exposure to the film,

c) the beam size is limited such that scatter is not introduced by the beam striking the bench, wall or objects other than the film at the greatest focal spot-film distance.

A chain drive running the length of the bench automatically moves the cassette carriage to prescribed focal spot-film distances (see Figure 3). These distances are defined by mechanical stops located on the side of the bench which activate a microswitch on the cassette carriage. The stops which define the exposure increments were positioned in the following way. A focal spot position was assumed. X-ray exposures at 80 KVP with 0.5 mm Cu + 3 mm Al filtration at the tube were made with the film at certain distances from the focal spot. Expected exposure

increments corresponding to the distance increments were calculated from the $1/r^2$ law. Tube output was adjusted to compensate for the expected exposure increments so that equal film density should have been obtained at all distances. After several such trials a focal spot position was found relative to which the $1/r^2$ law held for distances ranging from 10 inches to 126 inches. This resulted in 23 steps of 0.10 log exposure increments. The exposure latitude of 23 steps consisting of 0.10 log exposure increments ($\Delta \log E_{REL} = 2.2$) fulfills the requirements of obtaining the complete characteristic curve of medical x-ray film and screen film systems. The calibration was checked against an x-ray time-scale sensitometer (see Figure 2) using direct x-ray film.

Figure 5 shows the cassette with a screen film combination. The notches on the side of the cassette trigger a microswitch which causes the cassette to stop or start to its next position as

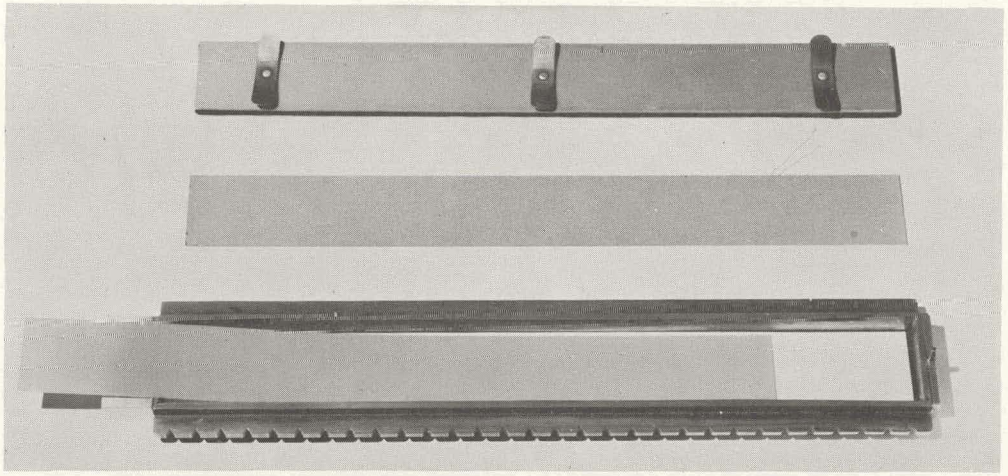

Figure 5. Cassette with film screen combination.

it is driven downward by a chain drive inside the cassette carriage as shown in Figure 6. The pin on the bottom of the cassette engages the chain drive when the carriage back is closed. Figure 7 shows the lead lined front of the carriage with the aperture determining the area of film to be exposed.

To sum up the sequence of happenings (ref. to Figure 3):

1. The operator sets the exposure time on the sector wheels,
2. the film cassette is placed in the carriage and driven to its first exposure position,
3. the operator leaves the room, turns on the x-ray machine, and with the main shutters closed sets exposure conditions,
4. when satisfied with x-ray output and stability the operator turns a switch which begins the following sequence: (a) main shutter opens allowing the film to be exposed at the first position through the rotating shutter, (b) main shutter closes with carriage and cassette moving automatically to exposure position 2, (c) main shutter opens and exposure 2 is made. This sequence continues for 23 steps.

Figure 8 shows an exposed film strip with measured film densities in column 1. The density across each step is uniform within ± .01. The film density can be plotted against its corresponding log relative exposure (column 2) or against relative exposure (column 3). Column 4 indicates

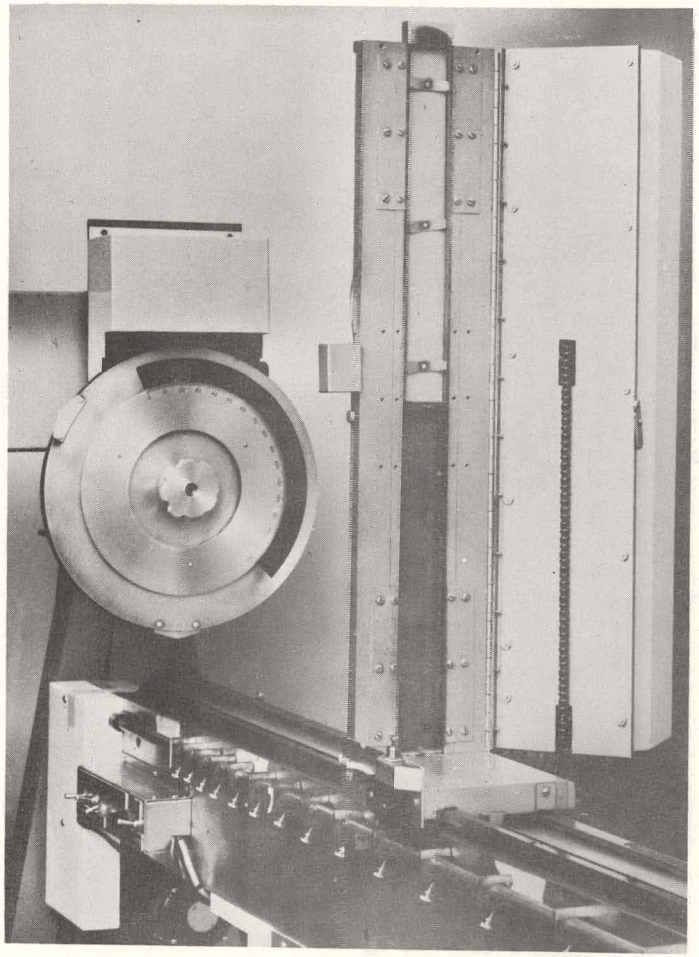

Figure 6. Cassette carriage.

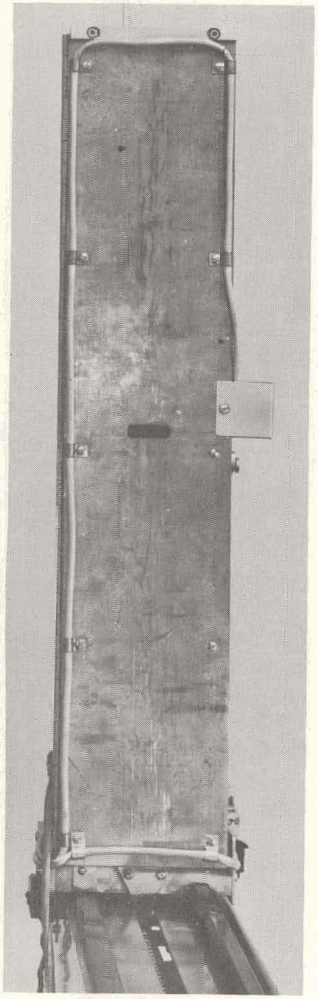

Figure 7. Lead lined front of carriage with aperture determining area of film to be exposed.

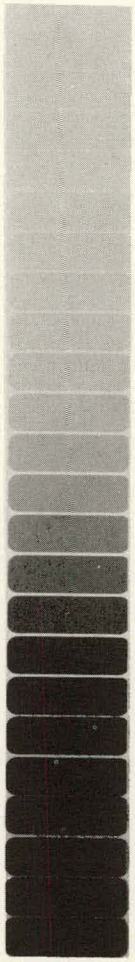

Density	Log relative exposure	Relative exposure	Focal spot-film distance (inches)
.21	0.0	1.00	126.0
.22	0.1	1.26	112.0
.23	0.2	1.59	100.0
.25	0.3	2.00	89.0
.28	0.4	2.51	79.3
.31	0.5	3.16	70.6
.37	0.6	3.98	63.0
.47	0.7	5.02	56.0
.59	0.8	6.31	50.0
.75	0.9	7.95	44.6
.97	1.0	10.0	39.8
1.26	1.1	12.6	35.5
1.57	1.2	15.9	31.6
1.91	1.3	20.0	28.2
2.27	1.4	25.1	25.1
2.57	1.5	31.6	22.4
2.80	1.6	39.8	20.0
2.98	1.7	50.2	17.8
3.11	1.8	63.1	15.8
3.21	1.9	79.5	14.1
3.25	2.0	100.0	12.6
3.29	2.1	125.8	11.2
3.32	2.2	158.5	10.0

Figure 8. Exposed film strip with corresponding measured film densities, log relative exposure, relative exposure and focal spot-film distance.

Figure 9. Characteristic curves of three typical film-screen combinations measured on the sensitometer under the same exposure conditions; fast screens (1), medium speed screens (2), slow screens (3), all exposed with the same film and processed simultaneously.

the focal spot-film distance corresponding to each step.

Characteristic curves of three typical intensifying screen-film combinations measured on the sensitometer under the same exposure conditions are shown in Figure 9. Sensitometric curves of this type can be reproduced within ±2 per cent of the exposure (±.01 log exposure).

The sensitometer is being used for the evaluation of screen film systems employed in medical diagnostic radiology, for routine evaluation of automatic processing machines, and for the exposure calibration of screen film systems in connection with modulation transfer function measurements.

LITERATURE CITED

1. Sensitometric Properties of X-ray Films. Rochester, New York: Radiography Markets Division Eastman Kodak Company.
2. Mees, C. E., and T. H. James. The Theory of the Photographic Process. New York. The Macmillan Co., 1966.

IMPROVEMENT IN THE IMAGE QUALITY OF CEREBRAL ANGIOGRAMS*

By

K. Rossmann, A. G. Haus, and G. D. Dobben†

It is common practice to perform cerebral angiography with fast intensifying screens and radiographic film of normal speed. Fast screens are used to increase system speed so that exposures can be made at a rapid rate with focal spots of relatively small size. The disadvantage of fast screens is their great unsharpness which results in a degradation of image quality. The present studies were designed to determine if other screen-film systems could be used to image blood vessels more sharply and to make smaller blood vessels visible. The answer to this question depends on the relative image degradation introduced by the main factors affecting the optical quality of the angiographic image. These are geometrical unsharpness, screen-film unsharpness and, possibly, poor screen-film contact and motion of the film changer.

The effect of geometrical unsharpness alone was measured in the following manner. A blood vessel phantom was constructed by drilling cylinders of 2 cm length in a 0.5 cm thick plastic plate. The diameter of the cylinders ranged from 0.5 to 4.0 mm. These cylinders were filled with a radiopaque medium used in cerebral angiography. The test object was radiographed by means of a Triplex Optimatic 1023 Elema-Schönander x-ray generator and a Phillips Super Rotelix x-ray tube with 0.3 and 1.2 mm focal spots. The kilovoltage used was 70 kVp with 1/2 mm copper and 4-1/2 mm aluminum filtration at the tube to approximate the radiation quality at the film under clinical conditions. The radiographic images were recorded on Kodak Industrial X-ray Film, Type R (single-coated) without intensifying screens. As has been shown in a previous investigation,[1] the unsharpness of this film is so small that images recorded on it can be used to calculate the effective, relative x-ray intensity in space or the x-ray pattern which is the input to the film. This is done by scanning the image with a microdensitometer and calculating the effective exposure received by the film by means of its sensitometric curve. To measure the effect of geometrical unsharpness on the input, the test object was first radiographed in contact with the film cassette. Air spacings of 2 and 10 cm were then introduced between test object and film to simulate the closest and farthest distances between object and film which are encountered in cerebral angiography. The focus-film distance was 100 cm, as it is in practice. No grid was used in this experiment. The measured input x-ray patterns for the 0.5 mm blood vessel phantom obtained with the 0.3 and 1.2 mm focal spot are shown in Figure 1a. Curve 1 is the x-ray pattern corresponding to the contact exposure without geometrical unsharpness. Curves 2 and 3 show the effect of the 2 and 10 cm spacing, respectively, with the 1.2 mm focal spot. The crosses and circles indicate the corresponding x-ray patterns obtained with the 0.3 mm focal spot. It is seen that the spacing increases the subject contrast because the intensity in the image plane of scattered radiation from the object has been reduced. Furthermore, the en-

*This report is taken from a paper that was presented at the 12th International Congress of Radiology, Tokyo, Japan, October 6-11, 1969, and appeared in Radiology, 96:361, 1970.

†Department of Radiology, The University of Chicago.

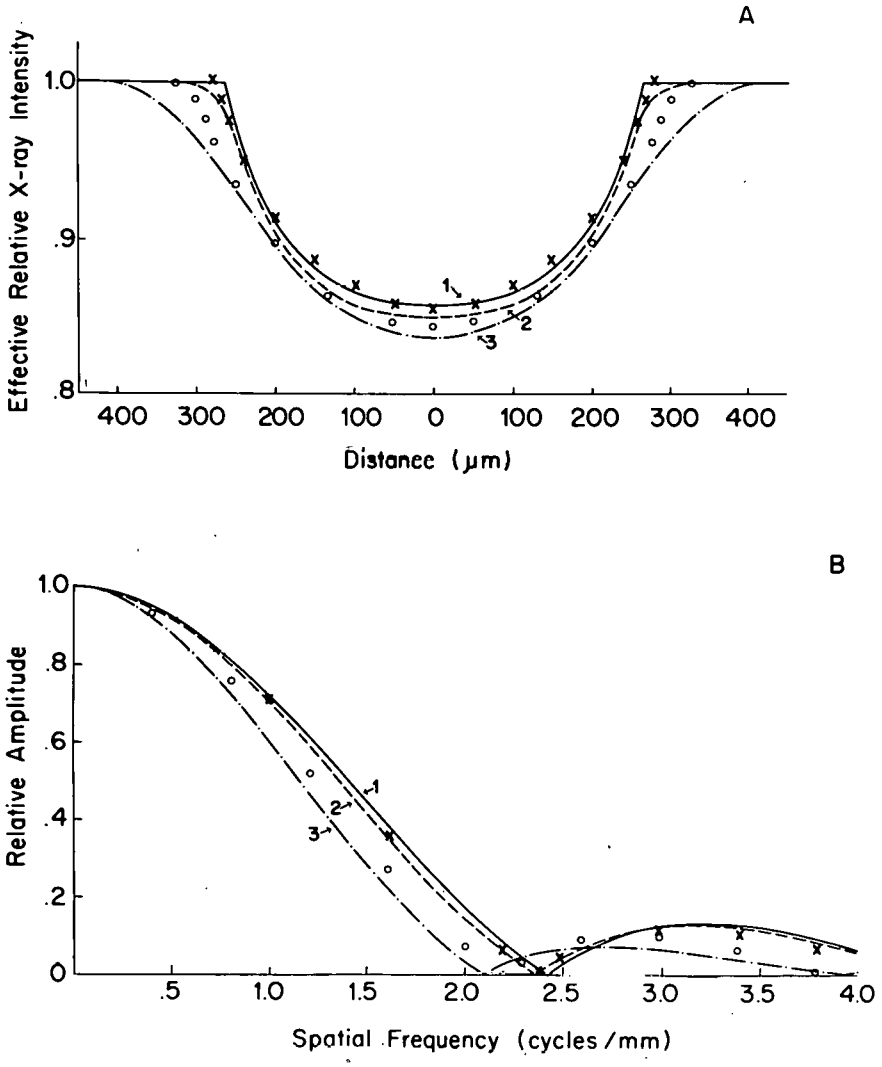

Figure 1. A. Input x-ray patterns of an 0.5-mm diameter blood vessel phantom. Curve 1: Phantom in contact with cassette. Curve 2: 2 cm air space between phantom and cassette (1.2 mm focal spot). Curve 3: 10 cm air space between phantom and cassette (1.2 mm focal spot). Crosses and circles indicate corresponding results obtained with an 0.3 mm focal spot. B. Normalized amplitude spectra calculated from x-ray patterns in Figure 1A.

largement of the x-ray shadow of the cylinder is apparent, and the intensity gradient at the edge of the cylinder is reduced, giving the impression of unsharpness in the recorded image. As expected, the smaller focal spot is most advantageous at the farthest spacing.

The results can be presented in a different manner, as in Figure 1B, which shows the normalized amplitude spectra of the cylinder inputs calculated from the x-ray patterns in Figure 1A. This representation of the inputs in the spatial frequency domain indicates the spatial frequency content of the inputs and is better suited to the analysis of the imaging process by means of optical communication theory than the representation in the spatial domain. The information gained from the two representations is basically the same. The enlargement effect results in a shift of the amplitude spectrum to lower frequencies, and the unsharpness is indicated by a re-

duction of the amplitude at the various spatial frequencies. The effect of the increase of subject contrast cannot be seen in the normalized spectra.

Based on these data, the relative effect of geometrical unsharpness and screen-film unsharpness can be determined. The following screen-film systems, whose characteristic curves are shown in Figure 2, were considered: Kodak Blue Brand Medical X-ray Film with Radelin TF-2 Intensifying Screens (Curve 2) and Kodak Royal Blue Medical X-ray Film with DuPont Par

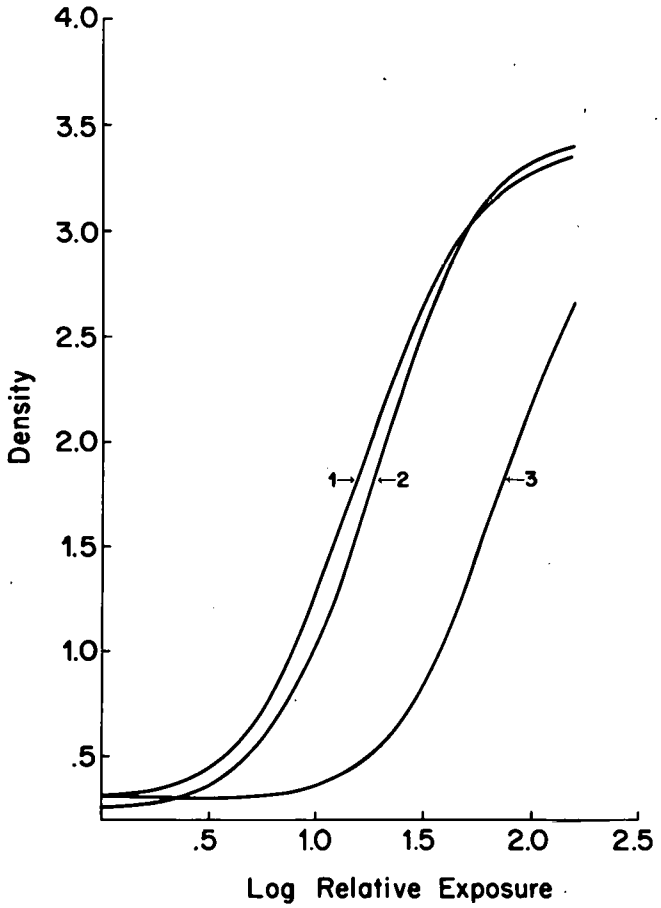

Figure 2. Characteristic curves of x-ray films. Curve 1: Kodak Royal Blue Medical X-ray Film with DuPont Par Speed Screens. Curve 2: Kodak Blue Brand Medical X-ray Film with Radelin TF-2 Intensifying Screens. Curve 3: Royal Blue film with DuPont Detail Intensifying Screens.

Speed (Curve 1) and DuPont Detail Intensifying Screens (Curve 3). These systems were chosen because the first is similar to systems commonly used in cerebral angiography, and the other two represent practical alternatives. Note that the speed of the system containing Par Speed screens is nearly identical to the commonly used system, and that the system containing Detail screens is slower by a factor of four. Films were processed in Kodak Rapid X-ray Developer, using nitrogen burst agitation to improve the reproducibility of the physical measurements. The principal conclusions, however, would be equally valid for machine-processed films.

The optical characteristics of these three screen-film systems are described in Figure 3. Line spread functions are shown in Figure 3A and modulation transfer functions in Figure 3B. Curves 1 correspond to the system with Par Speed screens, Curves 2 to the system with TF-2 screens, and Curves 3 to the system with Detail screens. It is seen that both the Par Speed and

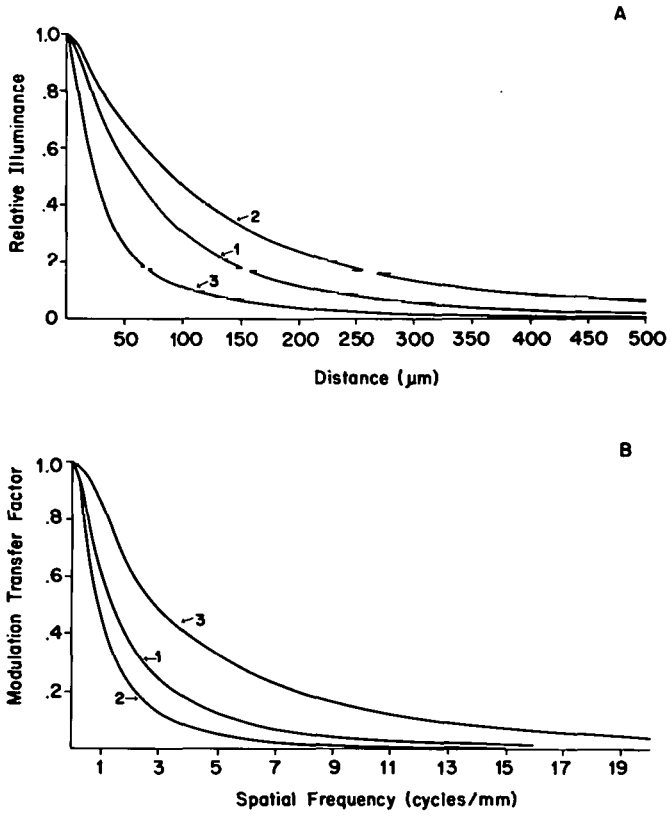

Figure 3. Optical characteristics of screen-film systems in Figure 2. A. Line spread functions; B. Modulation transfer functions.

Detail screen systems produce considerably greater sharpness and resolution than the conventionally used system. From the line spread functions and the input x-ray patterns, the output of the screen-film systems can be calculated by convolution. The results are shown in Figure 4. Curve 1 is the x-ray pattern corresponding to the 0.5 mm diameter cylinder in contact with the film cassette. Curves 2, 3 and 4 are the calculated relative illuminance distributions in the emulsion which result in the cylinder image when TF-2, Par Speed and Detail screens are used. The image produced by the conventionally used system (Curve 1) is considerably less sharp than that obtained with either of the other two systems, as indicated by the flaring-out of the illuminance distribution at the cylinder edges. Note that these outputs do not include the effect of geometrical unsharpness, since they were calculated from the contact input. Therefore, they can be compared directly with the inputs affected only by geometrical unsharpness, which were shown in Figure 1, to determine the relative effect of geometrical and screen-film unsharpness. Curve 5 is one of these x-ray patterns. It corresponds to the 0.5 mm diameter cylinder spaced 10 cm away from the cassette and radiographed with the 1.2 mm focal spot. It is apparent that, even for

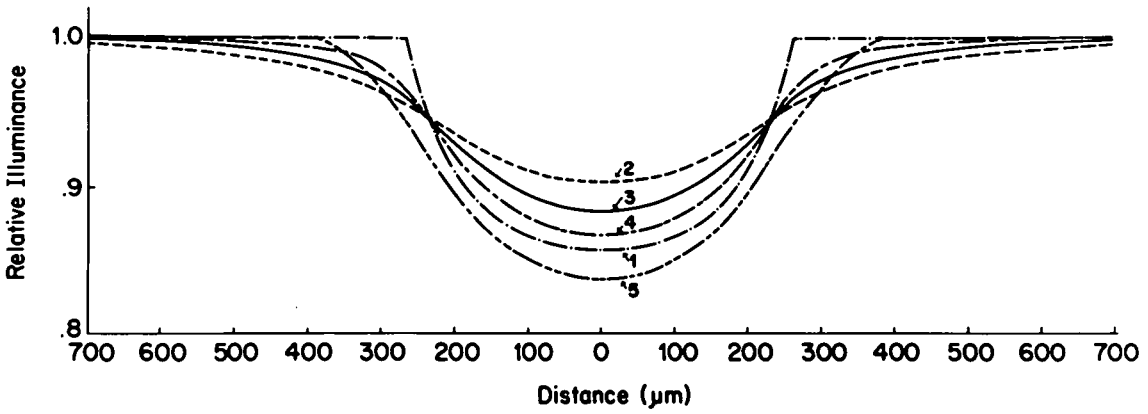

Figure 4. Curve 1: Input x-ray pattern of an 0.5-mm diameter blood vessel phantom in contact with cassette. Output calculated from Curve 1 and the line spread functions in Figure 3A. Curve 2: TF-2 screens. Curve 3: Par Speed screens. Curve 4: Detail screens. Curve 5: Input x-ray pattern of an 0.5-mm diameter blood vessel phantom spaced 10 cm away from cassette (1.2 mm focal spot).

the case showing the greatest geometrical unsharpness obtained in cerebral angiography, the unsharpness of all three screen-film systems plays a dominant role in the degradation of the image.

Two conclusions follow from this result. First, the use of a 0.3 mm focal spot will not result in a significant increase in sharpness under the radiographic conditions used in this experiment which are similar to conditions used in practice. Second, image sharpness can be increased significantly by the use of sharper screen-film systems even for blood vessels which are 10 cm away from the film. The latter can also be seen in Figure 5, which shows the calculated system outputs, including geometrical and screen-film unsharpness. Curve 1 in Figure 5a is the unsharp input and Curves 2, 3 and 4 are the outputs of the three screen-film systems calculated by convolving Curve 1 with the line spread functions. Curve 2 relates to the commonly used system. Figure 5B shows the corresponding amplitude spectra calculated from the input (Curve 1) by multiplying with the system MTF's. Curve 2, which has the lowest frequency content at all spatial frequencies, relates to the commonly used system.

It remains to be shown that these conclusions are also valid under practical conditions which differ from the idealized experimental conditions in several important aspects. First, the experiments were carried out in the absence of scattered radiation and without a grid, since an air space between test object and film was used. This was done because the presence of grid line images would have made the evaluation of the microdensitometer scans impossible, especially since the images were very sharp. It is feasible, however, that the presence of scattered radiation in practice might introduce image degradation which decreases the relative effect of the sharper screen-film systems. From Figure 6 it can be inferred that this is not the case. The smooth curve is the microdensitometer trace across the image of a 2 mm diameter cylinder on Type R film. An air space of 10 cm was introduced between cylinder and film. The other curve is a trace across the image of the same cylinder at the same spacing made on Blue Brand film with Detail screens. In this case, the test object was embedded in a plastic block simulating the head, and a 10:1 focused grid was used. The filtration at the tube was chosen to give roughly the same radia-

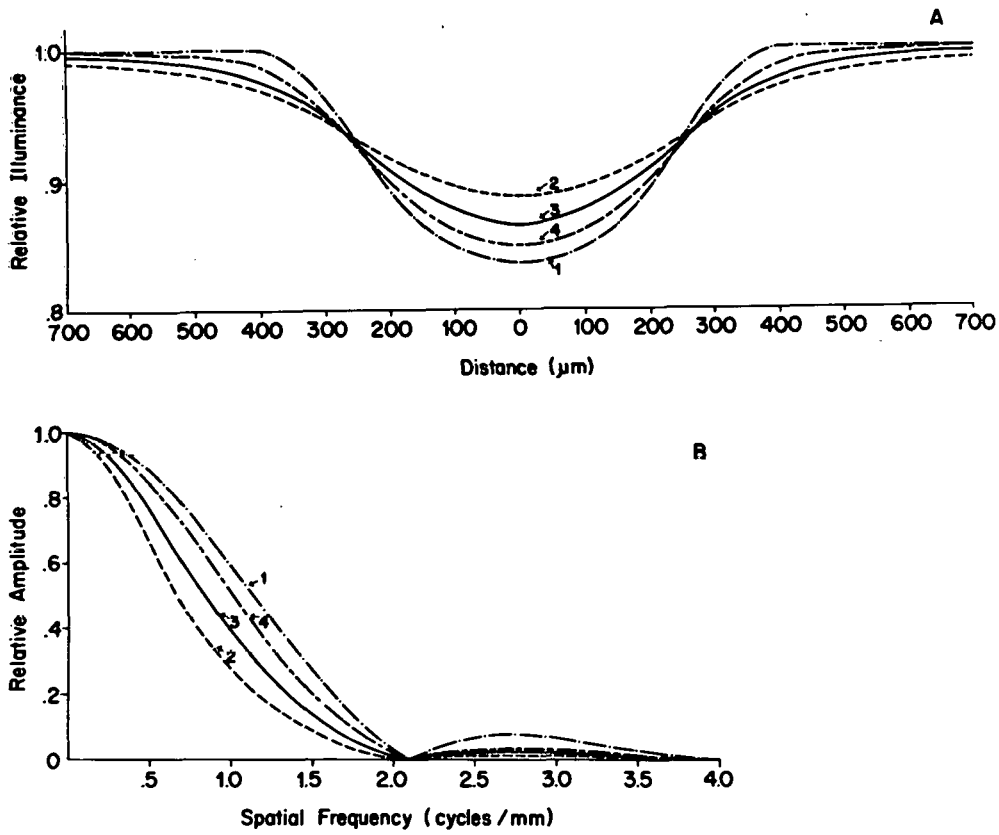

Figure 5. A. Curve 1: Input x-ray pattern of 0.5-mm diameter blood vessel phantom spaced 10 cm away from cassette (1.2 mm focal spot). Output calculated from Curve 1 and the line spread functions in Figure 3A. Curve 2: TF-2 screens. Curve 3: Par Speed screens. Curve 4: Detail screens. B. Corresponding amplitude spectra.

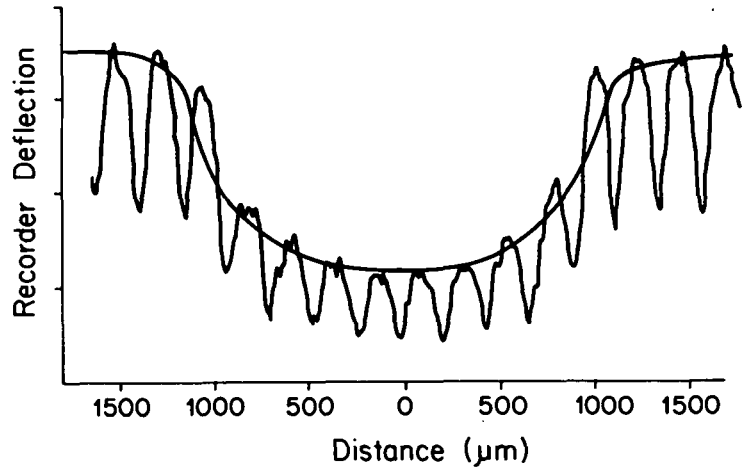

Figure 6. Smooth curve: Microdensitometer trace across image of 2-mm diameter blood vessel phantom on Type R film (10 cm air space between phantom and cassette, no grid). Second curve: Microdensitometer trace across image of 2-mm diameter blood vessel phantom in plastic block made on Blue Brand film with Detail screens (10 cm plastic spacer between phantom and cassette, 10:1 focused grid).

tion quality in the two cases. It appears that there is no significant contrast difference between the two images and that their profiles are about the same.

The second factor distinguishing the experimental conditions from practice was the use of a vacuum cassette for the measurement of the optical characteristics of the screen-film systems, which assured excellent contact between screens and film. Thus, poor screen-film contact and changer motion, which could conceivably degrade the image in practice when rapid film changers are used, were not taken into account during the measurements. However, tests performed on an Elema-Schönander AOT changer with a lead-line resolution test object normally used for this purpose by the manufacturer showed no evidence of unsharpness due to poor screen-film contact. No degrading effect due to changer motion was observed when the test object was placed on the changer as the head would be for a frontal radiograph, or when the test object was not in contact with the changer corresponding to a lateral radiograph of the head.

The third experimental condition which could be considered unrealistic is the use of stationary test objects, since in practice blood vessel pulsing might degrade the image to such an extent that the relative optical characteristics of the three screen-film systems become inconsequential. That this is not the case can be seen from actual cerebral angiograms of patients made with these systems. Figure 7 shows, on the left, a section of a lateral angiogram made with fast

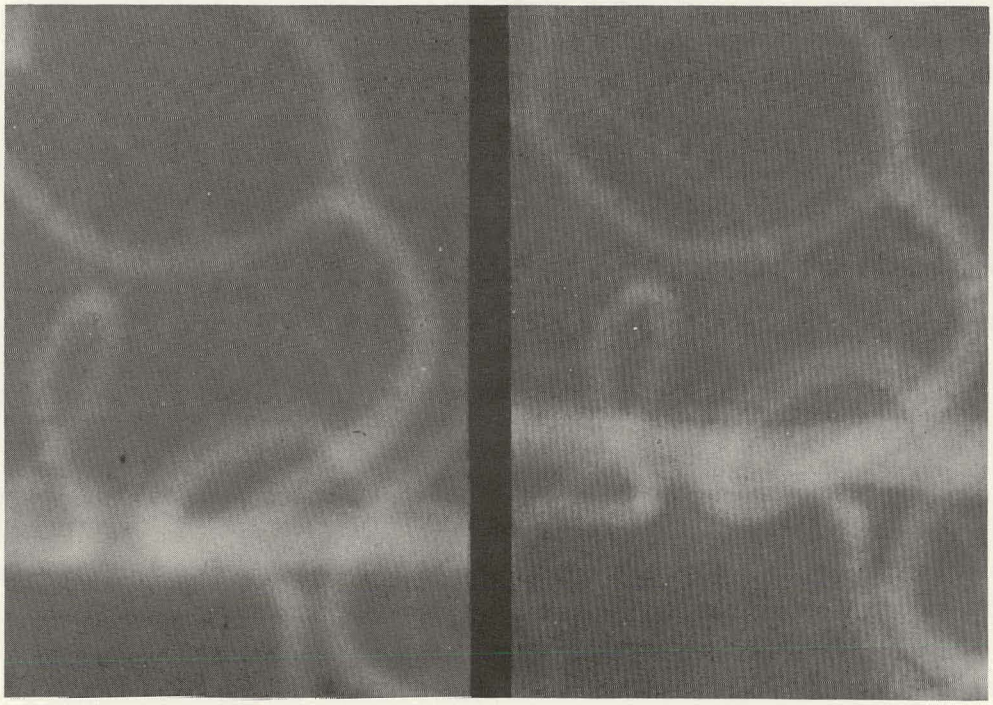

Figure 7. Lateral angiograms of patient. Left: TF-2 screens and Blue Brand film. Right: Par Speed screens and Royal Blue film.

screens and Blue Brand film, i.e., with the system which simulates present common practice. On the right is the same section radiographed with Par Speed screens and Royal Blue film under identical exposure conditions. The increased sharpness due to the new system is obvious to the radiologist and to the neurosurgeon. The attendant greater visibility of the grid lines, which is,

of course, overemphasized in the enlarged image, does not reduce the diagnostic usefulness of the image. Figure 8 shows, on the left, a radiograph made with the system simulating present common practice and, on the right, a radiograph of the same patient made with Detail screens and Royal Blue film at the same kilovoltage. Since this system has one-fourth the exposure speed of the commonly used system, radiographs had to be made at a rate of one frame/sec instead of the usual two frames/sec because of tube load limitations. However, if the kilovoltage were increased the higher frame rate could be used. In this case, also, the greater visibility of the grid lines was not found to be disturbing.

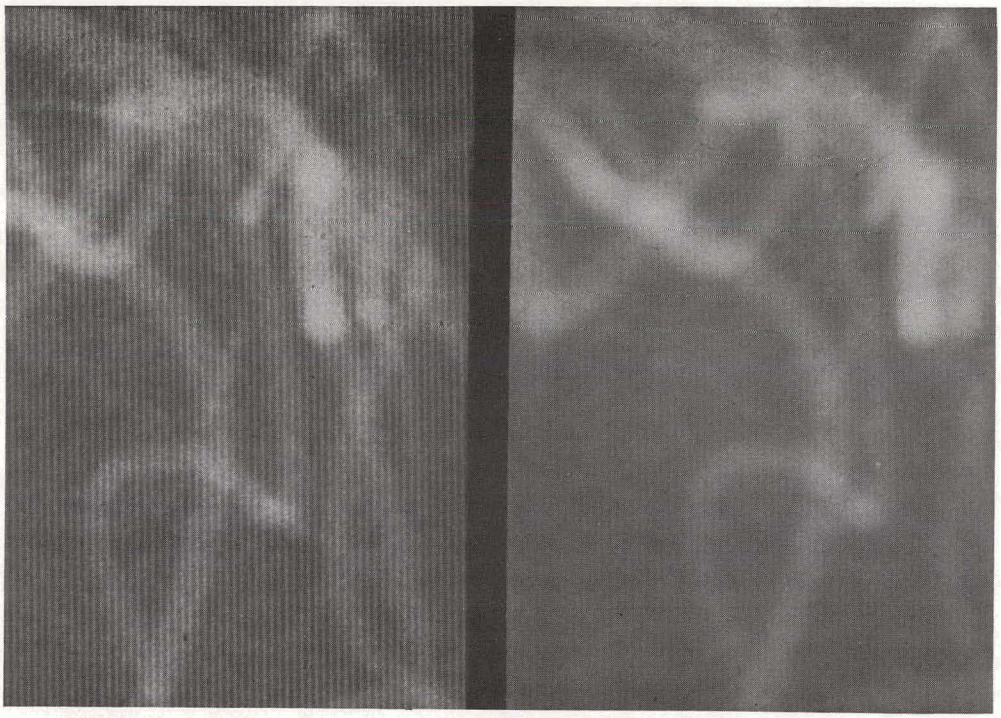

Figure 8. Lateral angiograms of patient. Left: TF-2 screens and Blue Brand film. Right: Detail screens and Royal Blue film.

Although rapid process films of Royal Blue speed are not yet available, Par Speed screens and Kodak RPS Medical X-ray Film can be used now to obtain lateral angiograms of improved sharpness. For frontal projections, the exposure speed of this system is marginal even at increased kilovoltages. The routine use of Detail screens and rapid process films to obtain angiograms of the greatest sharpness will have to await the development of rapid process films of higher speed or of x-ray machines with higher outputs at short exposure times.

LITERATURE CITED

1. Rossmann, K. In Television in Diagnostic Radiology. R. D. Moseley, Jr. and J. H. Rust, Eds. Birmingham, Alabama: Aesculapius Publishing Co., 1969.

COMPUTATION OF DISTRIBUTION OF ABSORBED DOSE AND ABSORBED DOSE RATE FROM A SCANNING ELECTRON BEAM*

By

M. Rozenfeld, L. H. Lanzl, Carol M. Newton,† and L. S. Skaggs

Most high-energy electron-therapy units spread their inherently small treatment beam with a scattering foil. The outer dimensions of the beam, so broadened, are subsequently defined by a collimator made of low atomic number material. The electron linear accelerator at the Argonne Cancer Research Hospital was designed to perform the functions of spreading and collimating in a different manner, namely by scanning the small, pencil-like beam over an arbitrarily shaped field, defined by a full-sized template.[1] The scanning device and the field resulting from a given template are shown in Figure 1.

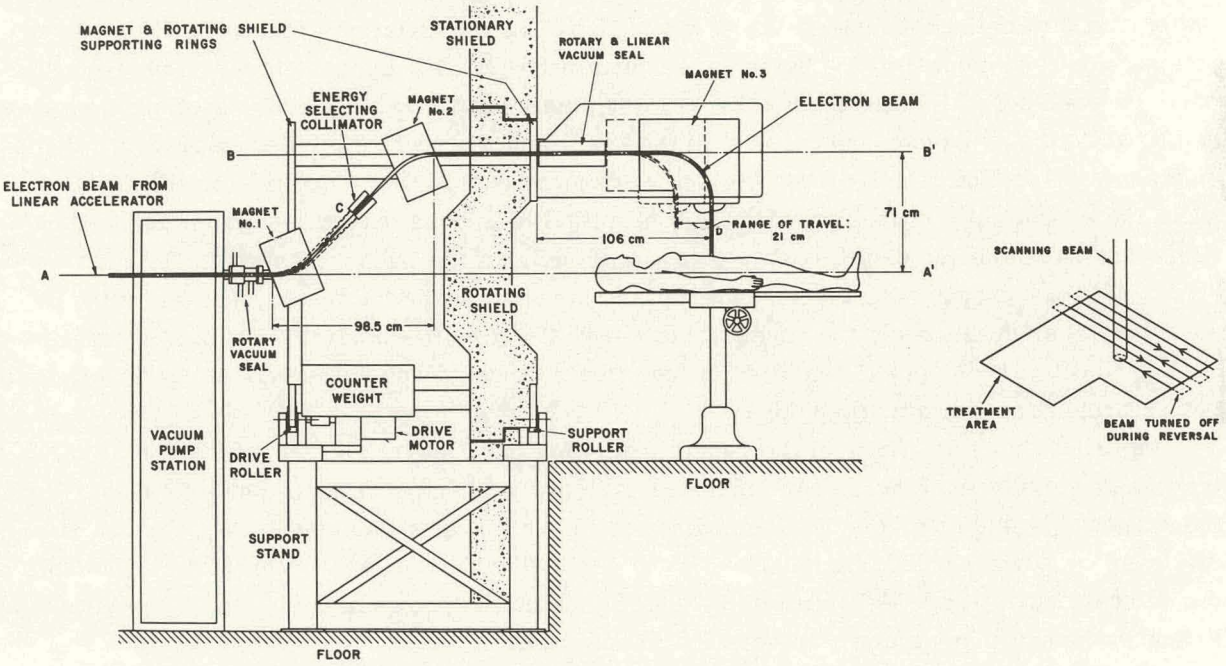

Figure 1. Schematic drawing of the electron beam scanning unit showing the arrangement of the magnet system, counterweight, rotating shield, treatment cot and patient. The electron beam is contained within a vacuum chamber that is not shown in this drawing. The inset on the right side illustrates scanning over a single portal field.

The scanning device operates with an index spacing of 5 mm between scan lines and a fixed scan speed of about 1 cm per second. The spacing was chosen to give reasonable overlap between the beams of adjacent scans and still allow a reasonable treatment time. For example, under

*This report is taken from a paper that appeared in Strahlentherapie, 138:651, 1969.

†Present address: The University of California at Los Angeles.

these conditions, it takes two hundred seconds to scan a field 10 cm by 10 cm. In general, the time of treatment is determined completely by the area of the field while the beam current is adjusted to deliver the required total dose in that time.

This mode of treatment has two dosimetric features that are amenable to computer calculations. (a) The dose distribution resulting from scanning over an arbitrarily shaped field is easily calculated by an appropriate summation of the distribution due to each individual pulse of the elemental pencil beam.[2] (b) The instantaneous dose rate is calculated from the same pencil beam data. During the scan, the dose rate has different values for any given point depending on the position of the beam relative to that point. These values at an arbitrary point within an irradiated medium depend on electron beam energy, depth in the medium, pulse length, repetition rate and location of the point in the field of irradiation.

MEASUREMENTS

The dose distribution study and the dose rate study require two separate computer programs. Both of these programs require, as input data, distributions of absorbed dose in unit density medium from the stationary pencil beam. These data were obtained by measuring the blackening of Adlux film irradiated between sheets of unit density Masonite. Irradiations with films placed both parallel and normal to the beam gave equivalent results in agreement with Dutreix.[3] The films exposed normal to the beam show any asymmetry in the beam's cross section at a given depth, while the films exposed parallel to the beam give correct relative results for all depths on a single film. The relative distributions were measured for each depth from the parallel films while the eccentricity of the approximately elliptical beam was determined from perpendicular films taken at the same depth. It should be mentioned that the magnet system of the linear accelerator does not produce a perfectly parallel and circular beam due to astigmatism in the magnetic lens system. To avoid the necessity of correcting for film nonlinearity, exposures were limited to give gross optical densities of less than 1.0, below which the net optical density is directly proportional to absorbed dose.

Figure 2 shows the films of the pencil beams for parallel irradiation with 5 and 35 MeV. The increased width of the 5 MeV beam at the surface of the phantom is mainly due to scattering in the exit window and transmission ion chamber. Figure 3 shows Polaroid films of the 35 MeV pencil beam for normal irradiation at 1 and 4 cm depth. The decrease in eccentricity with depth is due to scattering. The 5 MeV beam is essentially circular, probably due to large amounts of scattering in the exit window and transmission ion chamber.

Adlux film was also used to measure the distribution of absorbed dose resulting from a scan over an oddly shaped field to test the computer program. The distribution, in the form of isodose curves, was obtained from the films through use of a semi-automatic isodensity plotter. One or more percentage lines can be drawn which correspond to densities between the fog level and the maximum density read on the film. Care must be exercised in choosing the maximum to avoid film artifacts and local peaks due to instability of the linear accelerator.

DOSE DISTRIBUTION

The first program calculates the dose distribution at a given depth in a homogeneous unit density medium in a plane perpendicular to the beam for an arbitrary number of scan lines of arbitrary length. (A 7094 IBM computer was used here.) After the pencil beam distribution data

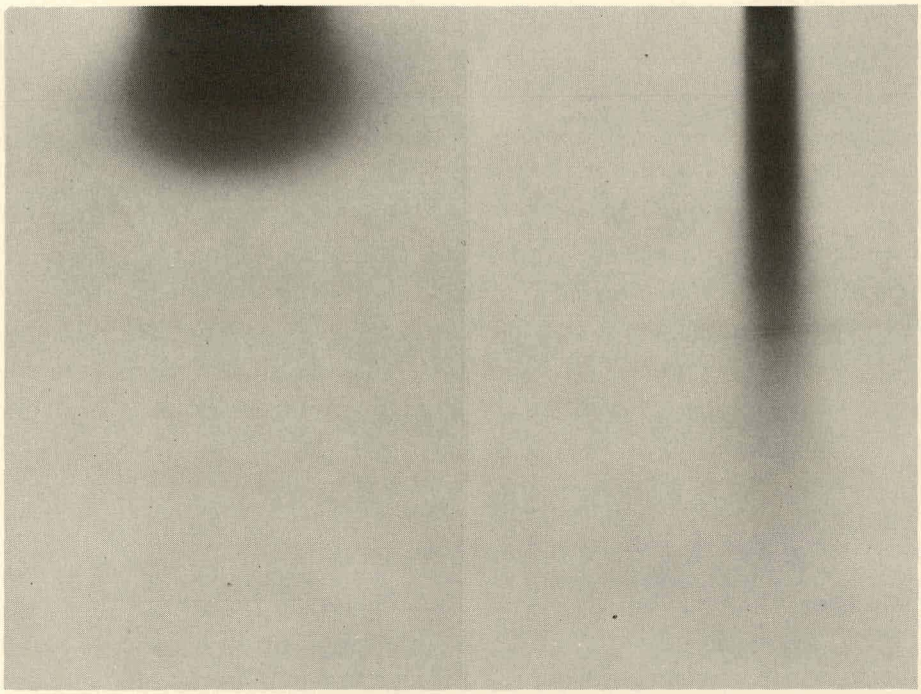

Figure 2. Films, located within a unit density phantom exposed parallel to the electron beam for 5 MeV (left) and 35 MeV (right).

for the appropriate energy and depth are entered into the computer, the number of scans of each length is entered relative to a grid of 100 x 100 points at 5 mm steps. The results of the calculation are the relative doses for each of the ten thousand points in the grid normalized to the maximum. If the relative dose distributions of the pencil beam for different depths are entered, the final distribution in each parallel plane can be normalized to the maximum dose at any chosen depth.

To avoid a summation for each individual pulse of electrons, the program starts out by calculating a new distribution by integrating the measured input data, i.e. for the pencil beam, over

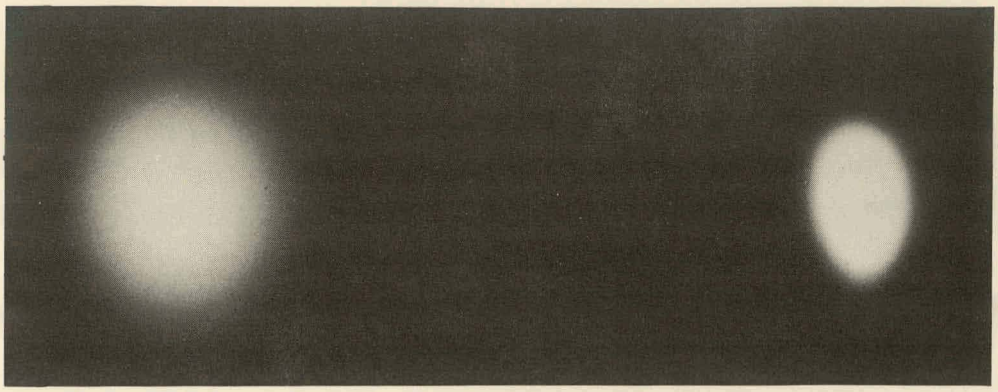

Figure 3. Elliptical shape of the 35 MeV pencil beam at a depth of 1 cm at the left and 4 cm at the right in unit density Masonite.

a scan length of 5 mm which is the grid spacing referred to above. This then represents a set of dose values at 5 millimeter spacing along the first scan line resulting from a movement of the beam from the left hand edge for a distance of 5 millimeters. The direct approach would then require repeating and summing this set of values for repeated 5 mm displacements of the beam up to the right hand edge.

Call the first set of values D(I) where I takes on integer values from 1 to 101 and represents the position along the scan line. The set of values D(I) is non-zero only for values of I corresponding to points near the left hand edge of the scan. The next 5 millimeter movement of the pencil beam will result in the same set of values displaced one step. Thus, the set of values corresponding to the second movement will be D(I-1). The total amount of radiation received at any point is the sum of the values from all the sets at that particular point. Thus, the total dose (TD) at the point I is

$$TD(I) = \sum_{J=0}^{K} D(I-J)$$

where K is one less than the total number at 5 millimeter movements of the beam along the scan line.

Thus, the dose at each point, I, has been reduced to a sum over the single set of values D. A further reduction in computation can be made by considering the total dose at the next point (I+1) in relation to the total dose at the present point I.

$$TD(I+1) = \sum_{J=0}^{K} D(I+1-J) = D(I+1) - D(I-K) + \sum_{J=1}^{K+1} D(I+1-J)$$

$$TD(I+1) = TD(I) + D(I+1) - D(I-K) \qquad (1)$$

Thus, the calculation of the total dose at the next point (I+1) has been reduced to adding just two more terms to the total dose for the present point. The left edge of the field must be chosen far enough from the extreme left edge of the array so the contribution there is zero. Then, the value of TD(I) for I = 1 is zero and the total dose for all points on the line is calculated from successive applications of formula (1).

The result for the top line is saved and entered into all lines of the same length and position. If the field is irregular, so that there are lines of different length or position, the above procedure is repeated for them. Then, starting again with the top line, a similar procedure is carried out to account for radiation contributed to each point from adjacent scan lines. When the line distributions have been summed for all scans within the range as given by the input data, the array is complete. This array can then be normalized relative to the highest value.

Another mode of treatment which would be valuable for some cases is to irradiate one segment of a field with electrons of one energy and another segment of the field with electrons of another energy while the patient remains immobile under the linear accelerator. A slight change in one control card allows the computer program to easily simulate this mode of treatment. Instead of normalizing the array after determining the results for one energy, the pencil beam distribution, number and length of scan lines for the second energy are read in, and their contribution is merely added to the previous array. Then, after the last energy field has been summed, the array is normalized relative to the highest value.

Normalization is, of course, not restricted to the peak value in the plane being calculated. By taking advantage of this feature, planes at different depths for a given field can all be represented relative to the maximum at one particular depth. In order to present the results in the more familiar form of isodose curves, an interpolation is then performed between the points in the array to find the positions of the desired percentages. The resultant isodose curves can be plotted with extreme resolution by a Calcomp plotter* or more quickly but less accurately on the high speed printer. Figures 4 and 5 show the printer output of the calculation for a test case

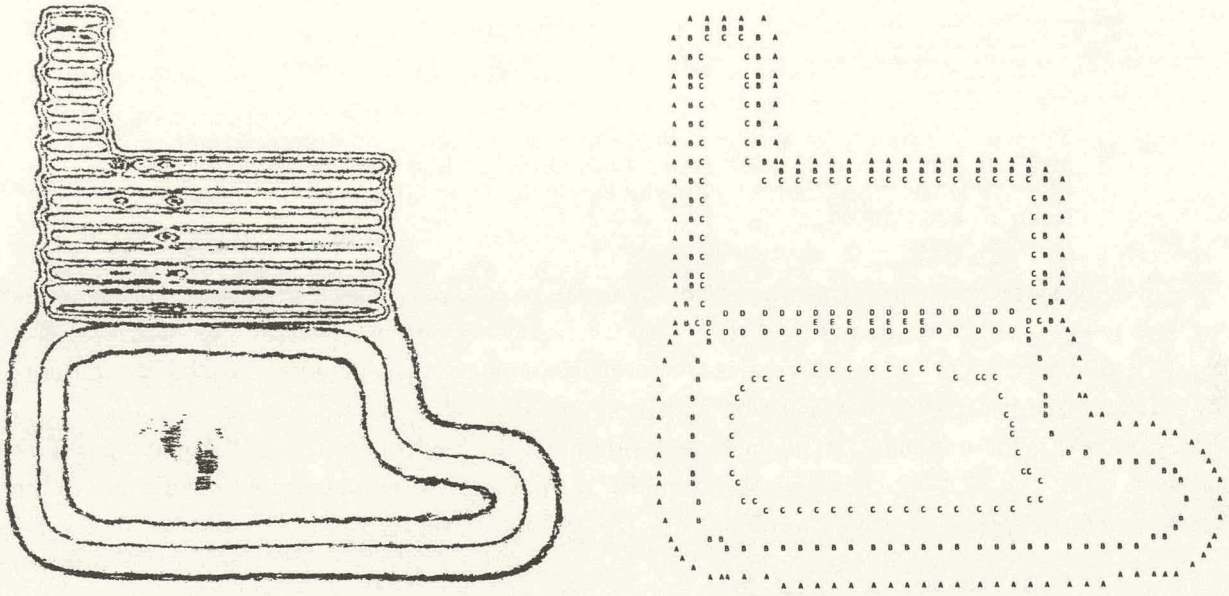

Figure 4. Comparison of measured and calculated dose distribution at 1 cm depth for combined 5 and 35 MeV yields. Both outputs show the 10, 40, 70, 90, and 100% isodose lines.

in comparison with the experimental curves obtained from an isodensity plot on Adlux film at two different depths. This test case was chosen to show some of the features of the linear accelerator and the program that has been described. Part of an irregular field was scanned with 35 MeV electrons and the other part with 5 MeV electrons. The calculations and measurements were made at 1 and 4 cm depth with all results normalized to the maximum at 1 cm.

The film shows structure in the scan lines in the 35 MeV field for the 1 cm depth where the beams of adjacent scans do not completely overlap. The computer output lacks this structure since the calculations are performed at a spacing equal to the distance between scan lines. The films for both depths were exposed simultaneously to the combined irradiation with both energies. The 5 MeV beam, however, does not penetrate to the 4 cm depth and the 35 MeV beam has been scattered sufficiently to smooth out all the structure evident at 1 cm.

DOSE RATE PROGRAM

The second program written specifically for the Argonne Hospital linear accelerator calculates the distribution of dose rate as the beam scans over a large field. (An IBM 360 Model 50

*A commercial digital incremental plotter.

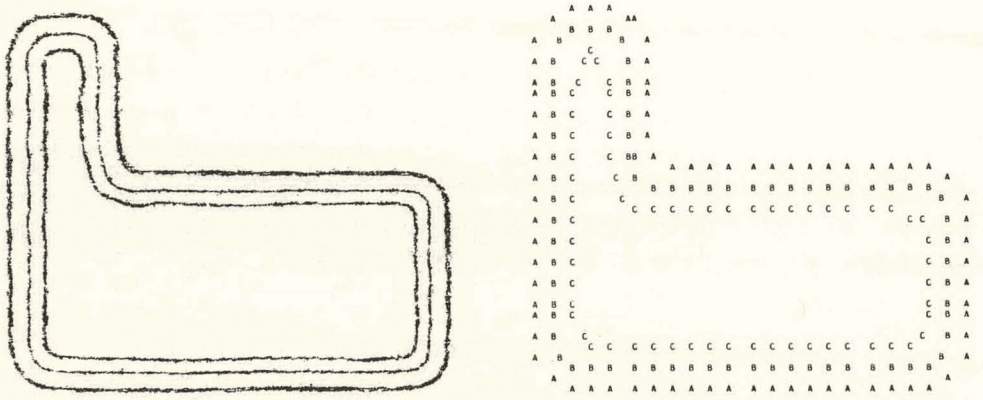

Figure 5. Comparison of measured and calculated dose distributions at 4 cm depth for a 35 MeV field. Both outputs show the 10, 40, and 70% isodose lines. Each output was independently normalized to the maximum at 1 cm depth.

computer was used for this program.) The dose rate during one pulse is the dose delivered during that pulse divided by the pulse length in seconds. Dose rates normalized per unit total dose can be calculated from the same relative input data as used in the previous program together with data on pulse length and repetition rate.

In general, the computation procedure determines the position of a pencil beam as it moves relative to a point stationary in the phantom, for all pulses that can contribute radiation to the point.

$$\text{Dose rate per unit total dose} = \frac{D}{\text{P.L.} \times \Sigma D}$$

where D = dose (in rad) from a pulse at a given point,

ΣD = total dose (in rad) at the given point from all pulses as the beam scans over a field, and

P.L. = the pulse length in seconds.

A wide range of dose rates will occur as the pencil beam approaches and then passes beyond the point of interest. The maximum dose rate will occur when the beam is centered over the point. The lowest non-zero value occurs when the beam is at a distance such that radiation can just be detected at the point.

The dose rate information is presented in different ways appropriate to different modes of operation. A continuous distribution of dose rates can be assumed for the nominal repetition rate of 60 pulses per second (pps) from the linear accelerator since in this case many pulses contribute to the total dose. First, the range of dose rates about each pulse is calculated and the results presented as the per cent of the total dose delivered per unit dose rate interval as a function of dose rate. Figure 6 shows the curves for the first depth, one cm deep in the phantom, used in the previous program and for the two energies, 5 and 35 MeV with a 0.5 μsec pulse length and 60 pps. Figure 7 presents the integration of the previous curves starting at the highest dose rate, thereby giving the per cent of the total dose delivered at rates higher than any given value.

The maximum dose rate per unit total dose for the 35 MeV beam at 1 cm depth is more than ten times larger than for the 5 MeV beam at the same depth since the smaller beam at the higher

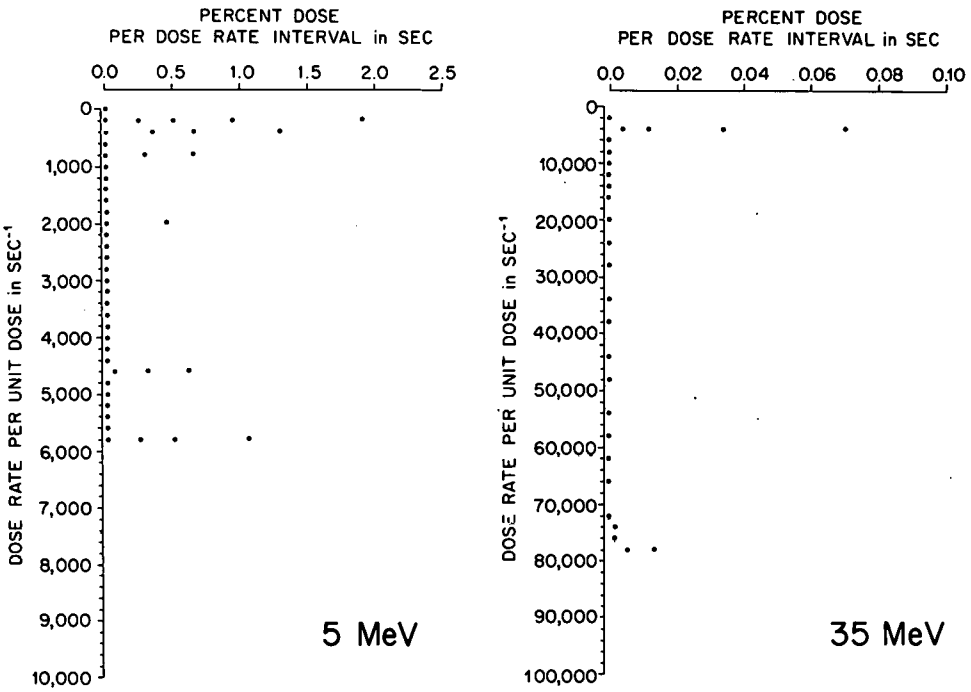

Figure 6. Per cent of the dose per unit dose rate interval for two energies at depth of 1 cm, pulse length 0.5 μsec and repetition rate of 60 pulses per sec.

energy contributes about ten times fewer pulses than the larger beam at the lower energy. The different number of peaks in the curves of Figure 6 are also due to the different size beams. Each peak indicates contribution from a scan line at a greater distance. The integral curves show a discontinuity corresponding to each peak in the differential curves.

The linear accelerator also has provision for reducing the repetition rate of the pulses of high energy electrons providing rates that equal 60 divided by any integer. At a rate of 6 pulses per second the beam moves approximately 2 millimeters between pulses, still providing a reasonable overlay during the scan. The peak current can easily be increased by the factor of ten necessary to provide the same average current and thereby the same total dose as for the nominal repetition rate of 60 pps. At this reduced rate, however, so few pulses contribute radiation to the point that a continuous distribution can no longer be assumed. For this case, the results are presented as the per cent of the total dose delivered per pulse. Figure 8 shows this function plotted against dose rate again for 5 and 35 MeV, 1 cm depth, 0.5 μsec pulse length but 6 pps. As expected, the maximum dose rate per unit total dose is ten times higher than in the previous case since the repetition rate has been reduced by a factor of ten. The curves for 35 MeV have so few points that no structure is evident, however, the differential curve for 5 MeV has a distinct structure.

Both Figures 6 and 8 can be explained by considering the relationship of the pencil beam distributions as they scan over a fixed point in the medium. Figure 9 shows a sample pencil beam distribution repeated at 5 mm intervals, which is the distance between scan lines. This figure shows the superposition of dose distributions of a series of scans with the direction of the scan perpendicular to the plane of the paper.

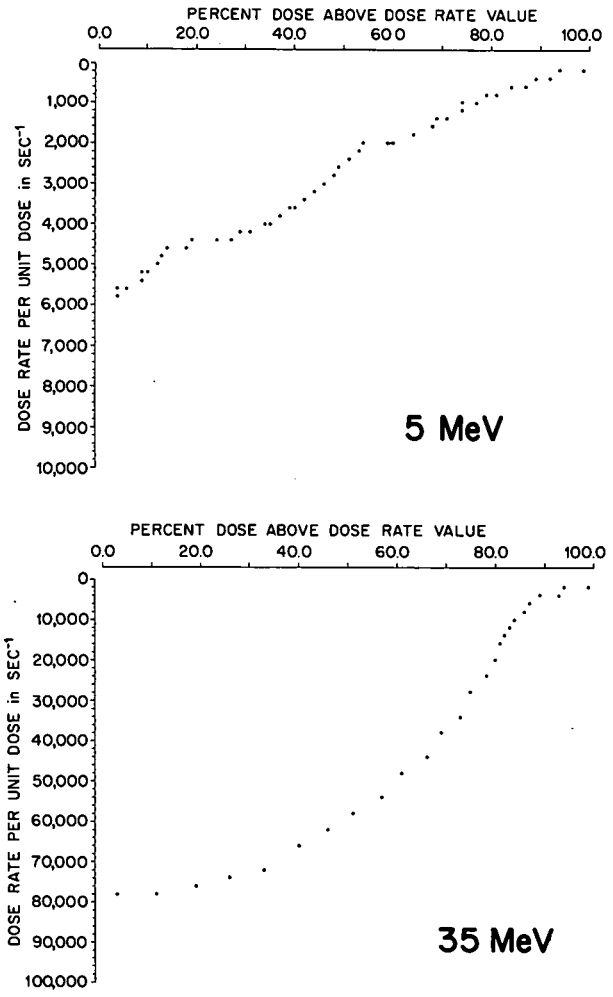

Figure 7. Per cent of the dose delivered at dose rates greater than the ordinate values. These are the integrals of the respective curves in Figure 6.

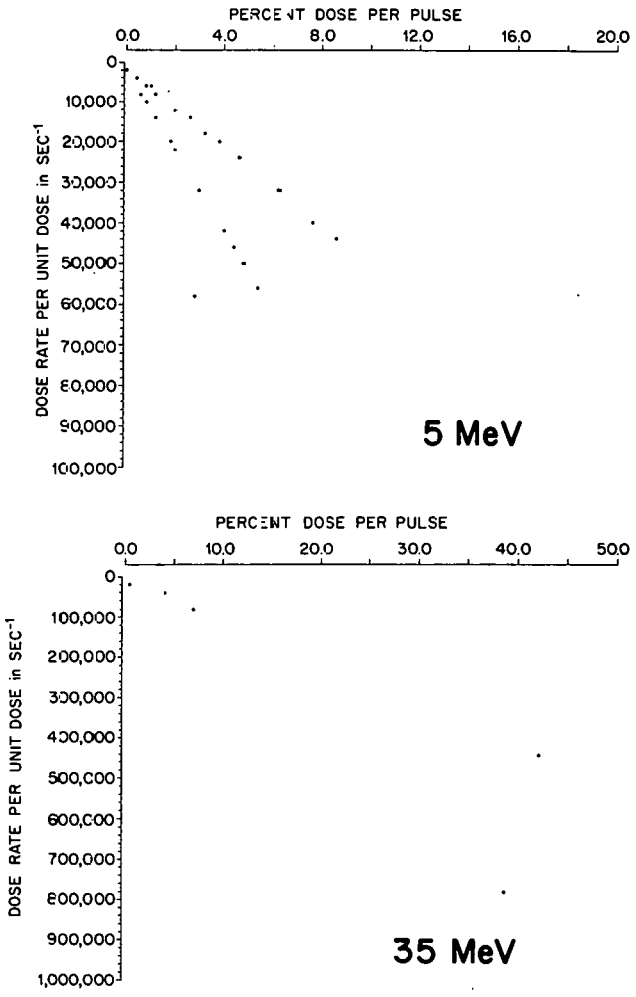

Figure 8. Per cent of the dose delivered per pulse at two energies at 1 cm depth, 0.5 μsec pulse length and repetition rate of 6 pulses per second.

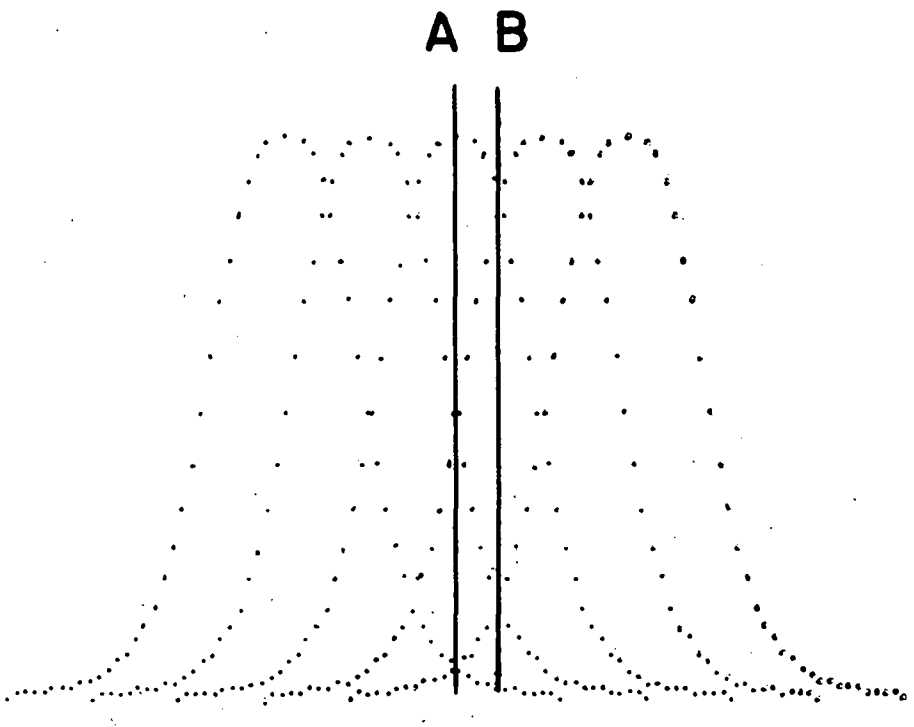

Figure 9. Superposition of sample pencil beam dose distribution repeated at the normal index spacing.

Point A, which has been taken as the point of reference thus far, will receive the highest dose rate when the beam scans directly over the point. Primarily because of the relatively flat top of the pencil beam distribution and the resultant small interval between the dose rates of consecutive pulses, the per cent of the dose per unit dose rate interval is large in this region, resulting in a peak. For adjacent scans, point A will receive additional radiation, but with a lower dose rate. When the adjacent scans pass the point, consecutive pulses again have approximately equal dose rates, thus, again, resulting in a small interval between pulses and another peak in the curve. Thus, each peak in Figure 6 is due to another pair of scan lines 5 mm further from point A.

The curve of per cent of the total dose per pulse shown in Figure 8 can similarly be explained. The highest dose rate is produced by the single pulse at the peak of the distribution when the beam scans directly over the point. All the other pulses due to the center scan must be considered in pairs of equal dose rate due to symmetry. This center scan accounts for the line of points in Figure 8 starting at about twice the per cent of the first point and sloping to zero. The adjacent scans that have a lower maximum dose rate, in addition, appear as symmetrical pairs. These scans produce the second string of points with twice the per cent of the first string.

Different points in the irradiated medium do not receive the same instantaneous dose rate. The distributions shown above are for point A which lies directly under the center of one of the scan lines. Point B, in Figure 9, which is midway between scan lines, will receive the lowest maximum dose rate of any point in the field. In addition, all scans contributing radiation to this point are symmetrically spaced. The points between A and B will all show slightly different dis-

tributions. The maximum dose rate will, of course, be intermediate, and no two scan lines contributing radiation to these points are at the same distance. In addition, for the lower repetition rates, one might consider points directly under a scan, but midway between two consecutive pulses which might be spaced as much as 2 millimeters apart. These points would have a lower maximum dose rate although they are on a scan line. A final parameter that alters the dose rate is depth in a phantom due to increase in the size of the beam. For example, the peak dose rate experienced at 4 cm depth due to irradiation at 35 MeV is about one third that at 1 cm at the same energy.

Thus, not only is the dose rate for one point distributed in a complicated fashion from some maximum to essentially zero, but this distribution depends strongly on the energy of the beam and the point chosen within the three dimensional volume being irradiated. The peak dose rate per unit total dose also varies inversely with the repetition rate and the pulse length.

Figure 5 shows that the maximum dose rate at 1 cm depth for 35 MeV, 0.5 μsec pulse length and 60 pps is about .08 megarad per sec per rad total dose. Since the usual patient dose is about 200 rad, the maximum dose rate is about 16 megarad per sec. This value should be compared to the dose rate of 55 kilorad per second obtained by an installation using the scattering method of beam spreading operating under identical conditions, assuming an output of 100 rad per minute. This dose rate would be constant rather than the maximum of a complicated distribution, and it would not vary with position in the field nor the total dose.

The maximum dose rate that was easily obtainable in a scanned field with our present installation was about 2×10^9 rad per sec. The conditions were 35 MeV, 1 cm depth, 0.2 μsec pulse length and 6 pps with a total dose of 1 krad. The limiting element is the final radiation monitor. With a newer monitor under development, higher doses could be delivered with consequent increase in dose rate.

From the theory of operation of traveling wave electron linear accelerators, it is to be expected that the electrons are bunched, thus producing a fine structure on the calculations presented here.[4] The bunching effect has not been measured, but it is estimated that it increases the dose rate during one bunch by a factor of ten to fifty over the average dose rate during a complete pulse.

LITERATURE CITED

1. Skaggs, L. S., L. H. Lanzl, and R. T. Avery. Isotopes in Medicine, Vol. 26, U.S.A., 1958, p. 312.
2. Skaggs, L. S., C. M. Newton, and L. H. Lanzl. Annual Meeting of Association of University Radiologists, Dallas, Texas, May 7-8, 1960 (Abstract).
3. Dutreix, J., and A. Dutreix. Ann. New York Acad. Sci., 161:33, 1969.
4. Carpender, J. W. J., L. S. Skaggs, L. H. Lanzl, and M. L. Griem. Am. J. of Roentgenol., Rad. Therapy, and Nucl. Med., 90:221, 1963.

Allen, L. W., and J. E. Ultmann. Laparotomy and Splenectomy in the Staging of Hodgkin's Disease. (Abstract) Clin. Res., 18(2):398, 1970.

Allen, L. W., J. E. Ultmann, D. J. Ferguson, and H. Rappaport. Laparotomy and Splenectomy in the Staging of Hodgkin's Disease. (Abstract) Proc. Central Soc. Clin. Res., 42:19, 1969.

Allen, L. W., J. E. Ultmann, and H. Rappaport. Laparotomy and Splenectomy in the Staging of Hodgkin's Disease. (Abstract) Proc. Am. College Physns., 51:37, 1970.

Aschenbrenner, V., R. Albin, R. Zak, K. G. Nair, and M. Rabinowitz. Increased Turnover of Mitochondrial Constituents in Cardiac Hypertrophy and Acute Hypoxia in the Rat. (Abstract) Third Annual Meeting of the International Study Group for Research in Cardiac Metabolism, Stowe, Vt., June 29 - July 1, 1970, p. 87.

Aschenbrenner, V., R. Druyan, R. Albin, and M. Rabinowitz. Haem a, Cytochrome c and Total Protein Turnover in Mitochondria from Rat Heart and Liver. Biochem. J., 119:157, 1970.

Aschenbrenner, V., M. Rabinowitz, R. Zak, and K. G. Nair. Effect of Severe Hypoxia on Turnover and Synthesis of Mitochondria from Rat Heart. (Abstract) J. Clin. Invest., 48(6):4a, 1969.

Beck, R. N. Modulation Transfer Function for Radioisotope Imaging Systems. In Handbook of Radioactive Nuclide. Y. Wang, Ed. Cleveland: The Chemical Rubber Company, 1969, p. 123.

Beck, R. N., P. V. Harper, L. T. Zimmer, and N. Lembares. Methods for Determining the Penetration and Scatter Fractions for Radioisotope Imaging Systems. (Abstract) Second International Conference on Medical Physics, "Abstracts of Papers," Boston, Massachusetts, 11-15 August 1969, p. 78.

Davis, M. E., L. H. Lanzl, and A. B. Cox. The Detection, Prevention and Retardation of Menopausal Osteoporosis. In Osteoporosis. U. S. Barzel, Ed. New York: Grune & Stratton, Inc., 1970, p. 140.

Davis, M. E., L. H. Lanzl, and A. B. Cox. Detection, Prevention and Retardation of Menopausal Osteoporosis. Obstetrics and Gynecology, 36(2):187, 1970.

DeGowin, R. L., A. R. Lavender, M. Forland, D. Charleston, and A. Gottschalk. Erythropoiesis and Erythropoietin in Patients with Chronic Renal Failure Treated with Hemodialysis and Testosterone. Ann. Intern. Med., 72(6):913, 1970.

Druyan, R., B. DeBernard, and M. Rabinowitz. Turnover Rates of Mitochondrial Hemeproteins. (Abstract) Fed. Proc., 28(2):729, 1969.

Fielding, C. J., C. T. Lim, and A. M. Scanu. A Protein Component of Serum High Density Lipoprotein with Co-Factor Activity Against Purified Lipoprotein Lipase. Biochem. Biophys. Res. Commun., 39(5):889, 1970.

Fogh, J. Studies on the Mechanism of the Increased Dose-Response of Erythropoietin After Stimulation with Erythropoietin. Blood, 35(4):476, 1970.

Gottschalk, A., J. D. Abatie, J. P. Petasnick, R. E. Polcyn, R. N. Beck, and D. B. Charleston. ACRH Brain Scanner. Comparison Between Sensitivity and Resolution Based on a Clinical Evaluation. In Medical Radioisotope Scintigraphy, Vol. II. Vienna: IAEA, 1968, p. 563.

Gottschalk, A., M. S. Usher, R. E. Polcyn, and J. L. Quinn, III. Scintillation Camera with Diverging Collimator: Physical Parameters and a Clinical Evaluation. (Abstract) J. Nucl. Med., 10(6):337, 1969.

Griem, M. L., D. J. Mewissen, P. Meier, and G. D. Dobben. Analysis of the Morbidity and Mortality of Children Irradiated in Fetal Life (II). In Radiation Biology of Fetal and Juvenile Mammal, AEC Symp. Series 17. M. R. Sihov and D. D. Mahlicon, Eds. Oak Ridge: USAEC Div. of Tech. Inform. Ext., 1969, p. 651.

Griem, M. L., L. S. Skaggs, and L. H. Lanzl. Radiation Therapy of the Laryngeal and Tracheal Tumors with High Energy Electrons Using Pencil Beam Scanning. In Proceedings of the Symposium on High-Energy Electrons, 26-28 September 1966, Madrid, Spain. General Directorate of Health, Spain, Eds. Madrid: Graficas Canales, S.L., Ciceron, 16, p. 345.

Gross, M., and E. Goldwasser. Effect of Erythropoietin on Synthesis of Hemoglobin Messenger RNA. (Abstract) Fed. Proc., 29(2): March-April, 1970.

Gross, M., and E. Goldwasser. On the Mechanism of Erythropoietin-induced Differentiation. VII. The Relationship Between Stimulated Deoxyribonucleic Acid Synthesis and Ribonucleic Acid Synthesis. J. Biol. Chem., 245(7):1632, 1970.

Gross, N. J., and M. Rabinowitz. Turnover of Mitochondrial DNA in Hypothyroid, Euthyroid and Hyperthyroid States. (Abstract) Clin. Res., 17(2):459, 1969.

Harper, P. V., R. N. Beck, and M. Reddy. Two-Dimensional Image Analysis in Radioisotope Scanning Systems. (Abstract) J. Nucl. Med., 10(6):340, 1969.

Harper, P. V., R. N. Beck, and T. D. Cohen. Evaluation of Scanning Procedures in Terms of Information Theory. In Medical Radioisotope Scintigraphy, Vol. I. Vienna: IAEA, 1969, p. 289.

Haus, A. G., and K. Rossmann. X-Ray Sensitometer for Screen-Film Combinations Used in Medical Radiology. Radiology, 94(3):673, 1970.

Hirz, R., and A. M. Scanu. Reassembly in vitro of a Serum High-Density Lipoprotein. Biochim. Biophys. Acta, 207:364, 1970.

Hunter, R. Antigen Trapping in the Lamina Propria and the Production of Secretory IgA Antibody. (Abstract) Fed. Proc., 29(2): March-April, 1970.

Kingdon, H. S., J. M. Baron, G. E. Byrne, Jr., and H. Rappaport. Malignant Histiocytosis. Results of Combination Vincristine-Prednisone Therapy. Ann. Intern. Med., 72(5):705, 1970.

Koka, M., and T. Nakamoto. Active 50S E. coli Ribosomes. (Abstract) Fed. Proc., 28(2):725, 1969.

Kranzler, J. K., P. V. Harper, R. E. Polcyn, and A. Gottschalk. Scintiphotographic Demonstration of Hepatic Pliability as a Diagnostic Criterion. J. Nucl. Med., 10(6):416, 1969.

Kyriazis, A. P., E. Douglas, K. Dzoga, and R. W. Wissler. Inhibition of Migration of Macrophages by Tumor Specific Antigens. (Abstract) J. Reticuloendothelial Society, San Francisco, 1-4 December 1969, p. 27.

Lanzl, L. H., T. J. Ahrens, M. Rozenfeld, and L. Bess. An Automatic Patient-Contour Measuring Apparatus. Am. J. Roentgenol., Radium Therapy Nucl. Med., CVIII(1):162, 1970.

Lanzl, L. H., A. Cox, G. Dobben, R. Olson, J. Toman, and A. Schrodt. An Additional System for Bone Densitometry Studies. Proc. of Bone Measurement Conference, Sheraton O'Hare Motor Hotel, Chicago, 22-23 May 1970. J. R. Cameron, Ed. Sponsored by University of Wisconsin Bone Mineral Laboratory and U. S. Atomic Energy Commission, CONF-700515, p. 33.

Lembares, N., R. N. Beck, and P. V. Harper. Determination of the Response to Scattered Radiation from ^{125}I. (Abstract) J. Nucl. Med., 10(6):417, 1969.

Lerch, I. A. Bioluminescence and Radiation Response of Photobacterium fischeri H-2. Rad. Res., 43(1):161, 1970.

Palmer, R. H. The Enzymatic Assay of Bile Acids and Related 3α-Hydroxysteroids; Its Application to Serum and Other Biological Fluids. In Methods in Enzymology, Vol. XV. S. P. Colowick and N. O. Kaplan, Eds. New York: Academic Press, 1969, p. 280.

Palmer, R. H. Toxic Effects of Lithocholic Acid and Related 5β-H Steroids. In Bile Salt Metabolism, Chapter 17. L. Schiff, J. B. Carey, Jr., and J. M. Dietschy, Eds. Springfield, Ill.: Charles C Thomas Publishers, 1969, p. 184.

Palmer, R. H., T. F. Gallagher, Jr., M. N. Mueller, and A. Kappas. The Effect of Natural and Synthetic Estrogens on the Excretion of BSP by the Liver. In Metabolic Effects of Gonadal Hormones and Contraceptive Steroids. H. A. Salhavick, D. M. Kysnis, and R. L. Vande Wield, Eds. New York: Plenum Press, 1969, p. 19. (Based on Workshop held in Boston, 1-5 December, 1968.

Pickleman, J. R., E. Paloyan, K. A. Lathrop, and P. V. Harper. Parathyroid Uptake of ^{75}Se-Selenomethionine in Thiazide-Induced "Hyperparathyroidism." (Abstract) J. Nucl. Med., 10(6):363, 1969.

Porter, J. W., P. V. Harper, and D. B. Charleston. Experimental Determination of Absolute Detection Efficiencies of NaI(Tl) Well Crystals Without Calibrated Standards. (Abstract) J. Nucl. Med., 10(6):428, 1969.

Rabinowitz, M., and H. Swift. Mitochondrial Nucleic Acids and Their Relation to the Biogenesis of Mitochondria. Physiol. Rev., 50(3):376, 1970.

Rappaport, H. The Pathologic Anatomy of the Splenic Red Pulp. In Die Milz/The Spleen. K. Lennert, and D. Harms, Eds. Berlin - Heidelberg: Springer-Verlag, 1970, p. 24.

Rappaport, H., and S. B. Strum. Vascular Invasion in Hodgkin's Disease: Its Incidence and Relationship to the Spread of the Disease. Cancer, 25(6):1304, 1970.

Reddy, M., P. V. Harper, and R. N. Beck. Calculation of the Figure of Merit for Imaging Systems Viewing Radially Symmetric Objects. (Abstract) J. Nucl. Med., 10(6):431, 1969.

Rossmann, K. A Method for Measuring One-Dimensional Spatial Frequency Spectra of Objects in Medical Radiology. In Television in Diagnostic Radiology, Chapter 24. R. D. Moseley, Jr. and J. H. Rust, Eds. Birmingham, Alabama: Aesculapias Publishing Company, 1969, p. 412.

Rossmann, K., A. G. Haus, and G. D. Dobben. Improvement in the Image Quality of Cerebral Angiograms. Radiology, 96(2):361, 1970.

Rowley, D. A., F. W. Fitch, M. A. Axelrad, and C. W. Pierce. The Immune Response Suppressed by Specific Antibody. Immunology, 16(4):549, 1969.

Rowley, J. D. Sex Chromosome Abnormalities and Neuropsychiatric Disorders. Ill. Med. J., May, 1970.

Rowley, J. D., and E. Pergament. Possible Non Random Selection of D Group Chromosomes Involved in Centric-Fusion Translocations. Ann. Genet., 12(3):177, 1969.

Rozenfeld, M., L. H. Lanzl, C. M. Newton, and L. S. Skaggs. Computation of Distribution of Absorbed Dose and Absorbed Dose Rate From a Scanning Electron Beam. Strahlentherapie, 138(6):651, 1969.

Scanu, A. M. The Effect of Reduction and Carboxymethylation on the Circular Dichroic Spectra of Two Polypeptide Classes of Serum High Density Lipoprotein. Biochim. Biophys. Acta, 200:570, 1970.

Scanu, A. Serum High Density Lipoproteins, Chapter C3. In Structural and Functional Aspects of Lipoproteins in Living Systems. A. Scanu and E. Tria, Eds. London: Academic Press, Ltd., 1969, p. 425.

Scanu, A., E. Cump, J. Toth, S. Koga, E. Stiller, and L. Albers. Degradation and Reassembly of a Human Serum High-Density Lipoprotein. Evidence for Differences in Lipid Affinity Among Three Classes of Polypeptide Chains. Biochemistry, 9:1327, 1970.

Scherberg, N. H., A. Guha, W.-T Hsu, and S. B. Weiss. Evidence for the Early Synthesis of T4 Bacteriophage-Coded Transfer RNA. Biochem. Biophys. Res. Commun., 40(4):919, 1970.

Sorensen, L. B. Mechanism of Excessive Purine Biosynthesis in Hypoxanthine-Guanine Phosphoribosyltransferase Deficiency. J. Clin. Invest., 49(5):968, 1970.

Stejskal, R., and F. W. Fitch. Tissue Agglutination Reaction with Normal Rat Spleen. J. Reticuloendothelial Soc., 7(1):121, 1970.

Strum, S. B., J. K. Park, and H. Rappaport. Observation of Cells Resembling Sternberg-Reed Cells in Conditions Other than Hodgkin's Disease. Cancer, 26(1):176, 1970.

Strum, S. B., and H. Rappaport. Significance of Focal Involvement of Lymph Nodes for the Diagnosis and Staging of Hodgkin's Disease. Cancer, 25(6):1314, 1970.

Ultmann, J. E., L. W. Allen, D. J. Ferguson, and H. Rappaport. Exploratory Laparotomy and Splenectomy in Staging of Hodgkin's Disease. (Abstract) International Integrated Cancer Congresses, Sao Paulo, Brazil, 7-13 September 1969, p. 143.

Ultmann, J. E., and D. D. Nixon. The Therapy of Disseminated Hodgkin's Disease. Editorial. Sangre, XV(1):1, 1970.

Waterston, R. H. Soluble Antigen from Sheep Erythrocytes: Preparation and Antigenic Properties. Immunology, 18(3):431, 1970.

Waterston, R. H., D. A. Rowley, and F. W. Fitch. Increase of the Antibody Response by "Antigenic Competition": A Paradox. (Abstract) Fed. Proc. 29(2): March-April, 1970.

Wong, T.-W., and S. B. Weiss. β-Mercaptopyruvate as the Sulfur-Donor for RNA Sulfur-Transferase from Bacillus subtilis. (Abstract) Fed. Proc., 28(2): March-April, 1970.

Wong, T.-W., S. B. Weiss, G. L. Eliceiri, and J. Bryant. Ribonucleic Acid Sulfurtransferase from Bacillus subtilis W168. Sulfuration with β-Mercaptopyruvate and Properties of the Enzyme System. Biochemistry, 9:2376, 1970.

Yachnin, S. Potentiation of Human Lymphocyte Transformation by Autologous Red Blood Cells and Platelets. (Abstract) J. Clin. Invest., 49(6):105a, 1970.